TECHNO-ECONOMIC AND SUSTAINABILITY ASSESSMENT OF SOLAR-AIDED LIGNOCELLULOSIC BIOREFINERIES

by

CHRISTIAN YAKAN A NWAI

submitted in accordance with the requirements for
the degree of

DOCTOR OF PHILOSOPHY

in the subject

CHEMICAL ENGINEERING

at the

UNIVERSITY OF SOUTH AFRICA

SUPERVISOR: PROF. BILAL PATEL

January 2023

DECLARATION

Name: Christian YAKAN A NWAI

Student number: 58551557

Degree: Doctor of Philosophy

Exact wording of the title of the thesis as appearing on the electronic copy submitted for examination:

TECHNO-ECONOMIC AND SUSTAINABILITY ASSESSMENT OF SOLAR-AIDED LIGNOCELLULOSIC BIOREFINERIES

I declare that the above thesis is my own work and that all the sources that I have used or quoted have been indicated and acknowledged by means of complete references.

I further declare that I submitted the thesis to originality checking software and that it falls within the accepted requirements for originality.

I further declare that I have not previously submitted this work, or part of it, for examination at Unisa for another qualification or at any other higher education institution.

(The thesis will not be examined unless this statement has been submitted.)

SIGNATURE

30 / 01 / 2023

DATE

Acknowledgments

I wish to thank my advisor, Prof Bilal Patel for his coaching and supervisory role. He is a patient advisor who always encouraged me to explore new ideas and think differently. His coaching role has made my PhD journey a pleasant one.

I would also like to thank Dr Henco Bezuidenhout, Purtunia Silinga, and all the staff of the research and development department of AECI Mining Explosives for their continuous support.

Dedication

This dissertation is dedicated to:

- The God of Abraham, Isaac, and Jacob for giving me health, strength, perseverance, and motivation throughout the completion of this work.
- All my teachers, lecturers and mentors for contributing to shaping my life.
- My father, Mr NWAI YAKAN for giving me the best gift ever; education.
- My mother, Mrs NWAI Genevieve for her unconditioned love and support.
- My wife KEDI IROUME Joelle Ines for continuously encouraging me.
- My family, friends, and colleagues for always cheering me up in difficult times.

"Trust in the LORD with all your heart, and do not lean on your own understanding. In all your ways acknowledge him, and he will make straight your paths" **(Proverbs 3: 5-6)**

Abstract

The aim of this thesis is to conduct a techno-economic and sustainability assessment of solar-aided biorefineries in South Africa. Previous studies on solar-aided lignocellulosic biorefineries are limited to concept illustration and biofuel cost estimation. Thus, a comprehensive assessment of the technical performance, environmental impact and manufacturing costs of potential co-products including lignin and biochar has never been conducted. In addition, although South Africa generates about 16 million metric tonnes of corn residues per annum, and possesses one of the highest solar irradiances in the world, a techno-economic study for solar-aided lignocellulosic biorefineries in South Africa is presently lacking.

In order to address the above-mentioned knowledge gaps, the conversion of corn stover into ethanol was simulated. Various scenarios in which solar energy could be added to the biorefinery to generate process steam and electricity were evaluated. Also, a novel gasification configuration allowing the integration of solar energy as a heat source for gasification chemical reactions was modelled and studied. Further, processes enabling the conversion of corn stover into methanol via gasification and CO_2 hydrogenation were developed. The techno-economic and environmental performance of all modelled scenarios was then assessed.

The results obtained revealed that by the incorporation of solar energy into a corn stover-to-ethanol biorefinery combined with the export of lignin as a co-product could enhance the biorefinery's overall energy conversion efficiency from 34.3 to 53 – 77%. Moreover, for the standalone scenarios, the minimum ethanol selling price (MESP) was 0.61 USD/litre (25.88 USD/GJ), which increased to 43.17 – 68.84 USD/GJ in the solar-aided scenarios. Lignin's minimum selling price was found to vary between 1.63 USD/kg to 3.55 USD/kg depending on the mode of solar energy integration. The incorporation of solar energy combined with export of lignin resulted in an overall potential environmental impact (PEI/hr) 14 to 46% lower. Also, in the solar-aided scenarios, up to 2.06 km^2 of land was required by the biorefinery.

In the corn stover-to-methanol biorefinery, the export of char was found to improve the overall conversion efficiency from 46.1 to 61.5%. Further, the introduction of a solar-aided gasifier enhanced net gasification efficiency by 56 to 87%. The minimum methanol selling price (MMSP) for the standalone and solar-aided configurations were respectively found to be 0.31 USD/litre (17.47 USD/GJ) and 0.50 USD/litre (27.88 USD/GJ). While the biochar minimum selling price was estimated to be 13.04 USD/GJ (0.37 USD/kg). The overall PEI/hr for the solar-aided biorefinery was found to be 36% lower that the standalone configuration. Also, the integration of solar energy required a total land area of 6.92 km^2, which is substantial.

Data generated in this study are expected to serve as a building block for the future implementation of the circular bioeconomy production concept. The study is also expected to be value-added to the literature by providing data that could be used as a reference point for the efficient integration of solar energy into lignocellulosic biorefineries.

Key terms: Biorefinery, biomass, solar-aided, solar-driven, circular economy, lignocellulose, biofuel, gasification, eco-efficient, bioeconomy, techno-economic analysis

List of publications

Yakan, C. & Patel, B., 2021. Techno-economic study and environmental analysis of a solar-aided lignocellulosic biorefinery: a South African case study. *Biomass Conversion and Biorefinery,* pp. 1-21. DOI: 10.1007/s13399-021-01859-2.

Yakan, C. & Patel, B., 2022. Techno-economic Study and Environmental Analysis for the Production of Bio-methanol Using a Solar-aided Dual-bed Gasifier. *Waste and biomass valorisation*. Accepted manuscript. DOI: 10.1007/s12649-023-02115-6.

Table of contents

List of figures

List of Tables

Glossary

Acronyms, abbreviations, and terms	Definition / explanation
AP	Acidification Potential
ATP	Aquatic toxicity potential
Biological conversion	Processing of biomass into biofuel using micrograms
Biorefinery	An integration of conversion processes aiming at producing power, bio-chemicals, and biofuels from biomass
CCE	Carbon conversion efficiency
CECPI	Chemical engineering cost plant index
CHP	Combined heat and power system
CS	Corn stover
CSP	Concentrated solar power
CST	Concentrated solar thermal
FCI	Fixed capital investment
FT-ICR MS	Fourier transform ion cyclotron resonance mass spectrometry
GWP	Global warming potential
HHV	Higher heating value
HMF	Hydroxymethylfurfural
HTPE	Human toxicity potential by dermal exposure or inhalation
HTPI	Human toxicity potential by ingestion
HVPR	High-velocity pneumatic riser
IRR	Internal rate of return
ISBL	Inside battery limit
LCA	life cycle analysis

LUE	Land-use efficiency
LVFB	Low-velocity fluidized bed
LVH	Lower heating value
MEA	Monoethanolamine
MESP	Minimum ethanol selling price
MLSP	Minimum lignin selling price
MMSP	Minimum methanol selling price
NPV	Net present value
NREL	National renewable energy laboratory
ODP	Ozone depletion potential
OPEC	Organization of the petroleum exporting countries
PCOP	Photochemical oxidation potential
PEI	Potential environmental impact
PV	Photovoltaic
RBPD	Regional biomass processing depots
SAM	System advisor model
SAM	System advisor model
TCI	Total capital investment
TEA	Techno-economic assessment
Thermochemical conversion	Processing of biomass into biofuel using high-temperature processes
TNEE	Tunzini Nessi Equipment Companies
TTP	Terrestrial toxicity potential
USD ($)	United States dollar
WAR	Waste reduction algorithm

CHAPTER 1 – INTRODUCTION

1.1 Background

Energy is a fundamental part of our daily lives. For many centuries, fossil fuels have been our primary source of energy. They supply most of the energy necessary to drive our industry, power our homes and keep our transportation system running. Fossil fuels consist of coal, crude oil and natural gas, and are currently the cheapest available sources of energy. Their extraction and refining processes are relatively cost-effective and offer the possibility to generate useful by-products such as polymers and chemicals. Moreover, the technologies used to harness energy from fossil fuels are already well established and we have become familiar with them (Gemna, 2014).

Despite their numerous favourable attributes, fossil fuels have been subject to various concerns. Firstly, the formation process of fossil fuels in the earth's crust requires hundreds of millions of years. Hence, these resources are practically non-renewable. Secondly, at the end of the year 2021, the global reserves of crude oil and natural gas were respectively estimated to be 545 billion barrels and 205.9 trillion cubic meters (OPEC, 2022). On the other hand, coal reserves as of January 1, 2021 were estimated to be 1.074 trillion metric tonnes (BP Statistical Review of World Energy, 2021). Given our current rate of extraction and consumption, the reserve of coal could be exhausted by the year 2159, while natural gas and crude oil could be depleted by the years 2069 and 2070 respectively unless discoveries are made (BP Statistical Review of World Energy, 2021). Thirdly, there is global consensus amongst climate scientists that the CO_2 released during the combustion of fossil fuels is a major contributor to global warming (Hoel & Kvermdokk, 1996); (Abbasi & Abbasi, 2011); (Londoño-Pulgarin, et al., 2021). Fossil fuels are therefore unsustainable.

Furthermore, it is common knowledge that geopolitical tensions involving oil-producing countries are prone to unsettle global fossil fuel prices. This was the case in 2022 when the conflict between Russia and Ukraine provoked an energy crisis. Indeed, during that period, most countries that depended on Russia for gas, oil or coal were compelled to find alternative suppliers. As a result, steep increases were observed in fossil fuel prices. It is

therefore crucial, especially for non-producing countries, to break the reliance on fossil fuels.

In the quest for sustainable alternative sources of energy that will gradually substitute fossil fuels in the long term, several sources of renewable energy have been explored. The most promising ones are solar energy, wind power and bioenergy (Babu, 2008). Amongst these promising alternatives, bioenergy which is energy derived from biomass, is the only option capable to substitute fossil fuels in all energy markets, mainly in the production of heat, electricity and transportation fuels (Bauen, et al., 2009).

Additionally, bioenergy is the only renewable carbon source that can be used for the production of chemicals, materials, and fuels (De Wild, 2015). Furthermore, considering that biomass can be produced in virtually every country, the adoption of bioenergy could minimize international conflicts driven by petroleum resources (Dale, 2003). Moreover, because plant-based biomass captures CO_2 from the atmosphere during its growth and releases it when burnt (refer to Equations 1.1 and 1.2 below), the adoption of bioenergy allows the level of carbon in the atmosphere to remain neutral with no increase in CO_2 (Naik, et al., 2010); (Cao, et al., 2017). Hence, the implementation of bioenergy can help mitigate climate change.

$$2CO_2 + 5H_2O \xrightarrow{Sun\ light} C_6H_{12}O_5 + 6O_2 \qquad \text{Eq. 1.1}$$

$$(CH_2O)_n + nO_2 \rightarrow nCO_2 + nH_2O + Heat \qquad \text{Eq. 1.2}$$

Bioenergy can be converted into petroleum-equivalent energy carriers with the help of a biorefinery. As illustrated in Figure 1.1, a biorefinery is an integration of conversion processes aiming at producing power, bio-chemicals, and biofuels from biomass. Biofuels are generally the main products of biorefineries and can be classified based on the biomass they are derived from. For instance, biofuels produced from edible biomass such as sugar cane, grains, and vegetable oils are referred to as first generation biofuels. While

biofuels derived from non-edible lignocellulosic biomass such as agricultural and forestry residues, energy crops, municipal solid waste and other crops are termed second generation biofuels or lignocellulosic biofuels (Paudel, et al., 2017); (Lee & Lavoie, 2013). Biofuels produced from algae are called third generation biofuels (Saha, et al., 2019).

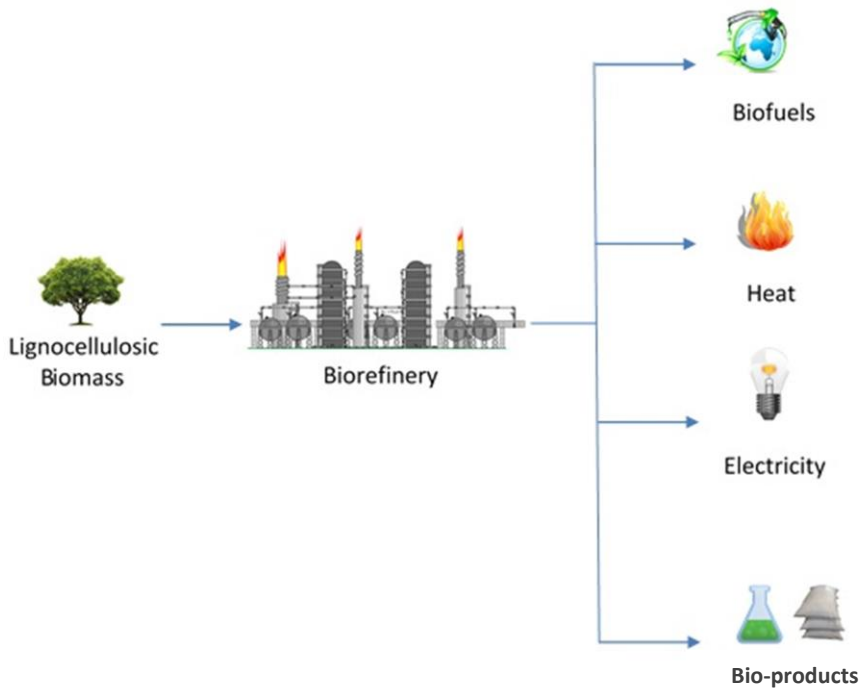

Figure 1.1: Graphical illustration of the biorefinery concept lignocellulose is converted into biofuels, heat, electricity and bioproducts

Because of the food vs. fuel dilemma, the first generation of biofuels has been fiercely opposed worldwide. Indeed, the idea of "turning food for the poor into fuel for the rich" (Kovarik , 1998) is highly controversial and raises ethical and sustainability concerns (Mohr & Raman , 2013). Hence, lignocellulosic biomass which is one of the cheapest and the most abundant renewable organic materials in the biosphere is regarded as a more sustainable option for biofuel production.

Lignocellulosic biomass can be converted into carbon-neutral liquid fuels via biological and thermochemical routes. The biological route relies on the depolymerisation of lignocellulose into monomeric sugars and the subsequent fermentation of sugars into

ethanol fuel. During this process, lignin remains inert due to its remarkable resistance to decay, biological attacks, and water ingression. Consequently, lignin, a renewable carbon source, is often combusted onsite for heat and electricity generation. The thermochemical conversion routes, on the other hand, are inherently endothermic as they require heat to decompose biomass into various fuels. Gasification is one of the most popular thermochemical conversion routes. As with biological conversion, this process also relies on the combustion of renewable sources of carbon (biomass feedstock, syngas products, or biochar by-products) to meet the thermal energy demand.

Considering that the combustion of renewable sources of carbon such as lignin, biomass, bio-syngas, or biochar for process heat is a low-value application and a drawback to the profitability of bio-based industries, early studies have explored alternative sustainable ways to meet the energy needs of lignocellulosic biorefineries. This includes the integration of solar energy to drive the conversion processes. Although this option is limited by geographical factors, solar-aided lignocellulosic biorefineries are gaining attention, and a few integration designs have already been proposed for both biological and thermochemical platforms (Nickerson, et al., 2015); (Vidal & Martín, 2015); (Ansari & Liu, 2019); (Ansari, et al., 2020).

One of the challenges solar-aided biorefineries are expected to face is finding energy-efficient and cost-effective integration options. And, as far as the author is aware, very few studies have addressed the subject. Therefore, the aim of this study was to investigate the techno-economic performances and environmental impact of solar-aided lignocellulosic biorefineries modelled using biological and thermochemical conversion routes. Although modelling results can be applied to any geographical location, economic performance is only applicable to the South African context.

1.2 Problem statement

All studies of solar-aided lignocellulosic biorefineries found in the literature are limited to concept illustration and estimation of bio-fuel production cost. Comprehensive studies assessing not only the technical performance but also the environmental impact and manufacturing costs of potential co-products including lignin and biochar are yet to be

conducted. In addition, despite having one of the highest solar irradiances in the world, a detailed techno-economic study for solar-aided lignocellulosic biorefineries in South Africa has never been conducted.

1.3 Objectives

The objectives of this study were set out as follows:

- Using the biological and thermochemical conversion platforms, develop models for the production of ethanol and methanol from corn stover, respectively.
- Evaluate the conversion efficiency and economic performances (in the South African context) of the modelled biorefineries.
- Investigate potential configurations for the integration of solar energy into the modelled lignocellulosic biorefineries.
- Using South Africa as a case study, evaluate the effect of solar energy integration on biorefineries' techno-economic and environmental performance.
- Determine the impact of exporting potential co-products, including lignin and bio-char, on the performance of the biorefinery.
- Comparatively analyze the thermochemical and biological conversion of corn stover into liquid fuels.

1.4 Contribution to knowledge

The novelties and contributions of the study include the followings:

- The study is the first techno-economic analysis conducted on solar-aided lignocellulosic biorefineries using parameters applicable to South Africa.
- The study is also the first to investigate the production of ethanol from corn stover in South Africa, as previous studies were based on bagasse.
- The study is equally the first to assess the costs of biochar and lignin co-products, which may be produced by solar-aided biorefineries.
- In addition, this is the first study to evaluate the economic performance of a biorefinery utilizing solar-aided gasification.
- Also, this study has presented a novel configuration for the integration of solar energy as the main energy source for gasification in a TNEE-type dual bed gasifier.

- Finally, this is the first study to assess the environmental benefits of solar-aided biorefineries.

1.5 Significance of the study

The study is expected to be a building block for the future implementation of the circular bioeconomy production concept. A concept where solar power is used as the main source of energy in biorefineries. And, carbonaceous residues generated during the conversion process are exported as co-products intended for the manufacturing of value-added products. The study is also expected to contribute to the literature by providing data that could be used as a reference point for the efficient integration of solar energy into lignocellulosic biorefineries. Furthermore, the study may equally assist investors and decision makers in selecting the ideal option for implementing the bio-economy concept in South Africa.

1.6 Outline

The thesis comprises eight chapters. The first chapter (current) serves as an introduction to the study. The second chapter first outlines general concepts regarding the conversion of lignocellulosic biomass into biofuels. It then discusses the energy supply methods currently employed by lignocellulosic biorefineries. And finally, it reviews previous work conducted on the integration of other renewable energy sources into biorefineries. Chapters 3 and 4 describe the approaches used to model the biological and thermochemical conversion of corn stover into ethanol and methanol respectively. The technical performance of biorefineries is also discussed. An in-depth description of the methods used to conduct economic modelling and assess environmental impacts is provided in chapter 5. Results from economic modelling and environmental studies are presented and discussed in chapter 6. Chapter 7 compares biological and thermochemical conversions with a focus on conversion efficiency, production costs, and eco-friendliness. Chapter 8 provides a summary of the study and highlights the findings.

CHAPTER 2 – LITERATURE REVIEW

2.1 Introduction

The literature on lignocellulosic biofuel production is substantial with numerous review articles published on the subject (Rodionova, et al., 2022); (Ibarra-Gonzalez & Rong, 2019); (Saravanan, et al., 2022); (Srivastava, et al., 2015); (Hosseini, et al., 2015); (Brown, 2015). In this chapter, the reader is introduced to basic concepts in lignocellulosic biofuel production. An emphasis is put on biological conversion and biomass gasification. Techniques commonly used to meet the energy needs of lignocellulosic refineries are also discussed. In addition, since this techno-economic analysis involved the integration of solar energy into lignocellulosic biorefineries, a summary of previous research work conducted on the incorporation of other renewable energy into biorefineries is presented as well.

2.2 General concepts in lignocellulosic biofuel production

2.2.1 Structure and composition of lignocellulosic biomass

Biomass is the term used to indicate any organic material that has not been derived from fossil fuels (Cao, et al., 2017). Lignocellulosic biomass, also known as lignocellulose, represents the most abundant renewable organic material on earth. It is mainly derived from agricultural and forestry residues (Paudel, et al., 2017). Although its composition depends on the specie, the main elements composing lignocellulosic biomass include carbon (40-51 wt%), hydrogen (3-5 wt%), oxygen (39-44 wt%) and nitrogen (0.1-1.6 wt%) (Dadile, et al., 2020); (Williams, et al., 2017). The structure of lignocellulosic biomass is illustrated in Figure 2.1.

Lignocellulosic biomass has a structure that consists predominantly of cellulose (30-50 wt%), hemicellulose (15-30 wt%), and lignin (10-30 wt%). It also contains other minor components such as proteins, lipids and extractives (Sindhu, et al., 2016). Hemicellulose and cellulose are both polysaccharides comprising about 200 and 10 000 monomers respectively. The former is an amorphous biopolymer made of hexoses (C6) and pentoses (C5) (Cabeza, et al., 2016), while the latter is highly crystalline and consists of hexoses units linked by β-1,4 glycosidic bonds. Lignin, on the other hand, acts as the glue that

holds cellulose and hemicellulose fibres together. It is a crucial component of plant cell walls as it provides support to the plants (Cheng & Timilsina, 2011). Also, lignin's composition is more complex than that of cellulose and hemicellulose. It consists of a mixture of phenolic compounds and derivatives, which are less prone to depolymerisation. As a result, lignin is highly resistant to decay, biological attacks, UV absorption, and water ingress. Indeed, only a limited number of organisms can degrade lignin (Azadi, et al., 2013). And once degraded, lignin generates a wide range of compounds, which include organic acids, phenols and vanillin (Hamelinck, et al., 2005).

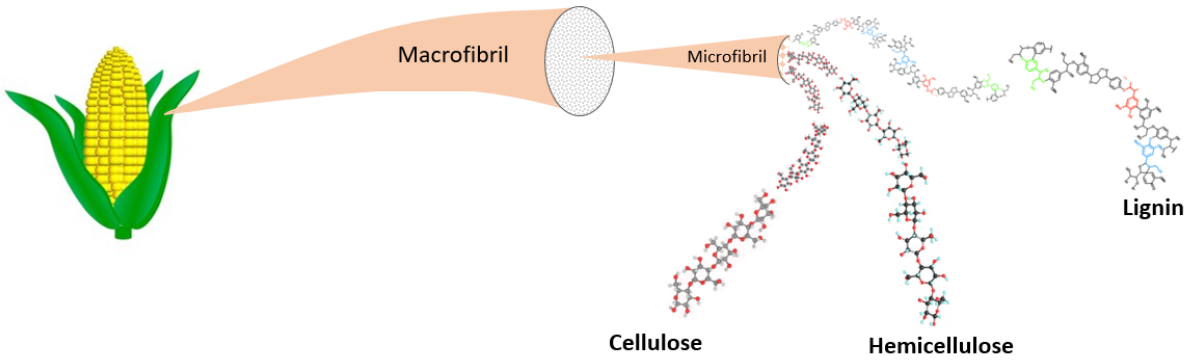

Figure 2.1: Illustration of the structure of lignocellulosic biomass

2.2.2 The biorefinery concept

A biorefinery can be defined as “the sustainable processing of biomass into a spectrum of marketable products and energy” (Jungmeier, et al., 2013). The technologies used by biorefineries to convert lignocellulose into biofuels are generally based on two main processing routes: biological and thermo-chemical.

2.2.3 Biological processing of lignocellulosic biomass

The biological route involves the conversion of lignocellulose into sugars using microbial and enzymatic processes. The sugars are subsequently metabolized into alcohol and/or other fuels and chemicals (Sindhu, et al., 2016). Although bio-butanol has a higher energy density than bio-ethanol, the latter is often the preferred fuel for the biological route.

This is due to several challenges faced during bio-butanol production such as the relatively low fermentation yield (Pfromm, et al., 2010).

2.2.3.1 Pretreatment

As illustrated in Figure 2.2, the production of ethanol from lignocellulosic biomass generally requires the combination of three fundamental conversion steps: pretreatment of lignocellulose, depolymerisation of carbohydrates (or saccharification/hydrolysis), and fermentation of monomeric sugars. The ultimate aim of the pretreatment step is to overcome the recalcitrance nature of lignocellulose and facilitate the depolymerisation of polysaccharides. Activities taking place during pretreatment include biomass size reduction, fragmentation of lignin structure, and disruption of cellulose's crystalline arrangement. These activities render the biomass more accessible to enzymes (Sindhu, et al., 2016). The effect of pretreatment on lignocellulose is depicted in Figures 2.3 (a) and 2.3 (b)

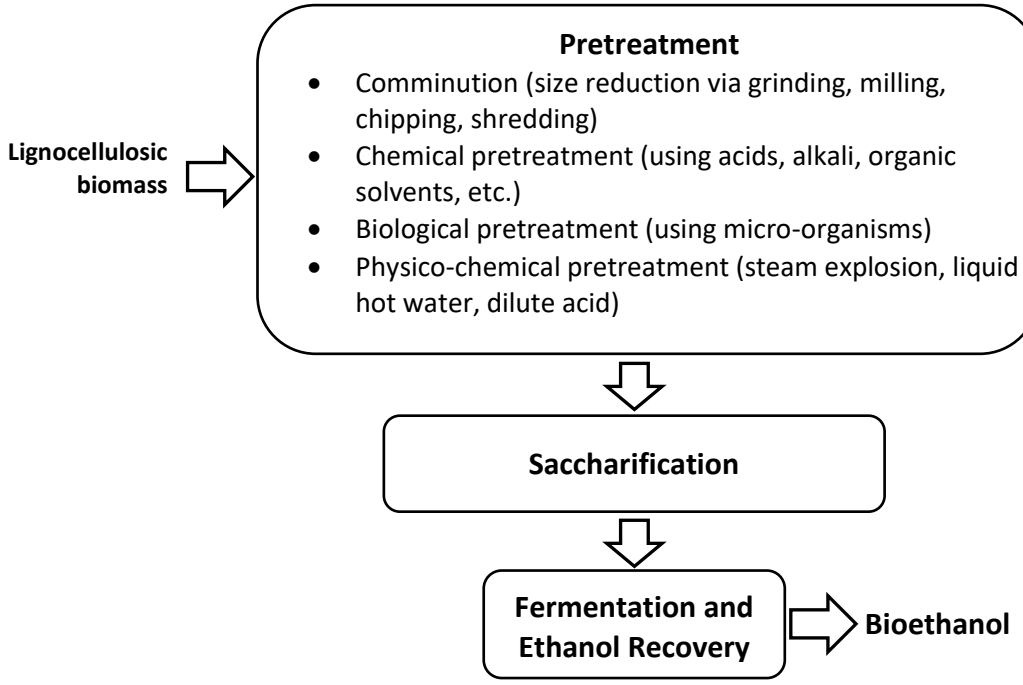

Figure 2.2: Major process steps for the production of bioethanol from lignocellulosic biomass using the biological conversion route

Several pretreatment techniques have been reported in the literature. These include the followings:

Comminution: Also known as mechanical size reduction, it is the starting point of lignocellulosic biofuel production. Comminution generally precedes all the other pretreatment methods, and includes operations such as grinding, shredding, and milling. The purpose of comminution is to facilitate biomass digestibility in the subsequent processing step, by increasing the biomass surface area (Agbor, et al., 2011).

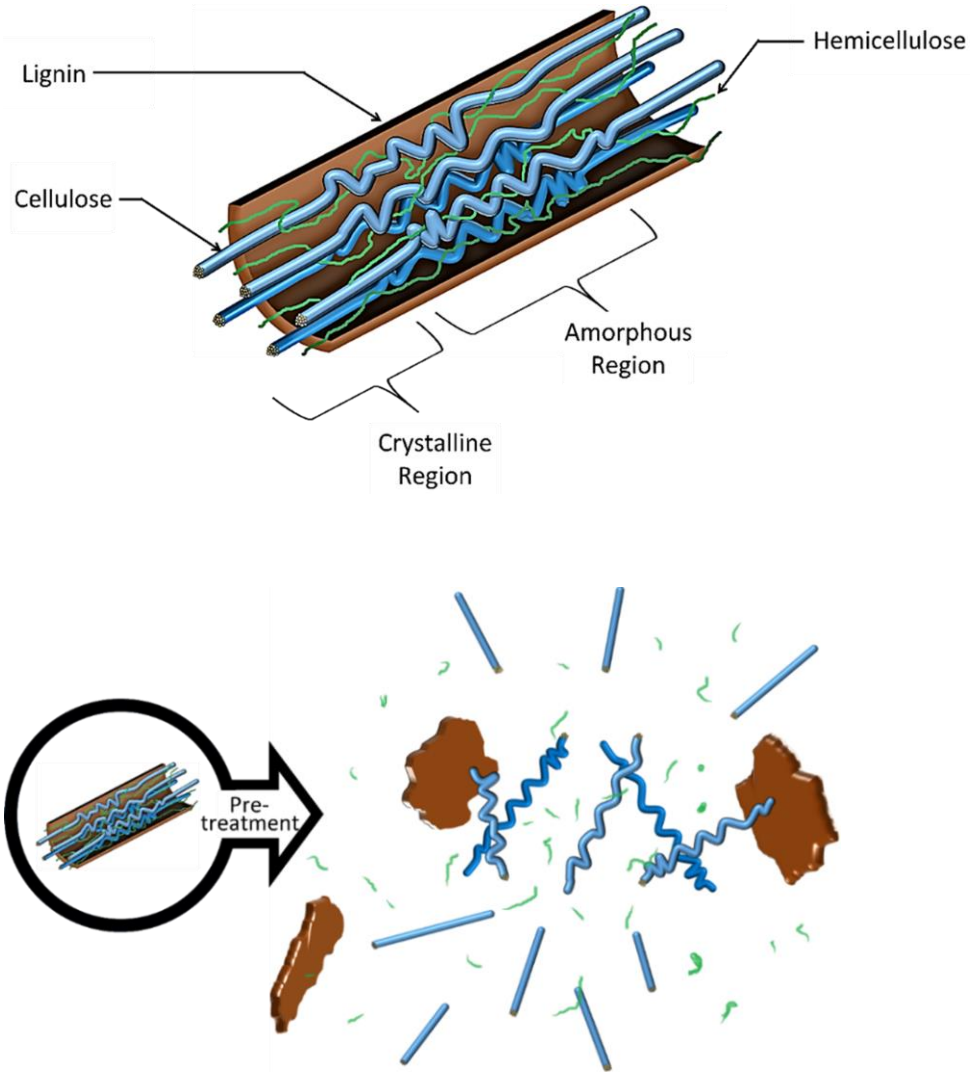

Figure 2.3: Illustration of the pretreatment effect on lignocellulose: (a) cellulose, hemicellulose held together by lignin; (b) lignin structure is broken, and the crystalline arrangement of cellulose is disrupted

Biological pretreatment: Just like other biomass pretreatment methods, biological pretreatment is generally performed after comminution. It entails the use of organisms such as fungi to degrade the biopolymers comprising lignocellulose (Sun & Cheng, 2002). Despite being capable of effectively degrading cellulose and lignin, biological pretreatment is considered unfavourable for industrial processes. This is because it is a slow process that requires a relatively long residence time (10-14 days) and special growth conditions (Agbor, et al., 2011).

Chemical pretreatment: Here, the structure of lignocellulose is disrupted using chemicals such as alkali and acids. Using alkali leads to the breakage of the lignin-cellulose/hemicellulose link, which renders both cellulose and hemicellulose more accessible. Alkali chemical pretreatment is usually suitable for biomass with a low lignin content such as agricultural residues. Acid pretreatment, on the other hand, breaks down the hemicellulose fraction of biomass into its monomers, which makes cellulose more accessible. This operation is generally carried out with diluted acid, as concentrated acid is more corrosive and must be recovered for the process to be economically feasible (Mosier, et al., 2005).

Physiochemical pretreatment: It includes several technologies as such as steam explosion, liquid hot water, dilute acid, ammonia fibre explosion, lime, organosolv, CO_2 explosion, ionic liquid pretreatment. The three most studied lignocellulose pretreatment methods are discussed below.

- Steam explosion makes use of pressurised saturated steam to break the bonds between lignocellulose components, and decompression to disrupt the lignocellulose structure. The process can be catalysed by adding sulphuric acid, CO_2 or SO_2 to steam. The successive compression and decompression actions result in the degradation of hemicellulose, which is then recovered in the water-soluble fraction. Cellulose on the other hand remains mostly undamaged (Shrotri, et al., 2017). Despite coming with a few challenges (incomplete disruption of lignin-carbohydrate matrix and the generation of fermentation inhibitors) (Agbor, et al., 2011), Steam explosive has several favourable attributes for industrial process. For instance, it requires a relatively low energy input.

Also, it does not excessively dilute the sugars. Moreover, the process is environmentally friendly and only marginally uses chemicals (Shrotri, et al., 2017).

- Liquid hot water is another popular physicochemical pretreatment method. It does have some similarities with steam explosion in a sense that water is also used to hydrolyse hemicellulose and render cellulose more accessible. However, in this case, water is utilized in the liquid state instead of steam. As a result, the formation of fermentation inhibitors and unwanted degradation compounds is minimized (Agbor, et al., 2011). Furthermore, given that no chemical is added during the process, liquid hot water eliminates the need to wash or neutralise the hydrolysate, which in turn, renders the process cost-effective for industrial applications. Despite its favourable attributes, liquid hot water pretreatment requires large volumes of water. Hence, substantial energy input is needed in the subsequent processes for evaporation (Zhang, et al., 2020); (Agbor, et al., 2011).

- Dilute acid is one of the most studied lignocellulose pretreatment method, mainly because it offers the possibility to eliminate the saccharification step (Agbor, et al., 2011). Just like chemical pretreatment, the dilute acid pretreatment makes use of acid to solubilize hemicellulose. However, in this case, thermal energy can also be applied either in the form of steam or via indirect heating to improve the reaction rate (Sathendra, et al., 2022). Dilute acid pretreatment often results in the generation of oligomers and monomeric sugars. And depending on the level of severity, sugars could be converted to furfural and hydroxymethylfurfural (HMF), which are fermentation inhibitors (Xu, 2015). Because of its low lignin removal, this method is often suitable for lignocellulosic biomass with low lignin content such as agricultural waste (Peral, 2016).

The capital cost required for dilute acid pretreatment is generally higher than other physiochemical pretreatment methods. This is due to the need for expensive construction materials to minimize the corrosive effect of acid (usually sulphuric acid) (Agbor, et al., 2011). Despite being costlier, dilute acid pretreatment can achieve relatively high reaction rates. Moreover, the process has a high efficiency and can metabolize almost the entire hemicellulose fraction of biomass into soluble sugars, which in turn, simplifies the

subsequent enzymatic hydrolysis of cellulose. Because of these favourable attributes, dilute acid pretreatment is one of the most preferred pretreatment methods (Peral, 2016).

2.2.3.2 Saccharification (hydrolysis)

During the saccharification step, carbohydrate biopolymers are depolymerised into monomeric sugars (Karimi, et al., 2013). The process is carried out with the help of chemicals or enzymes. Chemical saccharification takes place in concentrated or diluted acid, while enzymatic saccharification involves a reaction between the pre-treated substrate and enzymes. Enzymatic saccharification is often the preferred option of the two. This is because of its low energy requirement, low toxicity of products generated, relatively high product yield and low production of fermentation inhibitors (Madadi, et al., 2017).

Cellulase and hemicellulase are the two groups of enzymes generally used during lignocellulose saccharification. The former is a group of enzymes that can depolymerize cellulose into glucose monomers, while latter represents a category of enzymes with the ability to degrade hemicellulose into a variety of monomeric sugars (Madadi, et al., 2017). Currently, the high cost of enzymes combined with the low conversion efficiency is one of the obstacles to the commercialization of lignocellulosic bioethanol (Sindhu, et al., 2016); (Ko, et al., 2016).

2.2.3.3 Fermentation

During the fermentation process, sugars produced in the previous steps are metabolized to alcohol with the help of microorganisms (Gnansounou & Dauriat, 2005). Various types of microorganisms can be used for this purpose. These include bacteria, fungi, yeast, and some other fermenting agents. Although cellulose monomers can be fermented by several microorganisms, only a few yeast species are capable to ferment hemicellulose monomers. The most prominent ones include Candida shahatae, Pichia stipitis and Pachysolen tannophilus (Kudar, et al., 2011). Presently, finding suitable microorganisms capable to co-ferment cellulose and hemicellulose monomers', mainly hexose and

pentose sugars, remains a major technical challenge for the commercialisation of lignocellulosic ethanol (Malik, et al., 2021).

2.2.4 Thermo-chemical processing of lignocellulosic biomass

"A thermochemical biorefinery involves the processing of biomass and carbon-based waste, such as the organic fraction of municipal solid waste, to generate (simultaneously) products and services covering fuels, chemicals, heat, and electricity from syngas" (Haro, et al., 2013). Thermochemical processes have several advantages over biological processes such as the absence of a complex pretreatment step, the utilization of all the biomass components including lignin to produce biofuels and biochemical. In addition, thermochemical processes generally have a relatively shorter conversion time, and the ability to convert the whole biomass into biofuels. The main thermochemical conversion routes include gasification, direct combustion, liquefaction, pyrolysis, carbonisation and torrefaction. The next sections will briefly discuss each of these thermochemical conversion routes. However, an emphasis will be placed on gasification, because it is one of two biomass-to-fuel processes employed in the methodology (refer to chapter 4).

2.2.4.1 Direct combustion

Direct combustion is a basic thermochemical process that has been used for ages to produce heat and power from biomass. During this process, steam is generally generated along with CO_2, and a smaller fraction of other gases such as NOx, which poses environmental concerns (Patel et al., 2016); (Ma, et al., 2021). Equation 2.1 illustrates biomass decomposition during the combustion process.

$$\text{Biomass} + O_2 \rightarrow CO_2 + H_2O + \text{Heat} \qquad \text{Eq. 2.1}$$

2.2.4.2 Pyrolysis

Biomass pyrolysis is the thermal decomposition of biomass feedstock in an oxygen-free environment. The process generally produces char, bio-oil, bio-chemicals and fuel gases. Depending on the operating conditions, the pyrolysis of lignocellulosic biomass can be subdivided into three different categories: slow pyrolysis, fast pyrolysis and flash pyrolysis

- Slow pyrolysis, also known as conventional pyrolysis is a batch thermochemical conversion process carried out at low temperatures (≈ 200 – 300 ^{o}C) (Dhyani & Bhaskar, 2017) and slow heating rates (0.1 – 1 °C/s) (Font, 2018). Although the process generally requires a long residence time, it is more tolerant to biomass moisture content than the other types of pyrolysis. Slow pyrolysis generates a large fraction of solid fuel and limited bio-oil and gases (Dhyani & Bhaskar, 2017).

- Unlike slow pyrolysis, fast pyrolysis is continuous process performed at higher temperatures (450 – 600 ^{o}C) (Dhyani & Bhaskar, 2017), faster heating rates (10–200 °C/s) (Font, 2018), and with a shorter residence time (< 2 seconds). The process parameters are generally tailored to prevent unnecessary cracking of products, and therefore, achieve high oil yields. Because of the short residence time, a high heat transfer rate is crucial. High heat transfer rates can be obtained by using finely grounded biomass feedstock (Font, 2018).

Flash pyrolysis is sometime referred to as very fast pyrolysis due to the rapid heating rates (>1000 °C/s), and reaction temperatures are as high as the ones used for gasification (900 – 1300 °C). The residence time is also the shortest of all pyrolysis types (<0.5 second). Due to the very brief residence time, an extremely fine feedstock particle size (105 – 250 µm) is required. The process can achieve high bio-oil yield with low water content and conversion efficiencies as high as 70% (Li, et al., 2013).

2.2.4.3 Carbonisation and torrefaction

Carbonisation and torrefaction are very similar to slow pyrolysis; however, these processes are carried out at much lower temperatures and slower heating rates (Lu, et al., 2012). Additionally, unlike slow pyrolysis, carbonization and torrefaction do not require the condensation of vapours products. Although both carbonisation and torrefaction generally produce a significant quantity of solid fuels and only a limited amount of bio-oil and biogas (Patel, et al., 2016), the latter generates solid fuels with a much higher energy density (Lu, et al., 2012).

2.2.4.4 Liquefaction

Liquefaction involves the processing of biomass in a hot pressurised solvent to yield a mixture of liquefied biomass products resembling crude oil (Xue, et al., 2016). Although several solvents can be used for liquefaction, water is the solvent of choice. This is because of its low cost, environmentally friendliness, and its ability to process wet feedstock without pretreatment. When water is used as the solvent, the process is referred to as hydrothermal liquefaction (Brown, 2015).

Hydrothermal liquefaction (HTL) exhibits several attractive features such as, the potential to recover more than 70% of the carbon presents in the feedstock with an energy efficiency of 85 – 90% (Gollakota, et al., 2018). Hydrothermal liquefaction is typically carried out at temperatures ranging between 523 and 647 K and pressures around 4 to 22 MPa. The bio-crude produced is typically low in moisture and oxygen; therefore, it does not require a complex reaction mechanism during upgrading. In most cases, fine hydrotreatment is enough to enhance the quality and stability (Gollakota, et al., 2018).

2.2.4.5 Gasification

Gasification is an endothermic conversion process involving chemical reactions between carbonaceous materials and a gasifying agent, which typically includes gases such as O_2, air, steam, CO_2, or their mixtures. The process produces a variety of gases comprising CO, hydrogen, CO_2, methane, and nitrogen. These gases are known as producer gas or synthesis gas, and can be used for electricity generation, or upgraded into value-added fuels such as Fischer Tropsch liquid fuel, Dimethyl ether (DME), and methanol (Naik, et al., 2010); (Yang & Chen, 2015).

Biomass gasification is analogous to coal gasification in the sense that the chemistry and thermodynamics undergone by the feedstock are similar (Haro, et al., 2013). However, unlike coal gasification which takes place at temperatures ranging from 800 to 1800 °C (Haro, et al., 2013), biomass gasification does not usually exceed 1100 °C. This is due to the relatively low melting point of biomass ash (Link, et al., 2022); (Iqbal & Lewandowski, 2016). The gasification process is generally classified based on the mechanism used to

supply heat to the reactor (allothermal & autothermal); Or, the technology employed in the gasification bed (fixed & fluidized). Each of these is discussed below.

a) Allothermal vs autothermal gasification

Two mechanisms can be used to supply the thermal energy required for gasification: direct gasification also known as autothermal gasification, and indirect gasification also referred to as allothermal gasification. In autothermal gasification, the heat required in endothermic chemical reactions is supplied through partial oxidation within the gasifier. Hence, a portion of feedstock is combusted in the air or oxygen-enriched air inside the gasifier. The presence of air generally leads to the dilution of syngas with atmospheric nitrogen and results in syngas with a relatively low calorific value (~4 to 7 MJ/ Nm^3). The substitution of air with pure oxygen or oxygen-enriched air can improve the syngas calorific value. However, this approach requires costly air separators (Arena, 2013). Figure 2.4 illustrates the material flow during autothermal gasification.

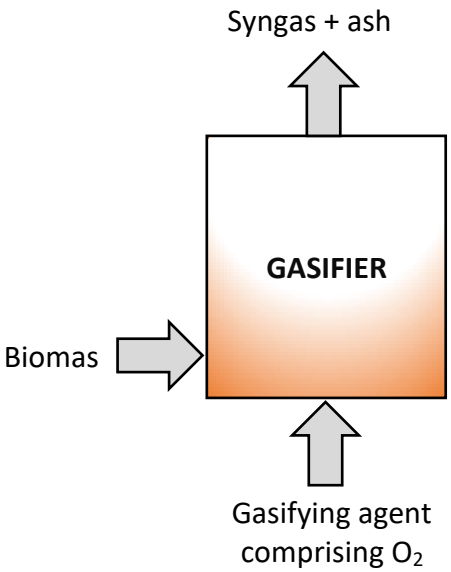

Figure 2.4: Schematic illustration of autothermal gasification

As opposed to autothermal gasification, allothermal gasification is conducted in an oxygen-free environment. Hence, does not require air separation. Here, steam, which is used as a gasification agent, reacts with biomass to generate syngas with a relatively high hydrogen concentration. The syngas produced is nitrogen-free, due to the air-free environment. Also, the syngas product obtained has a calorific value relatively higher than

autothermal gasification (~15 – 20 MJ/ N m^3) (Arena, 2013). The heat needed to maintain the gasification temperature is supplied to the reactor either using heat exchangers or by circulating hot-bed materials between a combustor and the gasifier (Bhaskar, et al., 2013). Fuel burned in the combustor includes carbonaceous by-products such as char. In some cases, a portion of biomass feedstock or syngas product is burnt in the combustor for heat generation. Figure 2.5 shows an illustration of heat and material flow during allothermal gasification

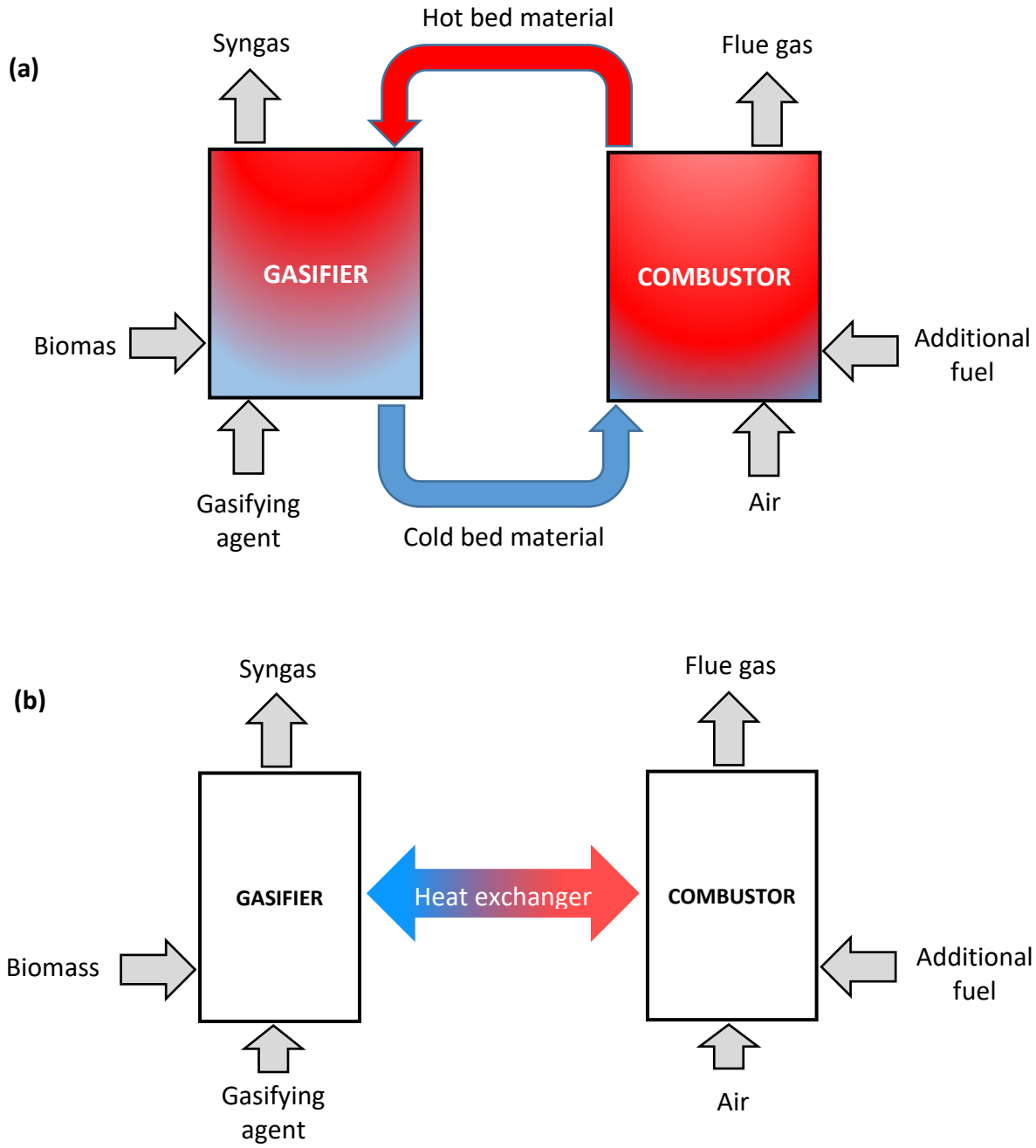

Figure 2.5: Schematic illustrations of allothermal gasification: (a) using circulating bed material as a heat carrier; (b) using a heat exchanger

It must be noted that both autothermal and allothermal gasification share a similar drawback: they both result in the partial consumption of feedstock or product gas for process heat generation, which minimizes the gas yield per unit of feedstock (Hebecker, et al., 2005); (Iliuta, et al., 2010).

b) Fixed vs fluidized bed gasifiers

The gasification bed can either occur in a fixed or fluidized form. Fixed bed gasifiers entail a stationary bed of biomass through which the oxidizing agent flows in an updraft or downdraft fashion. Although this type is generally simple to operate, it usually produces syngas containing considerable amounts of tar and char. This is due to the non-uniform heat flow and mass transfer between the biomass and gasifying agent (Dutta & Acharya, 2011).

Fluidized bed gasifiers, on the other hand, have a more complex operating mode. They involve the suspension of biomass particles in the upward flowing gasifier agent, which leads to turbulent mixing. When compared to fixed beds, fluidized bed gasifiers offer a more uniform temperature distribution, higher carbon conversion, and lower tar production (Ram & Mondal, 2022). Fluidized bed gasifiers include bubbling fluidized-bed, circulating fluidized-bed, and entrained flow fluidized-bed gasifiers (Ram & Mondal, 2022).

2.3 Techniques used to meet the energy needs of lignocellulosic biorefineries

2.3.1 Combustion of lignin residues

This technique, commonly applied to biological conversion, is motivated by the inability of current technologies to convert lignin into bioethanol. In fact, among the three main components of lignocellulose, cellulose and hemicellulose are the only polysaccharides that can presently be converted into ethanol, with a conversion rate of 85 – 90 % for the earlier and 30 – 85 % for the latter (Cheng & Timilsina, 2011). Lignin on the other hand remains inert during processing. For this reason, it is typically combusted in a combined heat and power system (CHP) to meet the energy needs of the biorefinery.

The advantage of combusting lignin in a combined heat and power system has been highlighted in several techno-economic analyses (TEA), such as the one disclosed by Quintero et al., (2013). The work involved the combustion of non-hydrolysed residues (mainly lignin) to generate steam, which was then used to partially cater for the process heating requirements. This approach was reported to reduce the overall external energy requirement of the biorefinery by 16 – 20 % depending on the feedstock used. Moreover, combining CHP (combined heat and power system) with a heat integration system was proven to further reduce the external energy requirement and generate surplus electricity that could be exported. The combustion of lignin-rich residues for process heat and power has also been employed in several other techno-economic analyses, including Gubicza et al., (2016); Do & Lim, (2016); Tewfik et al., (2015); Liu & Bao (2017).

Despite helping biorefineries to meet their energy demand, the combustion of lignin residues for energy generation not only produces CO_2 but also prevents the biorefinery from satisfying the principles of a circular economy. Principles that promote the upgrading of by-products and encourage the utilization of renewable energy where possible. The ultimate objective of these eco-efficient production principles is to maintain the value of products, materials and resources for as long as possible (Ubando , et al., 2020). And, this is not the case when lignin-rich residues are combusted for heat generation.

Also, the combustion of lignin for heat and power is rather a low-value application and a drawback in the profitability of lignocellulosic bio-based industries. In fact, lignin is a source of renewable carbon. Thus, its worth, when upgraded into bio-chemicals, is likely to be significantly higher. Furthermore, the combined heat and power system (CHP) used to generate heat and electricity from the combustion of lignin residues requires solid boilers that can account for up to 29% of the total installed equipment cost of a lignocellulosic biorefinery employing dilute acid pretreatment and enzymatic hydrolysis to produce 230 million litres of ethanol per year (Humbird, et al., 2011). For comparison's sake, a CHP system using methane gas as fuel could meet the biorefinery energy needs at a fraction of the capital cost required for a lignin CHP system (Scown, et al., 2014).

2.3.2 Combustion of biogas from the adjacent water treatment plant

Wastewater generated in biological conversion routes, mainly during biomass pretreatment and ethanol recovery, contains considerable amounts of carbonaceous residues. These residues are generally metabolized into biogas via anaerobic digestion in an adjacent plant. The biogas obtained is subsequently combusted in the CHP along with unconverted lignin residues.

The combustion of biogas in a CHP was evaluated by Liu & Bao, (2017) in a study that involved the production of ethanol from corn stover, wheat straw, rice straw, sugarcane bagasse and polar sawdust. The study revealed that 1946 – 2295 kWh of electricity could be generated from biogas combustion during the production of one tonne of bioethanol. Furthermore, Liu & Bao, (2017) disclosed that when both lignin residues and biogas are combusted, the electricity production could reach 7121 – 8180 kWh, which their case, was enough to meet the needs of the production processes and even generate a surplus that could be exported.

The wastewater-to-biogas approach has been employed in several other works, such as Gubicza et al., (2016) and Tao et al., (2017), where flash streams from the pretreatment and conditioning processes were anaerobically digested to produce biogas. The gas was subsequently combusted along with the solids fraction of the stillage to produce steam and electricity.

2.3.3 Combustion of char and non-condensable gases

This technique is generally used in pyrolysis processes where sizeable amounts of char and non-condensable gases (NCG) are generated along with the bio-oil product. The by-products (char and NCG) are then combusted in a CHP system to generate heat and/or electricity, which is used to cater for the energy needs of the biorefinery (Bridgwater, 2012).

The effectiveness of this technique was demonstrated in a techno-economic study conducted by Shemfe et al., (2015). The study simulated the conversion of pinewood into biofuel and electric power via fast pyrolysis and hydroprocessing. It was found that the

energy needed for the biomass drying operation and pyrolysis could be supplied by combusting char and non-condensable gas. Moreover, the residual energy produced could be exported in the form of electricity.

2.4 Incorporation of other renewable energy into lignocellulosic biorefineries

The idea of incorporating other renewable energy technologies into biorefineries has recently been enticing scientific curiosity. An attractive feature of this setup is the possibility to avoid combusting valuable renewable carbon for heat and power generation. Moreover, such biorefineries could facilitate the adoption of a circular bioeconomy model. This is because valuable carbonaceous residues that were initially intended for heat and power generation could be sold as co-products intended for the manufacturing of value-added chemicals and by-products.

Despite being limited by geographical factors, and hindered by sizable technological challenges to achieve efficient integration, the incorporation of other sources of renewable energy such as solar, wind, or geothermal into biorefineries, is gaining attention in the literature. The next sections review the main integration designs that have been proposed so far. The first part discusses the incorporation of solar energy into gasification processes, while the second part reviews the integration of various renewable energy sources into biorefinery processes.

2.4.1 The case of solar-aided gasification

An alternative option to the conventional autothermal and allothermal gasification schemes is the utilisation of concentrated solar energy as the energy source of high-temperature process heat. This approach, which is often referred to as “solar-aided” or “solar-driven” gasification, is analogous to allothermal gasification in the sense that the heat needed to drive the gasification reactions is supplied by an external source of energy. The solar-aided gasification process, however, has several unique features that distinguish it from conventional allothermal gasification. For instance, it eliminates the need to partially combust the biomass feedstock or syngas products for heat generation. This results in more syngas produced per unit of feedstock, with less discharge of pollutants into the environment (Gomaa, et al., 2020); (Piatkowski, et al., 2011).

Moreover, solar-aided gasification enables the upgrade of biomass energy content by an amount equivalent to the enthalpy change of endothermic reactions. Furthermore, because of solar energy input, solar-driven gasification can be assimilated as a way of storing the intermittent solar energy in a readily dispatchable chemical form, which can then be used on-demand as is with fossil fuels (Piatkowski, et al., 2011). In addition, given that solar-driven gasification does not require oxygen-enriched air, the need for costly oxygen separation technology is avoided. Also, solar-driven gasification has the potential to achieve temperatures as high as 1200 $^{\circ}$C, which results in high-quality syngas (Gomaa, et al., 2020); (Nzihou, et al., 2012) (Puig-Arnavat, et al., 2013).

The multiple benefits of solar-driven gasification have led to several studies being conducted on the subject. These include Ansari, et al., (2020) who used computer simulation software to model the gasification of wheat straw, coconut shells, groundnut shells, and corncobs, utilizing concentrated solar thermal as an intermittent heat source. The process was designed to co-produce electricity and bio-fertilizer. The heat was supplied to the gasifier using concentrated solar power during sun availability and syngas combustion during sun unavailability. Biochar and ash generated in the gasifier were collected as bio-fertilizer, while syngas was combusted for electricity generation. Syngas combustion for electricity generation was found to be more energy-efficient than combusting biomass for power generation. Furthermore, in the solar-assisted configuration, the net electricity output saw a 34% increase per unit biomass feed. Moreover, the solar-to-electricity efficiency was found to remain constant at gasification temperatures between 600 and 1200 ^{o}C. Also, when the gasifier was operated at 900 ^{o}C, the efficiency of the integrated gasification combined cycle (IGCC) for the standalone configuration was about 40%. The IGCC increased to 53% in the solar-assisted scenario.

Nickerson, et al., (2015) developed five biomass gasification designs for economic assessment. Four of these were solar-aided and one was based on conventional state-of-the-art gasification technology. The solar-aided configuration made use of a concentrated solar power system which comprised heliostats reflecting solar radiation to a focal point. Solar energy reflected on the focal point was absorbed by the cavity wall and subsequently transferred to a eutectic blend of carbonate molten salt. Biomass was then

injected into the molten salt where the gasification process took place. It was found that solar-aided gasification could compete with conventional gasification in certain situations. The breakeven prices of solar-aided gasification ranged from 10.90 $/GJ to 4.04 $/GJ.

Vidal & Martín, (2015) disclosed an integrated polygeneration system utilizing biomass gasification and concentrated solar power to produce electricity. The study involved the development of a superstructure considering both autothermal and allothermal gasification with two reforming modes (partial oxidation and steam reforming). The system was coupled with a concentrated solar plant consisting of a tower collector, molten salts storage tanks, and a regenerative Rankine cycle. Three options were considered for syngas utilization: water gas shift for hydrogen production, an open Brayton cycle, and syngas combustion in a furnace to heat the molten salt. The optimal integration consisted of allothermal gasification, steam reforming and a Brayton cycle. This integration resulted in an electricity generation of 340 MW, along with 97-kilo tons of hydrogen per year, which could translate into 0.073 €/kWh if the hydrogen is considered as a credit.

Further studies conducted on biomass gasification using solar radiation as the source of energy include Ansari & Liu, (2019). The study was performed using computer simulation software and employed concentrated solar power (CSP) as a heat source for a dual bed gasifier. The sand was used as a heat carrier and was fed to the gasification bed along with steam. The syngas intermediate product was used to generate power and Fischer Tropsch liquid fuel. During sun unavailability, syngas or recycled tail gas was combusted to supply heat to the gasifier. The hybrid configuration was found to have a peak net efficiency 45% higher than hybrid biorefineries previously disclosed in the literature. Moreover, it was reported that 17-18 kg of liquid fuel could be produced for every gigajoule of solar energy supplied to the biorefinery.

2.4.2 Other cases of renewable energy integrated into biorefineries

The literature on biorefineries integrated with other renewable energy technologies is gradually expanding with diverse designs being proposed. For instance, Banerjee et al., (2013) used geothermal energy to produce the steam required for biomass gasification. The production cost of biofuel obtained using such configurations was found to range

from $5.17 to $5.48 per gallon gasoline equivalent. This was comparable to the $5.14 obtained using steam generated from fossil fuel combustion.

Furthermore, Martín & Grossmann, (2017) reported the conceptual design of a hybrid biorefinery operating in conjunction with solar and/or wind energy. The biorefinery was designed to produce biodiesel by cultivating microalgae and accumulating lipid, which was then extracted and used in a trans-esterification process. Electricity required for the complex was assumed to be generated by photovoltaic (PV) panels or wind turbines. It was found that an investment of 120 million euros would be required to construct a plant capable of producing 60 Mgal of biodiesel per year, for a corresponding production cost of 0.80 €/gal.

Moreover, Zanotti et al., (2016) presented a hybrid biorefinery concept in a study involving the production of biodiesel from corn stover using solar power. Zanotti et al., (2016)'s biorefinery was based on corn stover hydrolysis followed by fungal lipid fermentation. Two scenarios were studied: in the first scenario, photovoltaic panels were used to cover the electricity need. Steam generated by the boiler was directly utilized in the conversion processes. While in the second scenario, concentrated solar power (CSP) was used as add-on energy to the boiler. Steam generated by the boiler was then used to drive a steam turbine and subsequently produced heat and electricity. Although the scenario employing CSP was found to require a smaller area for solar panel installation, the latter was reported to be more suitable for lignocellulosic biodiesel production. The preference of PV over CSP was because the thermal efficiency for electricity generation in CSP is significantly lower than PV.

Further studies on renewable energy incorporated into biorefineries include Gutiérrez, et al., (2022) who used a utility supply approach to evaluate the techno-economic performance of 500 MWth thermochemical biorefineries integrated with conventional concentrated solar power (CSP) systems. Various energy supply scenarios were considered. This included a standalone scenario where a portion of biomass feedstock or syngas was combusted to supply heat to the reactors. Electricity was imported from the grid. The solar-aided scenarios, where the CSP was used to supply electricity, to the plant

with a surplus that was exported to the grid in some scenarios. The standalone scenario was shown to have energy conversion efficiency in the range of 54 – 64%, and it increased by up to 4% in the solar-aided scenarios. Despite improving the conversion efficiency, the incorporation of CSP proved to be costly as it raised capital investment by 74%. DME's minimum selling price varied between 14 and 18.1 USD/GJ in the stand-alone scenarios and 18.3 – 21.2 USD/GJ in the solar-aided scenarios.

Moreover, Karan, et al., (2022) studied a solar biorefinery concept for the co-production of microalgae-based protein and renewable fuel. The study employed a combination of hydrothermal pretreatment, green chemical-based extraction and hydrothermal liquefaction to co-produce protein and diesel from microalgae. Experimental data generated was then utilized in TELCA 2.1 to conduct a Techno-Economic and Life-Cycle Analysis for a 500 ha microalgae production facility. It was found that for a minimum diesel selling price of US$0.67, the protein co-product with 32% purity would have to be sold for US$7.2/kg, to breakeven. Although this protein price was comparable to bulk plant proteins, it could not reach the price range of common proteins such as soybeans and fishmeal. Also, Karan, et al., (2022) reported that to compete against common protein sources, purity must be improved to at least 40%. this can be accomplished through biological and process optimization.

2.5 Summary and conclusions

Lignocellulosic biomass can be converted into biofuels either via biological or thermo-chemical processing routes. In both conversion routes, the biorefinery's energy needs are generally met by combusting carbonaceous by-products such as lignin, biogas, and char. This practice, however, not only produces CO_2 but also prevents the biorefinery from satisfying the principles of a circular economy. An alternative option is to use other renewable energy sources such as solar to supply energy to biorefinery processes. So far, only a few conceptual designs have been proposed in this regard in the literature.

2.6 Research topics identified

Despite the few studies conducted to date, many aspects of solar-aided biorefinery design are still unclear and need further investigation; these include the following:

- A comprehensive study assessing not only the production performance but also the manufacturing costs of potential co-products including lignin and biochar is yet to be conducted.
- A study comparatively evaluating biological and thermochemical solar-aided lignocellulosic biorefineries is non-existent.
- The potential environmental benefit pertaining to the implementation of solar-aided lignocellulosic biorefineries are not yet established in the literature

In this study, the technical and economic performances of two solar-aided lignocellulosic biorefineries are investigated. Biological conversion is employed in the first biorefinery (chapter 3), while thermochemical conversion, primarily gasification, is used in the second (chapter 4). Both biorefineries are compared to their standalone equivalents. The effect of generating carbonaceous co-products such as bio-char and lignin is also investigated. Moreover, the potential environmental benefits of using a solar-aided lignocellulosic biorefinery are presented. The next two chapters will discuss in detail the designs used for each biorefinery configuration.

CHAPTER 3 – MODELLING OF BIOLOGICAL PROCESSING

3.1 Introduction

Ethanol is the main fuel produced during the biological conversion of lignocellulosic biomass into biofuel. It can be blended with regular-grade gasoline at to obtain a fuel blend containing up to 85% (vol/vol) ethanol, and capable of being burned in internal combustion engines without major modifications (Nanda, et al., 2015). Moreover, large volumes of fossil fuels could be spared by producing the ethanol fraction of this fuel blend from lignocellulosic biomass. This, in turn, would result in a reduction in net carbon emissions from the transportation sector. Lignocellulosic bioethanol can therefore play a pivotal role in the transition from fossil fuels to green energy sources. This chapter first describes the methodology employed to model the standalone and solar-aided corn stover-to-ethanol biorefineries with capacities of 500 MWth (LHV). And then, it presents and discusses the biorefineries' technical performance.

3.2 Raw material selection and biomass composition

Although lignocellulosic bioethanol can be produced from a wide range of crop residues, this study used corn stover. The choice of corn stover was motivated by the fact that corn is the most widely cultivated energy crop in South Africa (Tongwane, et al., 2016); (Matsei, 2017). Also, corn farming in the country generates about 16 million tonnes of biomass residues per year. And, after subtracting the amount of corn stover required to maintain soil organic carbon, cattle feed, and control soil erosion, 5.1 million tonnes remain available (Batidzirai, et al., 2016). This excess corn stover could, therefore, be used to produce liquid fuel without requiring profound changes in land usage. Moreover, the conversion of corn stover into biofuels has been amply studied (Zanotti, et al., 2016); (Tao, et al., 2017); (Humbird, et al., 2011); (Zheng, 2013); (Kim, et al., 2003); (Mullen, et al., 2010); (Banerjee, et al., 2013); (Swanson, et al., 2010). Thus, there is a considerable pool of data in the literature enabling the modelling of a large-scale corn stover biorefinery.

The structural composition of corn stover used to model the biological conversion is shown in Table 3.1. The values displayed were obtained from a study conducted by Templeton et al., (2009) and represent the average composition of 508 corn stover

commercial grades. It should be noted that to simplify the modelling process, extractible organic, water-soluble, and other soluble components were combined and labelled as “others”. These "others" mainly consisted of sugars, organic acids, inorganic components, protein, and alcohols and were assumed to have an average composition of CH_2O.

Table 3.1: Corn stover composition used in the present modelling (dry basis, ash free) (Templeton, et al., 2009)

Component	Chemical formula used during modelling	wt (%)
Glucan	$C_6H_{10}O_5$	31.9
Xylan	$C_5H_8O_4$	18.9
Galactan	$C_6H_{10}O_5$	1.5
Arabinan	$C_5H_8O_4$	2.8
Mannan	$C_5H_8O_4$	0.3
Lignin	$C_{7.3}H_{13.9}O_{1.3}$	13.3
Sucrose	$C_{12}H_{22}O_{11}$	3.6
Acetate	$C_2H_3O_2$	2.2
Others	CH_2O	25.5
Total	-	100.0

3.3 Biorefinery location and logistic configuration

The Free State province was selected to host the biorefinery, due to the abundance of corn farms in the region. Indeed, as shown by Batidzirai, et al., (2016), the Free State alone can sustainably generate a total of 1.65 million tonnes of corn residues per year for biomass energy application. Furthermore, like most of South Africa, the Free State province has an abundance of solar irradiance (Jain & Jain, 2017); (Pegels, 2010). The region averages over 3 330 hours of sunshine per year (World Weather & Climate, 2022), with a direct normal irradiance of 5.4 kWh per square meter/day (see Figure 3.1) making the province's local solar resource one of the highest in the world. Also, the Free State's central location makes the province a convenient destination when collecting corn stover from other regions. Thus, the Free State is a convenient location to host a solar-aided corn stover biorefinery.

Corn stover feedstock was assumed to be collected from regional biomass processing depots (RBPD) as proposed by Carolan, et al., (2007). These cooperative facilities owned by farmers, would act as points of drop-off, densification, storage and pick-up. An illustration of the biomass transportation operation is shown in Figure 3.2. It is important

to note that operations taking place at the RBPD site and during biomass harvesting are not covered in this TEA study. The study focuses solely on the biorefinery conversion site.

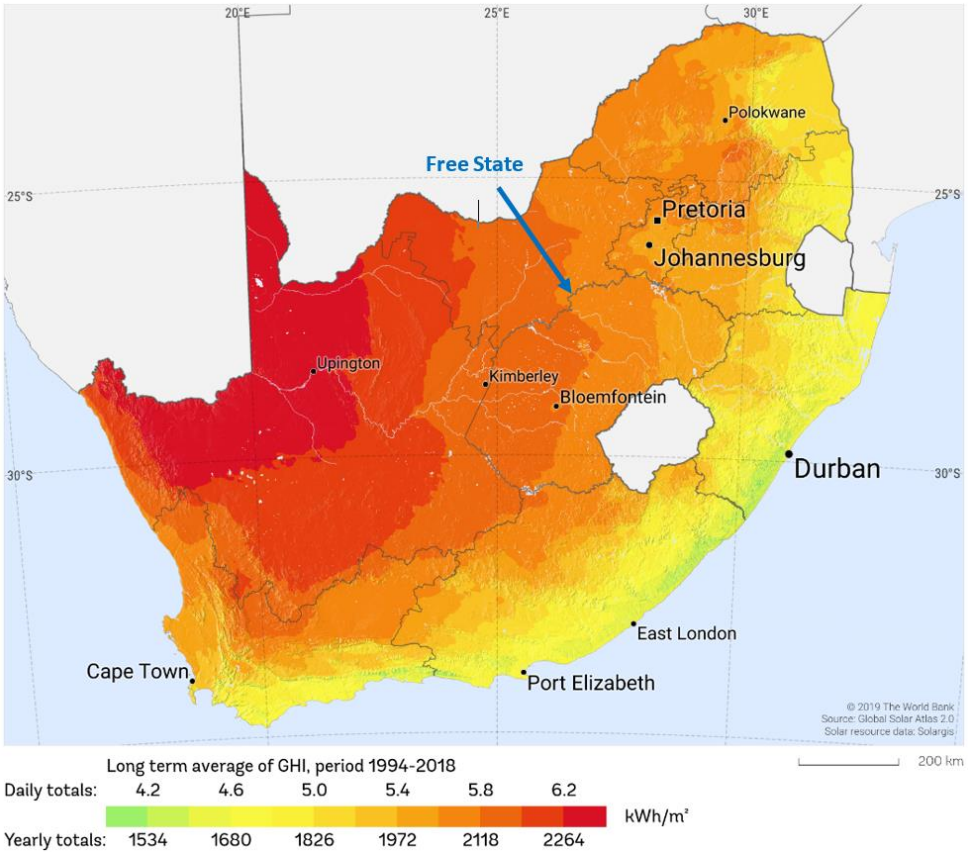

Figure 3.1: Solar resource map showing the global horizontal irradiance for South Africa (The world bank, 2019)

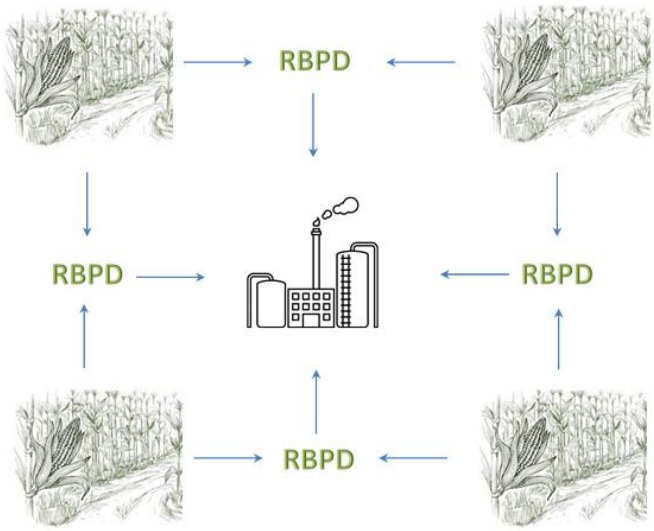

Figure 3.2: Illustration of corn stover transportation operations

The biorefinery was designed to process 83.33 tonnes of dry corn stover per hour. Assuming 20% moisture content, this translated into 104.17 tonnes of corn stover feedstock per hour or 0.83 million tonnes per year (assuming 8 000 operating hours per year). This Figure is well below the 1.65 million tonnes of corn residues that can be sustainably harvested in the Free State region as reported by Batidzirai, et al., (2016).

3.4 Conversion processes

The biorefinery was divided into five main conversion areas: pretreatment (deacetylation & dilute acid treatment), hydrolysis & fermentation, ethanol recovery, water treatment, and steam & power generation. Figure 3.3 shows a graphical illustration of the main conversion areas.

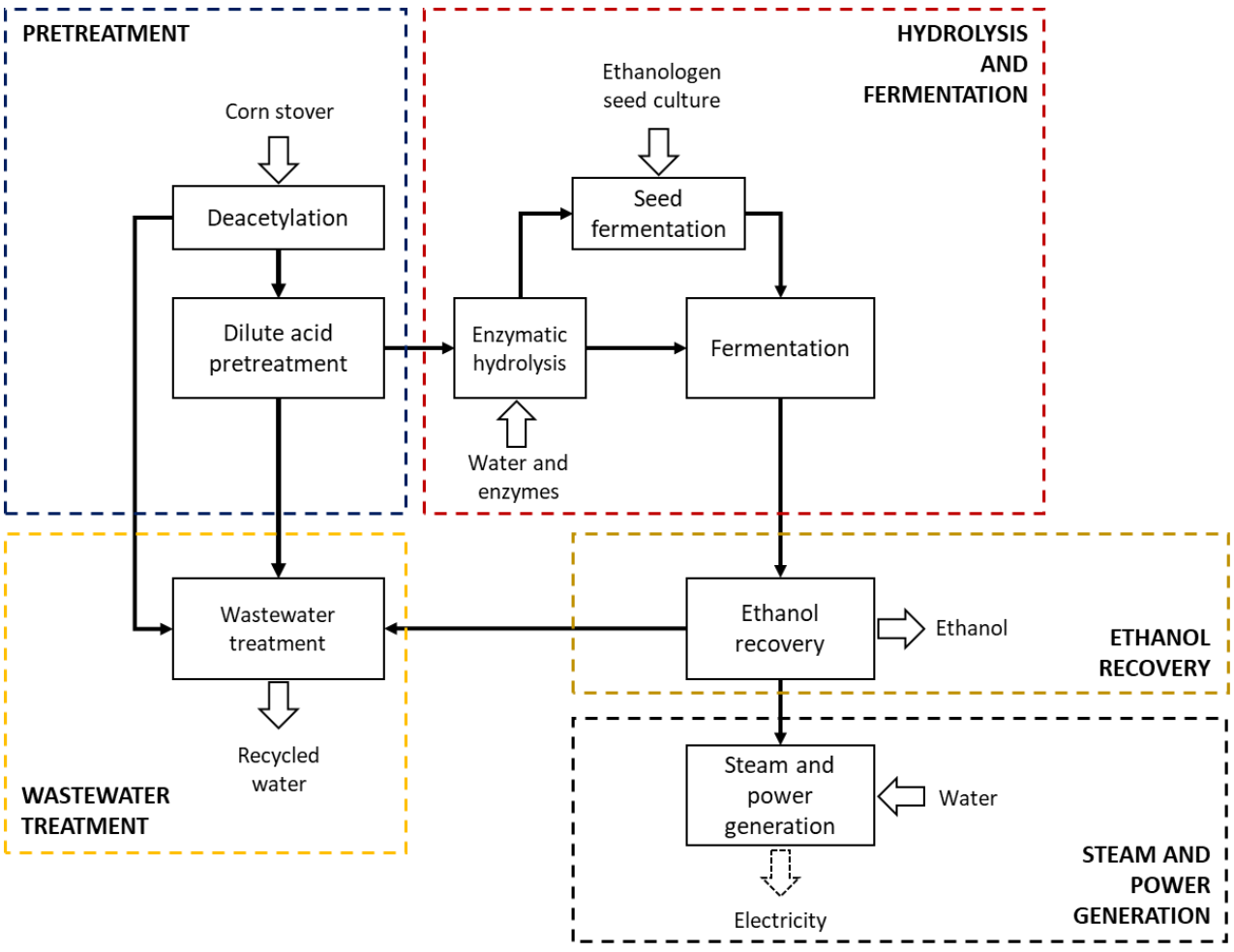

Figure 3.3: Graphical illustration of main conversion areas for the production of bioethanol from corn stover

3.4.1 Pretreatment

The pretreatment operation was divided into two sub-processes: deacetylation and dilute acid pretreatment.

3.4.1.1 Deacetylation

The objective of deacetylation was to selectively remove acetyl groups from the biomass. Thus, minimizing fermentation inhibition caused by acetate salts. Indeed, the acetyl groups present in corn stover are covalently bonded with xylan by ester bonds. And during dilute acid pretreatment, xylan is hydrolyzed into xylose which results in the acetyl groups being liberated and forming acetate salts. These salts are known to inhibit the activity of bio-catalysts used for ethanol production (Ranatunga, et al., 1997). Thus, it is beneficial to introduce a deacetylation step prior to pretreatment, especially when a dilute acid pretreatment is employed.

The deacetylation process employed in this work was based on the method described by Chen, et al., (2012). It involved the soaking of corn stover in a vessel containing 0.4% wt/v solution of sodium hydroxide (NaOH), with a solid loading of 8% (wt/wt). The mixture is heated to 80 ^{o}C in the vessel and then dewatered with the help of a pressure filter to produce deacetylized corn stover cake and caustic liquor. Corn stover cake is further washed with water. Caustic liquor generated is then sent to the wastewater treatment unit to be recycled. It was assumed that 99% of acetate would be solubilized and subsequently extracted from the corn stover during the deacetylation process. This assumption was based on experimental data reported by (Kuhn, et al., 2020). In addition, it was assumed that 1% (wt/wt) of biomass entering the deacetylation vessel is transferred to the caustic liquor after the deacetylation process. It should be noted that the thermal energy of the discharged slurry was recovered with the help of a heat exchanger.

3.4.1.2 Dilute acid pretreatment

Dilute H_2SO_4 acid pretreatment was chosen as the pretreatment method. This choice was motivated by several factors. Firstly, it can be performed at relatively low temperatures (Tomás-Pejó, et al., 2010); (Alvira, et al., 2010). Secondly, the process is capable of

achieving a relatively high conversion rate. And finally, the hydrolysis of cellulose and hemicellulose can be significantly improved by manipulating the pretreatment severity (Agbor , et al., 2011).

The dilute acid pretreatment method was similar to Humbird, et al., (2011)'s, and involved the impregnation of corn stover cake obtained from the deacetylation process with 0.8% w/v of sulphuric acid. Impregnated corn stover was then fed to the pretreatment reactor along with steam to achieve 30% (wt/wt) solid loading while maintaining the mixture temperature at 160 °C for 10 minutes. The pressure in the reactor was kept at the mixture bubble point. It should be noted that solid loading can have a direct impact on energy consumption, as excess water added during pretreatment and hydrolysis has to be evaporated in the subsequent ethanol concentration process; hence, the greater the volume of water added, the more energy is required to evaporate the excess water (Stickel, et al., 2009); (Hodge, et al., 2008); (Um & Hanley, 2008).

Note that, theoretically, the evaporation of excess water is most economical when the ethanol concentration after fermentation is greater than 4% (w/w). This translates into a glucose concentration ≥ 8% (w/w) in the fermentation inlet stream and a lignocellulose loading ≥ 20% (w/w) in the hydrolysis inlet stream. These estimates, however, assume that cellulose will only be converted during the process (Modenbach & Nokes, 2013).

Despite the energy-saving attribute of high solid loading (15 - 30% wt/wt), its usage promotes the formation of hydrolysis and fermentation inhibitors such as furfural and hydroxymethylfurfural (HMF). Moreover, high solid loading can also lower the solubility of sugars and decrease mass transfer by diffusion (Stickel, et al., 2009); (Hodge, et al., 2008); (Um & Hanley, 2008). Furthermore, high solid loading is known to increase slurry viscosity leading to elevated energy consumption during mixing, which then undermines its inherent benefits (Modenbach & Nokes, 2012). It is, therefore, essential for the pretreatment solid loading to be carefully considered during dilute acid pretreatment. The 30% (wt/wt) pretreatment solid loading used in this study was derived from previous works (Tao, et al., 2014); (Humbird, et al., 2011); (Hamelinck, et al., 2005); (Aden, et al.,

2002). And, according to Leibbrandt, (2010), this solid loading is close to the optimal value for dilute acid pretreatment.

Table 3.2: Major chemical reactions taking place during the conversion process

PROCESSES	MAIN CHEMICAL REACTIONS
Deacetylation	Acetic acid to sodium acetate: $C_2H_3O_2 + NaOH \rightarrow C_2H_3ONa + H_2O$
Pretreatment	Glucan to glucose: $C_6H_{10}O_{5\,(s)} + H_2O \rightarrow C_6H_{12}O_{6\,(aq.)}$
	Xylan to xylose: $C_5H_8O_{4\,(s)} + H_2O \rightarrow C_5H_{10}O_{5\,(aq.)}$
	Xylan to furfural: $C_5H_8O_{4\,(s)} \rightarrow C_5H_4O_{2\,(aq.)} + 2\,H_2O$
	Arabinan to arabinose: $C_5H_8O_{4\,(s)} + H_2O \rightarrow C_5H_{10}O_{5\,(aq.)}$
Hydrolysis	Glucan to glucose: $C_6H_{10}O_{5\,(s)} + H_2O \rightarrow C_6H_{12}O_{6\,(aq.)}$
Fermentation	Glucose to ethanol: $C_6H_{12}O_{6\,(aq.)} \rightarrow 2\,C_2H_6O_{\,(aq.)} + 2\,CO_2$
	Xylose to ethanol: $3\,C_5H_{10}O_{5\,(aq.)} \rightarrow 5\,C_2H_6O_{(aq.)} + 5\,CO_2$
	Arabinose to ethanol: $3\,C_5H_{10}O_{5\,(aq.)} \rightarrow 5\,C_2H_6O_{\,(aq.)} + 5\,CO_2$

3.4.2 Hydrolysis and fermentation

The pretreated slurry was discharged to a flash tank operated at atmospheric pressure, where most of the water is evaporated and sent to the wastewater treatment area. The flash tank bottom stream was fed to the hydrolysis reactor. Enzymes along with clean water were added to adjust the solid to liquid ratio to 20% (wt/wt). As previously done by Tao, et al., (2014), an enzyme loading of 26 g protein/gram cellulose was used. In addition, ammonia was fed to the reactor to neutralize the residual sulphuric acid, and subsequently raise the slurry's pH.

After hydrolysis, the resulting slurry was fermented using seed culture prepared onsite. The preparation procedure involved the revival of an ethanologen seed culture and its subsequent inoculation in the fermentation media. During fermentation, cellulose, xylose and arabinose were converted to ethanol as shown in Table 3.2, which led to the formation of an ethanol-rich beer with 6% (wt/wt) ethanol concentration.

3.4.3 Ethanol recovery

The configuration used for the ethanol recovery section consisted of two distillation columns, a water scrubber and molecular sieves. The fermentation broth was fed to the first distillation column (beer column) where 99% of the CO_2 was removed in the distillate, along with 94% of water in the bottom stream. The bottom stream from the beer column was then dewatered with the help of a filter. The resulting lignin-rich solid cake was stored, while the liquid product was sent to the wastewater treatment area. The top stream from the beer column was fed to a second distillation column (rectification column), where it was further purified and an ethanol/water azeotropic mixture was obtained. Finally, molecular sieves were used to achieve a purity of 99.5% anhydrous ethanol.

3.4.4 Wastewater treatment

Wastewater generated in the processes was cleansed before being recycled back to the processes. Wastewater main streams included the caustic liquor from the deacetylation stage, acid liquor from the dilute acid pretreatment stage, boiler blowdown, and wastewater from ethanol recovery. The method employed to purify wastewater was analogous to the one used by Humbird et al., (2011). It involved feeding wastewater to an anaerobic digester, where 86% of the organic compounds are metabolized into methane gas (CH_4) and carbon dioxide (CO_2). A combination of an active sludge lagoon equipped with floating aerators, a membrane bioreactor, and a reverse osmosis reactor is then used to remove residual sludge and obtain clean water.

3.4.5 Steam and power generation

3.4.5.1 Scenario 1

Five scenarios were considered for steam and power generation. In the first scenario, lignin-rich residues generated in the ethanol recovery area along with methane gas from the wastewater treatment area were combusted in a solid-fired combustor. Water was then fed into the heat exchanger circuit of the boiler, where it was heated to produce superheated steam. The steam was subsequently allowed to expand through multistage turbines, thus generating electricity. Moreover, the steam required for the conversion processes was withdrawn in two stages: a high-pressure steam stage followed by a low-

pressure steam stage. A simplified schematic illustration of the standalone configuration is shown in Figure 3.4.

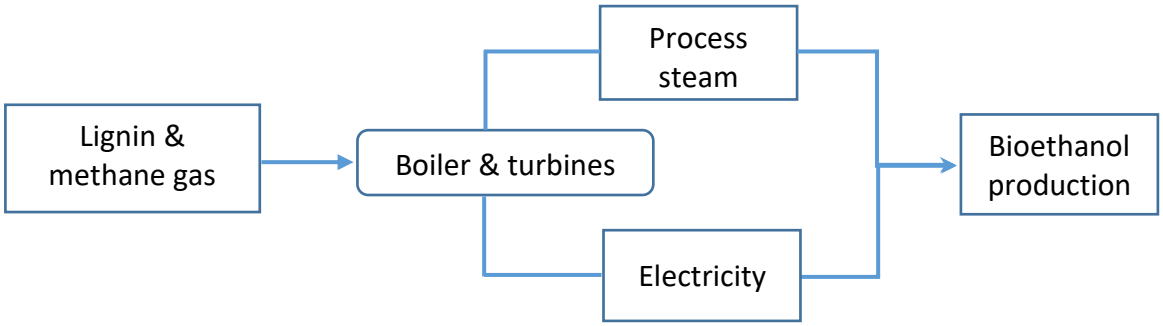

Figure 3.4: Simplified schematic illustration of the configuration used in the steam and power production area

3.4.5.2 Scenario 2

As illustrated in Figure 3.5, this scenario involved the integration of solar power into the biorefinery using a combination of concentrated solar thermal (CST) for steam generation, and solar photovoltaic panels (PV) for electricity supply. Linear Fresnel reflector were chosen as solar collectors for the CST. This is because of their relatively low initial cost compared to other commercially available solar collectors such as parabolic trough collector and solar tower (Pulido-Iparraguirre, et al., 2019); (Bellos & Tzivanidis, 2018); (Bellos, et al., 2018). Biogas from wastewater treatment plant was combusted, and the heat generated was used to preheat water fed to the boiler.

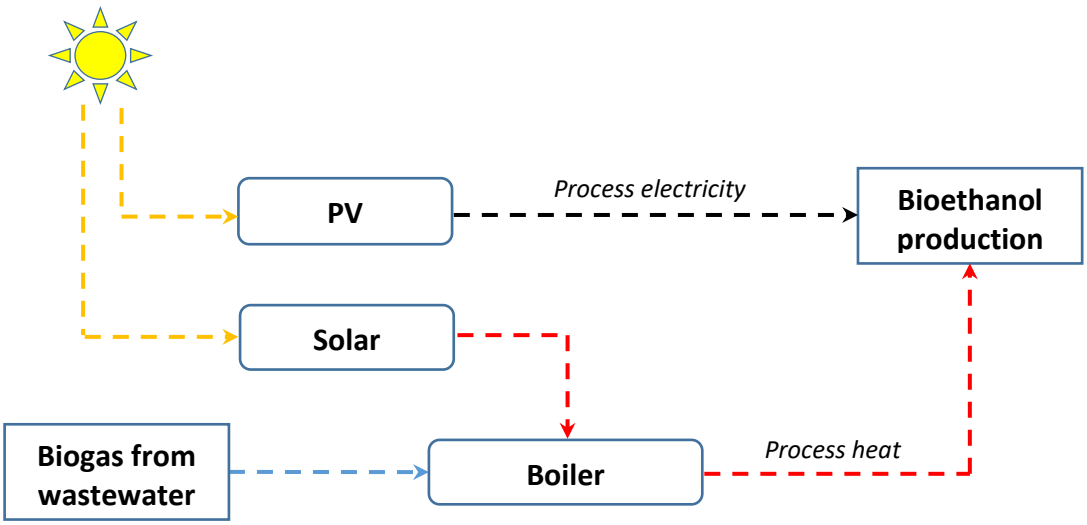

Figure 3.5: Simplified illustration of the configuration used in the steam and power production areas in scenario 2

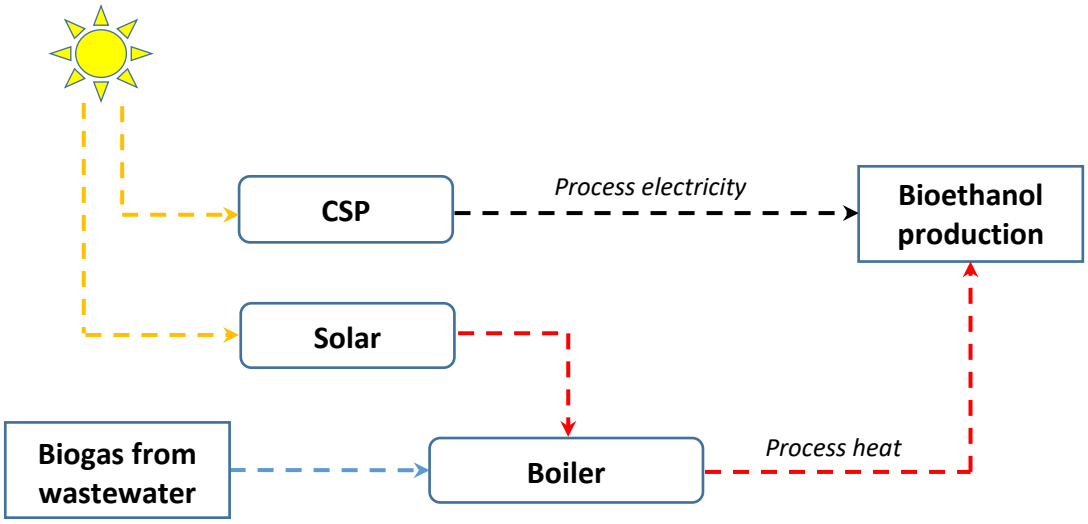

Figure 3.6: Simplified illustration of the configuration used in the steam and power production areas in scenario 3

3.4.5.3 Scenario 3

Scenario 3 was a duplicate of scenario 2, except for the fact that concentrated solar power (CSP) was used to supply the electrical power required in the processes rather than PV panels (refer to Figure 3.6). The CSP system used consisted of linear Fresnel reflectors concentrating solar energy into heat, which was subsequently used for steam generation. Steam was then fed to a turbine to produce electricity.

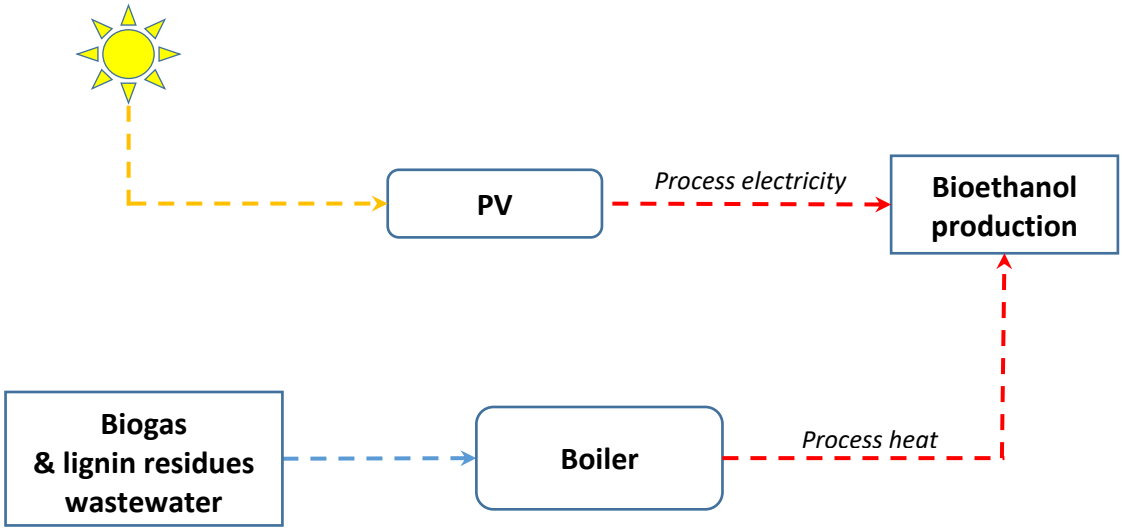

Figure 3.7: Simplified illustration of the configuration used in the steam and power production areas in scenario 4

3.4.5.4 Scenario 4 & 5

In Scenarios 4 and 5, solar PV and concentrated solar power were respectively used to supply electricity to the biorefinery, while biogas was combusted along with a portion of lignin-rich residues to generate process heat. The quantity of lignin-rich residue combusted was just enough to meet the process thermal energy demand. Refer to Figure 3.7 and Figure 3.8 for graphical illustrations of scenarios 4 and 5.

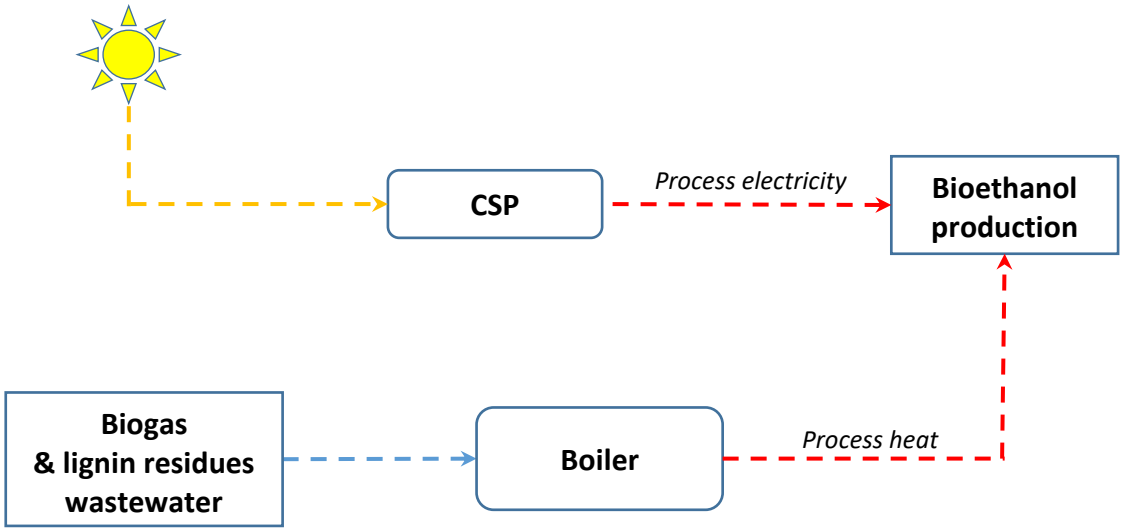

Figure 3.8: Simplified illustration of the configuration used in the steam and power production areas in scenario 5

3.5 Process simulation

The process was simulated using CHEMCAD simulation software. The physical properties for biomass cell, xylose, cellulose, xylan, lignin, and cellulase enzyme were obtained from Wooley & Putsche (1996). Considering that the process mostly involved vapour-liquid and liquid-liquid equilibrium, the Electrolyte Non-Random Two-Liquid (NRTL) property method was used throughout the simulation process to calculate the state parameters of components. Table 3.3 provides the key parameters used to simulate the major conversion units. Stoichiometric reactors were used to model the deacetylation, dilute acid pretreatment, hydrolysis and fermentation conversion processes. The conversion yields displayed in Table 3.3 were obtained from integrated bench and pilot-scale experimental results reported by Tao, et al., (2014). The combustion stoichiometry used

to simulate the chemical reactions occurring in the CHP's combustor can be found in Table A-13 of the appendix section.

Table 3.3: Model input parameters of the main unit operations used for Chemcad modelling

		Units	Value
Deacetylation	Temp	°C	80
	solid loading	%	8
	Corn stover loss	%	2
	Pressure	atm	1
	NaOH loading	%wt/v	0.4
	Acetic acid removal	%	99
Dilute acid treatment	Temperature	°C	159
	Pressure	atm	5.8
	Solid loading	%	30
	H_2SO_4 loading	%wt/v	0.8
	Glucan to glucose conversion	%	6.28
	Xylan to xylose conversion	%	84.96
	Xylan to furfural conversion	%	5.48
	Arabinan to arabinose conversion	%	95.08
Hydrolysis	Temperature	°C	50
	Solid loading	%	20
	Glucan to glucose conversion	%	95.08
Fermentation	Temperature	°C	33
	Glucose to ethanol conversion	%	95
	Xylose to ethanol conversion	%	93
	Arabinose to ethanol conversion	%	54
Ethanol recovery	CO_2 removal	%	99
	Overall ethanol recovery	%	99
Combustor/boiler	Boiler efficiency	%	80
Power generation (standalone scenario)	Turbines efficiency	%	85
	Water inlet Pump pressure	atm	62
	Turbine 1 exhaust pressure	atm	13
	Turbine 2 exhaust pressure	atm	9.5
	Turbine 3 exhaust pressure	atm	0.1

NB: The conversion yield used is the average yield obtained during the demonstration run conducted by Tao et al., (2014). Glucan, xylan and arabinan are in solid state while glucose, xylose, arabinose, and ethanol are in aqueous solution. 50% of extractives were also assumed to undergo fermentation.

3.6 Modelling of solar fields

The modelling of solar PV, CSP, and CST solar fields in the solar-aided scenarios was carried out with the help of the system advisor model (SAM) sourced from the National Renewable Energy Laboratory (NREL). The nominal capacity of modelled PV/CSP, and CST systems was 32.5 MW and 105 MW respectively. The weather data files for the plant location (Free State – South Africa) were obtained from the European Commission's Photovoltaic Geographical Information System (PVGIS, 2017). In order to minimize the impact of intermittent sunlight on the process's continuity, the solar field of all solar-aided scenarios was sized to sustain both daytime and night-time operations. Molten salt and lithium-ion batteries capable of powering the plant for 15 hours per day were employed as energy storage media for CSP/CST and PV respectively. Thus, surplus solar energy was continuously stored for use at night and on low-irradiance days.

The characteristics of the process steam produced (flow rate, pressure, temperature, vapour fraction) were identical in hybrid and standalone scenarios. The required solar energy input was determined based on the total energy demand of the standalone scenario. The sizing of solar fields was carried out using the system advisor model. The PV module used in the SAM modelling was assumed to be made of Mono-c-Si, with 96 cells, a surface area of 1.631 m^2, and a nominal efficiency of 19.02%. Linear Fresnel reflectors were utilized for CST and CSP. The solar multiple for the CSP linear Fresnel was 2.3 with a field aperture of 850 000 m^2, while CST's linear Fresnel had a solar multiple of 1.8 and a field aperture of 862 848 m^2.

3.7 Evaluation of conversion efficiency

3.7.1 Overall energy and conversion efficiency

Although energy conversion efficiency can be defined in various ways, its fundamental definition is “the useful energy output (benefit) divided by the energy input (cost)” (Shigenori, et al., 2018). This definition assesses the efficiency at which lignocellulosic biomass is transformed into ethanol and electricity. The energy inputs include the thermal energy of biomass raw materials as well as any energy supplied externally to the biorefinery such as solar energy. The total output energy includes the thermal energy of ethanol product, lignin co-product and electricity by-product (See Eq. 3.1). Ideally, the

unconverted lignin sold as a co-product from solar scenarios should not be burned by the end-users, but rather be used for the production of valuable bio-materials.

$$\eta_{Overall} = \frac{E_{ther.ethanol} + E_{ther.lignin\ co-product} + E_{elec.by-product}}{E_{ther.\ biomass} + E_{solar}} \quad \text{Eq. 3.1}$$

Where $\mu_{overall}$ is the overall energy conversion efficiency, $E_{ther.ethanol}$ is the thermal energy of ethanol product, $E_{ther.lignin\ co\text{-}product}$ is the thermal energy of lignin co-product, $E_{elec.by\text{-}product}$ is the electrical energy exported to the grid, $E_{ther.biomass}$ is the thermal energy of biomass feedstock, and E_{solar} is the solar energy input in solar-hybrid scenarios. Note that the thermal energy of ethanol, lignin and biomass were computed using their LHV.

3.7.2 Liquid fuel energy conversion efficiency

The expression used to determine the energy conversion efficiency based on liquid fuel production only, was obtained from Hamelinck, et al., (2005). Note that the portion of feedstock energy found in the by-products (surplus electricity and lignin in thermal units) was subtracted from the biomass feedstock energy to ensure that the Figure obtained is solely a reflection of the efficiency of the process to produce liquid fuels from the portion of the feed energy that is converted to liquid fuel energy. In other words, the contribution of by-products to the overall process energy efficiency was ignored. In order to convert surplus electricity into thermal energy, it was assumed that biomass could be directly converted into electricity at an electric conversion efficiency (μ_{elec}) of 45%. This value was based on Hamelinck, et al., (2005)'s biomass-integrated gasification combined cycle (BIGCC) system. Equation 3.2 shown the formula used to determine the energy conversion efficiency based on liquid fuel production only.

$$\eta_{liquid\ fuel} = \frac{E_{ther.liquid\ fuel\ (ethanol)}}{E_{ther.\ biomass} - E_{ther.\ lignin} - (E_{surplus\ elec.}/\mu_{elec})} \quad \text{Eq. 3.2}$$

3.7.3 Net energy

Net energy has often been used to evaluate the performance of biomass energy conversion systems (Weiss & Schebek, 2021); (Carlos, et al., 2017); (Jean-Christophe, et al., 2010). In the present study, both the net energy output (Eq. 3.3) and net energy ratios

(Eq. 3.4) were used to comparatively evaluate the performance of standalone and hybrid biorefineries, and appreciate the contrast between the total energy demands for operation and the energy content of products. The system boundary was limited to the raw materials inlet and product outlet.

$$Net\ energy\ output = Energy\ output - Energy\ demand \quad \text{Eq. 3.3}$$

$$Net\ energy\ ratio = \left|\frac{energy\ output}{energy\ demand}\right| \quad \text{Eq. 3.4}$$

A negative net energy output implies that the energy requirement of the biorefinery is greater than the energy content of energetic products. In contrast, positive net energy indicates a favourable system with a surplus of energy. Likewise, a net energy ratio greater than 1 indicates net energy loss, while a net energy ratio less than 1 suggests a surplus of energy, which is favourable.

3.8 Modelling results and discussions

3.8.1 Process energy demand

Ethanol production of 154 608 tonnes/annum was achieved at a corn stover feed rate of 833.34 kilo-tonnes/annum which was comparable to the 155.64 kilo-tonnes/annum reported by Tao et al (2014) using a similar conversion process with an identical corn stover feeding rate. The process energy demand was identical in all scenarios, given that the conversion areas were similar, except for the configuration used in the power generation unit. In all scenarios, the biorefinery initially required 29.4 MJ of energy input to generate 29.84 MJ of ethanol (the equivalent of 1 kg of ethanol). The energy input requirements dropped to 19.56 MJ/kg ethanol after heat integration.

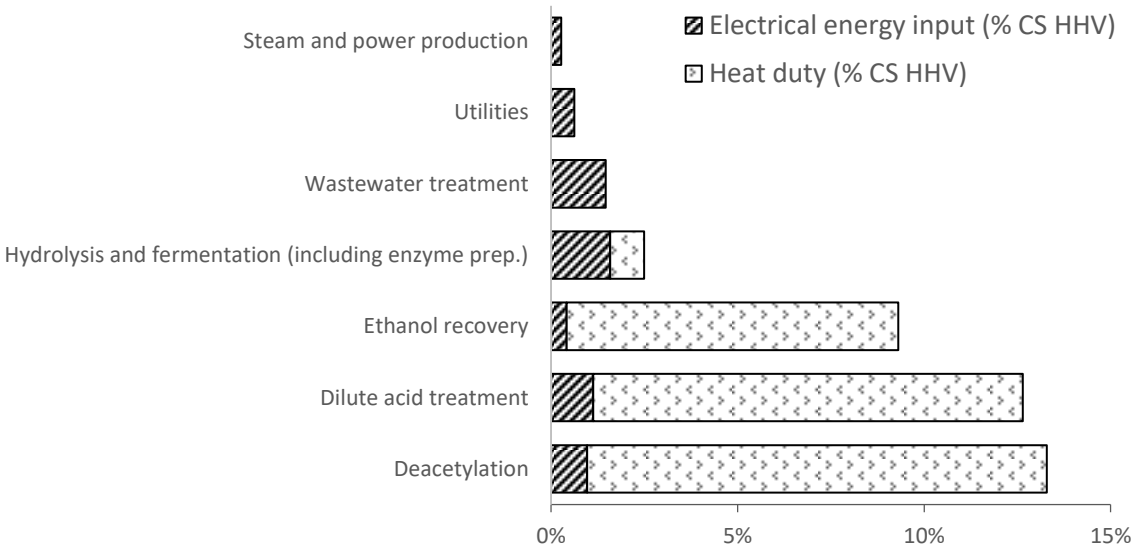

Figure 3.9: Energy demand as a function of corn stover (CV)'s HHV.

Thermal energy input accounted for more than 80% of the biorefinery energy needs while electrical energy accounted for the remaining 20%. The pretreatment process which included deacetylation and dilutes acid treatment was found to be the most energy-intensive process and required an energy input equivalent to 26% of the corn stover HHV (refer to Figure 3.9). The process energy demand could not be compared to previous studies such as Humbird (2011)'s and Tao (2014)'s. This is because the detailed data on process energy consumption are rarely disclosed in TEAs.

3.8.2 Energy conversion efficiency

As illustrated in Figure 3.10, depending on the scenario employed, energy enters the biorefinery either in the form of corn stover or solar energy. And then exits in the form of bioethanol, surplus electricity, and lignin-rich residues. Energy exiting as bioethanol represented 31.8% of the corn stover net calorific value. Considering that the primary purpose of the biorefinery is to convert biomass (corn stover) into liquid fuel (bioethanol), it can be deduced that most of the chemical energy contained in the corn stover feedstock is used for the generation of heat and electricity required in the conversion processes, with only a fraction recovered as bioethanol. The relatively low ethanol energy recovery can be attributed to several unfavourable occurrences. These include the formation of side products (e.g., furfural), the relatively low xylan conversion during pretreatment, and more importantly, the inertness of lignin during the entire conversion process.

Because the electricity generated in scenario 1 by the turbines was greater than the electricity required in the processes, surplus electricity was produced. This surplus electricity represented 2.44% of the net calorific value of the corn stover feedstock, and was exported to the grid as a way to enhance the biorefinery's profitability. The liquid fuel efficiency was respectively found to be 33.6% for scenario 1, 36.7% for scenarios 2 & 3, and 33.6% for scenarios 4 & 5.

In scenarios 2 and 3, where solar energy was used to meet the biorefinery's process energy demands, and the unconverted lignin-rich residues were exported as a co-product, the overall energy conversion efficiency was found to increase to 76.9%. A similar trend was observed in scenarios 4 and 5 where 60% of residues were combusted alongside biogas for process heat and only the remainder was sold as a co-product. The overall energy conversion efficiency in scenarios 2 and 3 was, however, much higher than in scenarios 4 and 5 due to partial lignin combustion in the latter scenarios. In light of these observations, it can be said that by exporting lignin as a co-product, and using solar power to meet the biorefinery's process energy requirements, the overall energy conversion efficiency is significantly enhanced.

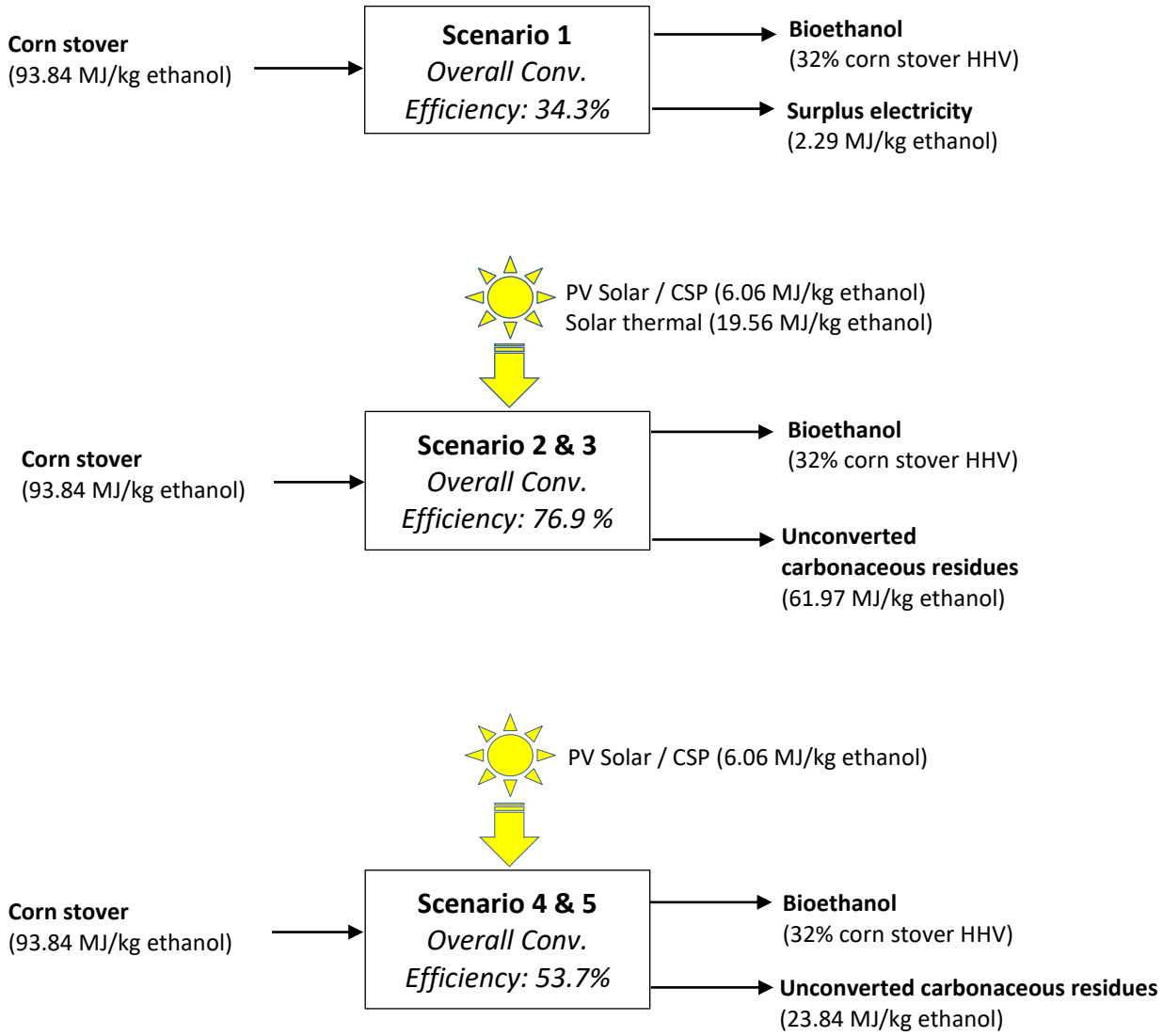

Figure 3.10: Conversion efficiency for different scenario

3.8.3 Net energy output

Process energy demand for all scenarios was found to be 6.06 $MJ/kg_{ethanol}$ for electrical energy, 19.56 $MJ/kg_{ethanol}$ for heat utility, and 0.1 $MJ/kg_{ethanol}$ for fossil energy (fuel consumed by trucks during biomass transportation). Also, in all scenarios, the net energy ratio was above 1 and the net energy output was positive. This implies that the energy contained in the products was greater than the process energy demand. Meanwhile, it is worth mentioning that both the net energy output and net energy ratio are a function of the extent to which energy recovery is applied in the biorefinery. For instance, if process

heat integration was not applied in scenario 1, the net energy output would have dropped to 1.82 MJ/kg ethanol produced. This corresponds to a net energy ratio of 1.06.

Table 3.4: Net energy of corn stover-to-ethanol biorefinery

	Scenario 1	Scenario 2 & 3	Scenario 4 & 5
ENERGY OUTPUT (MJ/kg of ethanol produced)			
Bioethanol	29,84	29,84	29,84
Surplus Electricity (With heat integration)	2.29	0	0
lignin-rich carbonaceous co-product	0	56.29	23.84
NET ENERGY			
Net energy output [a] (MJ/kg of ethanol produced)	6.51	60.50	28.06
Net energy ratio [b]	1.25	3.36	2.10

[a] Net energy ratio = |energy output/energy demand|. NB. Energy output includes the energy contents of the biofuels and the energetic co-products. [b] Net energy output = total energy output – total energy demand. *Value of net energy output/ratio if the energy content of lignin-residues is considered in the calculations

Furthermore, as seen in Table 3.4, the export of lignin-rich residues in solar-aided scenarios combined with the utilization of solar energy resulted in steep increases in both the net energy output and the net energy ratio. However, if lignin-rich residues were treated as a non-energy product, the opposite effect would be created. For instance, not including the energy content of lignin-rich residues in scenario 2 and 3 calculations would result in the net energy output declining from 60.5 to 0.42 MJ/kg ethanol and the net energy ratio dropping from 3.36 to 1.01. It can therefore be deduced that the sizable boost seen in the net energy is mainly the result of lignin-rich residues being considered as an energetic product. It should be noted that the net energy of scenarios 2 and 3 with the exclusion of lignin energy content is higher than scenario 1 because of the electricity co-product in the latter scenario.

3.8.4 Solar field requirements

Table 3.5 summarises the key modelling results of the three solar technologies (CSP, CST, and Solar PV) used to supply energy to the solar-aided biorefinery. It can be observed that the generation of process electricity from PV solar requires 0.35 km^2 of land. This value

increases further to 0.59 km^2 when CSP is used. Thus, the generation of process electricity using solar PV requires about 40% less land than CSP.

Table 3.5: Key modelling results of solar energy technologies used

	Scenario 2	Scenario 3	Scenario 4	Scenario 5
Total land area for PV / CSP (km^2)	0.35	0.59	0.35	0.59
Total land area for solar thermal (km^2)	1.47	1.47	0	0
Overall land required for solar field (km^2)	1.82	2.06	0.35	0.59

NB: Lithium iron phosphate battery was used as storage media for PV and CSP, while 12-hour molten salt thermal storage was used as storage media for solar thermal.

The generation of process heat using solar thermal required 1.47 km^2 of land, which was almost 4 folds larger than the land required for electricity generation using PV technology, and almost 3 folds larger than the land required for electricity generation from CSP. Consequently, solar energy will have a considerable impact on the physical footprint of biorefineries when used as their primary source of energy.

3.9 Conclusions

This chapter explained the approach applied to model the conversion of corn stover into ethanol. The rationale behind raw material selection and biorefinery location was given. The configuration used for each scenario was also described in detail. As part of the technical evaluation, modelling results were presented and discussed as well. In light of the results obtained, it can be asserted that although the incorporation of solar energy into a corn stover-to-ethanol biorefinery combined with the export of lignin as a co-product could enhance the biorefinery's overall energy conversion efficiency and net energy, it would also require substantial land to accommodate solar receivers.

.

CHAPTER 4 – MODELLING OF THERMOCHEMICAL PROCESSING

4.1 Introduction

This chapter describes the modelling of corn stover-to-methanol biorefineries via gasification. Two scenarios are explored: a standalone scenario where a conventional dual-bed gasifier is used to produce syngas from corn stover, and a solar-aided scenario where gasification is accomplished with the incorporation of solar energy. The production performances for each scenario are presented and discussed, with an emphasis on the solar-aided gasifier.

4.2 Logistic configuration and biorefinery location

The biorefinery location and logistic configuration were identical to the one discussed earlier in chapter 3, for the production of ethanol from corn stover. Thus, 2000 tonnes of corn stover was processed on a daily base (500 MWth LHV). Mechanical pretreatment, which involves size reduction (to 5 mm diameter), is performed at the regional biomass processing depots (RBPD). The milled biomass is then transported to the main biorefinery site for thermochemical processing.

4.3 Biomass characteristics

The ultimate and proximate analyses of the corn stover feedstock are summarized in Table 4.1. Corn stover's higher heating value (HHV) was calculated using the correlation developed by Noushabadi, et al. (2021). The correlation is presented in Equation 4.1, and was derived from experiments performed with 535 biomass samples. The lower heating value (LHV) on the other hand was estimated from the HHV, by subtracting the heat of evaporation of water present in the biomass feedstock.

$$HHV = -0.8738 \times N \times H^{-1.3101} - 0.1583 \times C \times O^{0.3497} + 0.3856 \times C \times (H \times O)^{0.1462} + 2.1436 \times \left(\frac{H}{O}\right)^{-0.3846} + 0.1076 \times C \times H^{-0.3846} + 0.1098 \times N \times S - 11.2794 \times \left(\frac{H}{C}\right) \quad \text{Eq.4.1}$$

Where N, H, C, O and S represent respectively the mass percentage of nitrogen, hydrogen, carbon, oxygen and sulphur in the biomass.

Table 4.1: Characteristics of corn stover feedstock (Li, et al., 2017)

Ultimate Analysis (wt%)	
C	48.59
H	6.28
O	33.27
N	1.31
S	0.18
Proximate Analysis (wt%)	
Volatile matter	71.27
Fixed carbon	18.37
Ash	10.36
Calorific value (MJ/kg)	
HHV*	19.83

*Value calculated using equation 4.1, Noushabadi, et al. (2021)

4.4 Design scenarios

The biorefinery was divided into four main conversion areas: pretreatment, gasification, methanol synthesis, and heat and power generation where fuel (unconverted syngas and biomass) was combusted in a CHP system to generate process steam and electricity. Two gasification configurations were considered: conventional gasification (standalone scenario) and solar-aided gasification (solar-aided scenario).

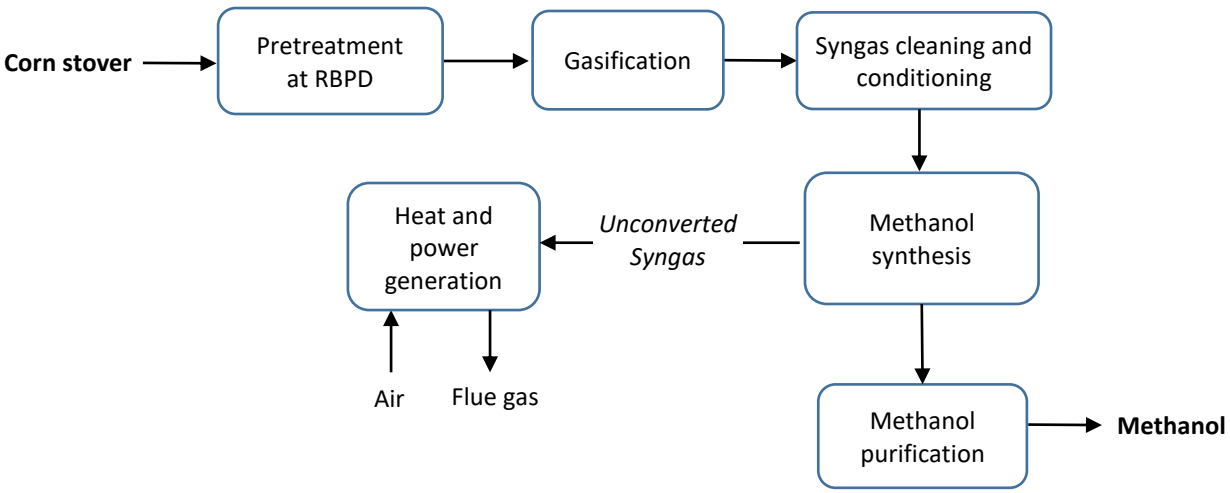

Figure 4. 1: Overview of main conversion areas used for standalone scenario

In conventional gasification, biochar was combusted in the gasifier's combustion bed to generate heat for the gasification process. While in the solar-aided gasifier, the thermal energy needed to drive the gasification reactions was obtained from concentrated solar

power, and biochar was commercialized as a co-product. The syngas generated in each scenario was upgraded to methanol. Overviews of both scenarios are illustrated in Figures 4.1 and 4.2. Further information on the gasification process is provided in the following sections.

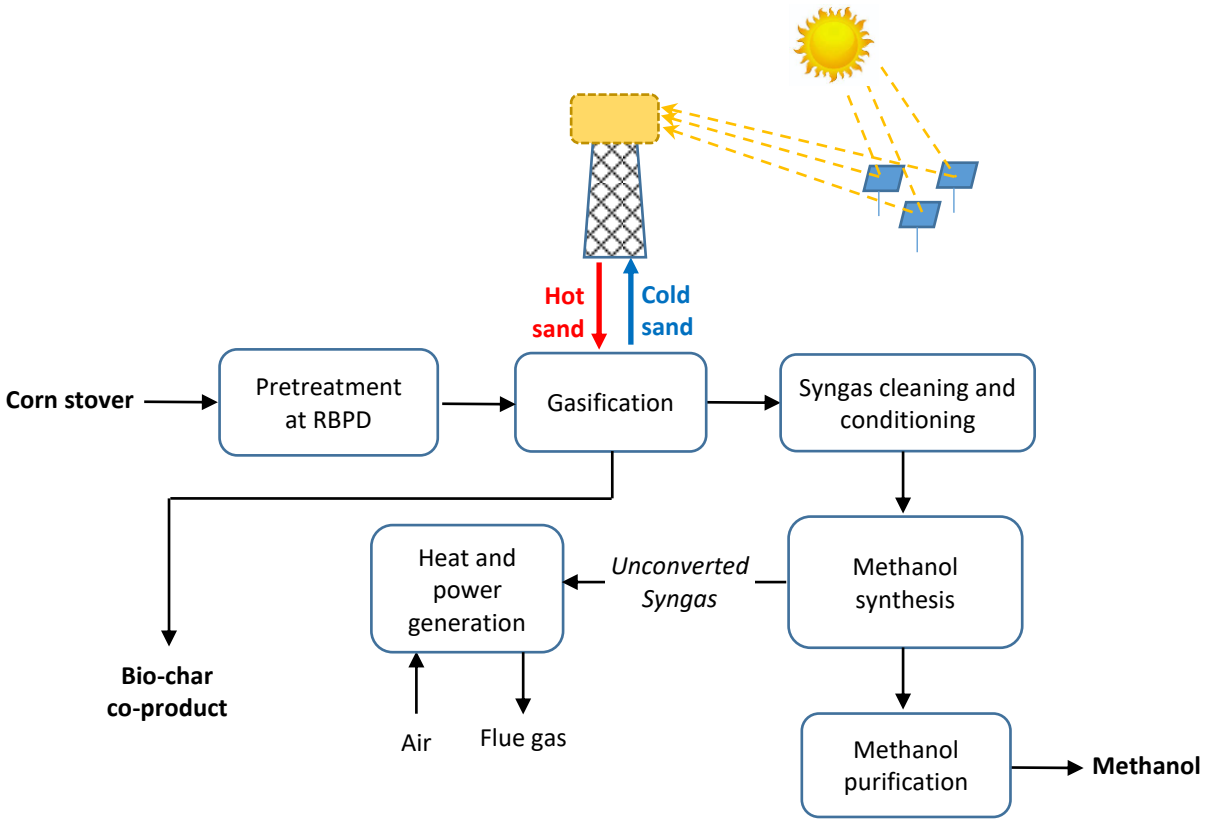

Figure 4.2: Overview of main conversion areas used for solar-aided scenario 2

4.5 Modelling of stand-alone scenario

4.5.1 Gasifier description and operation

An indirect fluidized bed gasifier was selected to model the conventional gasification process. This type of gasifier was chosen for its ability to uniformly transfer heat between biomass and oxidisers. Also, indirect fluidized bed gasifiers are known to achieve high carbon conversion, and low tar production compared to fixed bed gasifiers (Ram & Mondal, 2022). Moreover, its operation does not require pure oxygen. Hence, the need for an air separation unit (ASU) is avoided. In addition, it generally has a relatively long reactant residence time which leads to higher-quality syngas (Simanjuntak, et al., 2019).

Although several dual-bed gasifier configurations have been reported in the literature, such as FECO's (Hanchate, et al., 2021) and GAUSSING's (Bolhar-Nordenkampf, 2002), the study used a configuration similar to that developed in France by the Tunzini Nessi Equipment Companies (TNEE) and the Compiègne Universities. The choice of this gasifier setup was motivated by its ability to process feedstock with relatively high moisture content (Abdelouahed, et al., 2012). Moreover, it uses sand as bed material. Thus, it can be hybridized with solar power using the configuration discussed in section 4.6. The TNEE-type gasifier used in the study consisted of two separate beds: a low-velocity fluidized bed (LVFB) where gasification reactions occurred, as well as a combustion bed equipped with high-velocity pneumatic risers (HVPR) for combustion of char (Abdelouahed, et al., 2012). Due to the lack of detailed information on the TNEE gasifier in the literature, the energy involved during the movement of the pneumatic riser was not considered in this study.

Low-velocity fluidization is achieved in the gasification bed by recycling a portion of the product gas back into the gasifier. While in the combustion bed, air is injected bottom-up to create fluidization. Moreover, the combustion bed is equipped with a pneumatic riser that enables the bed to move and discharge into the adjacent gasification bed. As a result, hot sand circulates, and heat is exchanged from the combustion bed to the gasification bed. This configuration ensures that exhaust gas and product gas are kept unmixed throughout the process, which leads to high-quality syngas being produced. Also, it is worth noting that the TNEE indirect gasifier is capable of processing carbonaceous fuels with a relatively high moisture content (38% wt), and it does not require steam for its operation (Abdelouahed, et al., 2012). Figure 4.3 shows a simplified diagram of the TNEE gasifier and further details about its design are available in the literature (Simanjuntak, et al., 2019); (Abdelouahed, et al., 2012).

4.5.2 Gasifier modelling approach

In order to simplify the modelling process, an approach similar to that used by Abdelouahed, et al., (2012) was adopted. Consequently, the gasification bed was divided into two zones: a primary reaction zone where the biomass was pyrolyzed into a mixture CH_4, H_2, CO_2, CO, char and tar compounds, and a secondary reaction zone where pyrolysis product underwent further chemical reaction. As per TNEE's gasifier design, 5% of the

char was assumed to be conveyed to the secondary reaction zone, or "freeboard". The remaining 95% would exit the gasifier bed and be sent to the combustion bed along with sand. The remaining 95% would exit the gasifier bed and be sent to the combustion bed along with sand. Figure 4.4 illustrates the modelling approach used for the dual bed gasifier, while Figure 4.5 depicts the flow of material. It should be noted that the process was simulated using CHEMCAD software.

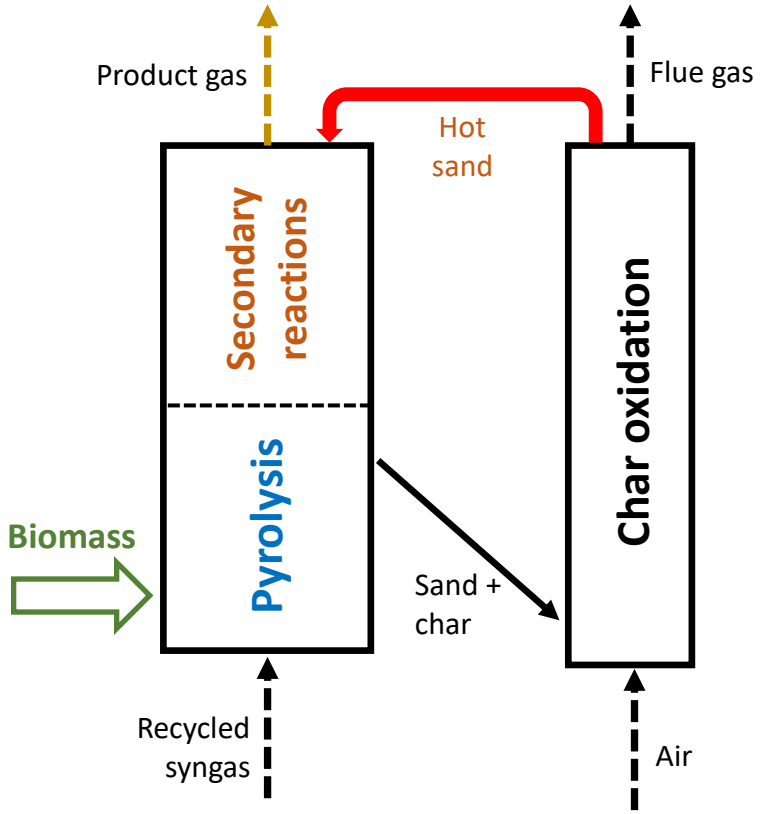

Figure 4.3: Simplified diagram of TNEE Gasifier. Redrawn from Abdelouahed, et al., (2012)

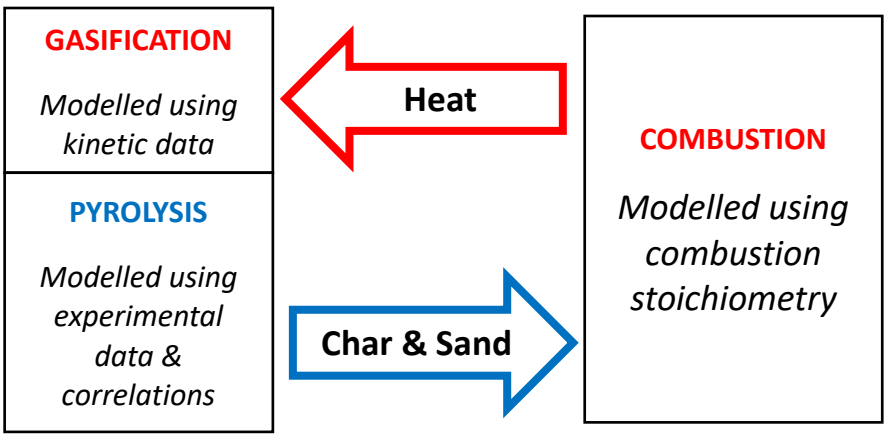

Figure 4.4: Illustration of modelling approach employed during biomass gasification

4.5.3 Modelling of pyrolysis zone

Biomass pyrolysis is a complex process which results in the formation of three major products: bio-char, condensable vapour (bio-oil) and non-condensable gases. The product yields are a function of several parameters, such as the type of biomass feedstock, processing parameters, and reaction pathways (Hu & Gholizadeh, 2019). Because of the complex nature of biomass pyrolysis, the pyrolysis product yield was predicted based on experimental data reported by You, et al., (2010), on corn stover pyrolysis.

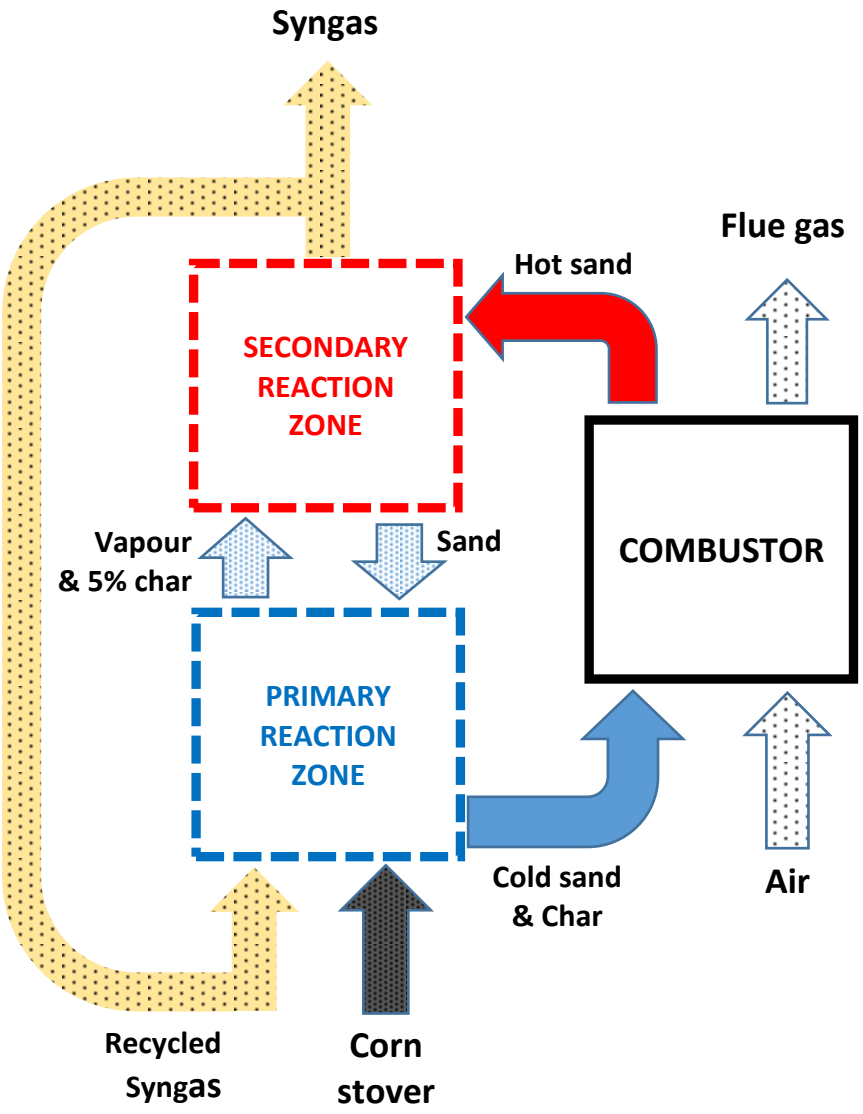

Figure 4.5: Material flow in the dual fluidized bed gasification system

It is worth pointing out that, although a few experimental works have been reported on the fast pyrolysis of corn stover, most of these were performed at relatively low

temperatures (Ali, et al., 2019); (Uzun & Sarioğlu, 2009); (Jianzhong, et al., 2000). And, as far as the author is aware, You et al., (2010)'s study is the only work conducted on corn stover fast pyrolysis with temperatures as high as 677 – 877 ^{o}C. Also, other studies using temperature of this magnitude mostly utilize wood as a feedstock. (Commandre, et al., 2011); (Dufour, et al., 2009).

Tables 4.2 and 4.3 show the product yield of corn stover pyrolysis obtained from You et al., (2010). The condensable vapour was modelled as a mixture of four compounds, mainly phenol (C_6H_6O), benzene (C_6H_6), naphthalene ($C_{10}H_8$) and toluene (C_7H_8). These compounds are generally among the prominent constituents of bio-oil formed during pyrolysis (Li & Suzuki, 2009). It is worth noting that the experimental results disclosed by You et al., (2010) using corn stover as feedstock (refer to Table 4.2) reveal a marginal drop in char yield as the temperature gradually increases from 477 to 877 ^{o}C. On the other hand, the yield of condensable vapour shows a more pronounced decline, while gas yield sharply increases with increasing temperatures.

Table 4.2: Yield of gas, char and condensable vapour generated during corn stover pyrolysis (kg/kg dry fuel). Data obtained from You et al., (2010)'s experimental data

Temperature (^{o}C)	477	677	777	877
Char	0.22	0.21	0.20	0.19
Gas (non-condensable)	0.27	0.62	0.66	0.71
Condensable vapour	0.50	0.19	0.16	0.09

Table 4.3: Gas composition. Data obtained from You et al., (2010)'s experimental data using corn stover as feedstock

Temperature (^{o}C)	477	677	777	877
CO	0.38	0.29	0.24	0.20
H_2	0.32	0.35	0.35	0.36
CO_2	0.13	0.14	0.14	0.15
CH_4	0.09	0.15	0.19	0.24
C_nH_m	0.08	0.08	0.07	0.06

It is important to note that You et al., (2010)'s paper didn't disclose the particle size used in their experiment. Hence, although this may affect the level of accuracy, the effect of particle size was not considered when predicting the product yield.

4.5.4 Kinetic modelling of gasification zone

Products generated in the pyrolysis sub-process were conveyed to the gasification zone where they were further heated up and underwent secondary reactions. The conversion taking place in the gasification zone was modelled using kinetic data implemented in an adiabatic plug flow reactor. The sand temperature in the combustion zone was varied by manipulating the fraction of biochar combusted, which in turn, impacted the temperature in the gasification and pyrolysis zones. Table 4.4 shows the chemical reactions considered in the secondary reaction zone along with the kinetic data used during modelling. Table 4.5 on the other hand shows the typical process parameters of TNEE dual bed gasifier technology. A flowsheet illustrating the gasification process is depicted in Figure 4.6.

Table 4.4: Rate laws considered in the secondary reaction zone

Chemical reaction	rate law (kmol/m^3·s)	source	
HOMOGENOUS REACTIONS			
$CO + H_2O \rightarrow CO_2 + H_2$	$1.35 \times 10^5 exp\left(-\frac{102400}{RT}\right) C_{H_2O} C_{CO}$	Forward water-gas shift (Bustamante, et al., 2005)	R1
$CO_2 + H_2 \rightarrow CO + H_2O$	$1.2 \times 10^{10} exp\left(-\frac{318000}{RT}\right) C_{H_2}^{0.5} C_{CO_2}$	Reverse water-gas shift (Bustamante, et al., 2004)	R2
$C_6H_6 + H_2O \rightarrow 3C + 2CH_4 + CO$	$10^7 exp\left(-\frac{10^5}{RT}\right) C_{C_6H_6}$	Tar reforming in the gas phase (Abdelouahed, et al., 2012)	R3
$C_7H_8 + H_2 \rightarrow C_6H_6 + CH_4$	$1.04 \times 10^{12} exp\left(-\frac{247000}{RT}\right) C_{C_7H_8} C_{H_2}^{0.5}$	Tar hydrogenation in the gas phase (Abdelouahed, et al., 2012)	R4
$C_6H_6O \rightarrow CO + 0.4C_{10}H_8 + 0.15C_6H_6 + 0.1CH_4 + 0.75H_2$	$10^7 exp\left(-\frac{10^5}{RT}\right) C_{C_6H_6O}$	Tar cracking in the gas phase (Abdelouahed, et al., 2012)	R5
$C_{10}H_8 \rightarrow 9C + 1/6C_6H_6 + 3.5H_2$	$3.04 \times 10^{14} exp\left(-\frac{350000}{RT}\right) C_{C_{10}H_8}^{1.6} C_{H_2}^{-0.5}$		R6
HETEROGENEOUS REACTIONS			
$C + H_2O \rightarrow CO + H_2$	$3 \times 10^{11} exp\left(-\frac{310000}{RT}\right) \frac{m_{char}}{V_R} C_{H_2O}$	Water-gas (Abdelouahed, et al., 2012)	R7
$CO_2 + C \rightarrow 2CO$	$5.81 \times 10^6 exp\left(-\frac{205600}{RT}\right) P_{CO_2}^{0.6}$	Boudouard reaction* (Basu, 2013)	R8
$CH_4 \rightarrow C + 2H_2$	$10^{-2} exp\left(-\frac{263000}{RT}\right) \frac{m_{char}}{V_R} P_{CH_4}$	Methane cracking (Abdelouahed, et al., 2012)	R9
$C_6H_6 + H_2O \rightarrow 3C + 2CH_4 + CO$	$21.11 exp\left(-\frac{61000}{RT}\right) \frac{m_{char}}{V_R} C_{C_6H_6}$	Tar cracking over char (Abdelouahed, et al., 2012)	R10
$C_7H_8 + H_2 \rightarrow C_6H_6 + CH_4$	$21.11 exp\left(-\frac{61000}{RT}\right) \frac{m_{char}}{V_R} C_{C_7H_8}$		R11
$C_6H_6O \rightarrow CO + 0.4C_{10}H_8 + 0.15C_6H_6 + 0.1CH_4 + 0.75H_2$	$95798\ exp\left(-\frac{79000}{RT}\right) C_{C_6H_6O}$		R12
$C_{10}H_8 \rightarrow 9C + 1/6C_6H_6 + 3.5H_2$	$21.11 exp\left(-\frac{61000}{RT}\right) \frac{m_{char}}{V_R} C_{C_{10}H_8}$		R13

Where P_i is the partial pressure of specie i (Pa), R is the ideal gas constant (8.314 kJ/kmol·K). V_R is the volume of the secondary reaction zone (m^3). C_i is the concentration of component i (kmol/m^3). m_{char} is the mass flow rate of char moving to the secondary reaction zone (kg/s). V_R stands for volume of secondary reaction zone (m^3). Reactions occur in plug flow reactors. *Rate law specific to char of corn stover origin could not be located in the literature. Hence, the rate law for bio-char of wheat straw origin was used.

It is important to note that, the water gas shift reaction was modelled using two separate forward and reverse kinetic rate laws obtained from Bustamante, (2005) and Bustamante, (2004). This is because as shown by (Abdelouahed, et al., 2012), the combination of these forward and reverse WGS rate laws gives a more accurate prediction of syngas composition for a TNEE-type dual-bed gasifier.

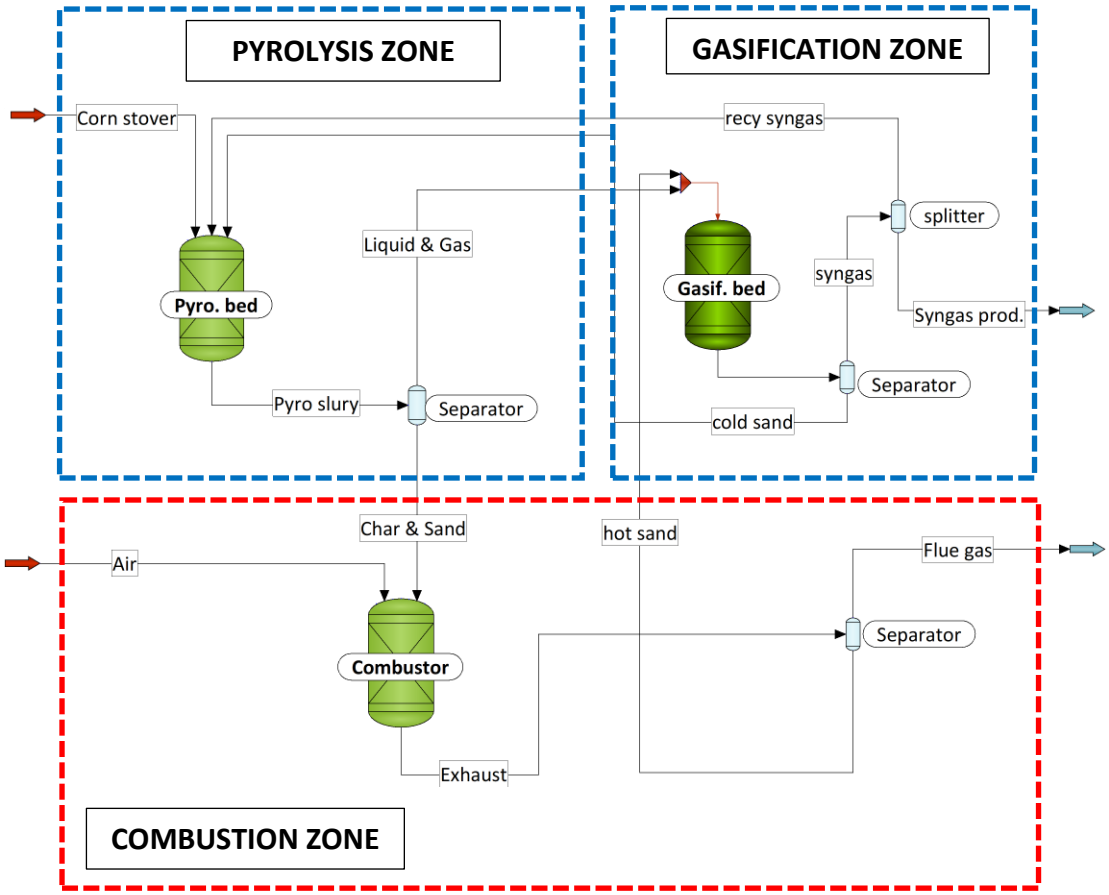

Figure 4.6: Flowsheet of the biomass gasification process

Table 4.5: Key process parameters of TNEE gasifier technology (Abdelouahed, et al., 2012)

PARAMETER	VALUE
Moisture content of biomass at the gasifier inlet	38% (wt/wt)
Mass flow rate of syngas used for fluidization	14% of syngas generated
Volume of secondary reaction zone	7.89 m^3 per 1 kg/s of anhydrous biomass fed to the gasifier
Temperature of combustor	980 ^oC
Temperature of pyrolysis zone	≈ 760 ^oC*
Temperature of gasification zone	≈ 980 - 940 ^oC*
Combustor pressure	1 atm
Pressure inlet of fluidization bed	1 atm
Mass flow rate of sand between combustor and gasifier bed	14.9 x dry biomass flow rate

*These temperatures can only be manipulated by adjusting the combustor's temperature and/or the sand flow rate.

4.5.5 Modelling of combustion sub-process

Char combustion was modelled using a stoichiometric reactor. The thermal energy released during char combustion was calculated from the heat of reaction. This energy was assumed to be entirely passed on to the sand, which resulted in the sand being heated. For the sake of simplicity, sand was modelled as 100% silica, and was assumed to remain inert during the entire conversion process. It is worth noting that 95% of the char generated in the pyrolysis bed is sent to the combustion bed. The remaining 5% is conveyed to the secondary reaction zone. Complete oxidation of char is assumed in the combustor.

4.6 Modelling of solar-aided scenario

4.6.1 Solar-aided gasification scenario

The gasifier employed in the solar-aided scenario had a gasification bed similar to the standalone scenario. The difference, however, was in the adjacent bed where char combustion was substituted with a concentrated solar power system (CSP) analogous to the one employed in power tower systems. Thus, sand was heated using solar energy rather than char combustion heat.

Solar tower systems typically comprise a central receiver mounted on a tower. The receiver is then surrounded by a sizeable heliostat field. The system is configured in such a way that sunlight from the heliostat's mirrors is directed to the receiver. To enable thermal energy absorption, the receiver is filled with a working substance such as water, molten salts, liquid sodium or air. Such systems can achieve temperatures as high as 2000 ^{o}C (Jin & Hong, 2012). Water is generally used as the working substance when the goal is to produce steam for heat and power generation via the Rankine cycle. While air is used as the working substance when the intent is to produce hot gases for turbines operating on the Brayton cycle (Kamran, 2021). Molten salts and liquid sodium on the other hand are used when the objective is to store thermal energy, which can then be utilized to extend the production time beyond sunlight hours, or for other heat-demanding processes (Singer, et al., 2014); (Boerema, et al., 2012).

One of the main challenges with concentrated solar power systems is ensuring that operations are extended beyond sunlight hours. This can be achieved via the use of

thermal energy storage (TES) systems. Such systems can store thermal energy in the form of heat for later use. For instance, in concentrated solar power plants, thermal energy produced during peak sunlight is generally stored as molten salt (Santos, et al., 2018). As of today, the molten salt thermal energy storage system remains the only proven technology for extending the operating hours of concentrated solar power plants. This technology, however, comes with several challenges. For instance, during circulation (charge and discharge), the molten salt temperature is usually unsteady (Diago, et al., 2018). Also, with an upper operating limit below 600 ^{o}C, storing thermal energy in the form of molten salt might not be suitable for applications such as gasification where higher temperatures are required.

Although numerous research works aimed at developing improved salt formulations capable of achieving higher storage temperatures have been ongoing (Lai, et al., 2022); (Gomez, et al., 2013); (Wu, et al., 2011); (Peng, et al., 2010), thermal decomposition of salts remains an obstacle to overcome (Bauer, et al., 2013). Thus, alternative thermal energy storage systems are being explored. These include phase change materials (PCM), which are capable of achieving higher energy densities and exchanging heat in narrow temperature ranges (Xu, et al., 2015). Despite the attractive features of phase change materials, a satisfactory material is yet to be developed (Diago, et al., 2018). Thermochemical energy storage is another option being explored. The technology, however, is in an embryonic phase, and needs to evolve further (Clark & Farid, 2022); (Prieto, et al., 2016).

The utilization of solids such as pack beds and solid blocks as thermal energy storage systems has also been investigated, and several favourable features have been established. For instance, a large variety of solids can be used, ranging from silica sand to limestone. Furthermore, depending on the material used, the system can store and dispatch solids at temperatures above 1000 ^{o}C (Laing-Nepustil & Zunft, 2021), which makes it ideal for gasification. Moreover, in contrast to molten salt, direct solar absorption with solid particles can be achieved through simple technology, and with minimal system exergy losses(Xu, et al., 2011).

Considering the above, the solar-aided gasification scenario employs desert sand as the working substance, heat carrier for the gasifier, and thermal energy storage medium. The ability of desert sand to act as a thermal energy storage material for solar receivers has been demonstrated in previous studies (Radwan, et al., 2021); (Hamdan, et al., 2020); (Diago, et al., 2018); (Diago, et al., 2016); (Diago, et al., 2015). Also, desert sand is a widely available resource that is currently unused. It can exhibit an average heat capacity as high as 926.1 $J \cdot kg^{-1} \cdot K^{-1}$ when heated in the range of 150 to 1100 °C (Diago, et al., 2015).

The solar-aided gasifier is configured in such a way that a pneumatic riser drops cold sand into the receiver, which is surrounded by heliostat reflectors. The sand is then heated to 980 ^{o}C before being fed to the secondary reaction zone of the gasifier's bed. To minimize the formation of hot spots, a static mixer is placed at the receiver's exit. The mixer is also expected to prevent sand agglomeration which, as discussed by Diago, et al., (2016) could occur at temperatures in the vicinity of 1000 ^{o}C and above. Heat lost during mixing was assumed to be marginal, hence the hot sand exited the receiver at a temperature of 980 ^{o}C. It should be noted that the propensity for agglomeration to take place is a function of sand composition and purity. For instance, when pure quartzose sand is used (≥99% quartz), agglomeration only occurs at temperatures above 1200 °C (Radwan, et al., 2021).

An illustration of material flow in the solar-aided gasifier is shown in Figure 4.7. For simplicity's sake, it was assumed that both the gasification and pyrolysis reaction mechanisms were similar to the ones taking place in the standalone dual-bed gasifier. During operation, the mixture of char and cold sand exiting the gasification bed is fed to a settling tank separator where the sand is recovered at the bottom, and the less dense char is captured at the surface and then exported as a co-product. A natural convection dryer is then used to remove excess moisture from the sand before being recycled back to the solar receiver.

Despite the fact that the heat capacity of desert sand (926 $J \cdot kg^{-1} \cdot K^{-1}$) (Diago, et al., 2015), is almost 60% that of molten salts (1542 $J \cdot kg^{-1} \cdot K^{-1}$) generally used for thermal energy storage (Sadeghi, 2022), the process was simulated with molten salt as working substance. This is because the simulation software used to model the solar field (SAM) is based on molten salt as the working substance and does not include sand as an option.

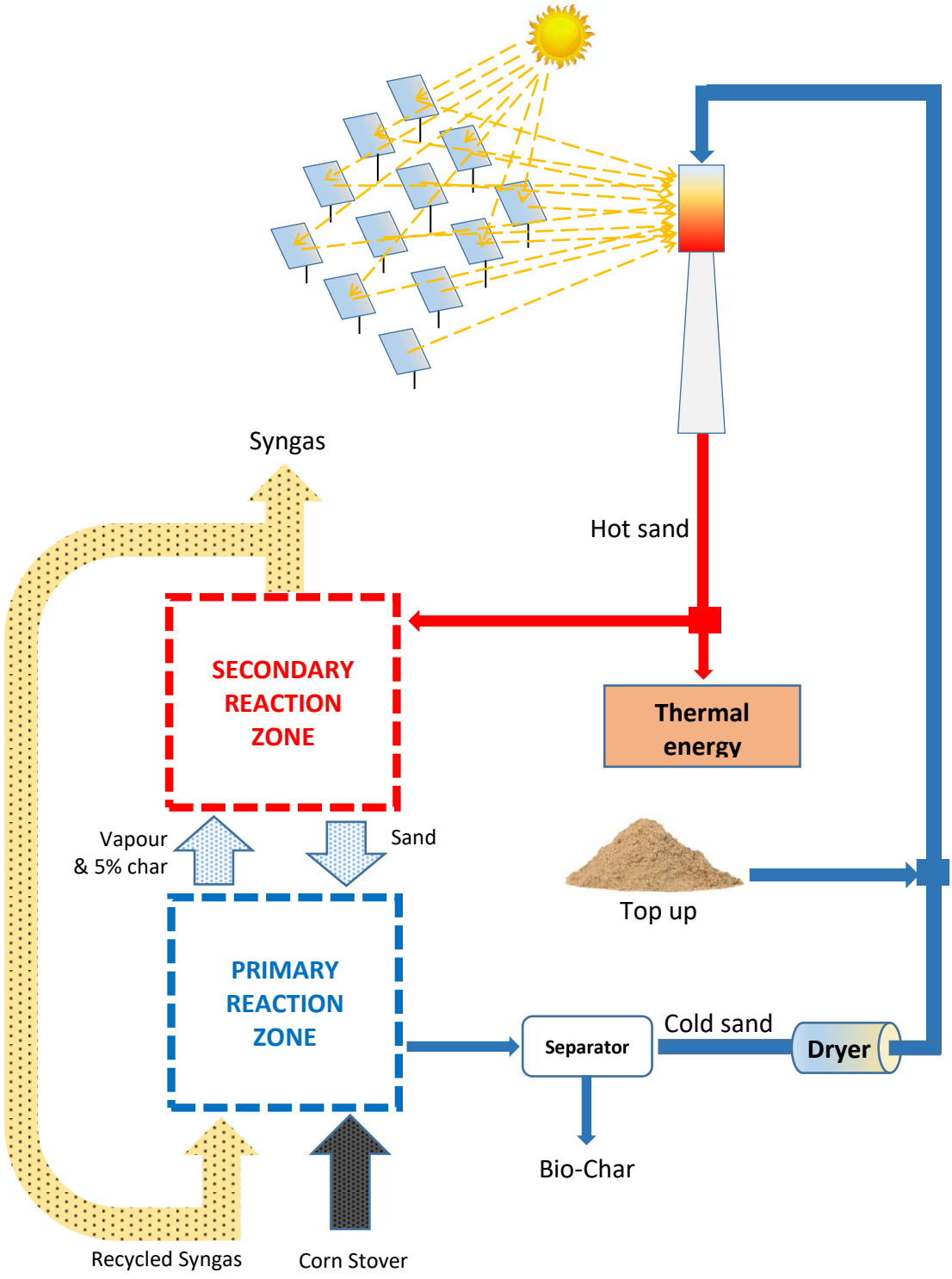

Figure 4.7: Illustration of material flow considered during the modelling of the proposed solar-aided gasifier

Moreover, considering the intermittent nature of sunlight, the field used to harness solar energy was designed to supply a heat load 50% greater than the gasifier's thermal energy requirements. Thus, extra thermal energy was continually stored in the form of hot sand to cater for night-time operations and hours of unfavourable solar irradiance. This would

minimize any unplanned production interruptions. Moreover, the oversized solar field was also a way to mitigate the effects of unforeseen disruptions in weather patterns during the biorefinery's lifespan.

4.6.2 Modelling of solar field

The design parameters of the gasifier's solar receiver are shown in Table 4.6. The System Advisor Model (SAM) was used to estimate the solar field size as well as the capital and variable costs of the solar power system. The weather data files for the plant location (Free State – South Africa) were obtained from the European Commission's Photovoltaic Geographical Information System (PVGIS, 2017).

Table 4.6: Design parameters of the solar receivers used in solar-aided gasification

Solar multiple	0.68
Design point DNI (W/m^2)	950
Receiver design thermal power (MWth)	187.3
Receiver start-up delay time	0.2
Receiver start-up delay energy fraction	0.25
Heat loss factor	1
Heat transfer fluid	Salt (60% $NaNO_3$ 40% KNO_3)

Also, as previously done in the solar-aided biological conversion process (chapter 3), the solar field was sized to sustain both daytime and night-time operations. Also, molten salt and lithium-ion batteries capable of powering the plant for 15 hours per day were employed as energy storage media for CSP/CST and PV respectively. Thus, surplus solar energy was continuously stored for use at night and on low-irradiance days.

4.7 Syngas cleaning and conditioning

Syngas produced through gasification processes generally contains contaminants. Tar, which is one of these contaminants, is a mixture of condensable organic compounds (Monir, et al., 2020). It includes single-ring to five-ring aromatic compounds, as well as other oxygenated hydrocarbons and polycyclic aromatic hydrocarbons (PAH) (Li & Suzuki, 2010). Tar compounds in the syngas can clog filters, block valves, and even cause premature corrosion of pipes (Pranolo, et al., 2022). As a result, maintenance intervals are increased and the production cost of syngas is adversely affected (Li & Suzuki, 2010). It is therefore essential to remove tar prior to downstream processing.

In order to remove tar contaminants, syngas exiting the gasifier was fed to a tar reformer similar to the one developed by Spath, et al., (2005) was used. During tar reforming, 90% of tar compounds were converted into CO and H_2, as well as 70% of benzene and 20% of methane. These conversion yields were obtained from the design performance of Spath, et al., (2005) tar reformer. Also, as per Spath, et al., (2005)'s design, the tar reformer was operated at 750 ^oC.

Because the syngas generated was intended for the production of methanol through CO and CO_2 hydrogenation, a few critical requirements needed to be met. Firstly, the stoichiometric number (SN) which is defined as the molar ratio of ($H_2 – CO_2$) to ($CO + CO_2$) should be equal to 2 (or slightly above 2 to minimize the formation of side products). Secondly, the carbon oxide ratio defined as the molar ratio of CO_2 to ($CO + CO_2$) should be lower than 0.6 (Nestler, et al., 2020).

Considering that the syngas generated in both the standalone and solar-aided gasification processes was relatively poor in H_2, with the carbon oxide ratio well above 0.6, a syngas enrichment step was required before methanol synthesis. This step consisted of a water-gas shift reaction followed by CO_2 removal via amine-based chemical absorption. The water-gas shift reaction was performed in two steps: a high-temperature water-gas shift at 350 ^oC followed by a low-temperature water-gas shift performed at 230 ^oC. Both reactors were modelled using CHEMCAD's built-in equilibrium data. The operating conditions of the water gas shift reactors are provided in Table 4.7.

Table 4.7: Characteristics of water gas shift reactors

Feed composition	Unit	Value
CO	% (mol/mol)	38
CO_2		12
H_2		43
CH_4		7
Reactor		
Steam/CO ratio	n/a	6
Inlet gas pressure	bar	20
Temperature of reactor 1	^oC	350
Temperature of reactor 2	^oC	230

Monoethanolamine (MEA) was used as the chemical solvent for absorption and was modelled using data from Götz, et al., (2012). Its amine solution regeneration sub-process consumed 3.3 MJ of thermal energy per kg of CO_2 removed, and the flow rate of amine solution was adjusted to achieve 69% (mol/mol) CO_2 removal. This resulted in syngas having a stoichiometry number of 2.98 and a CO_2 to (CO + CO_2) ratio of 0.50. Figure 4.8 shows a flowsheet for syngas cleaning and conditioning processes.

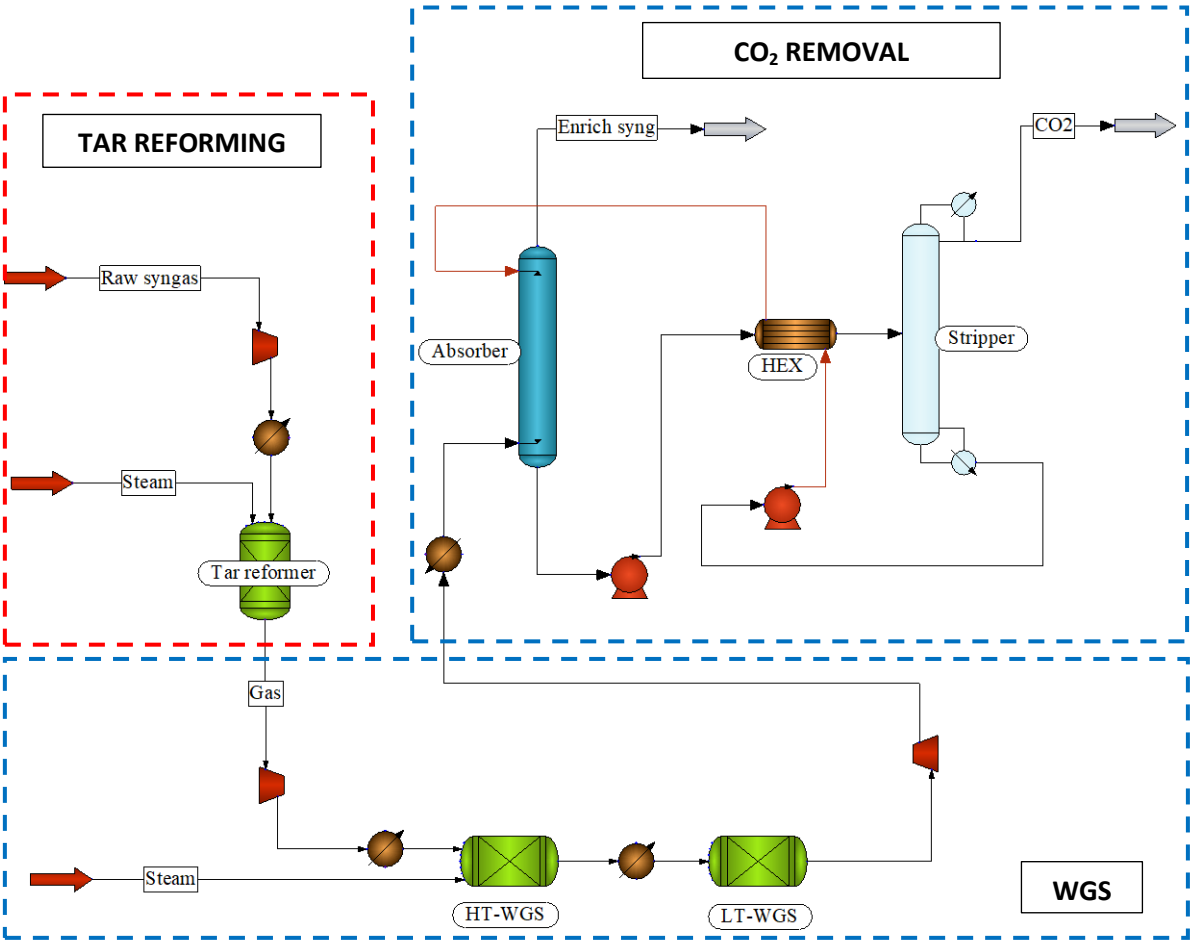

Figure 4.8: Flowsheet of syngas cleaning and conditioning processes

4.8 Syngas upgrade into methanol

The synthesis of methanol from syngas is a well-studied high-temperature high-pressure exothermic process typically carried out in a fixed bed tubular reactor loaded with a Cu/Zn/Al_2O_3 catalyst. The synthesis generally takes place at temperatures above 200°C to optimize the reaction rate, and below 300°C to avoid premature catalyst deactivation

(Nestler, et al., 2020). The pressure is typically in the range 50 – 150 atm (GhasemiKafrudi, et al., 2022); (Yang & Ge, 2016); (Van-Dal & Bouallou, 2013). The main chemical reactions occurring inside the reactor are as follows:

CO_2 hydrogenation: $CO_2 + 3H_2 \leftrightarrow CH_3OH + H_2O$ ΔH_R = - 50 kJ.mol^{-1} Eq. 4.2

Water-gas-shift reaction: $CO + H_2O \leftrightarrow CO_2 + H_2$ ΔH_R = - 41 kJ.mol^{-1} Eq. 4.3

CO hydrogenation: $CO + 2H_2 \leftrightarrow CH_3OH$ ΔH_R = -91 kJ.mol^{-1} Eq. 4.4

4.8.1 Reaction kinetics

Kinetic data were obtained from Bussche & Froment (1996), which is one of the pioneer works conducted on the kinetic modelling of methanol synthesis. This model is known to reliably predict the methanol yield and has been employed in a multitude of studies involving the modelling of methanol synthesis from syngas (Leonzio, et al., 2019); (Rafael Oliveira, et al., 2018); (Luyben, 2010).

$$r_{Methanol} = \left(k'_{5a}K'_2K'_3K'_4K_{H_2}P_{CO_2}P_{H_2}\right)\frac{\left[1-1/K^*\left(\frac{P_{CH_3OH}P_{H_2O}}{P_{CO_2}P_{H_2}^3}\right)\right]}{\left[1+k_3\left(P_{H_2O}/P_{H_2}\right)+k_1\sqrt{P_{H_2}}+k_2P_{H_2O}\right]^3} \quad \text{Eq. 4.5}$$

$$r_{RWGS} = \left(k'_1P_{CO_2}\right)\frac{\left[1-K_3^*\left(\frac{\left(P_{H_2O}P_{CO}/P_{CO_2}P_{H_2}\right)}{P_{CO_2}P_{H_2}}\right)\right]}{\left[\left[1+\left(K_{H_2O}/K_8K_9K_{H_2}\right)\left(P_{H_2O}/P_{H_2}\right)+\sqrt{K_{H_2}P_{H_2}}+K_{H_2O}P_{H_2O}\right]\right]} \quad \text{Eq. 4.6}$$

Table 4.8: Kinetic data constants used to predict methanol yield (Bussche & Froment, 1996)

	Unit	Kinetic parameter
$\boldsymbol{k'_{5a}K'_2K'_3K'_4K_{H_2}P_{CO_2}}$	$mol \cdot kg_{cat}^{-1}s^{-1}Pa^{-2}$	$1.07 \times 10^{-3}exp^{\frac{36696}{R.T}}$
$\boldsymbol{k'_1}$	$mol \cdot kg_{cat}^{-1}s^{-1}Pa^{-2}$	$1.22 \times 10^{9}exp^{\frac{94765}{R.T}}$
$\boldsymbol{K_{H_2O}/K_8K_9K_{H_2}}$	-	3.45338
$\sqrt{\boldsymbol{K_{H_2}P_{H_2}}}$	$Pa^{-0.5}$	$31.578 \times 10^{-3}exp^{\frac{17197}{R.T}}$
$\boldsymbol{K_{H_2O}}$	Pa^{-1}	$6.62 \times 10^{-16}exp^{\frac{124119}{R.T}}$

Bussche & Froment (1996)'s kinetic model is described by LHHW-type equations (Langmuir-Hinshelwood-Hougen-Watson) whereby the main kinetic term is multiplied by the ratio of the driving force term to the adsorption term (refer to equations 5 and 6). It should be noted that this kinetic model only accounts for the reverse water gas shift and CO_2 hydrogenation. Hence, CO hydrogenation is ignored. This is to remain consistent with experimental results which suggest that methanol is largely produced via CO_2 hydrogenation (Lee, et al., 1993); (Chinchen, et al., 1987). Kinetic data used to predict the conversion yield can be found in Table 4.8.

4.8.2 Characteristics of methanol reactor

Industrial reactors used for methanol synthesis are generally "Lurgi type" (Walid, et al., 2018); (Chen, et al., 2011); (Yusup, et al., 2010). Thus, they comprise a shell and tubes. The catalysts are packed inside the tubes, and the incoming syngas is allowed to flow through the catalyst bed. Considering the exothermic nature of chemical reactions occurring during methanol synthesis (refer to Equations 1, 2 and 3), a cooling stream is circulated through the shell for cooling and heat recovery. Water was used in this study as the cooling stream.

Since the design and optimization of a methanol synthesis reactor was beyond the scope of this study, the characteristics of the Lurgi reactor used to model methanol synthesis were obtained from Yusup, et al. (2010). These characteristics are summarized in Table 4.9, and they were obtained from an existing methanol plant. Interestingly, these characteristics are similar to those of the industrial methanol reactors described in Chen, et al., (2011). Notably, the stoichiometric number and carbon oxide ratio of the syngas used by Yusup, et al. (2010) were 3.20 and 0.51 respectively, which is close to the figures of the enrich syngas obtained in this study (section 4.7).

Considering that the syngas flow rate used in Yusup, et al. (2010)'s industrial reactor (40 789 kmol/hr) was considerably higher than the present work (14 200 kmol/hr), a scaling exercise was required. Scaling was based on the residence time of syngas in the reactor. Thus, the number of tubes in the reactor's shell was calculated to match Yusup, et al. (2010)'s residence time. The other reactor characteristics were the same as Yusup, et al. (2010). The syngas inlet temperature and pressure were both 225 ^{o}C and 82 bar,

respectively, in accordance with Yusup, et al. (2010). Also, the reactor shell was maintained at 250 ^{o}C.

Table 4.9: Characteristics of methanol reactor used during modelling

	Unit	Value
Inner diameter	m	0.0445
Outer diameter	m	0.0485
Number of tubes	n/a	1672
Tube length	m	7.260
Catalyst density	kg/m^3	1100
Catalyst porosity	m_g^3/m_g^3	0.4

NB. It was assumed that during methanol synthesis, the catalyst effectiveness would remain constant.

4.8.3 Methanol purification

The product stream exiting the methanol reactor consists mainly of methanol, water and unconverted syngas. To purify the methanol, the product stream is cooled to 38 ^{o}C, and subsequently fed to a flash tank operating at 106 bar. As previously shown by Luyben, (2010), the relatively high pressure allowed nearly the entire methanol to be recovered as liquid. After flashing, a portion of unconverted syngas is recovered in the vapour outlet, while a methanol-rich liquor is obtained in the liquid outlet. The liquid stream from the first flash tank is then fed to a second flash tank operating at 2 bar to further removed unconverted syngas. The syngas recovered in the vapour outlets of both flash columns is recycled back to the methanol reactor to maximize carbon-to-methanol conversion. The methanol-rich liquor exiting the second flash tank is fed to a distillation column where it is enriched to 99% (vol/vol) purity. A flowsheet illustrating the syngas to methanol conversion process can be found in Figure 4.9.

As typically done in syngas-to-methanol conversion processes (Luyben, 2010); (Pérez-Fortes, et al., 2016); (Van-Dal & Bouallou, 2013), a small fraction of unconverted syngas (1% mol/mol in this case) is purged to prevent inert gases such as CH_4 from accumulating in the reactor, and the remainder is fed to the flash columns. The off-gas (purge stream) is then combusted on-site for heat and electricity generation.

4.9 Heat and power generation

In the standalone scenario, a portion of biomass was combusted to generate steam used in the distillation column to purify methanol, and the electrical energy required to operate the compressors and pumps. While in the solar-aided scenario, solar PV was used for electricity generation and solar thermal was utilized to produce steam. Solar PV was preferred over CSP for electricity generation mainly because it was shown in the previous chapter that the former requires less land (refer to Table 3.5 of Chapter 3). Additionally, solar PV has a lower cost (refer to Table 6.1 of Chapter 6). It should be noted that in the steam and power generation area, unconverted syngas from the methanol synthesis area was combusted in a combined heat and power generation (CHP) system for steam and electricity production. While the biochar formed in gasifier bed was combusted in the combustion bed

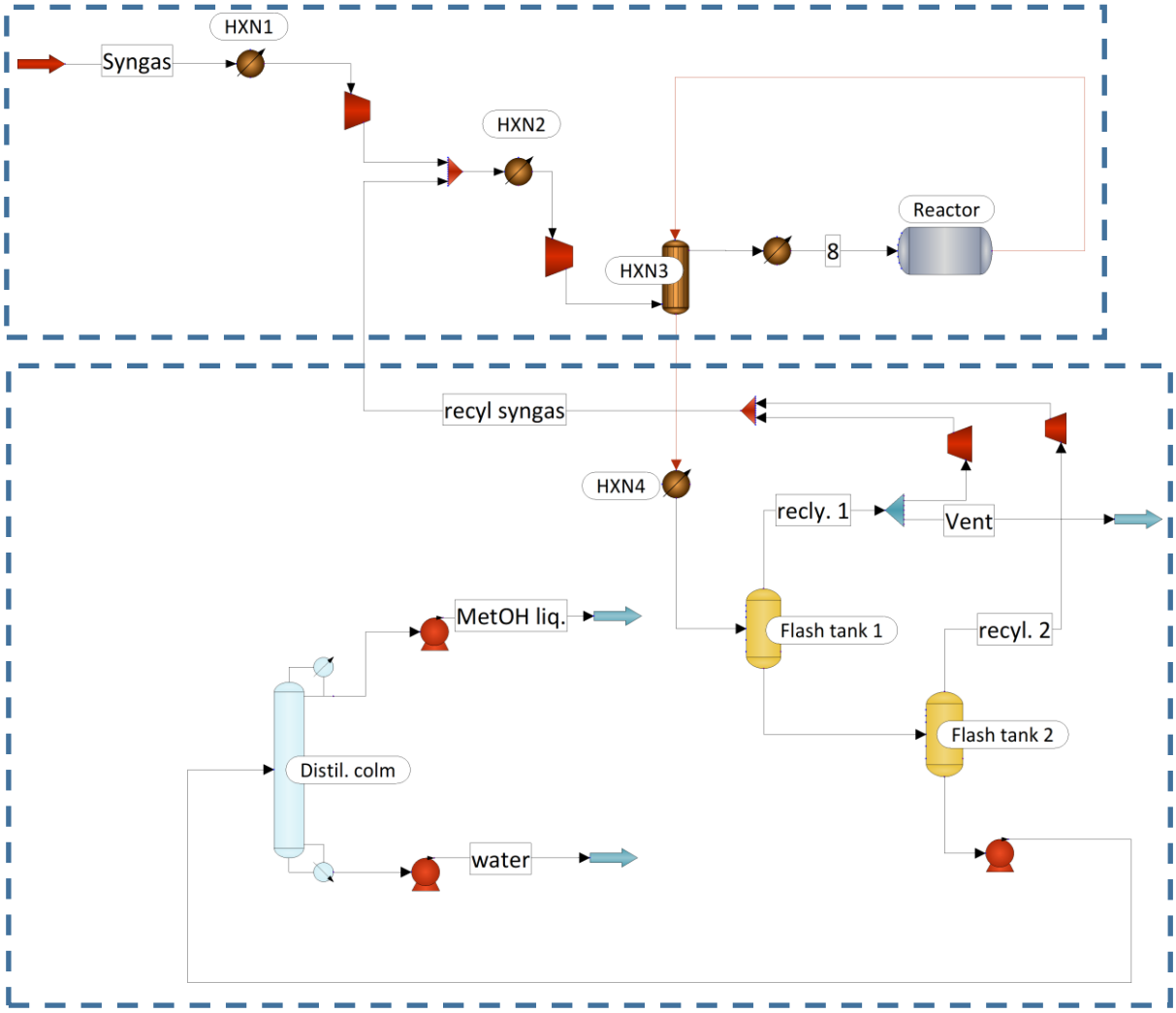

Figure 4.9: Flowsheet for the conversion of syngas into methanol

4.10 Conversion efficiency

Conversion efficiency is an essential key performance indicator used in energy conversion systems such as biorefineries. Four types of conversion efficiency were considered in this chapter: carbon conversion efficiency (CCE), net gasification efficiency, liquid fuel efficiency and overall energy conversion efficiency. The first is illustrated in equation 4.7 and represents the percentage of carbon in the biomass that is converted into methanol.

$$\eta_{CCE}\ (\%) = \frac{Carbon\ content\ in\ methanol\ \times Flow\ rate\ of\ methanol}{Carbon\ content\ in\ biomass\ feedstock \times Biomass\ fow\ rate} \qquad \text{Eq. 4.7}$$

The second is net gasification efficiency. It was applied around the gasification process (refer to equation 4.8), and was computed as the ratio of the net thermal energy of "the syngas products plus biochar co-product" to the net thermal energy of the biomass feedstock. The third efficiency used (refer to equation 4.9) was the liquid fuel efficiency, and was obtained from Hamelinck, et al., (2005). It was analogous to equation 3.2 applied in chapter 3. It should be noted that, in order to account for the portion of feedstock energy contained in the co-product, the thermal energy of co-product credit was subtracted from biomass feedstock. Thus, equation 4.9 measures the capability of the process to produce liquid fuel from the portion of the feedstock energy that is effectively gasified, leaving out the portion converted to biochar.

$$\eta_{gas.Net}\ (\%) = \frac{Flow\ rate\ of\ syngas \times LHV_{syngas} + LHV_{co-product\ credit}}{LHV_{biomass} \times Biomass\ input} \qquad \text{Eq. 4.8}$$

$$\eta_{liquid\ fuel} = \frac{LHV_{methanol}}{LHV_{biomass} \times Biomass\ input - LHV_{co-product\ credit}} \qquad \text{Eq. 4.9}$$

The last conversion efficiency considered is referred to as biomass overall energy conversion efficiency. It is applied around the entire biorefinery. Biomass energy conversion efficiency was calculated as illustrated in equation 4.10, and takes into account the solar energy input where applicable, as well as the thermal energy of all

products fuels including biochar. Also, in all the equations, the LHV of syngas was calculated by adding up the LHV of H_2, CO and CH_4 exiting the gasifier

$$\eta_{Overall\ energ.\ conv.}(\%) = \frac{LHV_{methanol} \times Flow\ rate\ of\ methanol + LHV_{biochar} \times Biochar\ output}{LHV_{biomass} \times Total\ biomass\ input + Solar\ energy\ input}$$

Eq. 4.10

4.11 Modelling results and discussions

4.11.1 Standalone gasification

4.11.1.1 Model validation

To validate the gasifier's model, TNEE gasifier parameters shown in Table 4.5 were used in the simulation, and the syngas composition obtained was compared to experimental data reported by Gourtay, et al., (1987). Considering that Gourtay, et al., (1987)'s results were based on woody biomass, the pyrolysis correlation used for the model validation exercise was for woodchips and was obtained from Abdelouahed, (2012).

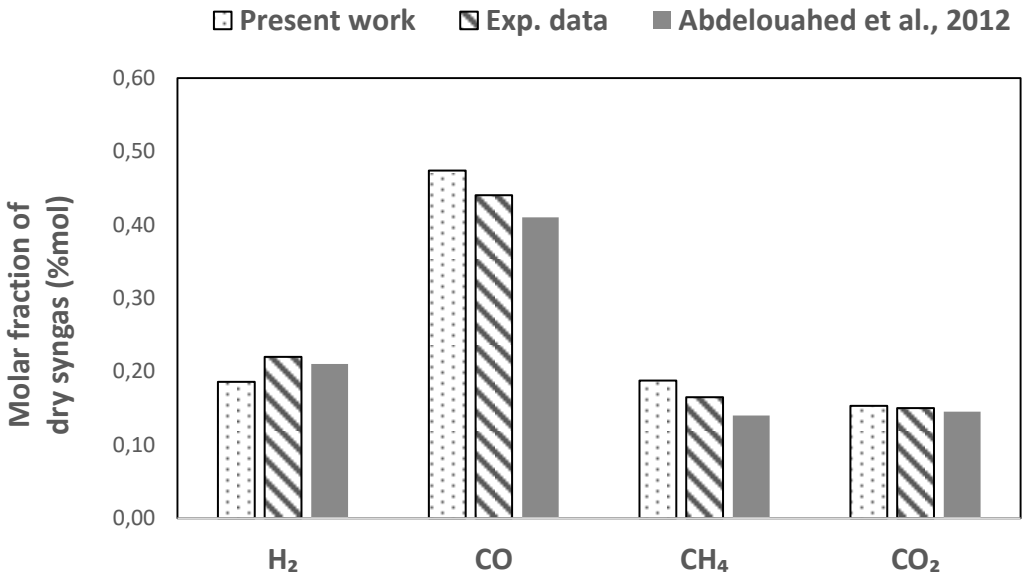

Figure 4.10: Comparison between syngas composition obtained during experimental works and present model. The gasifier operating conditions can be found in Table 4.5

As can be seen in Figure 4.10, the simulation results from this work and experimental data from Gourtay, et al., (1987) are in reasonable agreement. Hence, the gasification model developed in this work can predict the syngas composition of a TNEE-type dual bed gasifier. Furthermore, although the present model predicted H_2 and CO_2 concentrations comparable to modelling results reported by Abdelouahed, (2012), discrepancies were nonetheless observed in the CO and CH_4 concentrations. Indeed, the CO and CH_4 concentrations predicted by the present model were respectively 19 and 33% greater than the ones reported by Abdelouahed, (2012). These discrepancies could be attributed to the differences in kinetic parameters employed to model chemical reactions taking

place in the secondary reaction zone. For instance, in Abdelouahed, (2012)'s study, the pre-exponential factor for Bustamante, (2005)'s forward WGS rate law was modified to ensure that it could predict syngas composition for both TNEE and FERCO-types dual bed reactors. However, the present work used Bustamante, (2005)'s published rate law.

4.11.1.2 Effect of temperature on syngas generation

The effect of gasification temperature on the syngas composition was studied by adjusting the quantity of biochar fed to the combustor and simultaneously monitoring both the temperature in the gasification zones and the corresponding syngas composition. It was found that by operating the combustor at 980 ^{o}C, temperatures of 760 and 960^{o}C are respectively achieved in the primary and secondary reaction zones. It is interesting to note that these temperatures are close to the 760 and 948 ^{o}C obtained by Abdelouahed, (2012) using woodchips as feedstock. Figure 4.11 shows the dry syngas molar ratios as a function of combustor temperature. Note that the quantity of char formed in the gasification bed was insufficient to maintain the combustor at 1060 ^{o}C. Thus, in this particular case, additional corn stover fuel was combusted alongside char in the combustion bed.

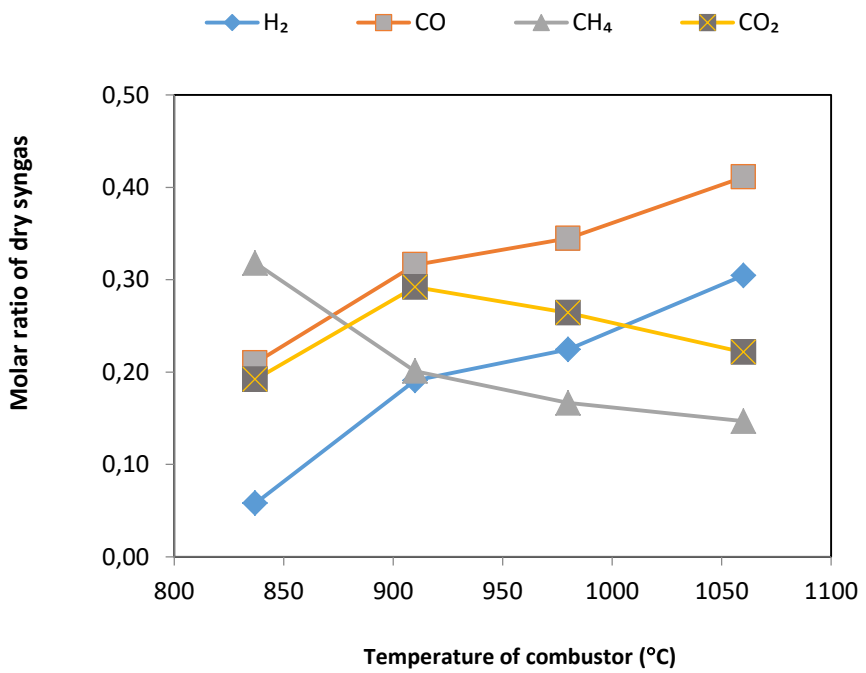

Gasifier Temperature profile (°C)	**Combustor**	**837**	**910**	**980**	**1060**
	Secondary reaction zone	786	884	960	1045
	Primary reaction zone	470	671	760	862

Figure 4.11: Effect of gasifier temperature on dry syngas flow rate

Moreover, it was observed that the H_2 and CO molar flow rates increased with an increasing gasification temperature. In contrast, the CH_4 flow rate followed the opposite trend. In addition, the CO_2 flow rate was found to increase with increasing temperatures, and then reach a plateau before subsequently decreasing. Although relatively high temperatures favoured the formation of H_2 and CO, it must be noted that the melting point for biomass ash is typically in the range of 1000 - 1100 °C (Link, et al., 2022); (Iqbal & Lewandowski, 2016). Therefore, reaching temperatures of that magnitude in the combustor is likely to lead to ash agglomeration, which in turn will compromise bed fluidization. Thus, to prevent potential bed agglomeration caused by melting ash, the combustor was operated at 980 ^{o}C.

4.11.1.3 Effect of biomass moisture content on gasifier's performance

The effect of biomass moisture on the syngas composition was studied by using a corn stover feedstock of various moisture content while operating the combustor at 980 ^{o}C. Hence, only the biomass moisture content was adjusted in the simulation. Figure 4.12 shows the syngas molar ratio at different biomass moisture content.

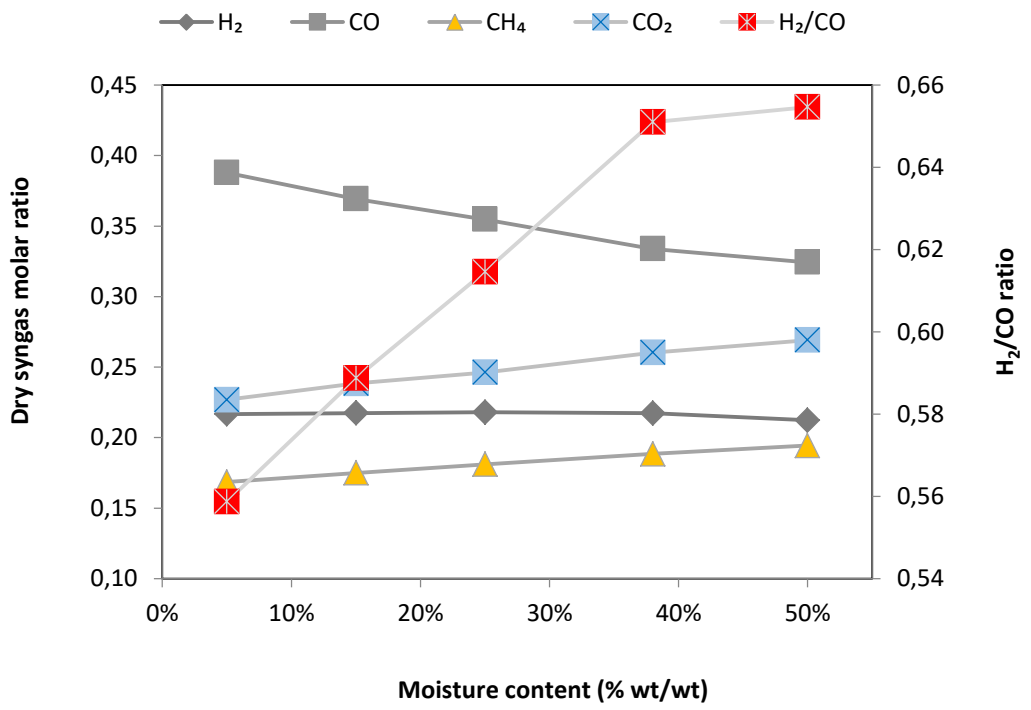

Figure 4.12: Dry syngas molar fraction and H_2/CO ratio as a function of feedstock moisture

As can be seen in Figure 4.12, the H_2 molar fraction almost remains unchanged as the moisture content increases while the CO molar fraction decreases. Moreover, CO_2 concentration increases considerably with increasing moisture content while CH_4 only shows a slight increase. The marginally affected H_2 concentration could be attributed to the fact that changes in moisture content have a more pronounced impact on the temperature of the primary reaction zone and a lesser effect on the secondary reaction zone temperature (refer to Table 4.10). Indeed, when feedstock with relatively high moisture is fed to the gasifier, extra thermal energy is required in the primary reaction zone for water evaporation, which results in a greater drop in temperature compared to the secondary reaction zone. Consequently, a gas such as H_2 which is mainly generated in the secondary reaction zone via methane and tar cracking would be less affected by variations in moisture content.

Moreover, the H_2/CO ratio was found to increase with increasing biomass moisture content. For instance, the lowest H_2/CO ratio was found to be 0.56 and was obtained when the moisture content was set to 5% (wt/wt), while the maximum H_2/CO ratio was 0.65 and was achieved at 50% (wt/wt) moisture content. Although high corn stover moisture appeared to favour an elevated H_2/CO ratio, it should be noted that variations in H_2/CO were mainly due to CO decreasing with increasing moisture content, while H_2 only marginally changed.

Also, it was found that when the feedstock had 50% (wt/wt) moisture content, the combustor needed external thermal energy input in addition to the heat from combusted biochar to attain a temperature of 980^{o}C. This external energy was estimated to be equivalent to about 6% of corn stover LHV. Therefore, the option of using corn stover with 50% (wt/wt) moisture content is unfavourable, as it compromises the energy self-sufficiency of the gasifier.

It is interesting to note that the present model, which is based on TNEE gasifier technology, does not involve the injection of steam into the gasification bed. Hence, as discussed by Donnot, et al., (1985), steam formed in this type of gasifier technology is exclusively from two sources: the moisture fraction of the biomass and the pyrolysis reactions occurring in the primary reaction zone. Therefore, utilizing biomass with

relatively high moisture content favours steam formation inside the gasifier. Although as shown in Table 4.10, steam formation via the evaporation of water-bound biomass inside the reactor lowers the bed temperature and minimizes the syngas calorific value. Similar trends have also been observed in other studies on biomass gasification (Doherty, et al., 2009); (Atnaw, et al., 2014); (Kirsanovs, et al., 2017). Thus, the present study recommends that corn stover be processed in a TNEE-type gasifier with a moisture content close to 15% (wt/wt).

Table 4.10: Effect of biomass moisture content on gasifier performance

Biomass moisture content (% wt/wt)	5	15	25	38	50
Combustor (°C)	980	980	980	980	980
Primary zone (°C)	871	850	817	761	684
Secondary zone (°C)	974	972	969	960	944
Syngas calorific value (MJ/kg)	13.5	13.2	13.0	12.6	12.5

The effects of feedstock moisture content and processing temperature could not be compared against experimental results because the data available on biomass gasification using TNEE-type technology do not specify the impact of processing parameters on the syngas composition. Thus, further experimental studies will be necessary to evaluate the accuracy of simulation results obtained. Moreover, the outcome of such studies is likely to contribute to the optimization of TNEE gasification technology.

4.11.2 Impact of solar hybridization on gasification efficiency

The incorporation of solar energy as the unique thermal energy source for the gasification reactions implied that biochar did not have to be combusted. As a result, the gasifier could generate two energy products: syngas and biochar. Thus, as promoted by the circular economy production model, carbon is kept in the system instead of ending up as CO_2. By assuming syngas to be the main product and biochar the co-product, energy credit status can be assigned to the biochar as per Equation 5, which results in an enhanced net gasification efficiency as shown in Figure 4.13. Therefore, it can be deduced that the incorporation of solar energy as the heat source of a TNEE-type gasifier could enhance the net gasification efficiency by 56 to 87%, depending on the biomass moisture

content. The enhancement in net gasification efficiency is mainly due to exported biochar, given that sand is entirely heated using solar energy.

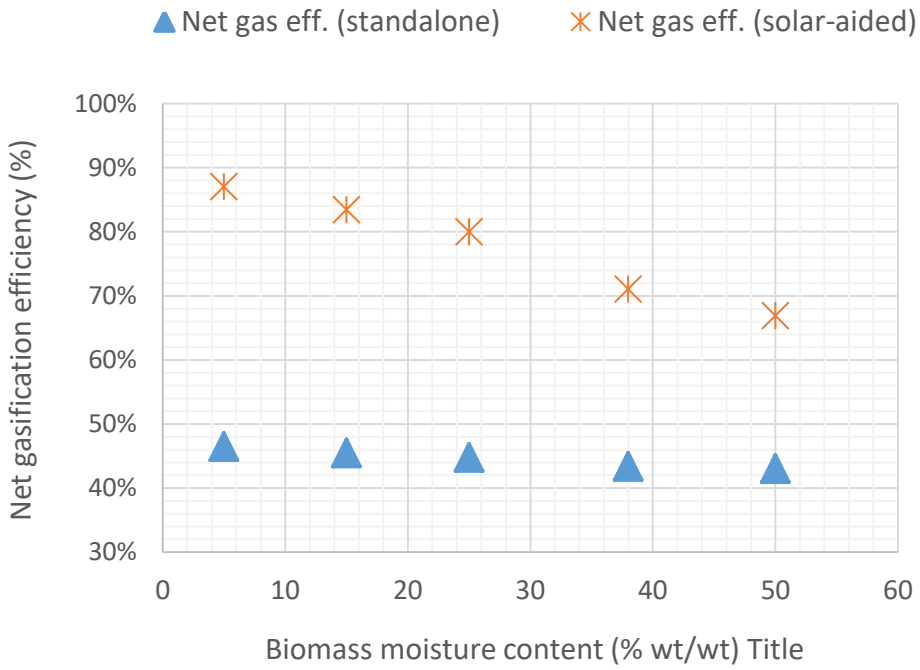

Figure 4.13: Net gasification efficiency for standalone and solar-aided scenarios

It is worth emphasizing that despite the enhancement in net gasification efficiency, the syngas flow rate remains identical to the standalone scenario. Thus, the incorporation of solar energy does not mean that more syngas is produced; rather, it virtually allows the storage of intermittent solar energy in a dispatchable bio-char form, which can then be used on-demand as bio-fertilizer, fuel, or starting materials for the production of other bio-materials.

Moreover, as shown in Figure 4.13, the use of high moisture content corn stover feedstock in a TNEE gasifier has a detrimental effect on the net gasification efficiency, with or without solar energy incorporation. This trend can be attributed to two factors: firstly, the syngas calorific value which increases with decreasing moisture content. Secondly, the drier the biomass, the lesser the fraction of biochar needed to be combusted to achieve 980^{o}C in the combustor, and the greater the fraction of biochar that can be exported as a credit.

4.11.3 Methanol production rate

The single-pass conversion of CO_2 and CO to methanol was 21% (mol/mol), which is relatively low. The relatively low yield was due to the chemical reactions being limited by thermodynamic equilibrium. To improve the yield, the unconverted syngas was recycled back to the reactor as commonly done in methanol synthesis (Luyben, 2010); (Yusup, et al., 2010); (Løvik, 2001). After the implementation of a recycled loop, the overall conversion of CO_2 and CO comprised in the fresh syngas, to the methanol exiting the reactor, was enhanced to 97% (mol/mol). This Figure was comparable to the 96% reported by Luyben, (2010) using similar process conditions, and the 99% reported by Yusup, et al., (2010). After purification via flashing and distillation, 1055 kmol/hr of methanol was recovered from the distillation column. Thus, the biorefinery produced 270 418 tonnes of methanol per year (assuming 8 000 yearly operating hours).

The carbon conversion efficiency, which is an estimation of how much carbon initially present in the feedstock is converted into methanol was calculated to be 31.0%. The overall energy conversion efficiency on the other hand was found to be 48.1% for the standalone scenario and 61.5% for the solar-aided scenario. The liquid only efficiencies as defined in Equation 4.9 were respectively found to be 42.3% and 70.8% for the standalone and solar-aided scenarios.

It is worth mentioning that despite increasing the methanol conversion yield, the implementation of a recycling loop is energy-intensive. This is because the large volumes of unconverted syngas have to be compressed before being recycled back to the reactor. This, in turn, impacts the plant's electrical energy demand. Further information on the effect of the recycling loop on methanol production can be found in Luyben, (2010).

4.12 Energy analysis of thermochemical conversion

Process energy demand for all scenarios was found to be 2.16 $MJ/kg_{methanol}$ for electrical energy, 1.26 $MJ/kg_{methanol}$ for heat utility, and 0.10 $MJ/kg_{methanol}$ for fossil energy (fuel consumed by trucks during biomass transportation). The thermal energy demand for the gasifier was 21.6 $MJ/kg_{methanol}$, which is equivalent to the calorific value of bio-char exported as a co-product. As can be seen in Table 4.11, in all scenarios, the net energy ratio was above 1 and the net energy output was positive. Thus, the products contained

more energy than what was required by the process. Furthermore, the export of biochar in the solar-aided scenario combined with the utilization of solar energy resulted in increases in both the net energy output and the net energy ratio.

Table 4.11: Net energy of corn stover-to-methanol biorefinery

	Scenario 1	Scenario 2
ENERGY OUTPUT (MJ/kg of methanol produced)		
Bio-methanol	27.0	27.0
Biochar co-product	0.0	21.6
NET ENERGY		
Net energy output [a] (MJ/kg of methanol produced)	1.9	23.5
Net energy ratio [b]	1.1	1.9

[a] Net energy ratio = |energy output/energy demand|. NB. Energy output includes the energy contents of the biofuels and the energetic co-products. [b] Net energy output = total energy output – total energy demand. *Value of net energy output/ratio if the energy content of lignin-residues is considered in the calculations

4.13 Land requirement

A summary of land requirements for the solar field is displayed in Table 4.12. As can be seen, the incorporation of solar energy could require a total land area of 6.92 km^2. Note that this Figure does not include the refinery site, which on its own, could be as little as 3 km^2 if the refinery was to match a medium size crude oil refinery such as Fos-sur-Mer refinery located in southern France (ESSO, 2019). Or, as large as 8 km^2 if the refinery site was to have a surface area comparable to SASOL's coal and gas refinery located in South Africa (SASOL, 2000).

Table 4.12: Requirements for solar power systems

	km^2
Total land area for CST of Heating utilities	0.11
Total land area for solar PV	2.98
Total land area for solar-aided gasification	3.83
Overall land required for solar field	6.92

4.14 Conclusion

This chapter explained the method used to design the corn stover-to-methanol refinery. Both standalone and solar-aided scenarios were described in detail. Also presented were

the criteria used to evaluate conversion efficiency. Detailed analysis and discussion of the modelling results were conducted. Considering that the main input point for solar energy was the gasifier, an emphasis was placed on the gasifier's performance. Considering the results obtained, it can be said that although the deployment of solar-aided gasifiers could enhance gasification efficiency and overall conversion efficiency, it will also adversely affect the biorefinery's physical footprint. The next chapter will focus on process economic modelling and evaluation of environmental impact.

CHAPTER 5 – ECONOMIC MODELLING AND ENVIRONMENTAL STUDY

5.1 Introduction

There is a global consensus among scientists and engineers that sustainable development should satisfy three main aspects: social, economic, and environmental (Tanzil & Beloff, 2006); (Krajnc & Glavič, 2003); (Azapagic & Perdan, 2000); (Sikdar, 2003); (Bakshi, & Fiksel, 2003). Therefore, in order to sustainably produce lignocellulosic biofuels, the production process should be socially beneficial, increase wealth, and be environmentally friendly. The purpose of this chapter is to explain how the economic performance and environmental impact of biorefineries modelled in chapters 3 and 4 were evaluated.

5.2 Economic modelling

Economic modelling is an exercise generally performed to determine the feasibility of processes that are yet to be commercialised. It is an essential part of techno-economic studies, and has been carried out in several studies as a means to estimate the production cost of biofuels (Fedeli, et al., 2022); (Zewdie & Ali, 2022); (Do & Lim, 2016); (Quintero, et al., 2013); (Leibbrandt, 2010); (Shemfe, et al., 2015); (Swanson, et al., 2010). In this section, economic models are developed for the processes described in chapters 3 and 4. Cost data are obtained from various sources in the literature, and financial parameters are adapted to South Africa. It should be noted the acronym "$" refers to the United States dollar (USD).

5.2.1 Total capital investment

5.2.1.1 Fixed capital investment

The equipment cost for the corn stover-to-ethanol biorefinery was obtained from Tao, et al., (2014)'s report, and adjusted to the year 2020 using the chemical engineering plant cost index (CEPCI). Tao, et al., (2014)'s equipment cost was used because it is based on actual vendor's quotation. Hence, it should offer a better level of accuracy than estimates from cost charts or equations. Also, given that the capacity of the corn stover-to-ethanol refinery was similar to Tao, et al., (2014)'s design with comparable equipment size, a scaling step was not necessary. To remain consistent with prior design practices, the main components of the indirect costs (engineering and office construction cost, start-up costs, field expenses, prorateable expenses, and the project contingency) were respectively

assumed to be 20, 10, 10, 10 and 20% of the inside battery limit (ISBL) (Davis, et al., 2018); (Tao, et al., 2014)

For the corn stover-to-methanol biorefinery, the factorial method was used to estimate the cost for major equipment. The base installed cost for the standalone scenario was obtained from previous studies, and can be found in Table B-4 of the appendix section. Also, in all solar-aided scenarios (biological and thermochemical conversion), the capital cost of the solar power system was estimated using the system advisor model.

5.2.1.2 Working capital and land cost

Working capital was assumed to be 5% of the fixed capital investment for both ethanol and methanol biorefineries. The land cost on the other hand was initially assumed to be $ 1 million and subsequently adjusted in a sensitivity analysis. It should be noted that capital investment and operating costs for photovoltaic panels, solar thermal, and concentrated solar power used in the solar-aided scenarios were obtained from the 2017 version of the system advisor model.

5.2.1.3 Variable operating cost

The major raw material used in all scenarios is corn stover. In the biological conversion route, substantial quantities of sulphuric acid and ammonia were also used. The bulk prices of sulfuric acid and ammonia were estimated based on quotations received from local chemical suppliers, while the corn stover price was based on (Batidzirai, et al., 2016)'s maize residues cost estimate for South Africa. A cost escalation exercise was performed to account for inflation and align the price of corn stover with the 2020 financial year. Both the freshwater cost and waste disposal costs were obtained from 2019/2020's local municipality tariff booklet.

5.2.1.4 Fixed operating cost

The number of employees required to operate the biorefinery was assumed to be 60. This is identical to the number reported by Humbird et al., (2011) for the operation of a biorefinery of a similar scale (500 MWth). Labour cost for each position was deduced by scrutinizing equivalent positions posted on South African job adverts. Also, as suggested in Humbird et al., (2011)'s report, the annual maintenance cost and property insurance

(plus tax) were respectively estimated to be 3% of the inside battery limit and 0.7% of the fixed capital investment. The salary structure and the estimated number of employees are provided in Table B-1 of the appendix section.

5.2.2 Financial valuation and economic performances

Three main approaches can be used to value businesses, assets, or business interests. These include the income approach, market approach and asset approach (Hitchner, 2011). In the present work, the financial value of each biorefinery scenario is evaluated using the income approach. It involves estimating future cash flows through a discounted cash flow analysis. The financial merit of each scenario was assessed using a combination of Net Present Value (NPV) and Internal Rate of Return (IRR). A brief explanation of each of these is provided below.

Net present value (NPV): It represents the cash flow offset between prospected investment, future benefits, and terminal values over the lifetime of the project. A positive NPV means that the financial model used will result in a favourable trade-off of cash inflows over outflows throughout the project's lifetime; in other words, the project will be profitable if implemented. While a negative NPV implies that the business model used will not result in the creation of wealth; thus, the project will not be profitable (Helfert, 2000). The NPV was calculated by adding up the after-tax present value for all periods (refer to equation 5.1). The annual cash flow was estimated based on anticipated net earnings and expenses.

$$NPV = \sum_{n=1}^{n=t} \frac{CF_n}{(1+i)^n} = \quad \text{Eq. 5.1}$$

Where ***CFn*** is the cash flow in year *n*, ***t*** is the project life in years, and ***i*** is the discount rate

Internal rate of return (IRR): It is a discount rate at which the present value of future cash flows equals the cost of the investment. In other words, it is a discount rate that enables the net present value of the discounted cash flow to equal zero. One of the attractive features of the IRR is that it provides a single number summarising the financial merit of a

project or an investment. The higher the IRR of the project, the more net cash it is expected to generate if implemented (Ross, et al., 2016).

5.2.3 Key financial parameters

The biorefineries were assumed to have 25 years' life span, with 8000 hours of operation per year. To minimize the effect of temporary financial relief measures implemented during the COVID-19 pandemic, key financial parameters such as the income tax and prime lending interest rate were based on the pre-COVID-19 period, mainly on the year 2019. Also, the interest rate on debt financing was assumed to be the prime lending rate for the year 2019 (10%), plus an additional 2%. Surplus electricity was sold to the local municipality for 0.5 Rand/kWh (0.037$/kwh) which was equivalent to 40% of the 2019-2020 average electricity residential tariff in South Africa for non-local electricity (before VAT) (Eskom, 2021). For this study, we used an exchange rate of 17.5 $/ZAR for the US dollar to RSA rand. A summary of key financial parameters used during the modelling process is shown in Table 5.1.

Table 5.1: Key financial parameters used for modelling

Annual operating hours (hr)	8 000
Depreciation (straight line) (%)	10
Tax income (%)	28
Annual inflation & Yearly escalation (%)	8
Discount rate	10%
Debt/equity ratio	60/40
Dividend paid out (% of net profit)	25
Debt repayment period (year)	10
Salvage value (% of initial capital investment)	20

5.2.4 Biomass transportation cost

Since the cost of collecting and transporting biomass raw materials impacts the fuel production cost, some attempts have been made to determine the optimal collection radius. For instance, Singh, et al., (2010) conducted a comparative study on the transportation of loose biomass in Sweden using trucks, and tractors with wagons. It was found that, for distances up to 30 km, using tractors is the most cost-effective option. And for distances exceeding 30 km, trucks are the preferred means of transport. Furthermore,

Gonzales, et al., (2013) reported that using trucks to transport woodchips is the most cost-effective method of transportation when travelling up to 386 km from the Midwest to the Eastern part of the United States. This result is, however, only valid in scenarios where barge transportation is not available. Moreover, Gonzales, et al., (2013) showed that when travelling from the Midwest to the West part of the United States, unit trains are the most cost-effective transportation mode for distances over 338 km. For shorter distances, trucks were the least expensive option.

In light of the above, using trucks for relatively short distances (30 – 338 km) could be considered to be a cost-effective transportation method. It is, however, worth mentioning that the road network varies from one location to another. Thus, the optimal solution would depend not only on the distance between the biorefinery and the main collection point but also on the quality of the road network. In this study, corn stover is collected from the regional biomass processing depots (RBPD) and transported by heavy-duty trucks to the biorefinery. Despite the fact that the dimensions of heavy-duty trucks are not universal, a payload (maximum load) of 22.7 tonnes was used for a volume of 70 m^3. This value was obtained from the study conducted by Sultana & Kumar (2011) on the delivery of lignocellulosic biomass feedstock to biorefineries.

It should be noted that the above-mentioned heavy-duty trucks could carry a maximum single load of 5.1, 9.2, 11.2, or 22.7 tonnes of loose, chopped, baled or pelleted agricultural biomass respectively. And given that in this study, the feedstock is collected from the RBPDs in pellet form, the daily processing of 2 000 tonnes of biomass would require 110 trips/day. Also, it was assumed that the RBPDs would be located within an average radius of 50 km.

Figure 5.1, obtained from Sultana & Kumar (2011), was used to estimate the round-trip cost of transportation. As can be seen, the cost curve for pelletized biomass is underneath all the other curves. Hence, it is cost-effective to transport agricultural biomass in pellets. This can be explained by the relatively high density of pelleted biomass compared to loosen, chopped, and balled biomass. It is also important to note that the gap between the costs of transportation widens at longer distances regardless of the form of biomass. Hence, for large-sized biorefineries where considerable quantities of biomass are

expected to be collected from distant locations, pelleted biomass is certainly the preferred form.

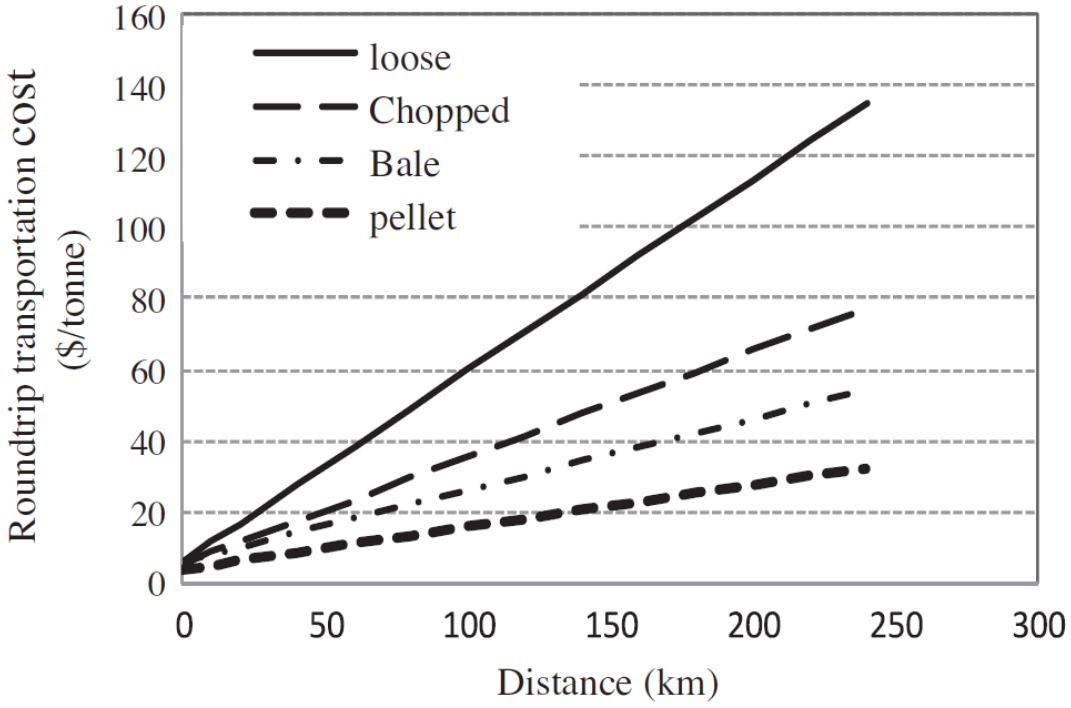

Figure 5.1: Transportation cost as a function of distance for agricultural biomass (Sultana & Kumar, 2011)

5.3 Environmental impact study

5.3.1 The waste reduction algorithm

The need to reduce waste generation and implement pollution prevention techniques at the design stage of processes has been discussed since the 1970s. Discussions eventually led to the development of a heat exchanger network (HEN) as a means to optimize thermal energy consumption in manufacturing processes. Later, the mass exchange network (MEN) concept was introduced to remove pollutants from desired streams and concentrate them on designated waste streams. Hence, minimizing waste generation in manufacturing processes (Young & Cabezas, 1999). Although both HENs and MENs could enhance the sustainability of manufacturing processes, neither technique addressed the impact waste generation within a process could have on the environment. In an effort to fill this knowledge gap, Hilaly and Sikdar (1994) developed the Waste Reduction

Algorithm (WAR) as a concept of pollution balance. This concept was later revised by Cabezas, et al., (1997) to potential environmental impact (PEI).

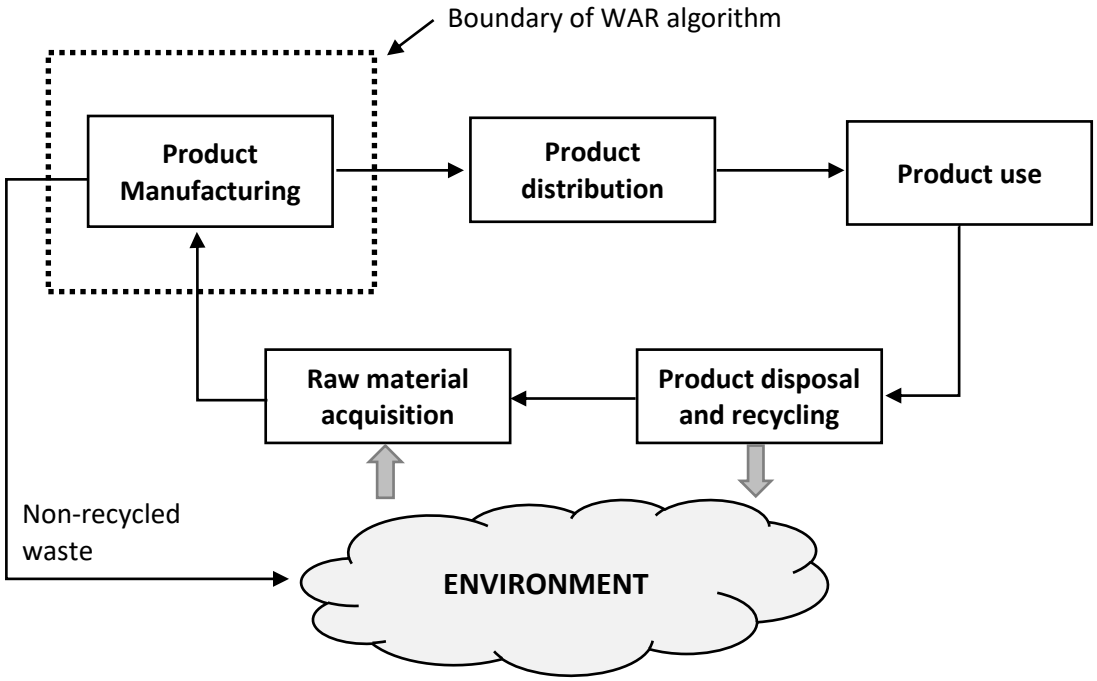

Figure 5.2: Illustration of product life cycle and boundary of WAR (waste reduction) algorithm. The boundary of WAR algorithm is indicated with dotted line

The WAR (waste reduction) algorithm is a swift methodology that measures the environmental impact of chemical processes. Unlike the comprehensive life cycle analysis (LCA) that considers all the stages of the life cycle of a product, the WAR algorithm solely focuses on the boundaries around the manufacturing process (Young & Cabezas, 1999). Hence, this methodology is ideal to evaluate the environmental performances of future chemical processes at the design and development phase, or for the retrofitting of existing processes. An illustration of the product life cycle using the WAR algorithm can be found in Figure 5.2.

Since its introduction, the WAR algorithm has been employed in numerous TEA studies. Among these are Giuliano, et al., (2015) who simulated an integrated biorefinery using Aspen plus software. The purpose of the work was to optimize the production of multiple products including alcohols (ethanol or butanol), value-added chemicals (levulinic acid

and succinic acid), and electricity from lignocellulosic biomass. Another example is Moreno-Sader, et al., (2021) who developed a shrimp biorefinery using process simulation and subsequently evaluated the environmental impact with the help of the waste reduction algorithm (WAR). The biorefinery was designed to produce shrimp meat as a primary product and convert shell residues into astaxanthin, chitin and chitosan using integrated sub-processes. The WAR algorithm revealed that the integrated biorefinery had a relatively low potential environmental impact. Moreover, fresh resource consumption was reduced by 56.63% compared to the non-integrated configuration.

5.3.2 The theory of waste reduction algorithm and potential environmental impact

Potential environmental impact (PEI) is a measure of the adverse effects a particular substance or energy would have on the environment if it were to be released in its present form. It is typically estimated using measurable quantities (Young & Cabezas, 1999). The PEI can be illustrated using the following mathematical expression (Equation 5.2):

$$\frac{\partial I_t}{\partial t} = \dot{I}_{in}^{(cp)} + \dot{I}_{in}^{(ep)} - \dot{I}_{out}^{(cp)} - \dot{I}_{out}^{(ep)} - \dot{I}_{we}^{(cp)} - \dot{I}_{we}^{(ep)} + \dot{I}_{gen}^{(t)} \qquad \text{Eq. 5.2}$$

Where $\frac{\partial I_t}{\partial t}$ is the quantified potential environmental impact of the system. $\dot{I}_{in}^{(cp)}$ and $\dot{I}_{out}^{(cp)}$ are the respectively the input and output rates of potential environmental impact pertaining to the chemical process. $\dot{I}_{in}^{(ep)}$ and $\dot{I}_{out}^{(ep)}$ constitute the input and output rates of potential environmental impact for energy generation processes. $\dot{I}_{we}^{(cp)}$ and $\dot{I}_{we}^{(ep)}$ respectively represent the potential environmental impact resulting from the emission of waste energy in a chemical process and energy generation process. $\dot{I}_{gen}^{(t)}$ is the rate of generation of potential environmental impact within the system. Also, for chemical processes, the depletion and creation of potential environmental impact via chemical reactions within the process is represented by $\dot{I}_{gen}^{(t)}$ (Young, et al., 2000); (Young & Cabezas, 1999).

In steady-state processes, $\frac{\partial I_t}{\partial t} = 0$. Thus, Equation 5.2 becomes Equation 5.3. In addition, as discussed by Young, et al., (2000), $\dot{I}_{we}^{(cp)}$ and $\dot{I}_{we}^{(ep)}$ can be neglected given that these

values will have a significantly lower impact compared to the energy consumed and produced by the chemical and energy generation processes. Moreover, for processes such as the ones modelled in chapters 3 and 4, the impact of input and output streams to the energy process ($\dot{I}_{in}^{(ep)}$ and $\dot{I}_{out}^{(ep)}$), can also be neglected. This is because biomass, lignin, and biochar, which are the major input and output streams are in solid matrix form and are all bio-based. Thus, these compounds are not expected to pose any meaningful risks to humans, animals or the environment. Equation 5.3, therefore, becomes Equation 5.4 and can be rewritten as Equation (5.5).

$$0 = \dot{I}_{in}^{(cp)} + \dot{I}_{in}^{(ep)} - \dot{I}_{out}^{(cp)} - \dot{I}_{out}^{(ep)} - \dot{I}_{we}^{(cp)} - \dot{I}_{we}^{(ep)} + \dot{I}_{gen}^{(t)} \quad \text{Eq. 5.3}$$

$$0 = \dot{I}_{in}^{(cp)} - \dot{I}_{out}^{(cp)} + \dot{I}_{gen}^{(t)} \quad \text{Eq. 5.4}$$

$$0 = \dot{I}_{in}^{(t)} - \dot{I}_{out}^{(t)} + \dot{I}_{gen}^{(t)} \quad \text{Eq. 5.5}$$

Where $\dot{I}_{out}^{(t)}$ represents the rate of total potential environmental impact output and can be approximated using known measurable quantities as shown in Equation 5.6.

$$\dot{I}_{out}^{(t)} = \sum_{i}^{Env.\ Cat} \alpha_i \sum_{j}^{NP\ Streams} \dot{M}_{j,out} \sum_{k}^{Comps} x_{kj} \varphi_{ki}^{s} \quad \text{Eq. 5.6}$$

Where: $\dot{I}_{out}^{(t)}$ is the PEI output index for category i; $\dot{P}$ is the mass flow rate of the product streams; $\dot{M}_j$ is the mass flow rate of the non-product output; x_{kj} is the mass fraction of component k in stream j; α_i is the weighting factor associated potential environmental impact category i; φ_{ki}^{s} is the specific potential environmental impact of component k associated with environmental impact category i.

$\hat{I}_{out}$ which represents the potential environmental impact output index with units of PEI/kg of product can be computed as shown in Equation 5.7.

$$\hat{I}_{out}^{(t)} = \frac{\dot{I}_{out}^{(t)}}{\sum_{P}^{Prod.\ Stream} \dot{P}_p} \quad \text{Eq. 5.7}$$

It is worth emphasizing that, $\dot{I}_{out}^{(t)}$ and $\hat{I}_{out}$ are the two most important indexes to characterize the relative environmental friendliness or efficiency of a chemical process. Essentially, the surrounding environment of a process with a relatively low $\dot{I}_{out}^{(t)}$ or $\hat{I}_{out}$ is more likely to effectively dissipate the waste emitted, compared to a process with a relatively high $\dot{I}_{out}^{(t)}$ or $\hat{I}_{out}$ (Young & Cabezas, 1999). Thus, the latter process represents a more environmentally efficient design. Figure 5.3 illustrates the mass and energy balance around chemical and energy processes, with the corresponding potential environmental impacts.

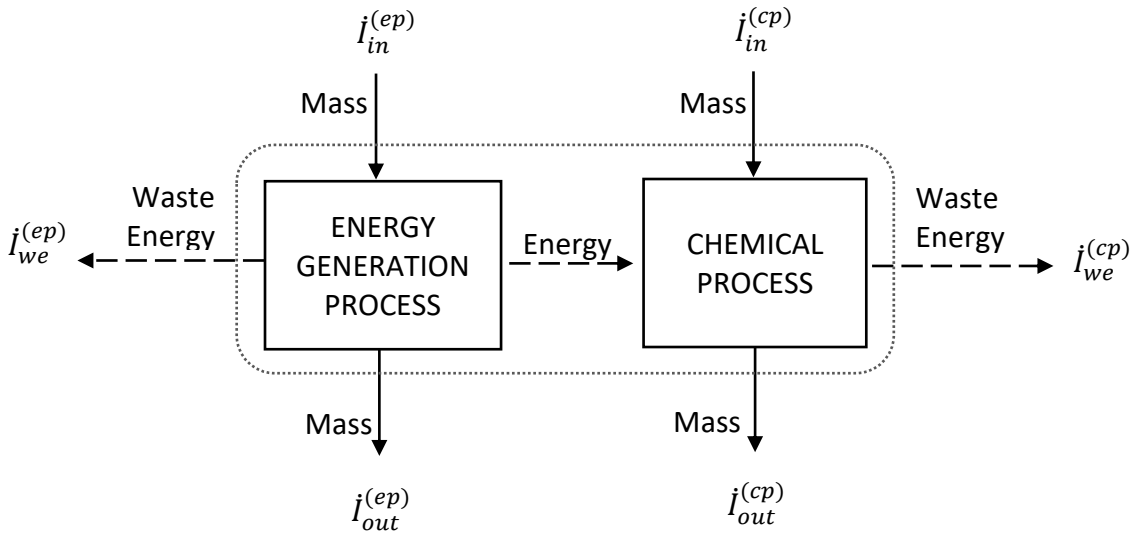

Figure 5.3: Illustration of mass and energy balance around chemical and energy generation processes. The system boundary is indicated with dotted line

5.3.3 Evaluation of environmental performances of modelled scenarios

The potential environmental impact (PEI) was computed using the WAR algorithm incorporated in Chemcad 7.1. Eight environmental categories were considered. These included: Human toxicity potential by ingestion (HTPI), Human toxicity potential by dermal exposure or inhalation (HTPE), Terrestrial toxicity potential (TTP), Aquatic toxicity potential (ATP), Global warming potential (GWP), Ozone depletion potential (ODP), Photochemical oxidation potential (PCOP), and Acidification potential (AP). Moreover, since the feed streams for both the standalone and hybrid scenarios were identical, only the output indexes ($\dot{I}_{out}^{(t)}$ and $\hat{I}_{out}$) were used in the evaluation.

5.4 Land use impact

Utility-scale solar power systems are defined as solar power plants designed to generate more than 20 MW. These facilities are known to require broad strips of flat space for solar energy collection. Thus, they involved trading-off sizeable plots of land for clean energy generation. Considering that such trade-offs could adversely impact existing land uses, it is crucial to quantify the efficiency at which land is utilized for energy generation. Capacity-based land use efficiency (LUE), is a ratio that can help gauge the efficient use of land in utility-scale solar energy systems. It is calculated by dividing the system's power output by the solar field area (W/m^2) (Hernandez, et al., 2013). LUE is particularly helpful at the early stage of projects involving large-scale solar energy generation, as it can guide in choosing an option that is likely to be more land-efficient (Ong, et al., 2013); (Hernandez, et al., 2013). LUE was used in this study to comparatively evaluate the land usage of the modelled solar-aided biorefineries.

5.5 Closing remarks

Economic modelling is an essential part of TEA studies. This is because it enables the financial performance of various processing routes to be comparatively assessed without having to construct costly experimental facilities. Also, environmental impact analyses such as the WAR algorithm, are key to gauging the potential environmental impacts of production systems at the design stage. Both these methodologies have previously been used in other studies to investigate the performance of biorefineries (refer to Table 5.2). In the following chapter, the results of the economic modelling exercise and the environmental impact assessment are discussed.

Table 5.2: Selection of previous studies on biorefineries employing computer-aided simulations to perform techno-economic analysis and/or environmental assessment via WAR algorithm

Authors	Type of study	Type of biomass raw material	Biofuel & Bio-products
(Moreno-Sader, et al., 2021)	Computer-aided simulation and environmental assessment via WAR algorithm	shrimp	Shrimp meat, astaxanthin, chitin and chitosan
(Duque, et al., 2015)	TEA and Environmental analysis via WAR algorithm	sugar cane bagasse, banana stem, corncob, rice husk, sawdust, woodbark, mango wastes, palm residues, pineapple peel, and plantain peel	Bio-ethanol
(Marticorena, et al., 2010)	Environmental impact analysis via WAR algorithm	soil bean oil	Bio-diesel, Bio-methanol
(Montoya, et al., 2006)	Environmental impact analysis via WAR algorithm	corn and sugar cane	Bio-ethanol
(Jin, et al., 2021)	TEA	grape pomace	seed oil, polyphenols, and biochar
(Dimitriou, et al., 2018)	TEA	wood chips	Liquid fuels (Methanol and Gasoline)
(Baral & Shah, 2017)	TEA	corn stover	Butanol
(Gubicza, et al., 2016)	TEA	sugar cane bagasse	Bio-ethanol
(Da Silva, et al., 2016)	TEA	corn stover	Bio-ethanol
(Do & Lim, 2016)	TEA	Empty fruit bunches of oil-palm	bioethanol. jet fuel by bioconversion, hydrocarbons through fast pyrolysis and bio-oil upgrading
Giuliano, et al., (2015)	TEA	not specifically mentioned	alcohols (ethanol or butanol)
(Shemfe, et al., 2015)	TEA	pine wood	Bio-oil, biogas, bio-char
(Tao, et al., 2014)	TEA	corn grain and corn stover	Jet-fuels
(Quintero, et al., 2013)	TEA	sugarcane bagasse, coffee cut-stems, rice husk, and empty fruit bunches)	Bio-ethanol
(Leibbrandt, 2010)	TEA	sugar cane bagasse	Bio-ethanol, bio-oil, Fischer-Tropsch liquid fuel

CHAPTER 6 – ECONOMIC PERFORMANCE AND ENVIRONMENTAL IMPACT

6.1 Introduction

In this chapter, results from economic models and WAR algorithm are presented and discussed. A sensitivity study is performed to determine the impact of key parameters on the production costs. The potential environmental impact of each biorefinery scenario is equally presented and compared to published data on other lignocellulosic biorefineries.

6.2 Economic performance of biological processing route

6.2.1 Analysis of fixed capital investment

The contribution of each conversion area to the fixed capital investment is shown in Figure 6.1. As can be seen, the incorporation of solar power as the principal source of energy resulted in a significant increase in fixed capital. This observation was made regardless of the type of solar energy used (PV, CSP, and solar thermal). Scenario 2 and 3 were found to be the most expensive options, and they respectively required a fixed capital investment of $1.61 and $1.68 billion. These Figures are substantially larger than the $402 million of fixed capital investment required for the standalone option (Scenario 1). In fact, the fixed capital required to build a single solar-aided biorefinery was high enough to build at least a couple of standalone lignocellulosic biorefineries.

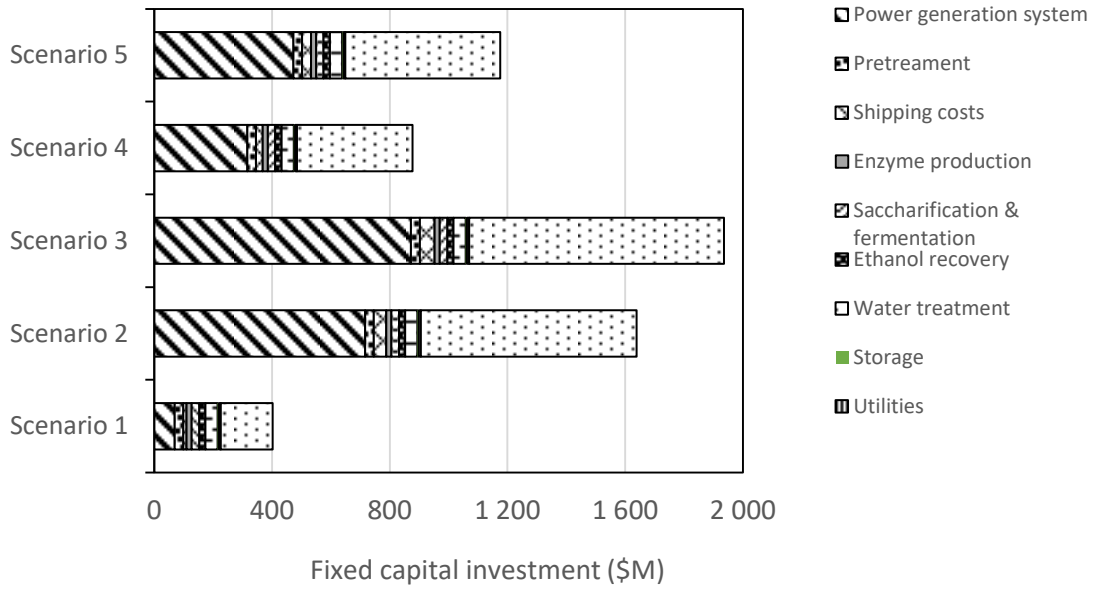

Figure 6.1: Breakdown of fixed capital investment for all scenarios (2020 dollar year)

The fixed capital investment of solar fields for solar-aided scenarios is shown in Table 6.1. It is evident that the generation of process heat using solar energy (refer to scenarios 2 and 3) renders the system particularly costly. Also, the capital cost required for the generation of process electricity using either PV or CSP was profoundly influenced by the energy storage cost. For instance, in scenarios involving solar PV, energy storage costs represented 93% of the capital cost of the solar PV system. While in scenarios involving CSP, energy storage costs represented 60% of the capital cost of the CSP system. Consequently, if energy was not continuously stored, the capital investment for the solar PV system would have dropped from $285 million to $21 million, while the CSP system would cost $177 instead of $441 million. Furthermore, the most expensive component of the concentrated solar thermal system was the module, accounting for 91% of the capital cost of the concentrated solar thermal system. This was despite the use of linear fresnel reflectors, which is currently the most cost-effective option to produce steam using solar power.

Table 6.1: Solar field costs ($M) for solar-aided scenarios in biological conversion

	Solar PV *Scenario 2 and 4*	CST *Scenario 2 and 3*	CSP *Scenario 3 and 5*
Module cost	20.8	392	177
Fixed operating cost	0.18	5.79	2.14
Energy storage cost	264	39.2	264
Capital cost of solar energy system	285	431	441

In summary, it can be said that high capital costs will certainly be a major challenge for the incorporation of solar power into lignocellulosic biorefineries. Thus, aggressive cost reductions or technological breakthroughs might be required to make solar-aided lignocellulosic more appealing.

6.2.2 Minimum ethanol selling price

6.2.2.1 A comparison with the NREL model

The minimum ethanol selling price (MESP), which is the price at which ethanol must be sold in order to achieve a net present value of zero, was found to be 0.61 $/litre (or 25.88 $/GJ) for the standalone scenario. This is equivalent to 10.63 Rand/litre assuming the

USD/ZAR exchange rate to be 17.5. In order to compare the MESP of this study to the value obtained by Tao, et al., (2014), a cost escalation exercise was needed. This is because Tao, et al., (2014)'s calculations were based on the 2007-dollar value. Cost escalation was performed by factoring the inflation rate into Tao, et al., (2014)'s MESP. And according to the Bureau of Labour Statistics consumer price index, $1 in 2007 was worth $1.24 in 2020 (USDL, 2007); (USDL, 2020). Hence, the MESP of Tao, et al., (2014) in 2020-dollar value was estimated to be equivalent to 0.70 $/litre, which is about 15% higher than the MESP of the present study.

The lower MESP obtained in this study can be explained by the discrepancies in parameters used during the economic modelling. For instance, although the total capital investment of Tao et al., (2014) after cost escalation using the chemical engineering plant cost index is about 3% greater than the value used in this study, the biomass cost for the present study is almost twice cheaper than the cost used by Tao et al., (2014). Also, it is worth mentioning that the relative low biomass cost in developing countries is now becoming evident (Domingues, et al., 2022), and this could play a key role in implementation of lignocellulosic biofuels in regions like South Africa. A comparison in economic parameters between Tao et al., (2014)'s study and the present study can be found in Table 6.2.

Table 6.2: Comparison between standalone scenario and Tao et al., (2014)'s biorefinery

Parameters	Present study	Tao et al., (2014)	Tao et al., (2014) (After cost escalation)
Biomass consumption rate (kg/hr)	104 167	104 167	-
Ethanol production rate (kg/hr)	19 326	19 455	-
Biomass cost ($/tonne)	22.2	53.1	65.7*
TCI ($M)	423	381	436 **
Percentage equity-financed (%)	40	40	-
Plant life (years)	25	30	-
After tax IRR (%)	10	10	-
Operating hours	8 000	8 000	-
Dollar value year	2020	2007	2020
Economic context	South Africa	USA	USA

*Cost escalation was performed using customer price index. **cost escalation was conducted using the chemical engineering plant cost index

6.2.2.2 A comparison with previous South African-based models

A comparison between the MESP of the present study and literature data on the production of lignocellulosic ethanol in South Africa is shown in Table 6.3.

Table 6.3: Comparison of economic evaluation between the standalone scenario and published South African based models

	Present study	(Petersen, et al., 2017)	(Leibbrandt, 2010)	(Leibbrandt, 2010)
Type of lignocellulosic raw material	Corn Stover	Bagasse	Bagasse	Bagasse
Capacity (MW)	500	600	600	600
Pretreatment method	Dilute acid 30% solid loading	Steam explosion	Steam explosion 50% solid loading	Dilute acid (35% solid loading)
Total Capital Investment ($M)	423	360	433	541
Specific operating costs ($/MJ thermal feed)	5.1	9.8	Not explicitly disclosed	Not explicitly disclosed
Operational hours	8000	6470	8000	8000
Income tax	28%	28%	28%	28%
Dividend paid (% net cash income)	25	25	25	25
Plant lifetime (years)	25	20	20	20
Debt to equity ratio	60/40	0/100	70/30	70/30
IRR (%)	10.0	15.4	14.4	14.4
Raw material price ($/dry tonne)	22.2	25.5	52	52
Exchange rate (ZAR/USD)	17.5	9.33	7.5	7.5
Dollar year	2020	2016	2009	2009
MESP ($/litre)	0.61	0.64	0.54	0.70
MESP after cost escalation to 2020 ($/litre)*	N/A	0.69	0.65	0.83

*Cost escalation was performed using customer price index.

It can be observed that after cost escalation, the MESP of the present study was close to the values reported by Petersen (2017) and Leibbrandt (2010) using steam explosion pretreatment. The MESP of the present work was however 13% lower than the ethanol production cost reported by Leibbrandt (2010) using dilute acid with 35% solid loading. It

is essential to note, however, that MESPs from techno-economic studies are always a function of the financial parameters considered during modelling. Thus, comparisons should always be carried out with caution.

6.2.3 Investment analysis and sensitivity study

Because the production cost from techno-economic studies is very sensitive to the assumptions made, it is essential to perform a sensitivity analysis and assess the MESP's response to variations in key parameters. The average South African gasoline and diesel inland prices for the year 2020 were 25 and 22 $/GJ respectively (DoE, 2021). These values were utilised for comparison purposes during the investment analysis.

Internal rate of return (IRR) and debt-to-equity ratio: Figure 6.2 shows the MESP's sensitivity to the internal rate of return (IRR) and percentage of equity finance (for the standalone scenario). It is evident that it would be advantageous to keep the debt-to-equity ratio as low as possible to minimise the MESP. Also, the IRR was found to profoundly impact the MESP.

Setting the IRR to 10% as recommended by Short, et al., (1995) for the economic evaluation of renewable energy technologies, resulted in an MESP of 0.61$/litre (25.88 $/GJ). It is interesting to note that this MESP is on the upper margin of 2020's South African inland petrol price. Hence, an IRR of 10% could be just low enough for lignocellulosic bioethanol to compete with a South African petrol price of 25 $/GJ. The main challenge here is the fact that fossil fuel prices are volatile and difficult to forecast.

Should the IRR be set to 20% to make the project more attractive to potential investors, or 30% which is generally desired for investment in new technologies, the MESP would increase to 1.09 $/litre (46.48 $/GJ) and 1.78 $/litre (75.75 $/GJ) respectively. With such high prices, bio-ethanol would require a significant price increase in fossil fuels in order to be competitive in the country and attract investors. Alternatively, the ZAR (local currency) will have to significantly weaken against the dollar during the plant's lifetime. Indeed, South Africa imports a large portion of its fossil fuels. Hence, the USD to ZAR exchange rate does affect fossil fuel affordability. That is why although the price of Brent crude oil

declined from $90.40 a barrel in December 2010 to $69.26 a barrel in December 2019, the stumbling local currency (8 ZAR/USD in 2010 to 17 ZAR/USD in 2019) forced the gasoline price to follow the opposite trend in the country.

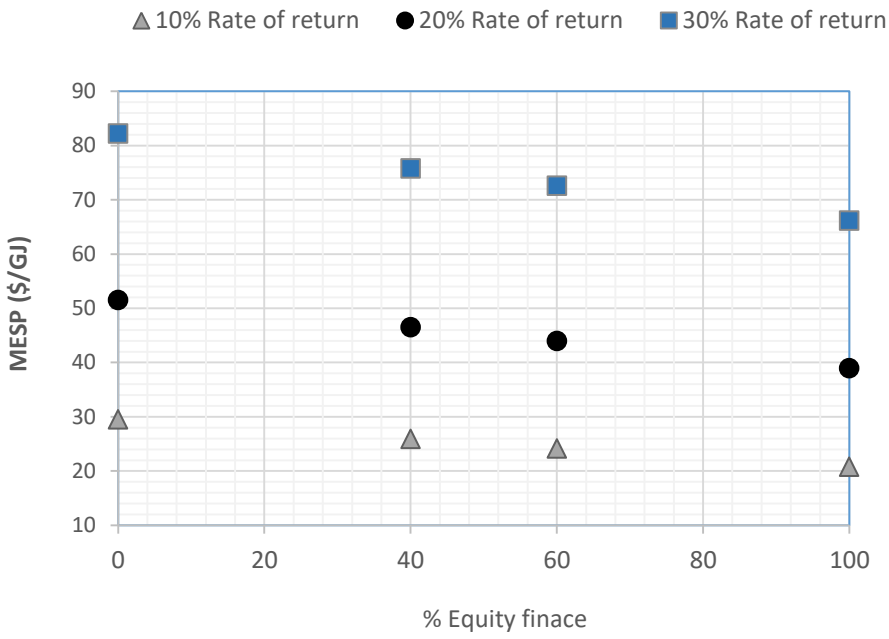

Figure 6.2: Sensitivity of MESP to IRR and % equity (for the standalone scenario)

Capital investment: Considering that the present study was largely based on factored estimates of major process equipment, which typically carry an accuracy of ± 30% (Peters & Timmerhaus, 1991), it was fundamental to determine the sensitivity of MESP to ± 30% variations in total capital investment (TCI). And as shown in Figure 6.3, a 30% reduction in TCI lowers the MESP by 17%. This means that should the total capital investment be reduced by 30% due to future technological breakthroughs, the production costs could be as low as 0.50 $/litre (or 21.50 $/GJ), which may allow bioethanol to compete with a gasoline price of 25 $/GJ. Moreover, it was observed that by reducing the TCI by 30% and simultaneously raising the IRR to 15%, the MESP would be 27.74 $/GJ, which is not low enough to compete with the 2020's South African petrol price. Hence, even with a 30% lower capital investment, it will be challenging to achieve an attractive IRR. On the other hand, a 30% increase in TCI resulted in the MESP rising to 30.5 $/GJ which could drastically upset the competitiveness of ethanol.

Electricity price: An increase in the electricity price in South Africa could also help to maximize the biorefinery profitability in the sense that the surplus electricity generated would be sold for a higher premium. Indeed, the price of electricity in South Africa has been considerably inflated for the last 10 years due to technical and financial challenges faced by the local electricity company and higher prices have been forecasted for the coming years. As illustrated in Figure 6.3, should the electricity price spike to 0.2 $/kWh, the MESP would be reduced to 0.52 $/litre (or 22.22 $/GJ), which would make investments in lignocellulosic biorefineries more attractive.

Biomass cost: Because the implementation of lignocellulosic ethanol is likely to increase the demand for lignocellulosic biomass, and cause an escalation in biomass price, it was essential to gauge the impact of biomass cost on the MESP. And as seen in Figure 6.3, should the biomass price increase to 27.73 $/tonne or 36.98 $/tonne, the MESP would shift to 28.00 and 30.11 $/GJ respectively, which could seriously upset the ability of bioethanol to compete with fossil fuels. The successful implementation of lignocellulosic bioethanol will therefore require some stability in the biomass price.

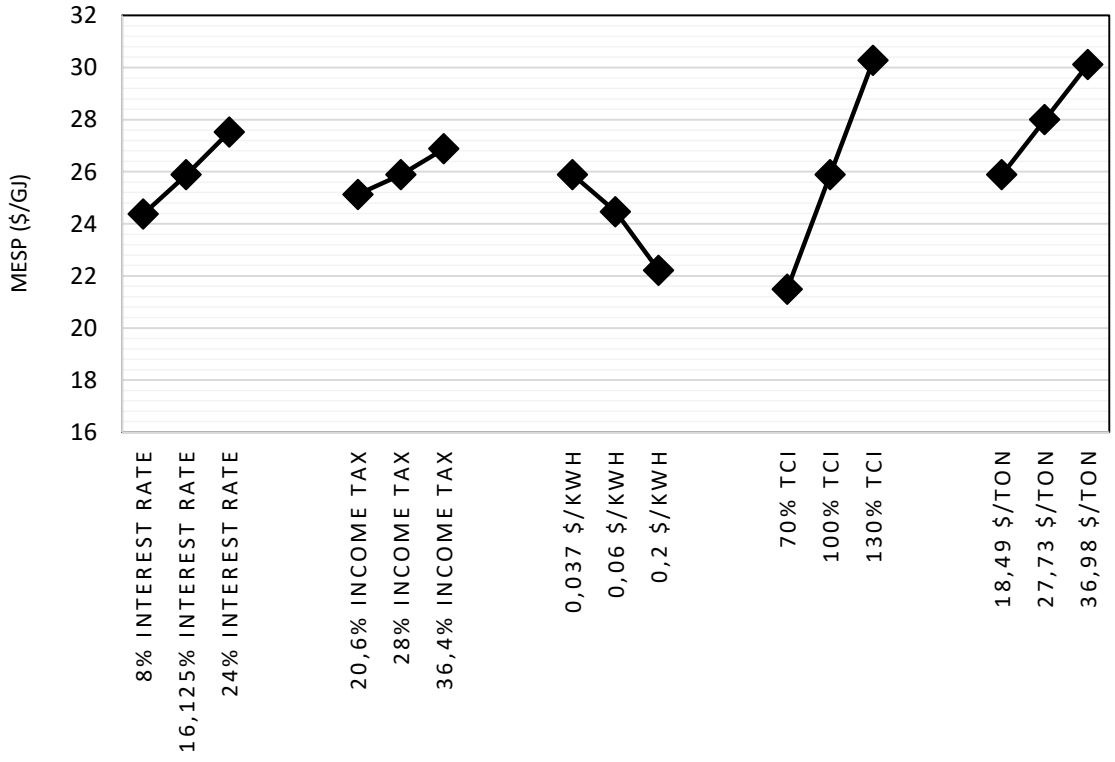

Figure 6.3: Sensitivity of MESP to interest rate, income tax, electricity selling price, total capital investment and biomass purchase prices (IRR = 10%) – standalone scenario

Considering the above, it can be stated that the commercialisation of lignocellulosic bioethanol in South Africa using a conventional biorefinery configuration is a possibility. However, its competitiveness will be influenced by several factors including the IRR, equity finance, biomass price and the electricity price.

6.2.4 Impact of solar hybridization and lignin commercialization on production cost

The MESP for the solar-aided scenarios were increased to 58.05 $/GJ for scenario 2, 68.84 $/GJ for scenario 3, 43.17 $/GJ for scenario 4, and 53.97 $/GJ for scenario 5. Hence, the ethanol selling price needs to be inflated by 32.16 $/GJ for scenario 2, 42.96 $/GJ for scenario 3, 17.29 $/GJ for scenario 4, and 28.09 $/GJ for scenario 5 to cover additional expenses related to the integration of solar energy. Furthermore, it was found that to lower the MESP back 25.88 $/GJ, the actual lignin fraction of lignin-rich residues had to be sold for 1 625 $/ tonne for scenario 2, 2 171 $/tonne for scenario 3, 2 184 $/tonne for scenario 4, and 3 549 $/tonne for scenario 5. These values, which could be referred to as "minimum lignin selling price" (MLSP) were determined by fixing the price of ethanol to a value equal to the MESP of the standalone scenario and adjusting the price of lignin until an NPV of zero was obtained.

Table 6.4: Lignin market from price obtained from Hodásová, et al., (2015)

	2015's price ($/tonne)	Escalated 2020 price* ($/tonne)
Lignosulphonates	180 – 500	198 – 550
Organosolv lignin	200 – 300	220 – 330
High purity lignin	750	825
Lignin from kraft process	260 – 500	286 – 550

*Cost escalation was performed using customer price index.

Lignin market value is shown in Table 6.4 for a comparison with the MLSP. Given that lignin market value was estimated in the 2015-dollar year, to compare the MLSP in the present study against lignin market value, a cost escalation exercise was performed. The values obtained after cost-escalation suggest that it is not currently economically viable

to generate lignin as a co-product of a lignocellulosic biorefinery, especially given the fact that a purification step that will incur additional costs will be required.

A sensitivity study revealed that a 50% reduction in the fixed capital investment of hybrid biorefinery would result in the MLSP of pure lignin dropping to 495 $/tonne for scenario 2, 780 $/tonne for scenario 3, 257 $/tonne for scenario 4 and 969 $/tonne for scenario 5. Thus, the commercialization of lignin as a co-product couple with the use of solar energy as the main energy supply might require a major decline in the capital investment for the solar energy plant. This could be achieved via major technology breakthroughs or substantial government subsidies.

Because land has been the subject of several controversies in South Africa and the forthcoming land reform proposals are likely to result in uncertainty in land cost in the country, it was important to assess the impact land price could have on the MESP, especially given the fact that a solar-hybrid lignocellulosic biorefinery requires considerable land size for the solar field. And, as shown in Figure 6.4, for prices as high as 50 $M, the land cost would have a marginal impact on the MESP.

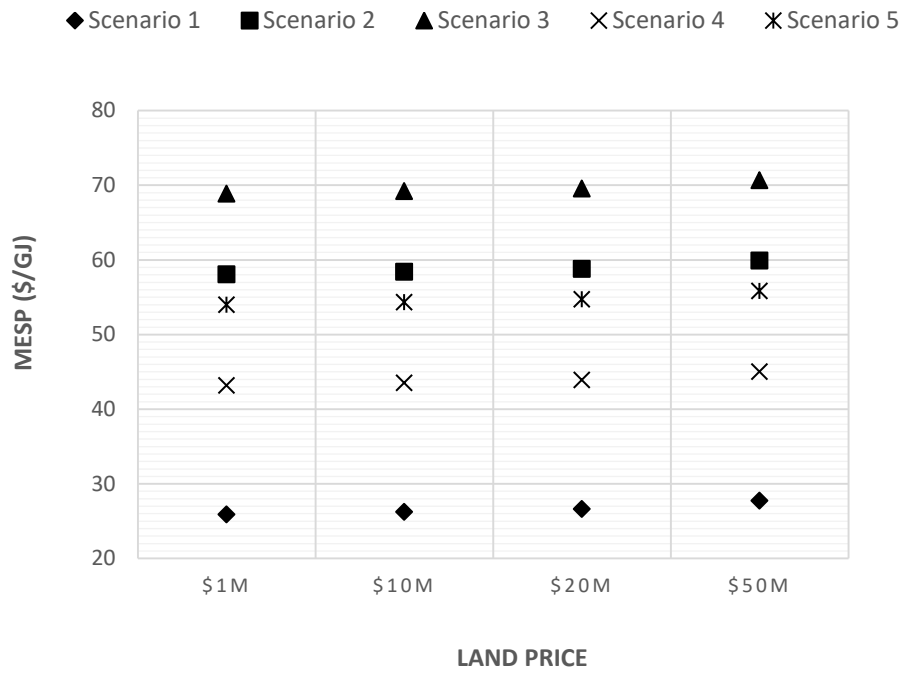

Figure 6.4: MESP as a function of land cost for all scenarios

6.3 Economic performance of thermochemical processing route

The minimum methanol selling price was estimated to be 0.31 $/litre (17.47 $/GJ) for the standalone scenario, which is equivalent to 5.48 Rand/litre, assuming the USD/ZAR exchange rate to be 17.5. To the best of the authors' knowledge, Amigun, et al., (2010) is the only techno-economic study published so far on the production of methanol from corn stover residues in South Africa. The study employed an allothermal gasifier equipped with a CO_2 absorption enhanced reforming (AER) process to produce syngas. Additionally, methanol synthesis was performed using a superconverter double tubular heat exchanger reactor, developed by Mitsubishi Gas Chemical Inc., (MGC) in collaboration with Mitsubishi Heavy Industry (MHI). In order to compare the production cost obtained in the present work to Amigun, et al., (2010)'s costs, a cost escalation exercise was needed. Table 6.5 shows a comparison between the production cost of the present work and Amigun, et al., (2010).

Table 6.5: Comparison between standalone scenario and previously published works conducted on the production of methanol from biomass in South Africa

	Present study	(Amigun, et al., 2010).
Type of biomass gasifier	TNEE-type circulating fluidized bed	Absorption Enhanced Reforming (AER) gasification process
Biomass input (MW_{th})	500	400
Methanol output (MW_{th})	213	220
Biomass cost ($/tonne) after time scaling to 2019 USD	22	141[a]
Initial annual operating costs	48 $M	4% of TCI
TCI	434 $M	448 $M [a]
Percentage equity-financed	40%	-
Plant life	25 years	-
After tax IRR	10%	-
Operating hours	8 000	8 000
Methanol production cost after time scaling to 2019 USD	0.31 $/litre	0.63 $/litre

A Value obtained after time scaling to 2019 USD. Note that in this case, the study was conducted using an average USA/ZAR exchange rate of 7.5.

A significant difference can be observed between the methanol production price of the present study and Amigun, et al., (2010). This is likely due to the major discrepancies in raw materials costs. Indeed, the biomass cost used in the present work was obtained from Batidzirai, et al., (2016)'s maize residues cost estimate for South Africa, and is nearly

6 folds lower than the cost used by Amigun, et al., (2010). Given that Amigun, et al., (2010) did not provide a rationale behind the relatively high biomass cost, it is rather complex to perform an objective comparison. In addition, the lack of key information such as the internal rate of return, and plant life complicates the task further.

6.3.1 Investment analyses and sensitivity study

As previously mentioned, the production cost from techno-economic studies is generally dependent on assumptions made during the study. Therefore, it is necessary to conduct a sensitivity study and assess the impact of economic parameters on production costs. Four main parameters were considered here. These included biomass cost, total capital investment, internal rate of return and fixed operating costs. Capital investment was varied within a 30% range, and its impact on methanol production costs was examined. The biomass cost, interest rate and fixed operating costs were also manipulated to assess their impact on production costs.

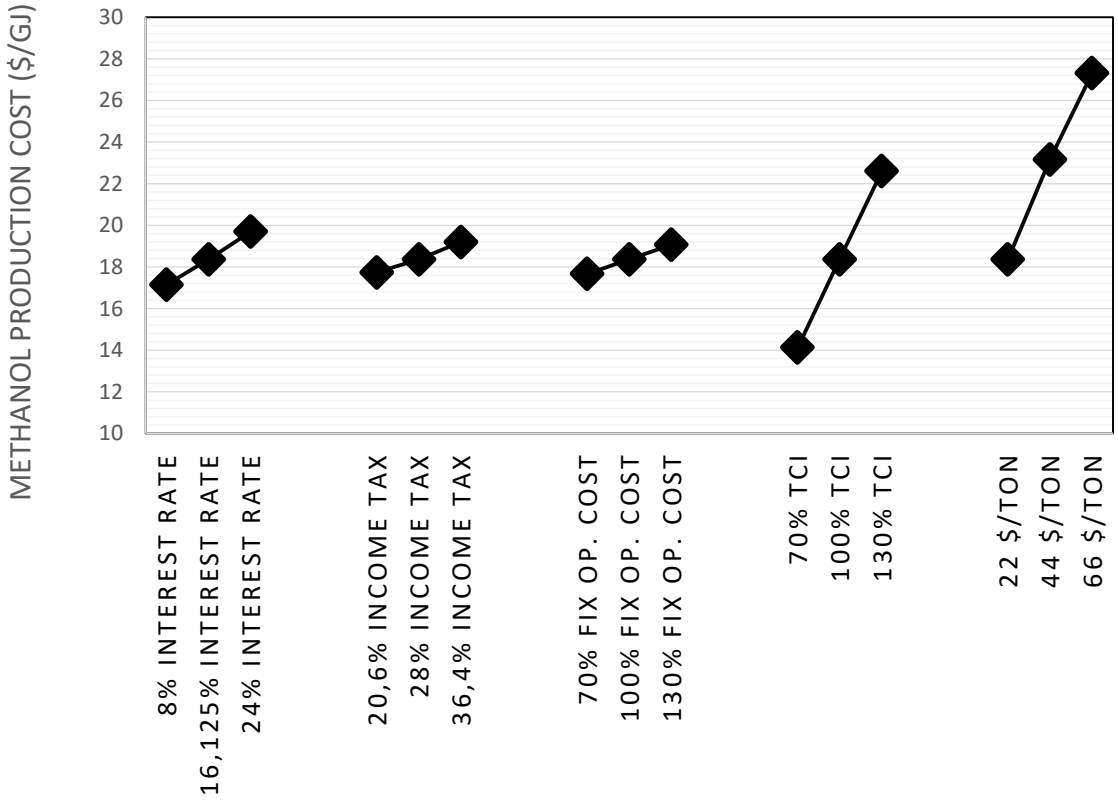

Figure 6.5: Sensitivity of methanol production cost to interest rate, income tax, fixed operating cost, total capital investment and biomass price (IRR = 10%) – standalone scenario

As can be seen in Figure 6.5, variations in TCI and biomass price appear to have a more pronounced impact on the methanol production cost compared to the other manipulated variables. The successful commercialisation of lignocellulosic bio-methanol in South Africa will therefore require some stability in the biomass price. Moreover, major technology breakthroughs allowing the reduction in capital costs could also play a major role in boosting the competitiveness of bio-methanol.

6.3.2 Impact of solar hybridization on methanol production cost

The minimum ethanol selling price in the solar-aided scenario was estimated to be 0.50 $/litre (27.88 $/GJ). Hence the methanol selling price needs to be inflated by 10.41 $/GJ to cater for expenses related to the incorporation of solar energy. Furthermore, to lower the production cost back to 0.31 $/litre, the bio-char by-product should be sold for 13.04 $/GJ (≈ 0.37 $/kg). This value, which could be referred to as the "minimum bio-char selling price" was determined by keeping the price of methanol fixed at 13.35 $/GJ and adjusting the price of bio-char until an NPV of zero is obtained.

6.4 Analysis of potential environmental impact

6.4.1 Environmental impact of biological conversion

During the production of ethanol from corn stover, non-product streams were released into the environment in three main conversion areas: steam and power generation (flue gases were released into the atmosphere); wastewater treatment (brine was discharged into the environment); and ethanol recovery (vapours rich in CO_2 and ethanol were released into the atmosphere by the scrubber).

The overall PEI/hr for scenario 1 was found to be $1.27x10^{+04}$. This value decreased to 1.09E+04 in scenarios 4 & 5 and 6.8E+03 in scenarios 2 & 3. Moreover, as seen in Table 6.7 and figure 6.7, the scenarios where lignin is combusted for energy generation (scenarios 1, 4 and 5) show a relatively high potential environmental impact per unit of ethanol produced (PEI/kg $_{ethanol}$). In fact, in scenarios 4 and 5 where lignin-rich residues are partially combusted, the PEI is reduced by 14%, while in scenarios 2 and 3 where they are entirely combusted, it is reduced by about 50%. This implies that the non-combustion of lignin could result in a lesser impact on the environment. It is however important to

emphasise that in order not to shift the environmental burden from the biorefinery to downstream value chain processes, the exported lignin-rich residues should ideally be used for a non-energy application where it will not be combusted. This is because combusting lignin residues in downstream processes will undermine its commercialisation purposes which are to promote a bio-based circular economy and further mitigate CO_2 emissions.

Table 6.6: Potential environmental impact values for pertinent polluting chemicals released into the environment. Values are given in PEI/kg ethanol produced

			HUMAN TOXICITY		**ECOTOXICITY**		**ENVIRONMENTAL POLLUTION**		
Conversion area	Pertinent pollutants	Flow rate (kg/hr)	HTPI	HTPE	ATP	TTP	GWP	PCOP	AP & ODP
Power generation (Scenario 1)	CO_2	81 000	0	1.36E-04	3.78E-01	0	1.33E-03	0	0
Power generation (Scenario 2 & 3)	CO_2	6 720		2.78E-05	7.76E-02		2.73E-04		
Power generation (Scenario 4 & 5)	CO_2	61 634		1.03E-04	2.88E-01		1.01E-03		
Wastewater treatment	CO_2	451	0	7.55E-07	2.11E-03	0	7.40E-06	0	
	Ethanol	133	3.52E-04	1.05E-06	1.10E-06	3.52E-04	0	3.78E-03	
	Methane	41.7	0	0	1.21E-04	0	7.55E-06	3.10E-05	
	NaOH	200 000	2.28E-04	5.85E-05	9.68E-05	2.28E-04	0	0	
	Furfural	309	8.90E-02	2.33E-04	1.08E-03	8.90E-02			
	Sodium Sulfate	92.8	5.33E-04	0	1.31E-06	5.33E-04			
	Sucrose	415	2.62E-04	4.17E-04	6.62E-09	2.62E-04			
Scrubber	CO_2	18 600	0	3.11E-05	8.69E-02	0	3.05E-04		
	Ethanol	107	2.84E-04	8.49E-07	8.90E-07	2.84E-04	0		
TOTAL (STANDALONE - SCENARIO 1)			9.07E-02	8.78E-04	4.68E-01	9.07E-02	1.65E-03	3.81E-03	0
TOTAL (SCENARIO 2 & 3)				7.70E-04	1.68E-01		5.93E-04		
TOTAL (SCENARIO 4 & 5)				8.45E-04	3.78E-01		1.33E-03		

ODP: Ozone Depletion Potential. GWP: Global Warming Potential. PCOP: Smog Formation Potential. ARP: Acid Rain Potential. HTPI: Human Toxicity Potential by Ingestion. HTPE: Human Toxicity Potential by Inhalation or Dermal Exposure. ATP: Aquatic Toxicity Potential. TTP: Terrestrial Toxicity Potential.

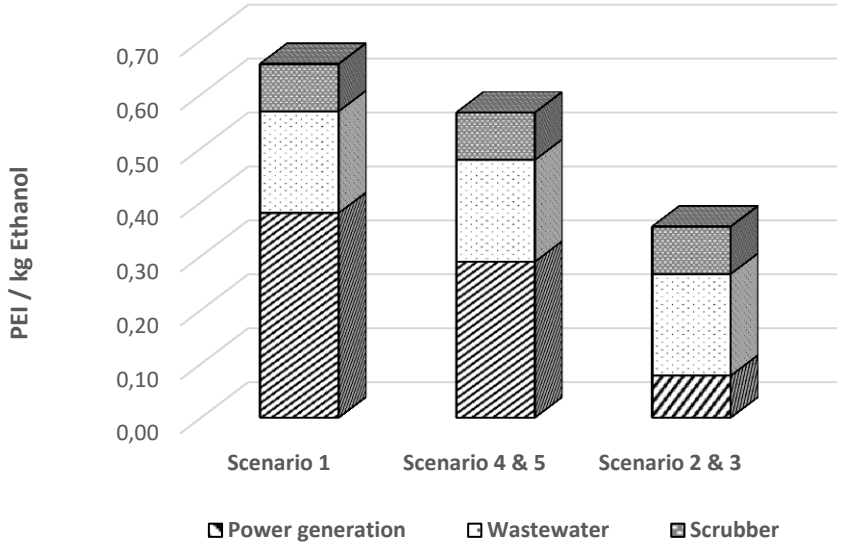

Figure 6.6: Potential environmental impact output indexes ($\hat{I}_{out}$)

6.4.2 Environmental impact of thermochemical conversion

Non-product streams were released into the environment in four main conversion areas: biomass gasification (flue gases from the combustion bed were released into the atmosphere); syngas cleaning and conditioning (stripper's effluent); heat and power generation (flue gases from the combustor), and methanol purification (effluent from the distillation column).

The overall PEI/hr for the standalone scenario was found to be 1.65E+04. This value decreased to 1.06E+04 in the solar-aided configuration. On the other hand, the overall potential environmental impact per unit of methanol produced (PEI/kg $_{methanol}$) was found to be 0.49 for the standalone scenario and 0.32 for the solar-aided configuration. The relatively low PEI/kg $_{methanol}$ observed in the solar-aided scenario is due to the elimination of char combustion which leads to less CO_2 being emitted into the environment. The utilisation of solar energy for biomass gasification could therefore considerably mitigate the environmental impact of a biomass-to-methanol biorefinery. Furthermore, as shown in Table 6.6, the Aquatic Toxicity Potential contributes the most to the environmental impact, followed by the global warming and Smog Formation Potentials.

Table 6.7: Potential environmental impact output indices for each category (PEI/kg $_{methanol}$)

			HUMAN TOXICITY		**ECOTOXICITY**		**ENVIRONMENTAL POLLUTION**		
Conversion area	Pertinent pollutants	Flow rate (kg/hr)	HTPI	HTPE	ATP	TTP	GWP	PCOP	AP & ODP
Biomass gasification (Combustion bed)	CO_2	63 202	0	6.07E-05	1.69E-01	0	5.95E-04	0	0
Heat and power generation	CO_2	55 900		5.36E-05	1.50E-01		5.24E-04		
Syngas cleaning and conditioning	CO_2	53 692		5.15E-05	1.44E-01		5.04E-04		
Methanol purification	Methanol	34	6.46E-05	1.12E-06	7.38E-08	6.46E-05	0	2.53E-04	
TOTAL (STANDALONE)			6.46E-05	1.67E-04	4.62E-01	6.46E-05	1.62E-03	2.53E-04	0
TOTAL (SOLAR-AIDED)				1.06E-04	2.93E-01		1.03E-03		

ODP: Ozone Depletion Potential. GWP: Global Warming Potential. PCOP: Smog Formation Potential. ARP: Acid Rain Potential. HTPI: Human Toxicity Potential by Ingestion. HTPE: Human Toxicity Potential by Inhalation or Dermal Exposure. ATP: Aquatic Toxicity Potential. TTP: Terrestrial Toxicity Potential.

6.5 Conclusion

The results of the economic modelling and environmental impact study were presented and discussed in this chapter. These results showed that solar-aided biorefineries would require a capital investment considerably larger than their standalone-equivalent. A sensitivity analysis was performed to determine how key financial parameters would affect production costs. The environmental benefit of solar-aided biorefineries was also assessed against the standalone equivalent. Results obtained demonstrated that the solar aided biorefineries could have a significantly lower impact on the environment. The next chapter compares biological and thermochemical routes.

CHAPTER 7 – COMPARATIVE EVALUATION

7.1 Introduction

Methanol and ethanol are similar in many ways. For instance, compared to gasoline, they both have relatively high-octane numbers with larger heats of vaporization, making them excellent candidates for combustion systems. In addition, as shown in the previous chapters, they can both be derived from lignocellulosic biomass, which positions them as key players in the transition from a fossil to a bio-based economy. Even though methanol and ethanol share many similarities, they also have distinct attributes that render each of them unique. As an example, methanol can be used as a precursor for the synthesis of various value-added chemicals, while ethanol is capable of being combusted in conventional internal combustion engines without major modifications.

In spite of their well-known similarities and differences, there are still some uncertainties regarding the comparison of ethanol and methanol derived from lignocellulosic biomass. For instance, which of the two production processes is the more favourable option in terms of energy conversion efficiency, economic performance, and potential environmental impact? Also, how would each of these conversion processes differ if they were integrated with solar energy? The objective of this chapter is to provide information enabling to answer these questions based on results generated from process simulation. The chapter is expected to guide investors and decision makers in selecting which of the two would be the more favourable option in the implementation of the bio-economy in South Africa.

7.2 Comparison of conversion efficiency

A comparison of liquid fuel conversion efficiency and overall energy conversion efficiency for all the modelled scenarios is shown in Figure 7.1. As can be observed the standalone scenario for the thermochemical conversion has a liquid fuel conversion efficiency greater than the standalone scenario for the biological conversion. This is mainly due to the relatively high liquid fuel yield obtained from the thermochemical conversion. Moreover, in both biorefineries, the incorporation of solar energy combined with the

export of lignin or biochar results in an enhancement of overall energy conversion efficiency.

Moreover, in both the thermochemical and biological conversions, adding solar energy increased the liquid fuel conversion efficiency, except for scenarios 4 & 5 of biological conversion, where it remained relatively unaffected. The unchanged liquid fuel conversion efficiencies in scenarios 4 & 5 of biological conversion are due to the fact that in these scenarios, 60% of lignin-rich residues were combusted and only 40% were exported as a co-product. The thermal energy equivalent of lignin-rich residues exported after solar energy input is almost equivalent to the surplus electrical energy in the standalone scenario. As a result, liquid fuel conversion efficiency remains unchanged.

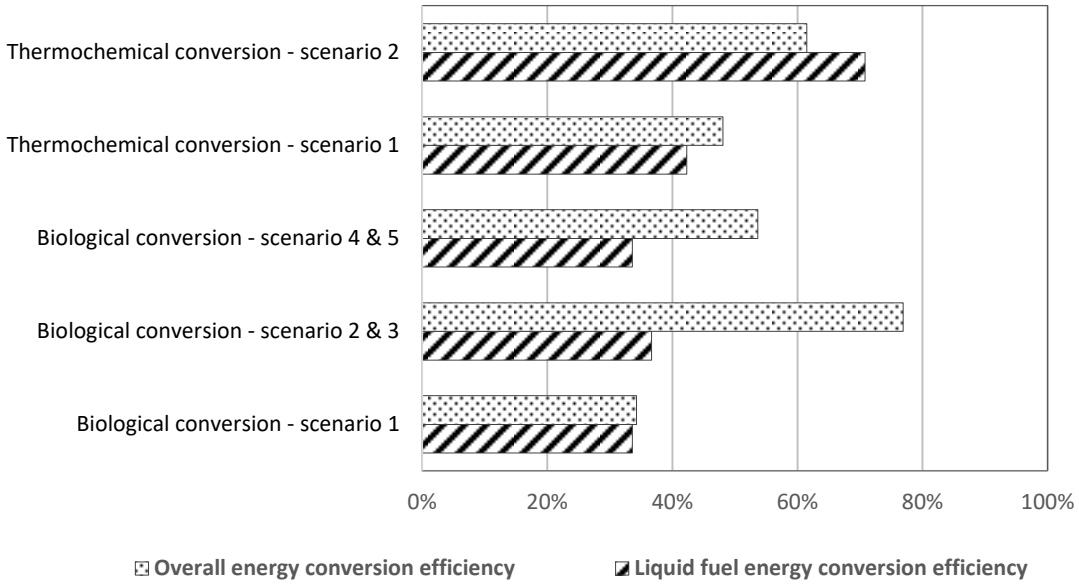

Figure 7.1: Comparison of energy conversion efficiency for modelled scenarios

Figure 7.2 shows a comparison between the conversion efficiencies obtained in this study and the literature data. As can be seen, the conversion efficiencies of modelled standalone scenarios are fairly comparable to literature data. However, solar-aided scenarios showed conversion efficiencies substantially greater than the standalone lignocellulosic biorefineries disclosed in the literature, with the exception once again of scenarios 4 & 5 for the reasons previously discussed. This trend confirms that the incorporation of solar energy combined with the export of carbonaceous co-products

does enhance the biorefinery's energy conversion efficiency. It is, however, worth noting that despite the enhancement in conversion efficiency, the liquid fuel output remains identical to the standalone scenario. Thus, as previously mentioned, the incorporation of solar energy does not mean that more liquid fuel is produced; rather, it simply allows the storage of intermittent solar energy in a dispatchable biochar or lignin form, which can then be used on-demand as bio-fertilizer, fuel, or starting materials for the production of other bio-materials.

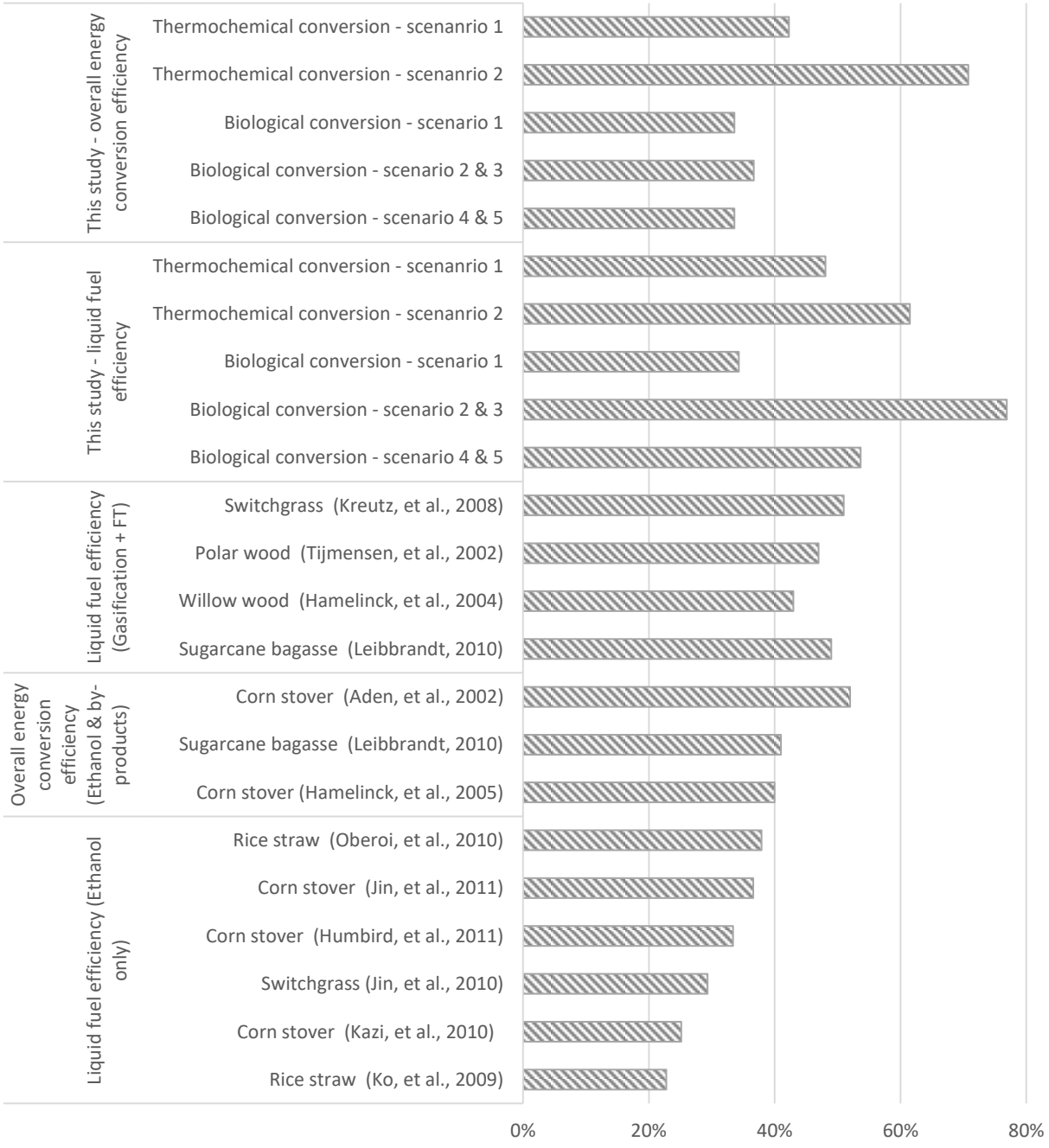

Figure 7.2: Comparison of energy conversion efficiency with literature data

Despite the comparison made between the literature data and results from this study, it is important for the reader to be reminded that the definitions used in the literature to calculate energy conversion efficiency vary from one author to another. And, in some cases, they are not even specified. Consequently, the calculated values may not always be accurately compared.

7.3 Comparison of production costs

A comparison in production costs between biological and thermochemical conversion routes is shown in Table 7.1. As can be seen, the relatively high methanol production rate led to a substantially low production cost (or minimum selling price). This was despite the fact that both biorefineries had comparable total capital investment. Please note that the production cost referred to in Table 7.1 is the minimum price at which liquid fuels must be sold in order to achieve a net present value of zero.

Although methanol had a lower production cost than ethanol, the latter is generally considered the more valuable of the two commodities. For instance, in 2019, a local chemical manufacturer sold methanol in bulk at 16.09 Rand/litre, while ethanol was priced at 18.75 Rand/litre. If the ethanol and methanol produced in the modelled biorefineries were sold at these prices, the internal rate of return would be 29.01% for the methanol and 19.87% for ethanol production from corn stover. These would correspond to returns on investment of 45.53 and 27.09% respectively. Thus, the modelled thermochemical biorefinery offers better investment potential.

Table 7.1: Comparison in production cost for biological and thermochemical conversions

	BIOLOGICAL CONVERSION *Ethanol production*	**THERMOCHEMICAL CONVERSION** *Methanol production*
Liquid fuel production rate (kg/hr)	19 326	33 760
Total capital investment ($M)	423	434
Annual Operating costs ($M)	49	36
Production cost of liquid fuel ($/GJ)	25.88	17.47
Production cost of liquid fuel (R/litre)*	10.63	5.48

*Based on 2019 financial year and dollar to ZAR exchange rate of 17.5

7.4 Comparison of environmental friendliness

7.4.1 Potential environmental impact

Figure 7.3 shows a comparison of the overall potential environmental impact obtained from the WAR algorithm. As can be seen, the standalone scenario for ethanol production had the highest overall potential environmental impact per kilogram of liquid fuel produced. However, in terms of hourly PEI, the standalone scenario for methanol production was the least eco-efficient option. Thus, this scenario is most likely to harm the environment around it. Of all the biorefineries modelled, scenarios 2 & 3 for ethanol production were the most environmentally friendly.

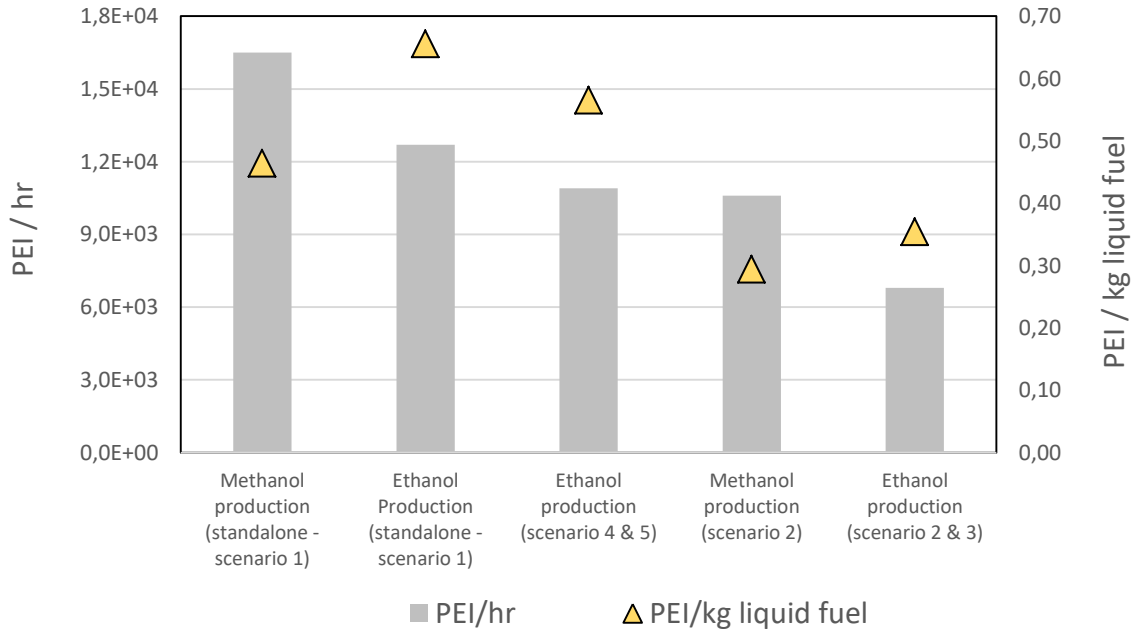

Figure 7.3: Comparison of overall potential environmental impact of modelled biorefineries

In spite of the differences in the feedstock and conversion processes, an attempt was made to compare the PEI values obtained in this study with those found in other studies (refer to Figure 7.4). As can be seen, the palm oil biorefinery disclosed by Herrera-Aristizábala, et al., (2017) had a PEI substantially higher than the values obtained in this study. Thus, the process used by Herrera-Aristizábala, et al., (2017) to produce crude palm oil, bio-hydrogen and palm kernel oil from African palm fruit might have a more

pronounced impact on the environment compared to the production of methanol and ethanol from corn stover.

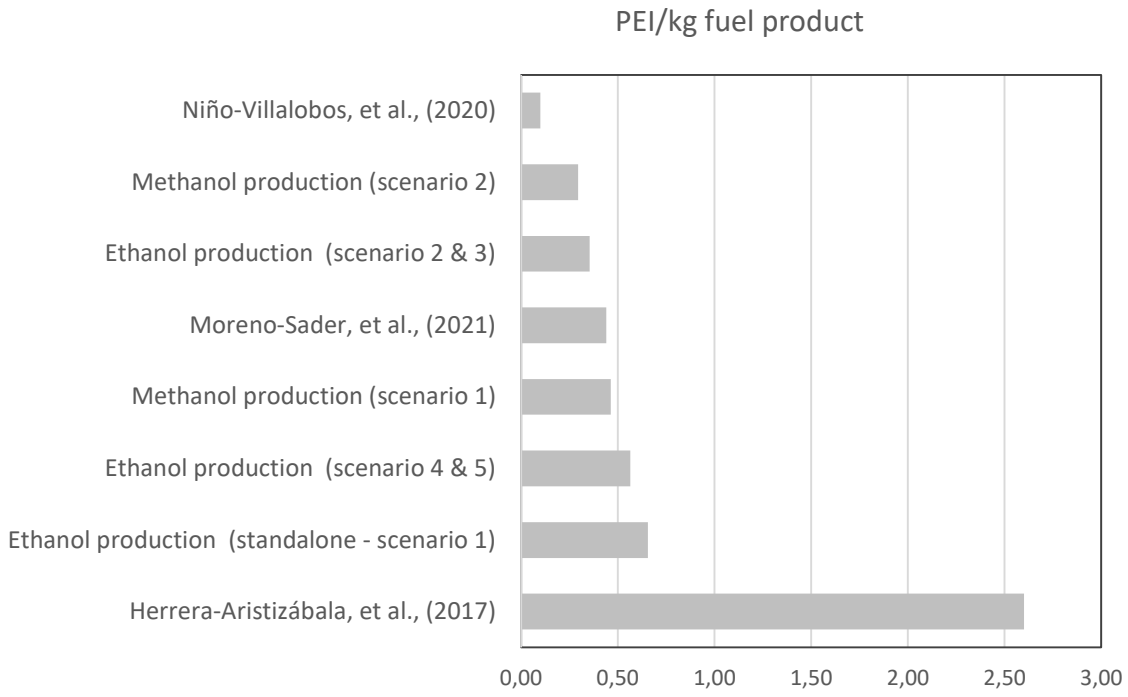

Figure 7.4: Comparison of overall potential environmental impact with literature data

Considering that Herrera-Aristizábala, et al., (2017) did not disclose the pertinent pollutant emitted, it would be difficult to precisely explain the rationale behind the relatively high PEI. However, one could speculate that this could be due to the fact that Herrera-Aristizábala, et al., (2017)'s biorefinery is an integration of three major conversion processes: firstly, the gasification of rachis for hydrogen production. Secondly, the extraction of palm oil from palm fruit. And finally, the conversion of palm fruit kernel into oil. Although the last two processes are not expected to emit major pollutants, H_2 production via gasification involves the complete removal and discharge of CH_4, CO and CO_2 to generate pure H_2.

Furthermore, the biorefinery modelled by Moreno-Sader, et al., (2021), which involved the conversion of fresh shrimp into shrimp meat, astaxantin, chitin and chitosan exhibited a PEI closer to the modelled biorefineries. Although the processes did not emit significant amounts of greenhouse gases, volatile organic compounds such as ethanol and

acetone used for product extraction were not entirely consumed. Hence, their partial emission adversely impacted the PEI output. Moreover, the combined palm and Jatropha Curcas biorefinery proposed by Niño-Villalobos, et al., (2020) exhibited a PEI output index considerably lower than the values obtained in this work.

7.4.2 Land use efficiency

Figure 7.5 shows a comparison between the land-use efficiency of solar fields used in the solar-aided biorefineries studied in this work and real-life utility-scale solar energy systems disclosed in the literature. Interestingly, most real-life utility scale solar energy systems shown in Figure 7.5 have land-use efficiencies lower than the values obtained in this study. This could be due to the simulation software assuming an ideal topography. Thus, no space is left empty, which in a real-life scenario, is rarely the case.

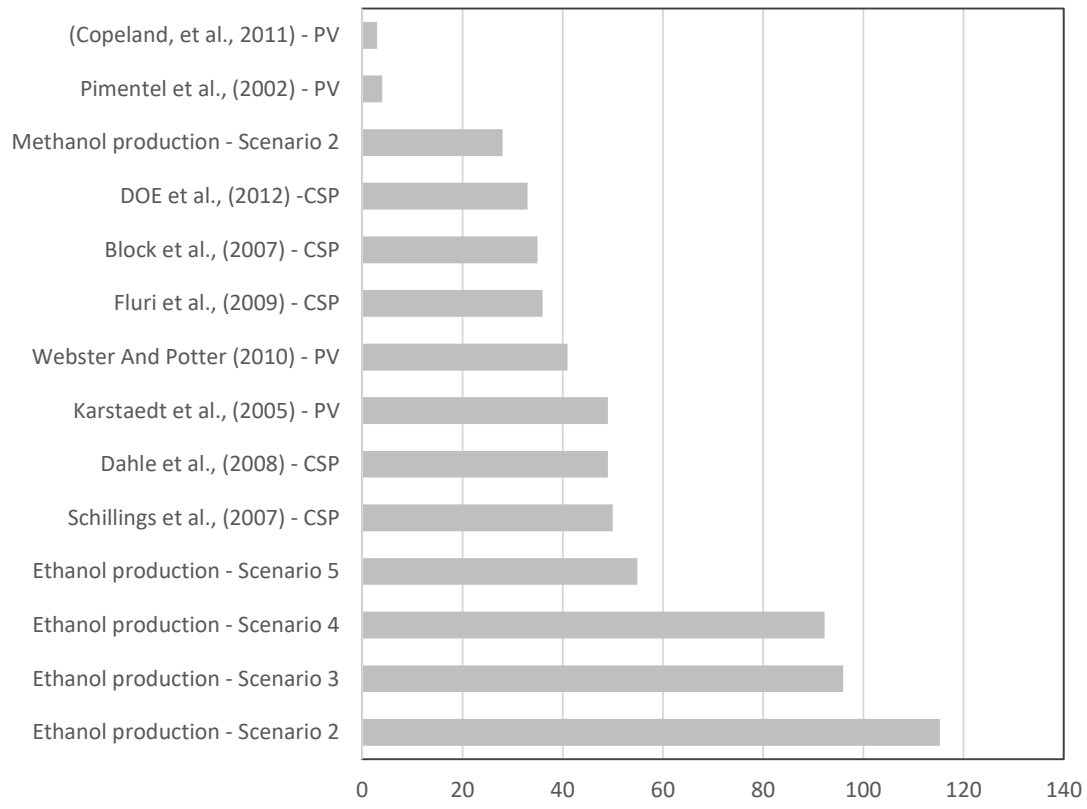

Figure 7.5: Land-use efficiency: solar power system of present study vs. literature data (W/m^2)

The LUE of solar-aided thermochemical conversion was found to be 28 (W/m^2), which almost 2 to 4 times lower than the Figure obtained for biological conversion. This is primarily because of the very high temperatures requires for gasification, which then results in a larger solar field needed for solar energy harvesting. For instance, solar aided gasification required 7.66 km^2 of land for the solar field, while biological conversion required between 0.35 and 2.06 km^2 depending on the scenario.

Furthermore, in biological conversion, the LUE corresponding to the generation of electricity with solar PV is considerably higher than CSP with a similar capacity. Hence, it is more land-efficient to use solar PV for the generation of process electricity. The highest LUE was obtained in scenario 2 of ethanol production, where solar PV was used for electricity generation and solar thermal was used for heat generation. Thus, scenario 4 is expected to have the least impact on land usage, followed by scenarios 3, 4, and 5. The solar-aided methanol production process is the least land-efficient process.

7.5 Conclusion

In conclusion, it can be said that the production of methanol from corn stover has a higher liquid fuel efficiency compared to the production of ethanol from corn stover. In addition, the thermochemical biorefinery offers greater investment potential. Furthermore, in terms of PEI, the standalone scenario for methanol production was the least eco-efficient option and scenarios 2 & 3 for ethanol production were the most environmentally friendly configurations. Finally, the integration of solar energy into the biorefinery is more land-efficient when biological conversion is employed.

CHAPTER 8: SUMMARY AND CONCLUSIONS

8.1 Summary

The study investigated the techno-economic performance and environmental impact of standalone and solar-aided lignocellulosic biorefineries using South Africa as a case study. Both biological and thermochemical conversion platforms were employed. In the biological platform (chapter 3), processes capable of converting corn stover into ethanol were developed. Five design scenarios were considered: one standalone scenario where lignin-rich residues were combusted alongside biogas from the adjacent wastewater treatment plant to supply energy to the biorefinery (scenario 1). Two solar-aided scenarios where lignin-rich residues were sold as a co-product, and combinations of concentrated solar thermal, concentrated solar power and solar photovoltaic were utilized to supply energy to the biorefinery (scenario 2 and 3). And two additional solar-aided scenarios where a portion of lignin-rich residues was combusted for process heat and solar photovoltaic/concentrated solar power were used for process electricity (scenario 4 and 5).

In the thermochemical platform (Chapter 4), corn stover was converted into methanol via gasification and syngas upgrading. The main focus was on the gasifier where two scenarios were considered: firstly, a standalone scenario involving gasification in a conventional TNEE-type dual-bed gasifier. And then, a solar-aided scenario where biochar generated in the gasification bed was exported as a co-product and solar energy was integrated into the biorefinery to drive the gasification chemical reactions using a novel solar-driven gasification approach. In addition, in the standalone scenario, a portion of the biomass feedstock was combusted alongside the unconverted syngas to generate process heat and electricity. While the solar-aided scenario used a combination of solar thermal and solar PV to generate process heat and electricity. The syngas generated was then upgraded to methanol through CO_2 hydrogenation.

The economic performance and environmental impact of all modelled biorefineries were assessed (Chapter 5) and discussed in detail (Chapter 6). A comparative analysis of biological and thermochemical conversions was then conducted (Chapter 7) with a focus on

conversion efficiency, production costs, and eco-friendliness. The main findings of the study can be summarized as follows:

- **BIOLOGICAL CONVERSION ROUTE:**

- A yearly ethanol production rate of 154 608 tonnes was achieved with corn stover feed rates of 833 336 tonnes/year. This was comparable to the 155 640 tonnes/year reported by Tao et al (2014) using a similar conversion process with an identical corn stover feeding rate.

- Process energy demand for all scenarios was found to be 6.06 MJ/$kg_{ethanol}$ for electrical energy, 19.56 MJ/$kg_{ethanol}$ for heat utility, and 0.1 MJ/$kg_{ethanol}$ for fossil energy (fuel consumed by trucks during biomass transportation).

- 31.8% of the LHV of corn stover was recovered in the bioethanol product. The relatively low ethanol energy recovery was attributed to the formation of side products, the relatively low xylan conversion during pretreatment, and more importantly, the inertness of lignin during the entire conversion process.

- For the standalone scenario, the overall energy conversion efficiency was 34.3%. In scenarios 2 & 3, it to 76.9%. While in scenarios 4 & 5, it was 56.7%. Thus, by exporting lignin as a co-product, and using solar power to meet the biorefinery's process energy requirements, the overall energy conversion efficiency is significantly enhanced.

- Liquid fuel efficiency was respectively found to be 33.6% for scenario 1, 36.7% for scenarios 2 & 3, and 33.6% for scenarios 4 & 5. The comparable liquid fuel conversion efficiencies in scenarios 1, 4 & 5 were explained by the fact that in these scenarios, 60% of lignin-rich residues were combusted and only 40% were exported as a co-product. The thermal energy equivalent of lignin-rich residues exported after solar energy input was almost equivalent to the surplus electrical energy in the standalone scenario. Therefore, liquid fuel conversion efficiency remained the same.

- The incorporation solar energy into to biorefinery processes led to the net energy ratio increasing from 1.25 (scenario 1), to 3.36 (scenarios 2 & 3) and 2.10 (scenarios 4 & 5). While the net energy output was enhanced from 6.61 MJ/kg $_{methanol}$ (scenario 1), to 60.50 MJ/kg $_{methanol}$ (scenarios 2 & 3), and 28.06 MJ/kg $_{methanol}$ (scenarios 4 & 5).

- The generation of process electricity from PV solar required 0.35 km^2 of land. This value increased further to 0.59 km^2 when CSP was used. Thus, the generation of process electricity using solar PV requires about 40% less land than CSP. Moreover, the generation of process heat using concentrated solar thermal equipped with linear Fresnel reflectors required 1.47 km^2 of land. It can therefore be deduced that solar energy will have a considerable impact on the physical footprint of biorefineries when used as their primary source of energy.

- Fixed capital investment for solar-aided biorefineries was 118 to 382% higher than the conventional standalone configuration. Thus, in order to make solar-aided lignocellulosic more attractive, substantial cost reductions or technological innovations may be required.

- The relatively high fixed capital was mainly due to two factors: firstly, the generation of process heat using concentrated solar thermal. Here, the most expensive component of the concentrated solar thermal system was the module, accounting for 91% of the capital cost of the concentrated solar thermal system. Secondly, the cost of energy storage: in scenarios involving solar PV, energy storage costs represented 93% of the capital cost of the solar PV system. While in scenarios involving CSP, energy storage costs represented 60% of the capital cost of the CSP system.

- The minimum ethanol selling price (MESP), was found to be 0.61 $/litre (25.88 $/GJ) for the standalone scenario. This was lower than the 0.70 $/litre (after cost-escalation) reported by Tao, et al., (2014). The relatively low MESP was mainly due to the discrepancies in biomass cost (18.49 $/tonne in the South African context vs 65.7 $/tonne after cost escalation in the American context). When compared to previous

South African-based models (both conducted with bagasse), the MESP of the present study was close to the values reported by Petersen (2017) and Leibbrandt (2010) using steam explosion pretreatment. The MESP of the present work was however 13% lower than the ethanol production cost reported by Leibbrandt (2010) using dilute acid with 35% (wt/wt) solid loading.

- Investment analysis revealed that, an IRR of 10% could be just low enough for lignocellulosic bioethanol from the standalone scenario to compete with a South African petrol price of 25 $/GJ. However, the main challenge here is the fact that fossil fuel prices are volatile and difficult to forecast. Additionally, an IRR of 10% might not be sufficiently rewarding to investors.

- Should the IRR be set to 20% to make the project more attractive to potential investors, or 30% which is generally desired for investment in new technologies, the MESP would increase to 1.09 $/litre (46.48 $/GJ) and 1.78 $/litre (75.75 $/GJ) respectively. And, with such high prices, bio-ethanol would require a significant price increase in fossil fuels in order to be competitive in the country and attract investors.

- Should the total capital investment of the standalone scenario be reduced by 30% due to future technological breakthroughs, the production costs could be as low as 0.50 $/litre (21.50 $/GJ), which may allow bioethanol to compete with a gasoline price of 25 $/GJ. However, by reducing the TCI by 30% and simultaneously raising the IRR from 10 to 15%, the MESP would be 27.74 $/GJ, which is not low enough to compete with the 2020's South African petrol price. Hence, even with a 30% lower capital investment, it will be challenging to achieve an attractive IRR.

- Furthermore, Should the biomass price increase from 18.49 $/ tonne to 27.73 $/tonne or 36.98 $/tonne, the MESP would shift to 28.00 and 30.11 $/GJ respectively, which could seriously upset the ability of bioethanol to compete with fossil fuels. The successful implementation of lignocellulosic bioethanol will therefore require some stability in the biomass price.

- In the solar-aided scenarios, the MESP were found to be 58.05 $/GJ for scenario 2, 68.84 $/GJ for scenario 3, 43.17 $/GJ for scenario 4, and 53.97 $/GJ for scenario 5. Thus, the ethanol selling price needs to be inflated by 32.16 $/GJ for scenario 2, 42.96 $/GJ for scenario 3, 17.29 $/GJ for scenario 4, and 28.09 $/GJ for scenario 5 to cover additional expenses related to the integration of solar energy.

- The minimum lignin selling price (MLSP), which was defined as the price at which lignin much be sold in order to achieve an ethanol production cost identical to the standalone scenario was found to be 1 625 $/tonne for scenario 2, 2 171 $/tonne for scenario 3, 2 184 $/tonne for scenario 4, and 3 549 $/tonne for scenario 5.

- A comparison with lignin market price showed that it is not currently economically viable to generate lignin as a co-product of a lignocellulosic biorefinery, especially given the fact that a purification step that will incur additional costs will be required.

- A 50% reduction in the fixed capital investment of solar-aided scenarios could result in the prices of lignin dropping to 495 $/tonne for scenario 2, 780 $/tonne for scenario 3, 257 $/tonne for scenario 4 and 969 $/tonne for scenario 5. These prices might be low enough for lignin co-product to compete on the market. Therefore, the commercialization of lignin as a co-product couple with the integration of solar energy as the main energy supply might require a major decline in the capital investment for the solar energy plant.

- The overall potential environmental impact (PEI/hr) for the standalone scenario was found to be $1.27x10^{+04}$. This value decreased to $1.09x10^{+04}$ in scenarios 4 & 5 and $6.8x10^{+03}$ in scenarios 2 & 3. Also, the scenarios where lignin is combusted for energy generation (scenarios 1, 4 and 5) had the least favorable potential environmental impact per unit of ethanol produced (PEI/kg ethanol). In order not to shift the environmental burden from the biorefinery to downstream value chain processes, the exported lignin-rich residues should ideally be used for a non-energy application where it will not be combusted.

- **THERMOCHEMICAL CONVERSION ROUTE:**

- The gasification model developed in this study was found to be in agreement with experimental data from Gourtay, et al., (1987). Hence, the model could predict the syngas composition of a TNEE-type dual bed gasifier. When comparing the gasification model developed in this work with Abdelouahed, (2012)'s modelling results, discrepancies were observed in the CO and CH_4 concentrations. These discrepancies were attributed to the differences in kinetic parameters employed to model chemical reactions taking place in the secondary reaction zone.

- The H_2 and CO molar flow rates were found to increase with an increasing gasification temperature. In contrast, the CH_4 flow rate followed the opposite trend. In addition, the CO_2 flow rate was found to increase with increasing temperatures, and then reached a plateau before subsequently decreasing. Although relatively high temperatures favoured the formation of H_2 and CO, the gasification bed was operated at 980 ^{o}C to prevent the ash from melting.

- The incorporation of solar energy as the heat source of a TNEE-type gasifier combined with the generation of biochar as a co-product improved the net gasification efficiency by 56 to 87%, depending on the biomass moisture content. The enhancement in net gasification efficiency was mainly due to exported biochar, given that sand would be entirely heated using solar energy.

- The biorefinery produced 270 418 tonnes of methanol per year which resulted in a carbon conversion efficiency of 31.0%. The overall energy conversion efficiency was found to be 48.1% for the standalone scenario and 61.5% for the solar-aided scenario. The liquid only efficiencies were respectively found to be 42.3% and 70.8% for the standalone and solar-aided scenarios.

- The syngas flow rate remained the same in the solar-aided scenario despite an increase in net gasification efficiency. Thus, the incorporation of solar energy does not mean that more syngas is produced; rather, it virtually allows the storage of intermittent solar energy in a dispatchable bio-char form, which can then be used

on-demand as bio-fertilizer, fuel, or starting materials for the production of other bio-materials.

- The thermal energy demand for the gasifier was 21.6 MJ/kg $_{methanol}$, which is equivalent to the calorific value of bio-char exported as a co-product when processing biomass with 38% (wt/wt) moisture. The other process energy demand was found to be 2.16 MJ/kg$_{methanol}$ for electrical energy, 1.26 MJ/kg$_{methanol}$ for heat utility, and 0.10 MJ/kg$_{methanol}$ for fossil energy (fuel consumed by trucks during biomass transportation).

- The incorporation solar energy into to biorefinery processes resulted in the net energy ratio increasing from 1.1 (standalone scenario), to 1.9 (solar-aided scenario). While the net energy output was improved from 1.9 MJ/kg $_{methanol}$ (standalone scenario), to 23.5 1.9 MJ/kg $_{methanol}$ (standalone scenario).

- The minimum methanol selling prices were respectively estimated to be **0.31 $/litre (17.47 $/GJ)** and **0.50 $/litre (27.88 $/GJ)** for the standalone scenario and solar-aided scenarios. While the minimum biochar selling price was estimated to be **13.04 $/GJ (0.37 $/kg)**. Sensitivity analysis revealed that that variations in TCI and biomass price have a more pronounced impact on the methanol production cost compared to the interest rate, fixed cost and income tax.

- When compared to the Amigun, et al., (2010)'s which is the only techno-economic study published so far on the production of methanol from corn stover residues in South Africa, a significant difference can be observed. This was attributed to the major discrepancies in raw materials costs.

- The integration of solar energy to drive the gasification process required a total land area of 6.92 km^2, which is substantial.

- The solar-aided scenario had an overall potential environmental impact almost 40% lower than the standalone scenario. This was mainly due to the elimination of char

combustion in the solar-aided scenario, which led to a reduction of CO_2 emissions. The integration of solar energy for biomass gasification could therefore considerably mitigate the environmental impact of a biomass-to-methanol biorefinery.

- The overall PEI/hr for the standalone scenario was found to be $1.65x10^{-04}$. This value decreased to $1.06x10^{+04}$ in the solar-aided configuration. The integration of solar energy could therefore considerably mitigate the environmental impact of a biomass-to-methanol biorefinery.

➢ **COMPARISON OF BIOLOGICAL AND THERMOCHEMICAL CONVERSION ROUTE:**

Methanol produced from corn stover had a liquid fuel conversion efficiency consistently higher than ethanol produced from corn stover. Furthermore, the corn stover-to-methanol biorefinery offered better investment potential than the corn stover-to-ethanol biorefinery. In both biorefineries, the incorporation of solar energy resulted in steep increases in capital investment and production costs. Moreover, the PEI/hr was the highest in the standalone scenario for methanol production. Thus, this configuration is the least eco-efficient option. On the other hand, scenarios 2 & 3 for ethanol production were the most environmentally friendly configurations. Finally, based on the scenarios studied, the integration of solar energy into the biorefinery is more land-efficient when biological conversion is employed.

8.2 Recommendation for future work

Following this study, several possible research initiatives have been identified. These include:

- Expand the modelling work to also consider the integration of other types of renewable energy sources such as geothermal into lignocellulosic biorefineries. This can be done by utilizing heat energy from geothermal well as add-on energy for gasification in thermochemical conversion or Physico-chemical pretreatment in biological conversion.

- Conduct a techno-economic analysis for the integration of solar energy into other biomass conversion processes such as pyrolysis and hydrothermal liquefaction.

- Conduct a comparative life cycle analysis of solar-aided biological and thermochemical conversion routes, to ascertain the trend observed using the WAR algorithm.

REFERENCES

Abbasi, T. & Abbasi, S., 2011. Decarbonization of fossil fuels as a strategy to control global warming. *Renewable and Sustainable Energy Reviews,* 15(4), pp. 1828-1834.

Abdelouahed, L. et al., 2012. Detailed Modeling of Biomass Gasification in Dual Fluidized Bed Reactors under Aspen Plus. *Energy & Fuels,* 26(6), p. 3840–3855.

Adapa, P., Tabil, L. & Schoenau, G., 2011. A Comprehensive Analysis of the Factors Affecting Densification of Barley, Canola, Oat and Wheat Straw Grinds. *The Canadian Society for Bioengineering - Paper written for presentation at the CSBE/SCGAB 2011 Annual Conference Inn at the Forks, Winnipeg, Manitoba,* Volume Paper No. CSBE11-513, pp. 1-31.

Aden , A. & Foust, T., 2009. Techno-economic analysis of the dilute sulfuric acid and enzymatic process for the converison of corn stover to ethanol. *Cellulose,* Volume 16, pp. 535-545.

Aden, A. et al., 2002. *Lignocellulosic Biomass to Ethanol Process Design and Economics Utilizing Co-Current Dilute Acid Prehydrolysis and Enzymatic Hydrolysis for Corn Stover,* Colorado: National Renewable Energy Laboratory.

Agbor , V. B. et al., 2011. Biomass pretreatment: Fundamentals toward application. *Biotechnology Advances,* 29(6), pp. 675-685.

Agbor, V. B. et al., 2011. Biomass pretreatment: Fundamentals toward application. *Biotechnology Advances,* 29(6), pp. 675-685.

Ali, N. et al., 2019. Fluidized bed fast pyrolysis of corn stover: Effects of fluidizing gas flow rate and composition. *Energy Sources,* Volume Part A: Recovery, Utilization, and Environmental Effects, pp. 1-3.

Alvira, P., Tomás-Pejó, E., Ballesteros, M. & Negro, M., 2010. Pretreatment technologies for an efficient bioethanol production process based on enzymatic hydrolysis: A review. *Bioresource Technology,* Volume 101, p. 4851–4861.

Amigun, B., Gorgens, J. & Knoetze, H., 2010. Biomethanol production from gasification of non-woody plant in South Africa: Optimum scale and economic performance. *Energy Policy,* 38(1), pp. 312-322.

Ansari, S. H. et al., 2020. Incorporation of solar-thermal energy into a gasification process to co-produce bio-fertilizer and power. *Environmental Pollution,* 266(3).

Ansari, S. H. & Liu, X., 2019. *ASPEN plus simulation study of concentrated solar power and biomass gasification for co-production of power and liquid fuel.* s.l., SOLARPACES 2018: International Conference on Concentrating Solar Power and Chemical Energy Systems.

Aranda , G. A. et al., 2013. Comparing direct and indirect fluidized bed gasification: Effect of redox cycle on olivine activity. *Environmental Progress & Sustainable Energy; Hoboken,* 33(3), pp. 711-720.

Arena, U., 2013. 17 - Fluidized bed gasification. In: F. Scala, ed. *Fluidized Bed Technologies for Near-Zero Emission Combustion and Gasification.* s.l.:Woodhead Publishing, pp. 765-812.

Arena, U., 2013. 17 - Fluidized bed gasification. In: F. Scala, ed. *Fluidized Bed Technologies for Near-Zero Emission Combustion and Gasification.* 1st ed. s.l.:Woodhead Publishing, pp. 765-812.

Asmar, B., 2010. *Fossil Fuels in the Arab World: Facts and Fiction - Global and Arab insights of oil, natural gas and coal.* s.l.:2050 Consulting.

Atabani, A. E. et al., 2022. Integrated biorefineries, circular bio-economy, and valorization of organic waste streams with respect to bio-products. *Biomass Conversion and Biorefinery,* 12(565).

Atnaw, S. M., Sulaiman, S. A. & Suzana, Y., 2014. Influence of Fuel Moisture Content and Reactor Temperature on the Calorific Value of Syngas Resulted from Gasification of Oil Palm Fronds. *The Scientific World Journal,* 2014(1), pp. 1-9.

Azadi, P., Inderwildi, O. R., Farnood, R. & King, D. A., 2013. Liquid fuels, hydrogen and chemicals from lignin: Acritical review. *Renewable and sustainable energy review,* Volume 21, pp. 506-523.

Azapagic, A. & Perdan, S., 2000. Indicators of Sustainable Development for Industry: A General Framework. *Process Safety and Environmental Protection,* 78(4), pp. 243-261.

Babu, 2008. Biomass pyrolysis: a state-of-the-art review. *Biofuels Bioproducts & Biorefining,* 2(5), pp. 2:393-414.

Bajwa , D., Pourhashem, G., Ullah, A. H. & Bajwa, S., 2019. A concise review of current lignin production, applications, products and their environmental impact. *Industrial Crops and Products,* Volume 139, pp. 111-526.

Bakshi,, B. R. & Fiksel, J., 2003. The quest for sustainability: Challenges for process systems engineering. *AIChE Journal,* 49(6), p. 1350–1358.

Balan, V., 2014. Current Challenges in Commercially Producing Biofuels from Lignocellulosic Biomass. *Hindawi Publishing Corporation. ISRN Biotechnology,* pp. 1-31.

Balat, M., 2008. Mechanisms of Thermochemical Biomass Conversion Processes. Part 1: Reactions of Pyrolysis. *Energy Sources, Part A,* Volume 30, pp. 620-635.

Baliban, R., Elia, J. & Floudas, C., 2010. Toward novel hybrid biomass, coal, and natural gas processes for satisfying current transportation fuel demands, 1: process alternatives, gasification modeling, process simulation, and economic analysis. *Industrial and engineering chemistry research,* 49(16), pp. 7343-7370.

Banerjee, S. et al., 2013. Technoeconomic Analysis of Biofuel Production and Biorefinery Operation Utilizing Geothermal Energy. *Energy & Fuels,* 27(3).

Baral, N. R. & Shah, A., 2017. Comparative techno-economic analysis of steam explosion, dilute sulfuric acid, ammonia fiber explosion and biological pretreatments of corn stover. *Bioresource Technology,* Volume 232, pp. 331-343.

Basu, P., 2013. Chapter 7 - Gasification Theory. In: P. Basu, ed. *iomass Gasification, Pyrolysis and Torrefaction (Second Edition).* s.l.:Academic Press, pp. 199-248.

Batidzirai, B. et al., 2016. Current and future technical, economic and environmental feasibility of maize and wheat residues supply for biomass energy application: Illustrated for South Africa. *Biomass and Bioenergy,* Volume 92, pp. 106-129.

Batidzirai, B. et al., 2016. Current and future technical, economic and environmental feasibility of maize and wheat residues supply for biomass energy application: illustrated for South Africa. *Biomass and Bioenergy,* Volume 92, pp. 106-129.

Bauen, A. et al., 2009. *MAIN REPORT "Bioenergy – a sustainable and reliable energy source. A review of status and prospects".* [Online]
Available at: http://www.ieabioenergy.com/wp-content/uploads/2013/10/MAIN-REPORT-Bioenergy-a-sustainable-and-reliable-energy-source.-A-review-of-status-and-prospects.pdf
[Accessed 14 Decembre 2017].

Bauer, T. et al., 2013. Material aspects of Solar Salt for sensible heat storage. *Applied Energy,* Volume 111, pp. 1114-1119.

Bellini, E., 2018. *Total completes solar plant at its biorefinery in France.* [Online]
Available at: https://www.pv-magazine.com/2018/01/18/total-completes-solar-plant-at-its-biorefinery-in-france/
[Accessed 23 April 2018].

Bellos, E., Mathioulakis, E., Papanicolaou, E. & Belessiotis, V., 2018. Experimental investigation of the daily performance of an integrated linear Fresnel reflector system. *Solar Energy,* Volume 167, pp. 220-230.

Bellos, E. & Tzivanidis, C., 2018. Multi-criteria evaluation of a nanofluid-based linear Fresnel solar collector. *Solar Energy,* Volume 163, pp. 200-214.

Bhaskar, T., Balagurumurthy, B., Singh, R. & Poddar, M. K., 2013. Chapter 12 - Thermochemical Route for Biohydrogen Production. In: J. C. P. C. H. C. L. Ashok Pandey, ed. *Biohydrogen.* s.l.:Elsevier, pp. 285-316.

Bhaskar, T., Balagurumurthy, B., Singh, R. & Poddar, M. K., 2013. Chapter 12 - Thermochemical Route for Biohydrogen Production. In: A. Pandey, J. Chang, P. C. Hallenbecka & C. Larroche, eds. *Biohydrogen.* s.l.:Elsevier, pp. 285-316.

Binder, J. B. & Raines, R. T., 2010. Fermentable sugars by chemical hydrolysis of biomass. *PNAS (Processings of the National Academy of Sciences of the United States of America),* Volume 10, pp. 4516-4521.

Bitra, V. S. et al., 2009. Direct mechanical energy measures of hammer mill comminution of switchgrass, wheat straw, and corn stover and analysis of their particle size distributions. *Powder Technology,* 193(1), p. 32 – 45.

Boerema, N., Morrison, G., Taylor, R. & Rosengarten, G., 2012. Liquid sodium versus Hitec as a heat transfer fluid in solar thermal central receiver systems. *Solar Energy,* 86(9), pp. 2293-2305.

Bolhar-Nordenkampf, M. &. H. H. &. R. R. &. T. H. &. A. C., 2002. *Biomass CHP Plant Güssing Using Gasification for Power Generation.* Phuket, Thailand, Conference: 2nd regional Conference on Energy Technology towards a clean envionnment: Volume: 1.

BP Statistical Review of World Energy, 2017. *Energy economics.* [Online]
Available at: https://www.bp.com/content/dam/bp/en/corporate/pdf/energy-economics/statistical-review-2017/bp-statistical-review-of-world-energy-2017-full-report.pdf
[Accessed 11 December 2017].

BP Statistical Review of World Energy, 2021. *Energy economics.* [Online]
Available at: https://www.bp.com/content/dam/bp/business-sites/en/global/corporate/pdfs/energy-economics/statistical-review/bp-stats-review-2021-full-report.pdf
[Accessed 26 May 2022].

Bridgwater, A., 2012. Review of fast pyrolysis of biomass and product upgrading. *Biomass and Bioenergy,* Volume 38, pp. 68-94.

Bridgwater, A., Meier, D. & Radlein, D., 1999. An overview of fast pyrolysis of biomass. *Organic geochemistry,* Volume 30, pp. 1479-1493.

Brown, T., 2015. A techno-economic review of thermochemical cellulosic biofuel pathways. *Bioresource Technology,* Volume 178, pp. 166-176.

Bussche, K. V. & Froment, G., 1996. A Steady-State Kinetic Model for Methanol Synthesis and the Water Gas Shift Reaction on a Commercial Cu / ZnO / Al 2 O 3 Catalyst. *Journal of Catlysis,* 161(ARTICLE NO. 0156), pp. 1-10.

Bustamante, F. et al., 2004. High-temperature kinetics of the homogeneous reverse water–gas shift reaction. *American Institute of Chemical Engineers,* Volume 50, pp. 1028-1041.

Bustamante, F. et al., 2005. Uncatalyzed and wall-catalyzed forward water–gas shift reaction kinetics. *American Institute of Chemical Engineers,* Volume 51, pp. 1440-1454.

Cabeza, A., Piqueras, C., Sobrón, F. & García-Serna, J., 2016. Modeling of biomass fractionation in a lab-scale biorefinery: Solubilization of hemicellulose and cellulose from holm oakwood using subcritical water. *Bioresource Technology,* Volume 200, pp. 90-102.

Cabezas, H., Bare, C. J. & Mallick, S. K., 1997. Pollution prevention with chemical process simulators: the generalized waste reduction (WAR) algorithm. *Computers in Chemical Engineering,* Volume 21, p. S305–S310.

Cabezas, H., Bare, J. C. & Mallick, S. K., 1999. Pollution prevention with chemical process simulators: the generalized waste reduction (WAR) algorithm—full version. *Computers and chemical engineering ,* 23(4-5), pp. 623-634.

Cao, L. et al., 2017. Hydrothermal liquefaction of agricultural and forestry wastes: state-of-the art review and future propects. *Bioresource Technology,* 245(Part A), pp. 1184-1193.

Carlos, Q.-A., John, S. & Thomas, B., 2017. Life cycle net energy and greenhouse gas emissions of photosynthetic cyanobacterial biorefineries: Challenges for industrial production of biofuels. *Algal Research,* Volume 26, pp. 445-452.

Carolan, J. E., Joshi, S. V. & Dale, B. E., 2007. Technical and Financial Feasibility Analysis of Distributed Bioprocessing Using Regional Biomass Pre-Processing Centers. *Journal of agricultural & food industrial organization,* 5(No. 2), pp. 1-29.

Channiwala, S. & Parikh, P., 2002. A unified correlation for estimating HHV of solid, liquid and gaseous fuels. *Fuel,* 81(8), pp. 1051-1063.

Channiwala, S. & Parikh, P., 2002. A unified correlation for estimating HHV of solid, liquid and gaseous fuels. *Fuel,* 81(8), pp. 1051-1063.

Chen , X. et al., 2012. The impacts of deacetylation prior to dilute acid pretreatment on the bioethanol process. *Biotechnology for Biofuels,* 5(8), pp. 1-14.

Cheng, J. J. & Timilsina, G. R., 2011. Status and barriers of advanced biofuel technologies: A review. *Renewable Energy,* 36(12), pp. 3541-3549.

Chen, L., Jiang, Q., Song, Z. & Posarac, D., 2011. Optimization of Methanol Yield from a Lurgi Reactor. *Chemical Engineering & Technology,* 34(5), p. 817–822.

Chinchen, G. et al., 1987. Mechanism of methanol synthesis from CO2/CO/H2 mixtures over copper/zinc oxide/alumina catalysts: use of14C-labelled reactants. *Applied Catalysis,* 30(2), pp. 333-338.

Clark, R.-J. & Farid, M., 2022. Experimental investigation into cascade thermochemical energy storage system using SrCl2-cement and zeolite-13X materials. *Applied Energy,* Volume 316, p. 119145.

Commandre, J.-M., Lahmidi, H., Salvador, S. & Dupassieux, N., 2011. Pyrolysis of wood at high temperature: The influence of experimental parameters on gaseous products. *Fuel processing technology,* 92(5), pp. 837-844.

Corella, J. & Sanz, A., 2005. Modelling Circulating Fluidized Bed Biomass Gasifiers. A Pseudo-Rigorous Model for Stationary State. *Fuel Processing Technology,* 86(No. 9), pp. 1021-1053.

Da Silva, A. R., Ortega, C. E. T. & Rong, B.-G., 2016. Techno-economic analysis of different pretreatment processes for lignocellulosic-based bioethanol production. *Bioresource Technology,* Volume 218, pp. 561-570.

Dadile, A. M. et al., 2020. Evaluation of Elemental and Chemical Compositions of Some Fuelwood Species for Energy Value. *International Journal of Forestry Research,* Volume 2020, pp. 1-8.

Dai, J. et al., 2008. Overview and some issues related to co-firing biomass and coal. *The Canadian journal of chemical engineering,* 86(3), pp. 367-386.

Dale, B. E., 2003. Biomass, Bioengineering. In: R. A. Meyers, ed. *Encyclopedia of Physical Science and Technology (Third Edition).* Michigan: Academic Press, pp. 141-157.

Dalgaard, T., Halberg, N. & Porter, J. R., 2001. A model for fossil energy use in Danish agriculture used to compare organic and conventional farming. *Agriculture, Ecosystems and Environment,* Volume 87, pp. 51-65.

Daugaard, D. E. & Brown, C., 2003. Enthalpy for Pyrolysis for Several Types of Biomass. *Energy & Fuels,* Volume 17, pp. 934-939.

Dávila, I., Gullón, B., Labidi, J. & Gullón, P., 2019. Multiproduct biorefinery from vine shoots: Bio-ethanol and lignin production. *Renewable Energy,* Volume 142, pp. 612-623.

Davis, R. et al., 2018. *Process Design and Economics for the Conversion of Lignocellulosic Biomass to Hydrocarbon Fuels and Coproducts: 2018 Biochemical Design Case Update. Biochemical Deconstruction and Conversion of Biomass to Fuels and Products via Integrated Biorefinery Path,* s.l.: National Renewable Energy Laboratory.

De Olivera, M. E. D., Vaughan, B. E. & Rykiel Jr., E., 2005. Ethanol as Fuel: Energy, Carbon Dioxide Balances, and Ecological Footprint. *Biofuel,* 55(7), pp. 593-602.

De Wild, P. J., 2015. Biomass pyrolysis for hybrid biorefineries. In: *Industrial biorefineries & white biotechnology.* s.l.:Elsevier B.V., pp. 341-367.

Dermibas, M., 2009. Biorefineries for biofuel upgrading: a critical review. *Applied energy,* 86(Supplement 1), pp. 151-161.

Dhyani, V. & Bhaskar, T., 2017. A comprehensive review on the pyrolysis of lignocellulosic biomass. *In Renewable Energy,* pp. 0960-1481.

Diago, M. et al., 2015. Characterization of Desert Sand for its Feasible use as Thermal Energy Storage Medium. *Energy Procedia,* Volume 75, pp. 2113-2118.

Diago, M. et al., 2016. Characterization of desert sand as a sensible thermal energy storage medium. *AIP Conference proceedings,* 1734(050011), pp. 1-9.

Diago, M., Iniesta, A. C., Soum-Glaude, A. & Calvet, N., 2018. Characterization of desert sand to be used as a high-temperature thermal energy storage medium in particle solar receiver technology. *Applied Energy,* Volume 216, pp. 402-413.

Dimitriou, I., Goldingay, H. & Bridgwater, A. V., 2018. Techno-economic and uncertainty analysis of Biomass to Liquid (BTL) systems for transport fuel production. *Renewable and Sustainable Energy Reviews,* Volume 88, pp. 160-175.

Din, Z. U. & Zainal, Z., 2016. Biomass integrated gasification–SOFC systems: Technology overview. *Renewable and Sustainable Energy Reviews,* Volume 53, pp. 1356-1376.

DOE, 2007. *Biofuels Industrial Strategy of the Republic of South Africa,* s.l.: s.n.

DoE, 2021. *The petrol price doubled over the past decade - with fuel tax jumping 132%.* [Online]
Available at: http://www.energy.gov.za/files/esources/petroleum/petroleum_arch.html
[Accessed 03 03 2021].

Doherty, W., Reynolds, A. & Kennedy, D., 2009. The effect of air preheating in a biomass CFB gasifier using ASPEN Plus simulation. *Biomass and Bioenergy,* 33(9), pp. 1158-1167.

Domingues, J., Pelletier, C. & Brunelle, T., 2022. Cost of ligno-cellulosic biomass production for bioenergy: A review in 45 countries. *Biomass and Bioenergy,* Volume 165, p. 106583.

Donnot, A., Reningovolo, J., Magne, P. & Deglise, X., 1985. Flash pyrolysis of tar from the pyrolysis of pine bark,. *Journal of Analytical and Applied Pyrolysis,,* 8(1), pp. 401-414.

Do, T. X. & Lim, Y.-i., 2016. Techno-economic comparison of three energy conversion pathways from empty fruit bunches. *Renewable Energy,* pp. 307-318.

Do, T. X. & Lim, Y.-i., 2016. Techno-economic comparison of three energy conversion pathways from empty fruit bunches. *Renewable Energy,* Volume 90, pp. 307-318.

Dufour, A., Girods, P., Masson, E. & Rogaume, Y. Z. A., 2009. Synthesis gas production by biomass pyrolysis: Effect of reactor temperature on product distribution. *International Journal of Hydrogen Energy,* 34(4), pp. 1726-1734.

Dupont, C., Chiriac, R., Gauthier, G. & Toche, F., 2014. Heat capacity measurements of various biomass types and pyrolysis residues. *Fuel,* Volume 115, pp. 644-651.

Duque, S. H., Cardona, C. A. & Moncada, J., 2015. Techno-Economic and Environmental Analysis of Ethanol Production from 10 Agroindustrial Residues in Colombia. *Energy & Fuels,* 29(2), p. 775–783.

Dutta, A. & Acharya, B., 2011. Chapter 16 - Production of bio-syngas and biohydrogen via gasification. In: R. Luque, J. Campelo & J. Clark, eds. *Handbook of Biofuels Production.* s.l.:Handbook of Biofuels Production, pp. 420-459.

Eskom, 2021. *ESKOM tarrif history.* [Online]
Available at: https://www.eskom.co.za/CustomerCare/TariffsAndCharges/Pages/Tariff_History.aspx
[Accessed 09 03 2021].

ESSO, 2019. *Raffinerie Esso de Fos-sur-Mer.* [Online]
Available at: https://corporate.esso.fr/-/media/France/Files/La-raffinerie-de-Fos-sur-Mer.pdf?la=fr-FR&hash=08EF118B06245AE0096D3D0480D71FD5F6645518
[Accessed 27 June 2022].

Fagernäs, L. et al., 2010. Drying of biomass for second generation synfuel production. *Biomass and Bioenergy,* 34(9), pp. 1267-1277.

Fao, 2000. *The Energy and Agriculture Nexus - Environment and Natural Resources Working Paper No. 4 ,* Rome: Fao.

Fedeli, M., Negri, F. & Manenti, F., 2022. Biogas to advanced biofuels: Techno-economic analysis of one-step dimethyl ether synthesis. *Journal of Cleaner Production,* Volume 376, p. 134076.

Font, R., 2018. Chapter 9 - Decomposition of Organic Wastes: Thermal Analysis and Evolution of Volatiles. In: S. Vyazovkin, N. Koga & C. Schick, eds. *Handbook of Thermal Analysis and Calorimetry.* s.l.:Elsevier Science B.V., pp. 339-397.

Friedl, A., Padouvas, E., Rotter, H. & Varmuza, K., 2005. Prediction of heating values of biomass fuel from elemental composition. *Analytica Chimia Acta,* 544(1-2), pp. 191-198.

Gemna, W., 2014. *9 Advantages Of Fossil Fuels: Enjoy Them While They Last.* [Online]
Available at: https://blog.udemy.com/advantages-of-fossil-fuels/
[Accessed 26 January 2018].

GhasemiKafrudi, E., Samiee, L., Mansourpour, Z. & Rostami, T., 2022. Optimization of methanol production process from carbon dioxide hydrogenation in order to reduce recycle flow and energy consumption. *Journal of Cleaner Production,* Volume 376, p. 134184.

Giuliano, A., Poletto, M. & Barletta, D., 2015. *Process Design of a Multi-Product Lignocellulosic Biorefinery.* Copenhagen, Denmark, s.n.

Gnansounou, E. & Dauriat, A., 2005. Ethanol fuel from biomass a review. *Journal of scientific and industrial research,* Volume 64, pp. 809-821.

Gollakota, A., Kishore, N. & Gu, S., 2018. A review on hydrothermal liquefaction of biomass. *Renewable and Sustainable Energy Reviews,* 81(1), pp. 1378-1392.

Gollakota, A., Kishore, N. & Gu, S., 2018. A review on hydrothermal liquefaction of biomass. *Renewable and Sustainable Energy Reviews,* 81(Part 1), pp. 1378-1392.

Gomaa, M. R., Mustafa, R. J. & Al-Dmour, N., 2020. Solar thermochemical conversion of carbonaceous materials into syngas by Co-Gasification. *Journal of Cleaner Production,* Volume 248, p. 119185.

Gomez, J., Calvet, N., Starace, A. & Glatzmaier, G., 2013. Ca (NO3) 2—NaNO3—KNO3 molten salt mixtures for direct thermal energy storage systems in parabolic trough plants. *Journal of solar energy engineering,* 135(2), p. 21016.

Gonzales, D., Searcy, E. M. & Ekşioğlu, S. D., 2013. Cost analysis for high-volume and long-haul transportation of densified biomass feedstock. *Transportation Research Part A: Policy and Practice,* Volume 49, pp. 48-61.

Götz, M., Köppel, W., Reimert, R. & Graf, F., 2012. Potential to Optimize Scrubbers for Biogas Cleaning Part 2.Chemical Scrubbers (in German; Optimierungspotenzial von Wäschen zur Biogasaufbereitung Teil 2. Chemische Wäschen).. *Chemie Ingenieur Technik,* 84(1-2), p. 81–87.

Gourtay, F., Nogues, J., Le Lan, . A. & Déglise, X., 1987. Le procédé TNEE de pyrolyse rapide Son application dans l'industrie de la pâte à papier. *Journées techniques MEI, Paris France*.

Graboski, M. S., 2002. *Fossil Energy Use in the Manufacture of Corn Ethanol,* Washington, DC: National Corn Growers Association.

Gubicza, K. et al., 2016. Techno-economic analysis of ethanol production from sugarcane bagasse using a Liquefaction plus Simultaneous Saccharification and co-Fermentation process. *Bioresource Technology,* pp. 42-48.

Gutiérrez, R., Guerra, K. & Haro, P., 2022. Exploring the techno-economic feasibility of new bioeconomy concepts: Solar-assisted thermochemical biorefineries. *Applied Energy,* Volume 322, pp. 119535,.

Hagman, L., Blumenthal, A., Eklund, M. & Svensson, N., 2018. The role of biogas solutions in sustainable biorefineries. *Journal of Cleaner Production,* Volume 172, pp. 3982-3989.

Hamdan, M., Sebastia-Saez, D., Hamdan, M. & Arellano-Garcia, H., 2020. CFD Analysis of the Use of Desert Sand as Thermal Energy Storage Medium in a Solar Powered Fluidised Bed Harvesting Unit. *Computer Aided Chemical Engineering,* Volume 48, pp. 349-354.

Hamelinck, C. N. & Faaij, A. P., 2002. Future prospects for production of methanol and hydrogen from biomass. *Journal of Power Sources,* 111(1), pp. 1-22.

Hamelinck, C. N., Faaij, A. P. & Uil, H. d., 2004. Production of FT transportation fuels from biomass;technical options, process analysis and optimisation, and development potential. *Energy,* Volume 29, p. 1743 – 1771.

Hamelinck, C. N., Hooijdonk, G. v. & Faaij, A. P., 2005. Ethanol from lignocellulosic biomass: techno-economic performance in short-, middle- and long term. *Biomass & Bioenergy,* 28(4), pp. 384-410.

Hanchate, N., Ramani, S., Mathpati, C. & Dalvi, V. H., 2021. Biomass gasification using dual fluidized bed gasification systems: A review. *Journal of Cleaner Production,* 280(part 1), pp. 123148,.

Haro, P., Ollera, P., Villanueva Perales, A. & Vidal-Barrero, F., 2013. Potential routes for Thermochemical biorefineries. *Biofuels bioproducts and biorefining,* 7(5), pp. 551-572.

Hebecker, D., Bittrich, P. & Riedl, K., 2005. Hierarchically structured exergetic and exergoeconomic analysis and evaluation of energy conversion processes. *Energy conversion and management,* Volume 46, p. 1247–1266.

Helfert, E. A., 2000. *Financial analysis: tools and techniques.* s.l.:McGraw-Hill.

Hernandez, R. R., Hoffacker, M. K. & Christopher, F. B., 2013. Land-Use Efficiency of Big Solar. *Environmental science and technology,* Volume 48, pp. 1315-1323.

Herrera-Aristizábala, R., Salgado-Dueñasa, J. S., Peralta-Ruizb, Y. Y. & González-Delgado, Á. D., 2017. Environmental Evaluation of a Palm-based biorefinery under North-Colombian Conditions. *Chemical engineering Transactions,* Volume 57, pp. 193-198.

Heyne, S. & Harvey, S., 2013. Impact of choice of CO2 separation technology on thermo-economic performance of Bio-SNG production processes. *International Journal of Energy Research,* Volume 38, pp. 299-318.

Hilaly, A. & Sikdar, S., 1994. Pollution balance: a new method for minimizing waste production in manufacturing processes. *J Air & Waste Manage Assoc,* Volume 44, pp. 1303-1308.

Hitcher, J. R., 2011. *Financial valuation: Applications and Models.* Hitcher, James R.; ed. s.l.:John Wiley & Sons, Inc., Hoboken, New Jersey.

Hitchner, J. R., 2011. *Financial Valuation: Applications and Models (Wiley Finance).* 3th ed. Hoboken, New Jersey.: John Wiley & Sons, Inc..

Hodásová, L., Jablonsky, M., Skulcova, A. & Haz, A., 2015. Lignin, potential products and their market value. *Wood reserach,* 60(6), pp. 973-986.

Hodge, D. B., Karim, N. M., Schell, D. J. & McMillan, J. D., 2008. Soluble and insoluble solids contributions to high-solids enzymatic hydrolysis of lignocellulose. *Bioresource Technology,* 99(18), pp. 8940-8948.

Hoel, M. & Kvermdokk, S., 1996. Depletion of fossil fuels and the impact of global warming. *Resource and energy economics,* 18(2), pp. 115-136.

Hosseini, S. E. et al., 2015. A review on biomass-based hydrogen production for renewable energy supply. *International Journal of Energy Research,* Volume 39, p. 1597–1615.

Hu, J., Yu, F. & Lu, Y., 2012. Application of Fischer–Tropsch Synthesis in Biomass to Liquid Conversion. *Catalysts,* 2(2), pp. 303-326.

Humbird, D. et al., 2011. *Process Design and Economics for Biochemical Conversion of Lignocellulosic Biomass to Ethanol: Dilute-Acid Pretreatment and Enzymatic Hydrolysis of Corn Stover.* [Online] Available at: https://www.nrel.gov/docs/fy11osti/47764.pdf
[Accessed 15 November 2017].

Humbird, D. et al., 2011. *Process Design and Economics for Biochemical Conversion of Lignocellulosic Biomass to Ethanol: Dilute-Acid Pretreatment and Enzymatic Hydrolysis of Corn Stover.* [Online] Available at: https://www.nrel.gov/docs/fy11osti/47764.pdf
[Accessed 04 October 2018].

Hu, X. & Gholizadeh, M., 2019. Biomass pyrolysis: A review of the process development and challenges from initial researches up to the commercialisation stage. *Journal of Energy Chemistry,* Volume 39, pp. 109-143.

Ibarra-Gonzalez, P. & Rong, B.-G., 2019. A review of the current state of biofuels production from lignocellulosic biomass using thermochemical conversion routes. *Chinese Journal of Chemical Engineering,* 27(7), pp. 1523-1535.

Iliuta, I., Leclerc, A. & Larachi, F., 2010. Allothermal steam gasification of biomass in cyclic multi-compartment bubbling fluidized-bed gasifier/combustor – New reactor concept. *Bioresource Technology,* 101(9), pp. 3194-3208.

Iqbal, Y. & Lewandowski, I., 2016. Biomass composition and ash melting behaviour of selected miscanthus genotypes in Southern Germany,. *Fuel,* 180(1), pp. 606-612.

Jain, S. & Jain, P. K., 2017. The rise of Renewable Energy implementation in South Africa. *Energy Procedia,* Volume 143, pp. 721-726.

Jambo, S. A., Abdulla, R., Azhar, S. H. M. & Marbawi, H., 2016. A review on third generation bioethanol feedstock. *Renewable and sustainable energy review,* Volume 65, pp. 756-769.

Jean-Christophe, B., Anne-Célia Disdier, C. G. & David, T., 2010. A quantitative assessment of the determinants of the net energy value of biofuels. *Energy Policy,* 38(5).

Jenkins, B., Baxter, L., Miles Jr., T. & Miles, T., 1998. Combustion properties of biomass. *Fuel Processing Technology,* 54(1-3), pp. 17-46.

Jianzhong, Y. et al., 2000. Fast pyrolysis of corn stover. *Engineering Chemistry and Metallurgy ,* Volume 21, pp. 434-437.

Jin, H. & Hong, H., 2012. Chapter 12 - Hybridization of concentrating solar power (CSP) with fossil fuel power plants. In: K. Lovegrove & W. Stein, eds. *Concentrating Solar Power Technology.* s.l.:Woodhead Publishing, pp. 395-420.

Jin, M., Balan, V., Gunawan, C. & Dale, B. E., 2011. Consolidated Bioprocessing (CBP) Performance of Clostridium phytofermentans on AFEX-Treated Corn Stover for Ethanol Production. *Biotechnology and Bioengineering ,* 108(6), p. 1290e7.

Jin, Q. et al., 2021. Techno-economic analysis of a grape pomace biorefinery: Production of seed oil, polyphenols, and biochar. *Food and Bioproducts Processing,* Volume 127, pp. 139-151.

Jones, W. & Lindstedt, R., 1988. Global reaction schemes for hydrocarbon combustion. *Combustion and Flame,* 73(3), pp. 233-249.

Jungmeier, G. et al., 2013. The "biorefinery fact sheet" and its application to wood based biorefining - Case studies of IEA Bioenergy task 42 "Biorefining". *Joanneum research resources.*

Kamran, M., 2021. Chapter 4 - Solar energy. In: M. Kamran & M. R. Fazal, eds. *Renewable Energy Conversion Systems.* s.l.:Academic Press, pp. 109-152.

Kan, T., Strezov, V. & Evans, T. J., 2016. Lignocellulosic biomass pyrolysis: A review of product properties and effects of pyrolysis parameters. *Renewable and Sustainable Energy Reviews,* Volume 57, p. 1126 –1140.

Karan, H. et al., 2022. Solar biorefinery concept for sustainable co-production of microalgae-based protein and renewable fuel. *Journal of Cleaner Production,* Volume 368, p. 132981.

Karimi, K., Shafiei, M. & Kumar, R., 2013. Progress in Physical and Chemical Pretreatment of Lignocellulosic Biomass. *Biofuel Technologies,* pp. 53-96.

Kazi, F. K. et al., 2010. Techno-economic comparison of process technologies for biochemical ethanol production fram corn stover. *Fuel,* Volume 89, pp. S20-S28.

Kazi, K. F., Fortman, J. & Anex, R., 2010. *Techno-economic analysis of biochemical scenarios for production of cellu- losic ethanol.* [Online]
Available at: https://www.nrel.gov/docs/fy10osti/46588.pdf
[Accessed 31 August 2019].

Kim, T. H., Kim, J. S., Sunwoo, L. C. & Y.Y, 2003. Pretreatment of corn stover by aqueous ammonia. *Bioresource Technology,* 90(1), pp. 39-47.

Kirsanovs, V. et al., 2017. *Experimental investigation of downdraft gasifier at various conditions.* Riga, Latvia, Elsevier.

Ko, J. K. et al., 2009. Ethanol production from rice straw using optimized aqueous-ammonia soaking pretreatment and simultaneous saccharification and fermentation processes. *Bioresource Technology,* 100(19), pp. 4374-4380.

Ko, J. K. et al., 2016. Ethanol production from lignocellulosic hydrolysates using engineered saccharomyces cerevisiae harboring xylose isomerase-based pathway. *Bioresource Technology,* Volume 209, pp. 290-296.

Korhonen, J., Honkasalo, A. & Seppälä, J., 2018. Circular Economy: The Concept and its Limitations. *Ecological Economics,* Volume 143, pp. 37-46.

Kovarik , B., 1998. Henry Ford, Charles F. Kettering and the fuel of the future. *Automotive history review,* Volume 32, pp. 7-27.

Krajnc, D. & Glavič, P., 2003. Indicators of sustainable production. *Clean Technologies and Environmental Policy,* 5(3-4), pp. 279-288.

Kraszkiewicz, A., Kachel-Jakubowska, M. & Niedziolka, I., 2017. The chemical composition of ash from the plant biomass in terms of indicators to assess slagging and pollution of surface heating equipment. *Fresenius Environmental Bulletin,* 26(No. 11), pp. 6383-6389.

Kreutz, T. G., Larson, E. D., Liu, G. & Williams, R. H., 2008. *Fischer-Tropsch Fuels from Coal and Biomass.* Pittsburgh, Pennsylvania, USA, 25th Annual International Pittsburgh Coal Conference.

Kudar, R. C. et al., 2011. Bioethanol production from pentose sugars: Current status and future prospects. *Renewable and Sustainable Energy Reviews,* 15(9), pp. 4950-4962.

Kuhn, E. M., Chen, X. & Tucker, M. P., 2020. Deacetylation and Mechanical Refining (DMR) and Deacetylationand Dilute Acid (DDA) Pretreatment of Corn Stover, Switchgrass, and a 50:50 Corn Stover/Switchgrass Blend. *Sustainable Chemistry and Engineering,* pp. 6734 - 6743.

Kumbhar, S. & Khot, S., 2023. Experimental investigations of ethanol-gasoline blends on the performance, combustion, and emission characteristics of spark ignition engine spark ignition (S.I) engine with partial addition of n-pentane. *Materials Today: Proceedings,* 77(part 3), pp. 647-653.

Kurian, J. K., Nair, G. R., Hussain, A. & Raghavan, G. V., 2013. Feedstocks, logistics and pre-treatment processes for sustainable lignocellulosic biorefineries: A comprehensive review. *Renewable and Sustainable Energy Reviews,* Volume 25, pp. 205-219.

Laing-Nepustil, D. & Zunft, S., 2021. Chapter 4 - Using concrete and other solid storage media in thermal energy storage systems. In: L. F. Cabeza, ed. *Advances in Thermal Energy Storage Systems (Second Edition).* s.l.:Woodhead Publishing, pp. 83-110.

Lai, X. et al., 2022. Design optimization and thermal storage characteristics of NaNO3-NaCl-NaF molten salts with high latent heat and low cost for the thermal energy storage. *Journal of Energy Storage,* 52(Part A), p. 104805.

Larson, E. D. & Tingjin, R., 2003. Synthetic fuel production by indirect coal liquefaction. *Energy for Sustainable Development,* 7(4), pp. 79-102.

Laskar, D. & Yang, B., 2013. Pathways for biomass-derived lignin to hydrocarbon fuels. *Biofuels Bioproducts & Biorefining,* 7(5), pp. 602-626.

Lee, J., Lee, K., Lee, S. & Y.G. Kim, 1993. A Comparative Study of Methanol Synthesis from CO2/H2 and CO/H2 over a Cu/ZnO/Al2O3 Catalyst. *Journal of Catalysis,* 144(2), pp. 414-424.

Lee, R. A. & Lavoie, J.-M., 2013. From first- to third-generation biofuels: Challenges of producing a commodity from a biomass of increasing complexity. *Animal Frontiers,* 3(2), p. 6–11.

Lee, S. H., Doherty, T. V., Linhardt, R. J. & Dordick, J. S., 2008. Ionic liquid-mediated selective extraction of lignin from wood leading to enhanced enzymatic cellulose hydrolysis. *Biotechnology and Bioengineering,* 102(5), pp. 1368-1376.

Leibbrandt, N. H., 2010. *Techno-economic study for sugarcane bagasse to liquid biofuels in South Africa: a comparison between biological and thermochemical process routes,* thesis: Stellenbosch University, Cape Town: s.n.

Leibbrandt, N. H., 2010. Techno-Economics Study for Sugarcane Bagasse to Liquid Biofuels in South Africa: A Comparison between Biological and Thermochemical Process Routes. *PhD Dissertation - Department of Process Engineering.*

Leksawasdi, N., Joachimsthal, E. L. & RogersEmail , P. L., 2001. Mathematical modelling of ethanol production from glucose/xylose mixtures by recombinant Zymomonas mobilis. *Biotechnology Letters,* 23(13), p. 1087–1093.

Leonzio, G., Zondervan, E. & Foscolo, P. U., 2019. Methanol production by CO2 hydrogenation: Analysis and simulation of reactor performance. *International Journal of Hydrogen Energy,* 44(16), pp. 7915-7933.

Li, C. & Suzuki, K., 2009. Tar property, analysis, reforming mechanism and model for biomass gasification—An overview. *Renewable and Sustainable Energy Reviews,* 13(3), pp. 594-604.

Li, C. & Suzuki, K., 2010. Resources, properties and utilization of tar. *Resources, Conservation and Recycling,* 54(11), pp. 905-915.

Li, H. et al., 2012. Evaluation of a biomass drying process using waste heat from process industries: A case study. *Applied Thermal Engineering,* Volume 35, pp. 71-80.

Li, J. et al., 2017. Correlation of Feedstock and Bio-oil Compound Distribution. *Energy & Fuel,* 31(7), p. 7093–7100.

Li, L., Rowbotham, J. S., Greenwell, H. C. & Dyer, P. W., 2013. Chapter 8 - An Introduction to Pyrolysis and Catalytic Pyrolysis: Versatile Techniques for Biomass Conversion. In: S. L. Suib, ed. *New and Future Developments in Catalysis.* s.l.:Elsevier, pp. 173-208.

Link, S., Yrjas, P., Lindberg, D. & Trikkel, A., 2022. Characterization of Ash Melting of Reed and Wheat Straw Blend. *ACS Omega,* 7(2), p. 2137–2146.

Li, Q., Zhang, Y. & Hu, G., 2015. Techno-economic analysis of advanced biofuel production based on bio-oil gasification. *Bioresource Technology,* Volume 191, pp. 88-96.

Litterick, A. M. & Watson, C. A., 2017. Organic Farming. *Encyclopedia of Applied Plant Sciences (Second Edition),* Volume 3, pp. 311-317.

Liu, G. & Bao, J., 2017. Evaluation of electricity generation from lignin residue and biogas in cellulosic ethanol production. *Bioresource Technology,* pp. 1232-1236.

Liu, G. et al., 2011. Making Fischer−Tropsch Fuels and Electricity from Coal and Biomass: Performance and Cost Analysis. *Energy & Fuels,* 25(1), pp. 415-437.

Lizotte , P.-L., Savoie , P. & Champlain , A. D., 2015. Ash Content and Calorific Energy of Corn Stover Components in Eastern Canada. *Energies,* Volume 8, pp. 4827-4838.

Londoño-Pulgarin, D., Cardona-Montoya, G., Restrepo, J. C. & Muñoz-Leiva, F., 2021. Fossil or bioenergy? Global fuel market trends. *Renewable and Sustainable Energy Reviews,* Volume 143, p. 110905.

Løvik, I., 2001. *Modelling, Estimation and Optimization of the Methanol Synthesis with Catalyst Deactivation,* s.l.: s.n.

Lu, K.-M.et al., 2012. Torrefaction and low temperature carbonization of oil palm fiber and eucalyptus in nitrogen and air atmospheres. *Bioresource Technology,* Volume 123, pp. 98-105.

Luo, L., van der Voet, E. & Huppes, G., 2009. An energy analysis of ethanol from cellulosic feedstock–Corn stover. *Renewable and Sustainable Energy Reviews,* 13(8), pp. 2003-2011 .

Lu, X. & Wang, T., 2013. Water–gas shift modeling in coal gasification in an entrained-flow gasifier. Part 1: Development of methodology and model calibration. *Fuel,* Volume 108, pp. 629-638.

Luyben, W. . L., 2010. Design and Control of a Methanol Reactor/Column Process. *Ind. Eng. Chem. Res.,* 50(13), p. 6150–6163.

Lynd, L. R. et al., 2008. How biotech can transform biofuels. *Nature Biotechnology,* Volume 26, pp. 169-172.

Madadi, M., Tu, Y. & Abbas, A., 2017. Recent Status on Enzymatic Saccharification of Lignocellulosic Biomass for Bioethanol Production. *Electronic Journal of Biology,* 13(2), pp. 135-143.

Malik, K. et al., 2021. Co-fermentation of immobilized yeasts boosted bioethanol production from pretreated cotton stalk lignocellulosic biomass: Long-term investigation. *Industrial Crops and Products,* Volume 159, p. 113122.

Mani, S., Tabil, G. L. & Sokhansanj, S., 2004. Grinding performance and physical properties of wheat and barley straws,corn stover and switchgrass. *Biomass and Bioenergy,* 27(4), pp. 339-352.

Mani, S., Tabil, L. G. & Sokhansanj, S., 2006. Effects of compressive force, particle size and moisture content on mechanical properties of biomass pellets from grasses. *Biomass and Bioenergy,* 30(7), pp. 648-654.

Manochioa, C., Andrade , B., Rodriguez, R. & Moraes, B., 2017. Ethanol from biomass: A comparative overview. *Renewable and Sustainable Energy Reviews,* Volume 80, pp. 743-755.

Marticorena, A. A., Mandagaran, B. A. & Campanella, E. A., 2010. Environmental impact analysis of methanol recovery in biodiesel production using the waste reduction algorithm WAR. *Centro de Informacion Tecnologica; Información Tecnológica,* 21(1), pp. 23-30.

Martinez, D. M., Ebenhack, B. W. & Wagner, T. P., 2019. *Energy Efficiency: Concepts and Calculations.* s.l.:Joe Hayton.

Martín, M. & Grossmann, I. E., 2017. Optimal integration of a self sustained algae based facility with solar and/or wind energy. *Journal of Cleaner Production,* pp. 336-347.

Martín, M. M., 2016. Chapter 5 - Syngas. In: M. M. Martín, ed. *Industrial Chemical Process Analysis and Design.* s.l.:Elsevier, pp. 199-297.

Matsei, E., 2017. *Crop estimates committee.* [Online]
Available at: http://www.daff.gov.za/docs/Cropsestimates/Media%20May%202017.pdf
[Accessed 15 February 2018].

Ma, W. et al., 2021. Nox formation in fixed-bed biomass combustion: Chemistry and modeling. *Fuel,* Volume 290, p. 119694.

Mayer-Laigle, C., Blanc,, N., Rajaonarivony, R. K. & Rouau, X., 2018. Comminution of Dry Lignocellulosic Biomass, a Review: Part I. From Fundamental Mechanisms to Milling Behaviour. *Bioengineering,* 5(41), pp. 1-14.

Mikkola, H. J. & Ahokas, J., 2010. Indirect energy input of agricultural machinery in bioenergy production. *Renewable Energy,* 35(1), pp. 23-28.

Modenbach, A. A. & Nokes, S. E., 2012. The use of high-solids loadings in biomass pretreatment—a review. *Biotechnology and Bioengineering,* 109(6), pp. 1430 - 1442.

Modenbach, A. A. & Nokes, S. E., 2012. The use of high-solids loadings in biomass pretreatment—a review. *Biotechnology and Bioengineering,* Volume 109, p. 1430–1442.

Modenbach, A. A. & Nokes, S. E., 2013. Enzymatic hydrolysis of biomass at high-solids loadings – A review. *Biomass and Bioenergy,* Volume 56, pp. 526-544.

Mohr , A. & Raman , S., 2013. Lessons from first generation biofuels and implications for the sustainability appraisal of second generation biofuels. *Energy Policy,* Volume 63, pp. 114-122.

Monir, M. U., Khatun, F., Ramzilah, U. R. & and Aziz, A. A., 2020. *Thermal Effect on Co-product Tar Produced with Syngas Through Co-gasification of Coconut Shell and Charcoal.* s.l., Engineering Science and Technology, p. 022007.

Montoya, M. I. R., Quintero, J. A. S., Sánchez, Ó. J. T. & Cardona, C. A. A., 2006. Environmental impact assessment for ethanol production process using the waste reduction algorithm. *Revista Facultad de Ingeniería ,* Volume No. 36, pp. 85-95.

Moreno-Sader, K. A., Martínez-Consuegra, J. & González-Delgado, Á. D., 2021. An integrated biorefinery approach via material recycle/reuse networks for the extraction of value-added components from shrimp: Computer-aided simulation and environmental assessment. *Food and Bioproducts Processing,* Volume 127, pp. 443-453.

Mortensen, P. et al., 2011. A review of catalytic upgrading of bio-oil to engine fuels. *Applied Catalysis A: General,* 407(1-2), pp. 1-19.

Mosier, N. et al., 2005. Features of promising technologies for pretreatment of lignocellulosic biomass. *Bioresource Technology,* 96(6), pp. 673-686.

Mullen, C. A. et al., 2010. Bio-oil and bio-char production from corn cobs and stover by fast pyrolysis. *Biomass and Bioenergy,* 34(1), pp. 67-74.

Mumford, K. A., Wu, Y., Smith, K. H. & Stevens, G. W., 2015. Review of solvent based carbon-dioxide capture technologies. *Frontiers of Chemical Science and Engineering,* 9(2), pp. 125-141.

Naik, S. N., Goud, V. V., Rout , P. K. & Dalai, A. K., 2010. Production of first and second generation biofuels: a comprehensive review. *Renewable and sustainable energy review,* 14(2), pp. 14:578-597.

Nanda, S., Azargohar, R., Dalai, A. K. & Kozinski, J. A., 2015. An assessment on the sustainability of lignocellulosic biomass for biorefining. *Renewable and Sustainable Energy Reviews,* Volume 50, pp. 925-941.

Nestler, F. et al., 2020. Kinetic modelling of methanol synthesis over commercial catalysts: A critical assessment. *Chemical Engineering Journal,* 394(124881), pp. 1-13.

Nickerson, T. A., Hathaway, B. J., Smith, T. M. & Davidson, J. H., 2015. Economic assessment of solar and conventional biomass gasification technologies: Financial and policy implications under feedstock and product gas price uncertainty. *Biomass and Bioenergy,,* Volume 74, pp. 47-57.

Nielsen, K. M., 2019. Organic Farming. *Encyclopedia of Ecology (Second Edition),* Volume 4, pp. 550-558.

Niño-Villalobos, A., Puello-Yarce, J., González-Delgado, Á. D. & González-Delgado, Á. D., 2020. Biodiesel and Hydrogen Production in a Combined Palm and Jatropha Biomass Biorefinery: Simulation, Techno-Economic, and Environmental Evaluation. *ACS Omega,* Volume 5, pp. 7074-7084.

Noushabadi, A. S. et al., 2021. Estimation of higher heating values (HHVs) of biomass fuels based on ultimate analysis using machine learning techniques and improved equation. *Renewable Energy,* Volume 179, pp. 550-562.

Nzihou, A., Flamant, G. & Stanmore, B., 2012. Synthetic fuels from biomass using concentrated solar energy – A review. *Energy,* 42(1), pp. 121-131.

Olsson, L. & Hahn-Hägerdal , B., 1996. Fermentation of lignocellulosic hydrolysates for ethanol production. *Enzyme and Microbial Technology,* 18(5), pp. 312-331 .

Ong, S. et al., 2013. *Land-Use Requirements for Solar Power Plants in the United States,* s.l.: National Renewable Energy Laboratory.

OPEC, 2022. *2022 OPEC annual statistical bulletion, 57th edition,* s.l.: OPEC.

Özyuğuran, A. & Yaman, S., 2017. Prediction of Calorific Value of Biomass from Proximate Analysis. *Energy Procedia,* Volume 107, pp. 130-136.

Patel, M., Zhang, X. & Kumar, A., 2016. Techno-economic and life cycle assessment on lignocellulosic biomass thermochemical conversion technologies: a review Renewable and sustainable energy review. *Renewable and sustainable energy review,* Volume 53, pp. 1486-1499.

Patzek, T. W., 2004. Thermodynamics of the Corn-Ethanol Biofuel Cycle. *Critical Reviews in Plant Sciences,* 23(6), pp. 519-567.

Paudel, S. R. et al., 2017. Pretreatment of agricultural biomass for anaerobic digestion: Current state and challenges. *Bioresource Technology,* Volume 245, pp. 1194-1205.

Pegels, A., 2010. Renewable energy in South Africa: Potentials, barriers and options for support. *Energy Policy,* 38(9), pp. 4945 - 4954.

Peng, Q. et al., 2010. The preparation and properties of multi-component molten salts. *Applied Energy,* 87(9), pp. 2812-2817.

Peral, C., 2016. Chapter 5 - Biomass Pretreatment Strategies (Technologies, Environmental Performance, Economic Considerations, Industrial Implementation). In: P. Poltronieri & O. F. D'Urso, eds. *Biotransformation of Agricultural Waste and By-Products.* s.l.:Elsevier,, pp. 125-160.

Perez-Cantu, L. et al., 2013. Comparison of pretreatment methods for rye straw in the second generation biorefinery: Effect on cellulose, hemicellulose and lignin recovery. *Bioresource Technology,* Volume 142, pp. 428-435.

Pérez, E., Tuck, C. O. & Poliakoff, M., 2018. Valorisation of lignin by depolymerisation and fractionation using supercritical fluids and conventional solvents. *The Journal of Supercritical Fluids,* 133(2), pp. 690-695.

Pérez-Fortes, M., Schöneberger, J. C., Boulamanti, A. & Tzimas, E., 2016. Methanol synthesis using captured CO2 as raw material: Techno-economic and environmental assessment. *Applied Energy,* Volume 161, pp. 718-732.

Petersen, A. M., Van der Westhuizen, W. A., Mandegari, M. A. & Görgens,, J. F., 2017. Economic analysis of bioethanol and electricity production from sugarcane in South Africa. *Biofuels, Bioproducts, Biorefinering,* Volume 12, pp. 224 - 238.

Peters, M. S. & Timmerhaus, K. D., 1991. Chapter 6: Cost estimation. In: *Plant design and economics for chemical engineers.* McGraw-Hill International Editions ed. s.l.:s.n., pp. 150-160.

Peters, M. S. & Timmerhaus, K. D., 1991. Chapter 6: Cost estimation. In: M. Professional, ed. *Plant design and economics for chemical engineers.* 5th ed. New York, NY: Chemical Engineering Series, pp. 150-160.

Pfromm, P. et al., 2010. Bio-butanol vs. bio-ethanol: A technical and economic assessment for corn and switchgrass fermented by yeast or Clostridium acetobutylicum,. *Biomass and Bioenergy,* 34(4), pp. 515-524.

Piatkowski, N., Wieckert, C., Weimer, A. W. & Steinfeld , A., 2011. Solar-driven gasification of carbonaceous feedstock - a review. *Energy and Environmental Science,* Issue 1, p. 2010.

Pimentel, D., Berardi, G. & Sarah, F., 1983. Energy efficiency of farming systems: Organic and conventional agriculture. *Agriculture, Ecosystems & Environment,* 9(4), pp. 359-372 .

Pimentel, D. et al., 2005. Environmental, Energetic, and Economic Comparisons of Organic and Conventional Farming Systems. *BioScience,* 55(7), pp. 573-582.

Plevin, R. J. et al., 2006. Ethanol Can Contribute to Energy and Environmental Goals. *Science,* 311(5760), pp. 506-508.

Ponnusamy, V. K. et al., 2019. A review on lignin structure, pretreatments, fermentation reactions and biorefinery potential. *Bioresource Technology,* Volume 271, pp. 462-472.

Popovski, K., 2003. *Political and public acceptance of geothermal energy - IGC2003 - Short Course Geothermal training,* Grensásvegur: s.n.

Pranolo, S. H. et al., 2022. Feasible tar cleaning method of producer gas from palm kernel shell and mahogany fruit shell gasification. *Materials Today: Proceedings,* 63(Supplement 1), pp. S237-S243.

Prieto, C., Cooper, P., Fernández, A. I. & Cabeza, L. F., 2016. Review of technology: Thermochemical energy storage for concentrated solar power plants. *Renewable and Sustainable Energy Reviews,* Volume 60, pp. 909-929.

Puig-Arnavat, M., Tora, E., Bruno, J. & Coronas, A., 2013. State of the art on reactor designs for solar gasification of carbonaceous feedstock. *Solar Energy,* Volume 97, pp. 67-84.

Pulido-Iparraguirre, D., Valenzuela, L., Serrano-Aguilera, J.-J. & Fernández-García, A., 2019. Optimized design of a Linear Fresnel reflector for solar process heat applications. *Renewable Energy,* Volume 131, pp. 1089-1106.

PVGIS, 2017. *European Commission - PHOTOVOLTAIC GEOGRAPHICAL INFORMATION SYSTEM.* [Online]
Available at: http://re.jrc.ec.europa.eu/pvg_tools/en/tools.html#TMY
[Accessed 26 March 2019].

Quintero, J. A., Moncada, J. & Cardona, C. A., 2013. Techno-economic analysis of bioethanol production from lignocellulosic residues in Colombia: A process simulation approach. *Bioresource Technology,* pp. 300-307.

Radwan, O. A., Humphrey, J. D., Hakeem, A. S. & Zeama, M., 2021. Evaluating properties of Arabian desert sands for use in solar thermal technologies. *Solar Energy Materials and Solar Cells,* Volume 231, p. 111335.

Rafael Oliveira, d. S., Lizandro, d. S. S. & Diego Martinez, P., 2018. Simulation and optimization of a methanol synthesis process from different biogas sources. *Journal of Cleaner Production,* Volume 86, pp. 821-830.

Rahman, S. & Hasan, K. M., 2014. Energy productivity and efficiency of wheat farming in Bangladesh. *Energy,* Volume 66, pp. 107-114 .

Raman, J. K. & Alves, C. M., 2018. A review on moringa tree and vetiver grass – Potential biorefinery feedstocks. *Bioresource Technology,* Volume 249, pp. 1044-1051.

Ram, M. & Mondal, M. K., 2022. Chapter 13 - Biomass gasification: a step toward cleaner fuel and chemicals. In: B. Gurunathan, R. Sahadevan & Z. A. Zakaria, eds. *Biofuels and Bioenergy.* s.l.:Elsevier, pp. 253-276.

Ram, M. & Mondal, M. K., 2022. Chapter 13 - Biomass gasification: a step toward cleaner fuel and chemicals,. In: B. Gurunathan, R. Sahadevan & Z. A. Zakaria, eds. *Biofuels and Bioenergy.* s.l.:Elsevier, pp. 253-276.

Ranatunga, T. . D. et al., 1997. Identification of inhibitory components toxic toward zymomonas mobilis CP4(pZB5) xylose fermentation. *Applied Biochemistry and Biotechnology,* 67(185), pp. 185-198.

Rebrov, E., 2011. Chapter 13 - Advances in water-gas shift technology: modern catalysts and improved reactor concepts,. In: M. R. Khan, ed. *Advances in Clean Hydrocarbon Fuel Processing.* Belfast,UK: In Woodhead Publishing Series in Energy, pp. 387-412.

Rezaiyan, J. & Cheremisinoff, N. . P., 2005. *Gasification Technologies: A Primer for Engineers and Scientists.* Boca Raton: CRC Press.

Rodionova, M. V. et al., 2022. A comprehensive review on lignocellulosic biomass biorefinery for sustainable biofuel production. *International Journal of Hydrogen Energy,* 47(3), pp. 1481-1498.

Ross, S. A., Westerfield, R. W., Jaffe, J. & Jordan, B. D., 2016. *Corporate Finance.* 11th ed. New York: The McGraw-Hill/Irwin Series in Finance, Insurance, and Real Estate.

Sacramento-Rivero, J. C., 2012. A methodology for evaluating the sustainability of biorefineries: framework and indicators. *Biofuels, Bioproducts and Biorefining,* 6(1), pp. 32-44.

Sadeghi, G., 2022. Energy storage on demand: Thermal energy storage development, materials, design, and integration challenges,. *Energy Storage Materials,* Volume 46, pp. 192-222.

Saha, S. et al., 2019. *Chapter 14 - Bio-plastics and Biofuel: Is it the Way in Future Development for End Users?.* Al-Salem, S.M.; ed. New Delhi: William Andrew Publishing.

Santos, J. J. et al., 2018. Chapter 12 - Concentrating Solar Power. In: I. Yahyaoui, ed. *Advances in Renewable Energies and Power Technologies.* s.l.:Elsevier, pp. 373-402.

Saravanan, A. et al., 2022. Recent advances and sustainable development of biofuels production from lignocellulosic biomass. *Bioresource Technology,* 344(Part B), p. 126203.

SASOL, 2000. *SASOL, 50 years of innovation.* [Online]
Available at:
https://www.sasol.com/sites/sasol/files/content/files/Sasol%2050%20year%20Brochure_1039069422306_0_0_1.pdf
[Accessed 27 June 2022].

Sathendra, E. R. et al., 2022. Chapter 5 - Refining lignocellulose of second-generation biomass waste for bioethanol production. In: B. Gurunathan, R. Sahadevan & Z. A. Zakaria, eds. *Biofuels and Bioenergy.* s.l.:Elsevier, pp. 87-110.

Schell, D. J. & Harwood, C., 1994. Milling of lignocellulosic biomass. *Applied Biochemistry and Biotechnology,* 45(1), p. 159–168.

Scown, C. D. et al., 2014. Role of lignin in reducing life-cycle carbon emissions, water use, and cost for United States cellulosic biofuels. *Environmental Science and Technology,* 48(15), pp. 8446-8455.

Shapouri, H. & McAloon, A., 2002. *The 2001 Net Energy Balance of Corn-Ethanol,* Washington DC: Department.

Shemfe, M. B., Gu, S. & Ranganathan, P., 2015. Techno-economic performance analysis of biofuel production and miniature electric power generation from biomass fast pyrolysis and bio-oil upgrading. *Fuel,* Volume 143, pp. 361-372.

Shigenori, M., Bernhard, G. & Viktor, H., 2018. Chapter 1 - Introduction. In: *Fuel Cells and Hydrogen.* s.l.:s.n., pp. 1-13.

Short, W., Packey, D. J. & Holt, T., 1995. *A Manual for the Economic Evaluation of Energy Efficiency and Renewable,* s.l.: National Renewable Energy Laboratory.

Shrotri, A., Kobayashi, H. & Fukuoka, A., 2017. Chapter Two - Catalytic Conversion of Structural Carbohydrates and Lignin to Chemicals. In: C. Song, ed. *Advances in Catalysis.* s.l.:Academic Press, pp. 59-123.

Shrotri, A., Kobayashi, H. & Fukuoka, A., 2017. Chapter Two - Catalytic Conversion of Structural Carbohydrates and Lignin to Chemicals. In: C. Song, ed. *Advances in Catalysis.* s.l.:Academic Press, pp. 59-123.

Sikdar, S. . K., 2003. Sustainable development and sustainability metrics. *American Institute of Chemical Engineers - Journal,* 49(8), p. 1928–1932.

Silaen, A. & Wang, T., 2009. *Comparison of instantaneous, equilibrium and finite rate gasification models in an entrained flow coal gasifier.* Pittsburgh, Pennsylvania, s.n., pp. September 21–24,.

Simanjuntak, J. P., Al-attab, K. A. & Zainal, Z. A., 2019. Hydrodynamic Flow Characteristics in an Internally Circulating Fluidized Bed Gasifier. *Journal of Energy Resoource Technology,* 141(3), p. 032001.

Sims, R. & Taylor, M., 2008. *International energy agency.* [Online]
Available at: https://www.iea.org/publications/freepublications/publication/2nd_Biofuel_Gen.pdf
[Accessed 17 June 2016].

Sindhu, R., Binod, P. & Pandey, A., 2016. Biological pretreatment of lignocellulosic biomass – An overview. *Bioresource technology,* Volume 199, pp. 76-82.

Singer, C., Giuliano, S. & Buck, R., 2014. Assessment of Improved Molten Salt Solar Tower Plants. *Energy Procedia,* Volume 49, pp. 1553-1562.

Singh, J., Panesar, B. & Sharma, S., 2010. A mathematical model for transporting the biomass to biomass based power plant. *Biomass and Bioenergy,* 34(4), pp. 483-488.

Souza, G. M. et al., 2017. The role of bioenergy in a climate-changing world. *Environmental Development,* Volume 23, pp. 57-64.

Spath, P. et al., 2005. *Biomass to hydrogen production detailed design and economics utilizing the battelle columbus laboratory indirectly-heated gasifier,* s.l.: National Renewable Energy Laboratory.

Speight, J., 2017. Chapter 3 - Industrial Organic Chemistry . In: *Environmental Organic Chemistry for Engineers.* s.l.:s.n., pp. 87-151 .

Srivastava, N., Rawat, R., Oberoi, H. S. & Ramteke, P. W., 2015. A Review on Fuel Ethanol Production From Lignocellulosic Biomass. *International Journal of Green Energy,* 12(9), pp. 949-960.

Stampe, S., Alcock, R., Westby, C. & Chisholm, T., 1983. Energy consumption of a farm-scale ethanol distillation system. *Energy in Agriculture ,* 2(1983), pp. 355-368.

Stickel, J. J. et al., 2009. Rheology measurements of a biomass slurry: an inter-laboratory study. *Rheologica Acta,* 48(9), p. 1005–1015.

Sultana, A. & Kumar, A., 2011. Optimal configuration and combination of multiple lignocellulosic biomass feedstocks delivery to a biorefinery. *Bioresource Technology,* 102(21), pp. 9947-9956.

Sun, N. et al., 2009. Complete dissolution and partial delignification of wood in the ionic liquid 1-ethyl-3-methylimidazolium acetate. *Green Chemistry ,* 11(5), pp. 646-655.

Sun, Y. & Cheng, J., 2002. Hydrolysis of lignocellulosic materials for ethanol production: a review. *Bioresource Technology,* 83(1), pp. 1-12.

Swanson, R. M., Platon, A., Satrio, J. A. & Brown, R. C., 2010. Techno-economic analysis of biomass-to-liquids production based on gasification. *Fuel,* Volume Volume 89, Supplement 1, pp. S11-S19.

Tanzil, D. & Beloff, B. R., 2006. Assessing impacts: Overview on sustainability indicators and metrics. *Environmental Quality Management,* 15(4), pp. 41-56.

Tao, L., Markham, J. N., Haq, Z. & Biddy, M. J., 2017. Techno-economic analysis for upgrading the biomass-derived ethanol-to-jet blendstocks. *Green Chemistry,* Issue 4, pp. 1082-1102.

Tao, L. et al., 2014. *NREL 2012 Achievement of Ethanol Cost Targets: Biochemical Ethanol Fermentation via Dilute-Acid Pretreatment and Enzymatic Hydrolysis of Corn Stover.* [Online] Available at: https://www.osti.gov/biblio/1129271-nrel-achievement-ethanol-cost-targets-biochemical-ethanol-fermentation-via-dilute-acid-pretreatment-enzymatic-hydrolysis-corn-stover [Accessed 05 Septembre 2018].

Templeton, D. W. et al., 2009. Assessing corn stover composition and sources of variability via NIRS. *Cellulose,* 16(4), pp. 621-639.

Tewfik, S. R., Abulnour, A. G. M. & Sorour, M. H., 2015. Techno-economic and environmental aspects of the production of medium scale ligno-cellulosic ethanol under Egyptian conditions. *Egyptian Journal of Petroleum,* 24(4), pp. 375-381.

The world bank, 2019. *Global solar atlas.* [Online] Available at: https://globalsolaratlas.info/download/south-africa?c=-28.265682,22.565918,6 [Accessed 13 July 2022].

Tijmensen, M., Faaij, A., Hamelinck, C. & Hardeveld, M., 2002. Exploration of the possibilities for production of Fischer Tropsch liquids and power via biomass gasification. *Biomass and Bioenergy,* Volume 23, pp. 129-152.

Tingey, G. L., 1966. Kinetics of the Water—Gas Equilibrium Reaction. I. The Reaction of Carbon Dioxide with Hydrogen. *The Journal of Physical Chemistry,* 70(5), p. 1406–1412.

Tock, L., Gassner, M. & Maréchal, F., 2010. Thermochemical production of liquid fuels from biomass: Thermo-economic modeling, process design and process integration analysis. *Biomass and Bioenergy,* 34(12), pp. 1838-1854.

Tomás-Pejó, E., Ballesteros, M., Alvira, P. & Negro, M., 2010. Pretreatment technologies for an efficient bioethanol production process based on enzymatic hydrolysis: A review. *Bioresource Technology,* 101(13), pp. 4851-4861.

Tongwane, M. et al., 2016. Greenhouse gas emissions from different crop production and management practices in South Africa. *Environmental Development,* Volume 19, pp. 23-35.

Torres, A. F., Visser, R. G. & Trindade, L. M., 2015. Bioethanol from maize cell walls: genes, molecular tools, and breeding prospects. *Global change biology,* 7(4), pp. 591-607.

Ubando , A. T., Felix , C. B. & Chen , W.-H., 2020. Biorefineries in circular bioeconomy: A comprehensive review. *Bioresource Technology V,* Volume 299.

Ubando, A. T., Felix, C. B. & Chen, W.-H., 2020. Biorefineries in circular bioeconomy: A comprehensive review. *Bioresource Technology,* Volume 299, pp. 1-18.

Um, B.-H. & Hanley, T. R., 2008. A Comparison of Simple Rheological Parameters and Simulation Data for Zymomonas mobilis Fermentation Broths with High Substrate Loading in a 3-L Bioreactor. *Applied Biochemistry and Biotechnology,* 145(1-3), pp. 29-38.

USDL, 2007. *CONSUMER PRICE INDEX: JUNE 2007,* Washington, D.C. : Bureau of Labor Statistics.

USDL, 2020. *Bureau of labor statistics - US department of labor.* [Online]
Available at: https://www.bls.gov/news.release/pdf/cpi.pdf
[Accessed 14 November 2020].

Uzun, B. B. & Sarioğlu, N., 2009. Rapid and catalytic pyrolysis of corn stalks. *Fuel Processing Technology,* 90(5), pp. 705-716.

Van-Dal, É. S. & Bouallou, C., 2013. Design and simulation of a methanol production plant from CO2 hydrogenation. *Journal of Cleaner Production,* Volume 57, pp. 38-45.

Van-Dal, É. S. & Bouallou, C., 2013. Design and simulation of a methanol production plant from CO2 hydrogenation. *Journal of Cleaner Production,* Volume 57, pp. 38-45.

Vidal Jr, B. C., Dien, B. S., Ting, K. C. & Vijay Singh, 2011. Influence of Feedstock Particle Size on Lignocellulose Conversion - A Review. *Applied Biochemistry and Biotechnology,* 164(8), pp. 1405-1421.

Vidal, M. & Martín, M., 2015. Optimal coupling of a biomass based polygeneration system with a concentrated solar power facility for the constant production of electricity. *Computers & Chemical Engineering,* Volume 72, pp. 273-283.

Vigants, E. et al., 2015. Analysis of Energy Consumption for Biomass Drying Process. *Environment Technology Resources - Proceedings of the 10th International Scientific and Practical Conference,* Volume 2, pp. 317-322.

Virginia , E.-B.et al., 2019. High resolution fourier transform ion cyclotron resonance mass spectrometry (FT-ICR MS) for the characterisation of enzymatic processing of commercial lignin. *New Biotechnology,* Volume 52, pp. 1-8.

Wagemann, K., 2012. Biorefinery - Prerequisite for the realization of a future bioeconomy. *Presented at the DGMK Tagungsbericht,* pp. 133-143.

Walid, B. A. B. T., Hassiba, B., Boumediene, H. & Weifeng, S., 2018. Improved Design of the Lurgi Reactor for Methanol Synthesis Industry. *Chemical engineering and technology,* 41(No.10), p. 2043–2052.

Weber, C. W., Kohlhepp, E. A., Idouraine, A. & Ochoa, L. J., 1993. Binding capacity of 18 fiber sources for calcium. *Journal of Agricultural and Food Chemistry,* 41(11), pp. 1931-1935.

Weiss, A. & Schebek, L., 2021. The net energy ratio of microalgae biofuels production based on correlated cultivation parameters in flat plate photobioreactors. *Journal of Cleaner Production,* Volume 287.

Weiss, R., Guebitz, G. M., Pellis, A. & Nyanhongo, G. S., 2020. Harnessing the Power of Enzymes for Tailoring and Valorizing Lignin. *Trends in biotechnology,* pp. 1-17.

Williams, C. L., Emerson, R. M. & Tumuluru, J. S., 2017. Chapter 11: Biomass Compositional Analysis for Conversion to Renewable Fuels and Chemicals. In: J. S. Tumuluru, ed. *Biomass Volume Estimation and Valorization for Energy.* s.l.:IntechOpen, pp. 251-270.

Wooley, R. J. & Putsche, V., 1996. *Development of an ASPEN PLUS Physical Property Database for Biofuels Components,* Gold n, Colorado 80401 -3393: National Renewable Energy Laboratory.

World Weather & Climate, 2022. *World Weather & Climate: Average monthly hours of sunshine in Bloemfontein (Free State).* [Online]
Available at: https://weather-and-climate.com/average-monthly-hours-Sunshine,bloemfontein,South-Africa
[Accessed 13 01 2023].

Wu, Y.-t., Ren, N., Wang, T. & Ma, C.-f., 2011. Experimental study on optimized composition of mixed carbonate salt for sensible heat storage in solar thermal power plant. *Solar Energy,* 85(9), pp. 1957-1966.

Xu, B., Li, P. & Chan, C., 2015. Application of phase change materials for thermal energy storage in concentrated solar thermal power plants: A review to recent developments. *Applied Energy,* Volume 160, pp. 286-307.

Xu, C., Wang, Z., Li, X. & Sun, F., 2011. Energy and exergy analysis of solar power tower plants. *Applied Thermal Engineering,* 31(17–18), pp. 3904-3913.

Xu, D., Gu, X. & Dai, Y., 2023. Concentrating solar assisted biomass-to-fuel conversion through gasification: A review. *Frontier in energy research,* pp. 1-26.

Xue, Y. et al., 2016. A review on the operating conditions of producing bio-oil from hydrothermal liquefaction of biomass. *International Journal of Energy Research,* 40(7), pp. 865-877.

Xu, J., 2015. Chapter 9 - Microwave Pretreatment. In: A. Pandey, S. Negi, P. Binod & C. Larroche, eds. *Pretreatment of Biomass.* s.l.:Elsevier, pp. 157-172.

Yakan, C. & Patel, B., 2021. Techno-economic study and environmental analysis of a solar-aided lignocellulosic biorefinery: a South African case study. *Biomass Conversion and Biorefinery,* pp. 1-21.

Yakan, C. & Patel, B., 2022. Techno-economic Study and Environmental Analysis for the Production of Bio-methanol Using a Solar-aided Dual-bed Gasifier. *Waste and biomass valorisation.*

Yakan, C. & Patel, B., 2022. Techno-economic Study and Environmental Analysis for the Production of Bio-methanol Using a Solar-aided Dual-bed Gasifier. *Waste and biomass valorisation.*

Yang, H. & Chen, H., 2015. Chapter 11 - Biomass gasification for synthetic liquid fuel production,. In: R. Luque & J. G. Speight, eds. *Gasification for Synthetic Fuel Production.* s.l.:Woodhead Publishing, pp. 241-275.

Yang, H. et al., 2013. Estimation of Enthalpy of Bio-Oil Vapor and Heat Required for Pyrolysis of Biomass. *Energy & Fuels,* Volume 27, p. 2675−2686.

Yang, L. & Ge, X., 2016. Chapter Three - Biogas and Syngas Upgrading. In: Y. Li & X. Ge, eds. *Advances in Bioenergy.* s.l.:Elsevier,, pp. 125-188.

Young, D. . M. & Cabezas, H., 1999. Designing sustainable processes with simulation: the waste reduction (WAR) algorithm. *Computers & Chemical Engineering,* 23(10), pp. 1477-1491.

Young, D., Scharp, R. & Cabezas, H., 2000. The waste reduction (WAR) algorithm: environmental impacts, energy consumption, and engineering economics. *Waste Management,* Volume 20, pp. 605-615.

You, Z. et al., 2010. *The Carbonization Characteristics Studies of Corn Stalk in a Fixed Bed Reactor.* s.l., institute of electrical and electronics engineers, pp. 1-4.

Yusup, S., Nguyen Phuong, A. & Haslinda, Z., 2010. A simulation study of an industrial methanol reactor based on simplified steady-state model. *International Journal of Recent Research and Applied Studies,* 5(3), pp. 213-222.

Yusup, S., Phuong Anh, N. & Zabiri, H., 2010. A simulation study of an industrial methanol reactor based on simplified steady-state model. *International Journal of Recent Research and Applied Studies,* 5(3), pp. 213 - 222.

Z'Graggen, A. & Steinfeld, A., 2009. Heat and mass transfer analysis of a suspension of reacting particles subjected to concentrated solar radiation – Application to the steam-gasification of carbonaceous materials. *International Journal of Heat and Mass Transfer,* 52(1-2), pp. 385-395.

Zanotti, M. et al., 2016. A sustainable lignocellulosic biodiesel production integrating solar- and bio-power generation. *Green Chemistry,* Issue 18, pp. 5059-5068.

Zewdie, D. T. & Ali, A. Y., 2022. Techno-economic analysis of microalgal biofuel production coupled with sugarcane processing factories. *South African Journal of Chemical Engineering,* Volume 40, pp. 70-79.

Zhang, J., Zhou, H., Liu, D. & Zhao, X., 2020. Chapter 2 - Pretreatment of lignocellulosic biomass for efficient enzymatic saccharification of cellulose. In: A. Yousuf, D. Pirozzi & F. Sannino, eds. *Lignocellulosic Biomass to Liquid Biofuels.* s.l.:Academic Press, pp. 17-65.

Zheng, H., 2013. *Corn stover steam gasification,* s.l.: PhD Thesis submitted to the faculty of faculty of the graduate school of the university of minesota.

APPENDIX A

KEY SIMULATION PARAMETERS, STREAM COMPOSITIONS, AND MASS BALANCE AROUND MAJOR PROCESSING UNITS

Table A-1: Thermodynamic settings used in CHEMCAD 7.1.2 to simulate the conversion processes. Note that each conversion area was simulated separately.

Process	Thermodynamic Global K-Value Model	Thermodynamic Global Enthalpy Model
Deacetylation reactions	NRTL	Latent heat
Filtration after deacetylation		
Dilute acid Pretreatment		
Flash cooling after pretreatment		
Hydrolysis reactions		
Fermentation reaction		
Flash cooling		
Distillation reactions		
Molecular sieving		
Gasification process	NRTL	Latent heat
Wastewater treatment		
Heat and power Steam generation	SRK	SRK
Electricity generation		
Methanol synthesis from syngas		
Syngas cleaning and conditioning		

Table A-2: Chemical formulas used for biomass compounds in biological conversion

COMPOUND NAME	CHEMICAL FORMULA	NOTES
Acetate	$C_2H_4O_2$	Use Xylan Properties
Arabinan	$C_5H_8O_4$	Use Xylose properties
Arabinose	$C_5H_{10}O_5$	Use Glucose properties
Cellobiose	$C_{12}H_{22}O_{11}$	
Cellulose	$C_5H_{10}O_5$	Modelled as water
Corn steep liquor (CSL)	Unknown	
Furfural	$C_5H_4O_2$	Use cellulose properties
Galactan	$C_6H_{10}O_5$	Use cellulose properties
Galactose	$C_6H_{12}O_6$	
Glucose	$C_6H_{12}O_6$	Use Furfural properties
HydroxyMethylFulfural (HMF)	$C_5H_4O_2$	
Lignin	$C_{10}H_{13.9}O_{1.3}$	Use Cellulose properties
Mannan	$C_6H_{10}O_5$	Use glucose properties
Mannose	$C_6H_{12}O_6$	Use Glucose properties for Liquid-Liquid interactions
Soluble Lignin	$C_{10}H_{13.9}O_{1.3}$	Use Xylan properties
Tar	$C_5H_8O_4$	
Xylan	$C_5H_8O_4$	
Xylose	$C_5H_{10}O_5$	
Z. mobilis	$CH_{1.8}O_{0.5}N_{0.2}$	

DEACETYLATION

Acetyl groups of the biomass are hydrolysed to acetic acid once in solution. Thus, the deacetylation reaction takes place between acetic acid and NaOH and results in the formation of sodium acetate and water as follows: $C_2H_3O_2 + NaOH \rightarrow C_2H_2O_2Na + H_2O$.

During the deacetylation process, 5% of the biomass mass is loss through filtering and unaccounted chemical reactions

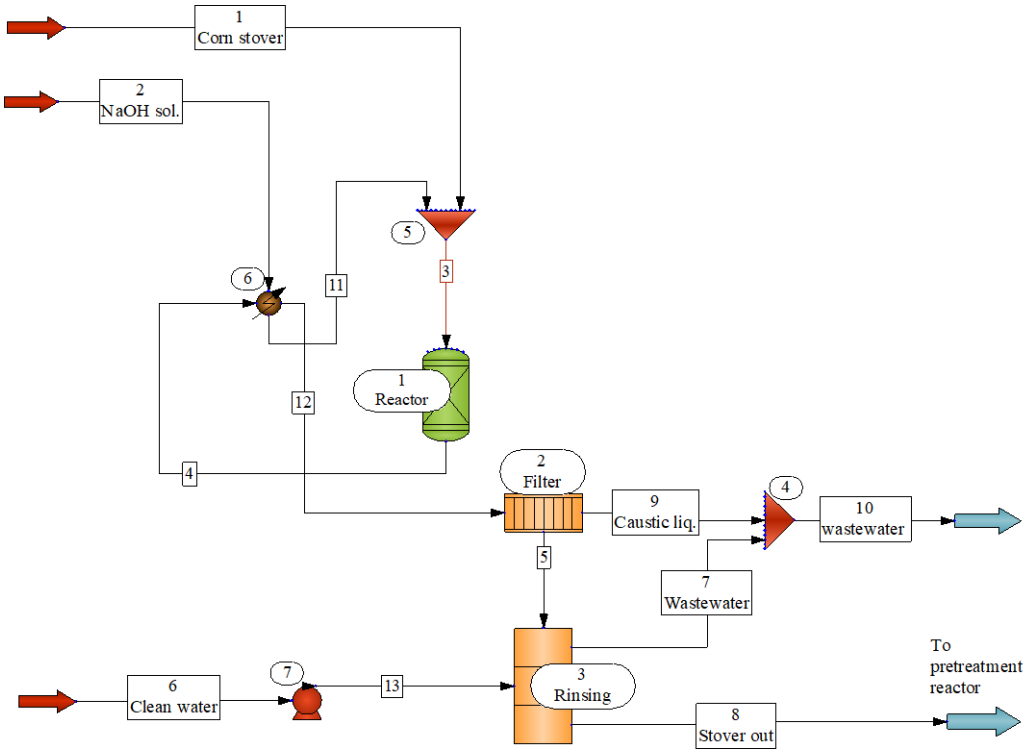

Figure A-1: Chemcad Flowsheet of deacetylation process

Table A-3: Mass balance around deacetylation process

	kmol/h		kg/h	
	Input	Output	Input	Output
Water	53 249	53 283	959 281	959 899
Acetic Acid	31	0	1 832	0
Glucan	164	164	26 583	26 583
Xylan	119	119	15 750	15 750
Lignin	90	90	11 083	11 083
Sucrose	9	9	3 000	3 000
Others	708	708	21 250	21 250
Mannan	2	2	250	250
Arabinan	18	18	2 333	2 333
Galactan	8	8	1 250	1 250
H+	1	0	1	0
OH-	96	64	1 630	1 095
Na+	96	96	2 203	2 203
CH3CO2-	1	31	54	1 856
Total	54 590	54 592	1 046 552	1 046 552

Table A-4: Stream composition for deacetylation process

Stream No.	1	2	3	4	5	6	7	8	9	10	11	12	13
Temp ^{o}C	**25**	**25**	77	80	28	**25**	28	28	28	28	79	28	25
Pressure (atm)	**2**	**2**	2	2	1.5	**1.5**	1.5	1.5	1.5	1.5	2	2	1.5
Total kmol/h	2 306	52 230	54 540	54 540	2 246	56	764	1 538	52 290	53 050	52 230	54 540	56
Total kg/h	104 200	941 300	1 046 000	1 046 000	101 900	1 000	16 850	86 030	943 700	960 500	941 300	1 046 000	1 000
Flow rates in kg/h													
Water	20 830	937 500	958 900	958 900	20 270	1 000	12 710	8 559	938 600	951 300	937 500	958 900	1 000
Acetic Acid	1 832	0	0	0	0	0	0	0	0	0	0	0	0
Glucan	26 580	0	26 580	26 580	26 580	0	1 329	25 250	0	1 329	0	26 580	0
Xylan	15 750	0	15 750	15 750	15 750	0	788	14 960	0	788	0	15 750	0
Lignin	11 080	0	11 080	11 080	11 080	0	554	10 530	0	554	0	11 080	0
Sucrose	3 000	0	3 000	3 000	3 000	0	150	2 850	0	150	0	3 000	0
Others	21 250	0	21 250	21 250	21 250	0	1 062	20 190	0	1 062	0	21 250	0
Mannan	250	0	250	250	250	0	13	238	0	13	0	250	0
Arabinan	2 333	0	2 333	2 333	2 333	0	117	2 216	0	117	0	2 333	0
Galactan	1 250	0	1 250	1 250	1 250	0	63	1 188	0	63	0	1 250	0
OH-	0	1 630	1 095	1 095	23	0	14	9	1 072	1 086	1 630	1 095	0
Na+	0	2 203	2 203	2 203	47	0	28	19	2 157	2 184	2 203	2 203	0
CH3CO2-	54	0	1 856	1 856	39	0	23	16	1 816	1 840	0	1 856	0

PRETREATMENT

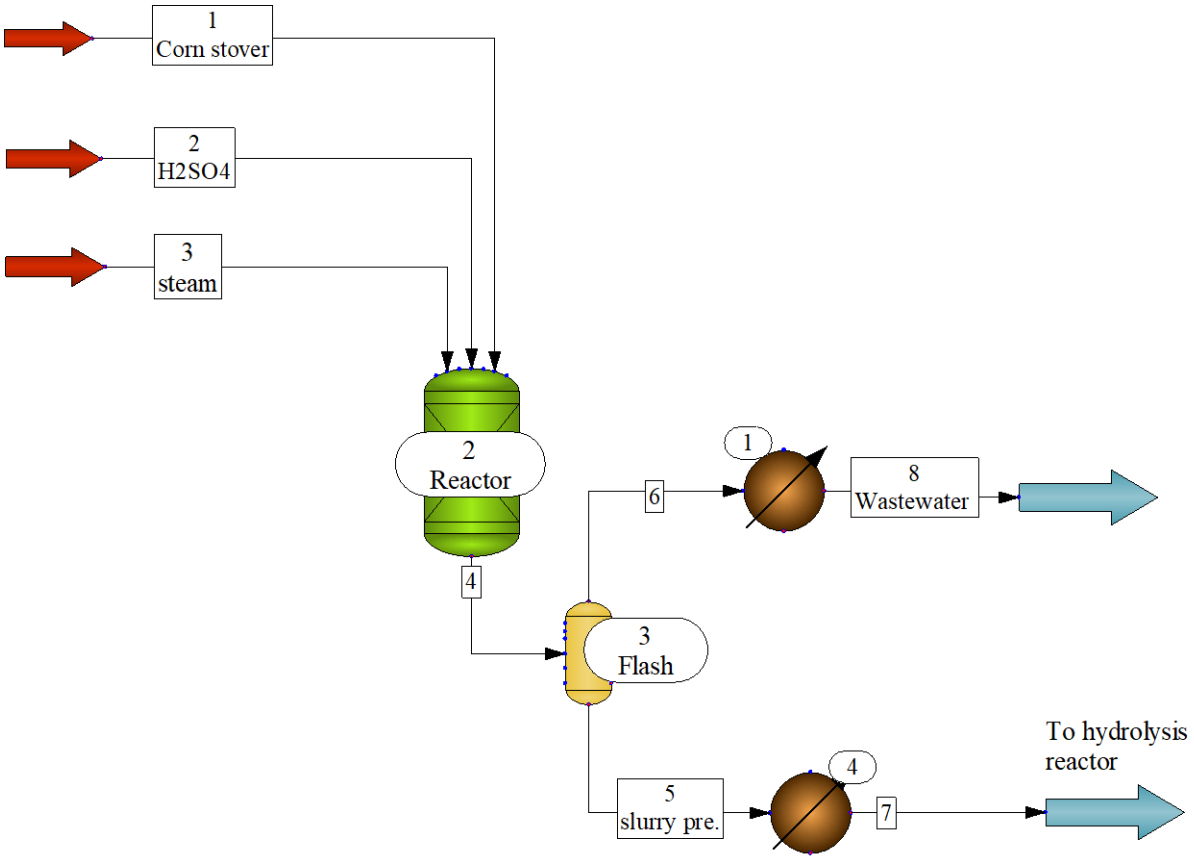

Figure A-2: Chemcad Flowsheet of pretreatment process

Table A-5: Mass balance around pretreatment process

	kmol/h		kg/h	
	Input	Output	Input	Output
Water	13600.82	13491.28	245018.8	243045.4
Glucan	155.751	145.969	25253.85	23667.91
Xylan	113.252	10.827	14962.5	1430.415
Lignin	85.957	85.957	10528.85	10528.85
Sucrose	8.326	8.326	2850	2850
Others	672.326	672.326	20187.5	20187.5
Mannan	1.798	1.798	237.5	237.5
Arabinan	16.776	0.825	2216.35	109.044
Galactan	7.324	7.324	1187.5	1187.5
OH-	0.548	0.548	9.317	9.317
Na+	0.815	0.815	18.74	18.74
CH3CO2-	0.267	0.267	15.783	15.783
Sulfuric Acid	0.661	0.661	64.872	64.872
Furfural	0	6.206	0	596.331
Alpha-D-Glucose	0	9.781	0	1762.15
Xylose	0	96.219	0	14445.55
Arabinose	0	15.95	0	2394.659
Total	14664.62	14555.08	322551.5	322551.5

Table A-6: Stream composition for pretreatment process

Stream No.	1	2	3	4	5	6	7	8
Temp ^{o}C	27.9335	**25**	157.3479	160	101.1585	101.1585	95	30
Pressure (atm)	**5.7**	**6**	5.7	5.7	1	1	1	1
Total kmol/h	1 538	1	13 130	14 560	3 297	11 260	3 297	11 260
Total kg/h	86 030	65	236 500	322 600	119 300	203 300	119 300	203 300
Flow rates in kg/h								
Water	8 559	0	236 500	243 000	40 330	202 700	40 330	202 700
Glucan	25 250	0	0	23 670	23 670	0	23 670	0
Xylan	14 960	0	0	1 430	1 430	0	1 430	0
Lignin	10 530	0	0	10 530	10 530	0	10 530	0
Sucrose	2 850	0	0	2 850	2 850	0	2 850	0
Others	20 190	0	0	20 190	20 190	0	20 190	0
Mannan	238	0	0	238	238	0	238	0
Arabinan	2 216	0	0	109	109	0	109	0
Galactan	1 188	0	0	1 188	1 188	0	1 188	0
OH-	9	0	0	9	9	0	9	0
Na+	19	0	0	19	19	0	19	0
CH3CO2-	16	0	0	16	16	0	16	0
Sulfuric Acid	0	65	0	65	65	0	65	0
Furfural	0	0	0	596	27	569	27	569
Alpha-D-Glucose	0	0	0	1 762	1 762	0	1 762	0
Xylose	0	0	0	14 450	14 440	4	14 440	4
Arabinose	0	0	0	2 395	2 395	0	2 395	0

HYDROLYSIS AND FERMENTATION

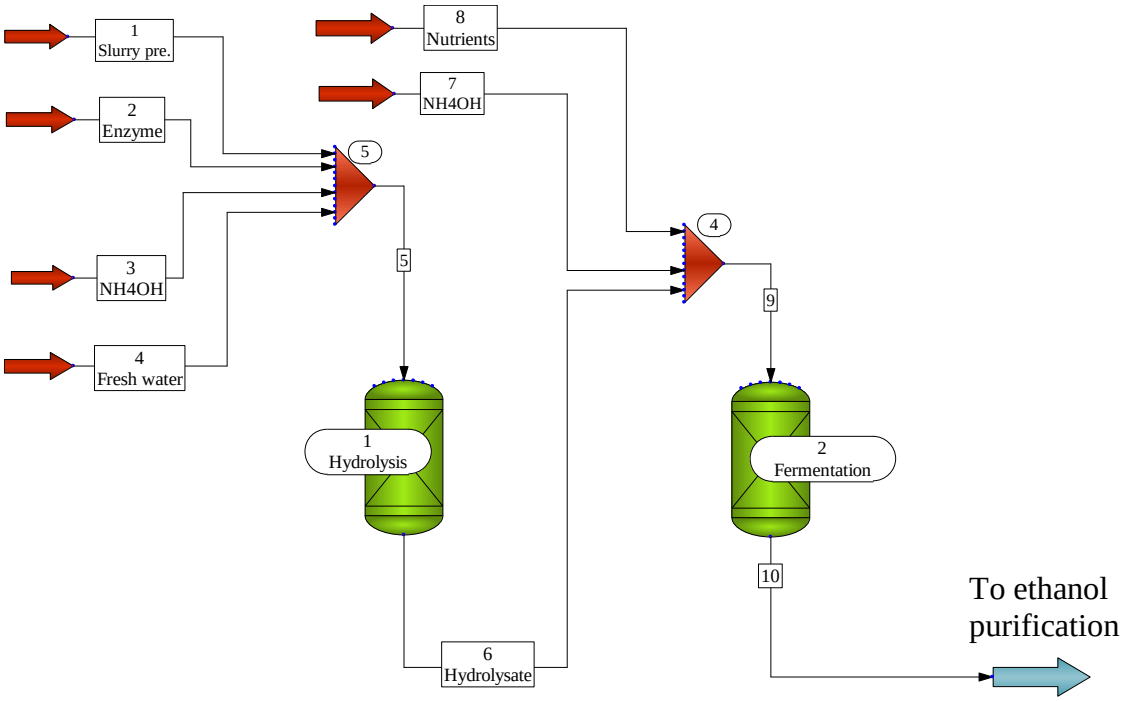

Figure A-3: Chemcad Flowsheet of hydrolysis and fermentation processes

Table A-7: Mass balance around hydrolysis and fermentation processes

	kmol/h		kg/h	
	Input	Output	Input	Output
Water	17226.21	17099.95	310330	308055.5
Glucan	145.969	19.706	23667.91	3195.167
Xylan	10.827	10.827	1430.415	1430.415
Lignin	85.957	85.957	10528.85	10528.85
Sucrose	8.326	8.326	2850	2850
Others	672.326	672.326	20187.5	20187.5
Mannan	1.798	1.798	237.5	237.5
Arabinan	0.825	0.825	109.044	109.044
Galactan	7.324	7.324	1187.5	1187.5
OH-	0.548	0.548	9.317	9.317
Na+	0.815	0.815	18.74	18.74
CH3CO2-	0.267	0.267	15.783	15.783
Sulfuric Acid	0.661	0.661	64.872	64.872
Furfural	0.285	0.285	27.36	27.36
Alpha-D-Glucose	9.781	6.802	1762.15	1225.478
Xylose	96.196	6.734	14442	1010.94
Arabinose	15.95	7.337	2394.659	1101.543
Ammonium Hydroxide	0.057	0.057	2	2
Cellulase (Enzyme)	0.044	0.044	1	1
Microorganism (C	0.041	0.041	1	1
Ethanol	0	421.943	0	19438.51
Carbon Dioxide	0	421.943	0	18569.73
Total	18284.21	18774.51	389268	389268

Table A-8: Stream composition for hydrolysis and fermentation processes

Stream No.	1	2	3	4	5	6	7	8	9	10
Stream Name	Slurry pre.	Enzyme	NH4OH	Fresh water		Hydrolysate	NH4OH	Nutrients		
Temp ^{o}C	95	**25**	**25**	**25**	38.0557	50	**25**	**25**	49.9915	33
Pressure (atm)	1	**1**	**1**	**1**	1	1	**1**	**1**	1.5	1.5
Total kmol/h	3 297	0	0	14 990	18 280	18 160	0	0	18 160	18 770
Total kg/h	119 300	1	1	270 000	389 300	389 300	1	1	389 300	389 300
Flow rates in kg/h										
Water	40 330	0	0	270 000	310 300	308 100	0	0	308 100	308 100
Sodium Hydroxide	0	0	0	0	0	0	0	0	0	0
Acetic Acid	0	0	0	0	0	0	0	0	0	0
Glucan	23 670	0	0	0	23 670	3 195	0	0	3 195	3 195
Xylan	1 430	0	0	0	1 430	1 430	0	0	1 430	1 430
Lignin	10 530	0	0	0	10 530	10 530	0	0	10 530	10 530
Sucrose	2 850	0	0	0	2 850	2 850	0	0	2 850	2 850
Others	20 190	0	0	0	20 190	20 190	0	0	20 190	20 190
Mannan	238	0	0	0	238	238	0	0	238	238
Arabinan	109	0	0	0	109	109	0	0	109	109
Galactan	1 188	0	0	0	1 188	1 188	0	0	1 188	1 188
Sodium Acetate	0	0	0	0	0	0	0	0	0	0
OH-	9	0	0	0	9	9	0	0	9	9
Na+	19	0	0	0	19	19	0	0	19	19
CH3CO2-	16	0	0	0	16	16	0	0	16	16
Sulfuric Acid	65	0	0	0	65	65	0	0	65	65
Furfural	27	0	0	0	27	27	0	0	27	27
Alpha-D-Glucose	1 762	0	0	0	1 762	24 510	0	0	24 510	1 225
Xylose	14 440	0	0	0	14 440	14 440	0	0	14 440	1 011
Arabinose	2 395	0	0	0	2 395	2 395	0	0	2 395	1 102
Ammonium Hydroxi	0	0	1	0	1	1	1	0	2	2
Cellulase (Enzym	0	1	0	0	1	1	0	0	1	1
Microorganism (C	0	0	0	0	0	0	0	1	1	1
Ethanol	0	0	0	0	0	0	0	0	0	19 440
Carbon Dioxide	0	0	0	0	0	0	0	0	0	18 570

ETHANOL RECOVERY

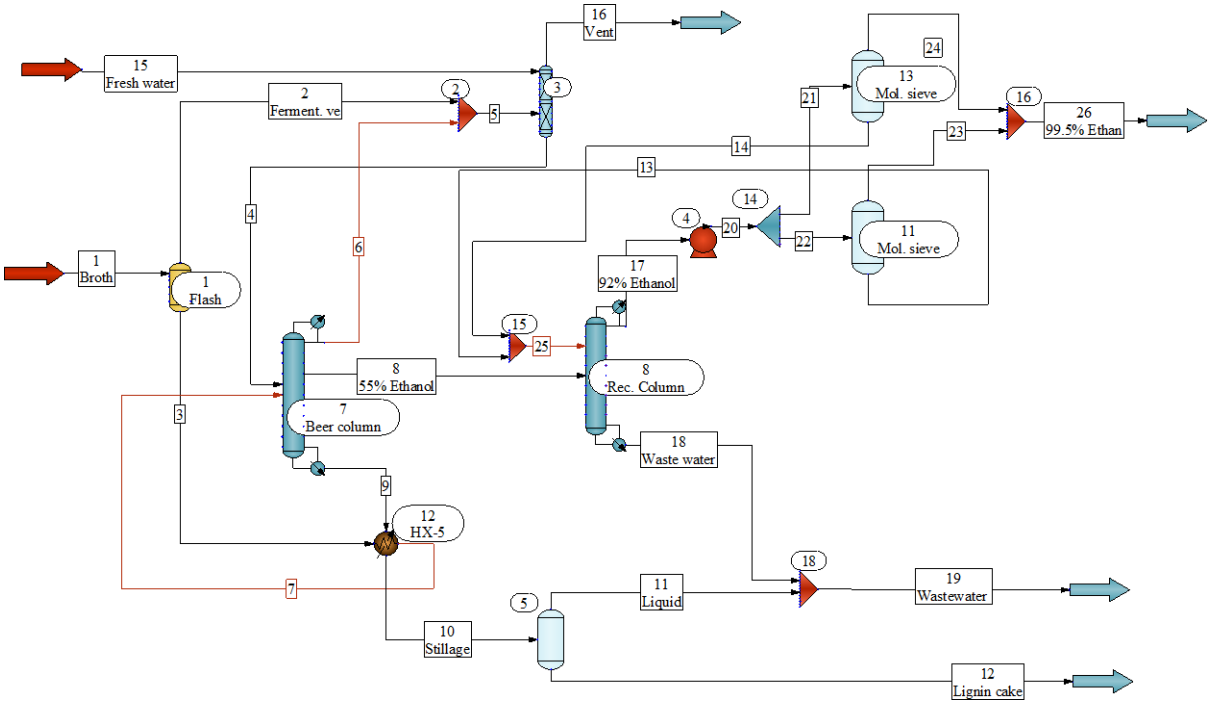

Figure A-4: Chemcad Flowsheet of hydrolysis and fermentation processes

Table A-9: Mass balance around hydrolysis and fermentation processes

	kmol/h		kg/h	
	Input	Output	Input	Output
Water	17655.04	17655.04	318055.5	318055.6
Glucan	19.706	19.706	3195.167	3195.167
Xylan	10.827	10.827	1430.415	1430.415
Lignin	85.957	85.957	10528.85	10528.85
Sucrose	8.326	8.326	2850	2850
Others	672.326	672.326	20187.5	20187.5
Mannan	1.798	1.798	237.5	237.5
Arabinan	0.825	0.825	109.044	109.044
Galactan	7.324	7.324	1187.5	1187.5
OH-	0.548	0.548	9.317	9.317
Na+	0.815	0.815	18.74	18.74
CH3CO2-	0.267	0.267	15.783	15.783
Sulfuric Acid	0.661	0.661	64.872	64.872
Furfural	0.285	0.285	27.36	27.36
Alpha-D-Glucose	6.802	6.802	1225.478	1225.478
Xylose	6.734	6.734	1010.94	1010.94
Arabinose	7.337	7.337	1101.543	1101.543
Ammonium Hydroxide	0.057	0.057	2	2
Cellulase (Enzyme)	0.069	0.069	1.579	1.579
Microorganism (C	39.51	39.51	973	973
Ethanol	421.943	421.944	19438.51	19438.54
Carbon Dioxide	421.943	421.942	18569.73	18569.69
Total	19369.1	19369.1	400240	400240

Table A-10: Stream composition for ethanol recovery process

Stream No.	1	2	3	4	5	6	7	8	9	10	11	12	13	14	15	16	17	18	19	20	21	22	23	24	25	26
Temp °C	33	33	33	107.0618	31.02	63.16	88.1518	85.5697	105.3039	47	45	47	50	50	25	-79.845	38.1164	81.5786	46.5202	38.4158	38.4158	38.4158	50	50	50	50
Pressure (atm)	1.5	1.5	1.5	1.5	1.2	1.2	1.5	1.2	1.2	1.2	1.2	1.2	3	3	1.5	1.5	0.5	5	1.2	3	3	3	3	3	3	3
Total kmol/h	18 810	428	18 390	553	451	22	18 390	1 147	17 770	17 770	16 780	989	51	51	555	453	521	727	17 510	521	260	260	210	210	101	420
Total kg/h	390 200	18 490	371 700	10 250	19 430	942	371 700	32 440	348 600	348 600	303 500	45 070	943	943	10 000	19 190	21 210	13 120	316 700	21 210	10 610	10 610	9 663	9 663	1 887	19 330
Flow rates in kg/h																										
Water	308 100	249	307 800	9 783	292	43	307 800	13 100	304 500	304 500	301 400	3 045	893	893	10 000	510	1 786	13 100	314 500	1 786	893	893	0	0	1 786	0
Glucan	3 195	0	3 195	0	0	0	3 195	0	3 195	3 195	160	3 035	0	0	0	0	0	0	160	0	0	0	0	0	0	0
Xylan	1 430	0	1 430	0	0	0	1 430	0	1 430	1 430	0	1 430	0	0	0	0	0	0	0	0	0	0	0	0	0	0
Lignin	10 530	0	10 530	0	0	0	10 530	0	10 530	10 530	53	10 480	0	0	0	0	0	0	53	0	0	0	0	0	0	0
Sucrose	2 850	0	2 850	0	0	0	2 850	0	2 850	2 850	285	2 565	0	0	0	0	0	0	285	0	0	0	0	0	0	0
Others	20 190	0	20 190	0	0	0	20 190	0	20 190	20 190	101	20 090	0	0	0	0	0	0	101	0	0	0	0	0	0	0
Mannan	238	0	238	0	0	0	238	0	238	238	0	238	0	0	0	0	0	0	0	0	0	0	0	0	0	0
Arabinan	109	0	109	0	0	0	109	0	109	109	0	109	0	0	0	0	0	0	0	0	0	0	0	0	0	0
Galactan	1 188	0	1 187	0	0	0	1 187	0	1 188	1 188	119	1 069	0	0	0	0	0	0	119	0	0	0	0	0	0	0
OH-	9	0	9	0	0	0	9	0	9	9	9	0	0	0	0	0	0	0	9	0	0	0	0	0	0	0
Na+	19	0	19	0	0	0	19	0	19	19	19	0	0	0	0	0	0	0	19	0	0	0	0	0	0	0
CH3CO2-	16	0	16	0	0	0	16	0	16	16	16	0	0	0	0	0	0	0	16	0	0	0	0	0	0	0
Sulfuric Acid	65	0	65	0	0	0	65	0	65	65	64	1	0	0	0	0	0	0	64	0	0	0	0	0	0	0
Furfural	27	0	27	0	0	0	27	20	8	8	8	0	0	0	0	0	0	20	27	0	0	0	0	0	0	0
Alpha-D-Glucose	1 225	0	1 225	0	0	0	1 225	0	1 225	1 225	123	1 103	0	0	0	0	0	0	123	0	0	0	0	0	0	0
Xylose	1 011	0	1 011	0	0	0	1 011	0	1 011	1 011	101	910	0	0	0	0	0	0	101	0	0	0	0	0	0	0
Arabinose	1 102	0	1 102	0	0	0	1 102	0	1 102	1 102	110	991	0	0	0	0	0	0	110	0	0	0	0	0	0	0
Ammonium Hydroxide	2	0	2	0	0	0	2	0	2	2	2	0	0	0	0	0	0	0	2	0	0	0	0	0	0	0
Cellulase (Enzyme)	2	0	2	0	0	0	2	0	2	2	2	0	0	0	0	0	0	0	2	0	0	0	0	0	0	0
Microorganism (C	973	0	973	0	0	0	973	0	973	973	963	10	0	0	0	0	0	0	963	0	0	0	0	0	0	0
Ethanol	19 440	231	19 210	465	571	341	19 210	19 330	4	4	3	0	49	49	0	107	19 420	2	5	19 420	9 712	9 712	9 663	9 663	97	19 330
Carbon Dioxide	18 570	18 010	558	0	18 570	558	558	0	0	0	0	0	2	2	0	18 570	4	0	0	4	2	2	0	0	4	0

Table A-11: Modelling results of beer column

Unit type:	SCDS		Unit name:	Beer column	Eqp # 7		
			* Net Flows *				
	Temp	Pres	Liquid	Vapor	Feeds	Product	Duties
Stage	C	atm	kmol/h	kmol/h	kmol/h	kmol/h	MW
1	63.2	1.2	2248.4			22.48	-26
2	83.8	1.2	2361.72	2270.89			
3	85.6	1.2	1158.24	2384.21			
						1146.66	side product
4	93.8	1.2	1682.21	2327.38	553.12		
5	98.3	1.2	1689.88	2298.23			
6	99.2	1.2	1691.62	2305.9			
7	99.3	1.2	1691.86	2307.64			
8	99.3	1.2	1691.9	2307.88			
9	99.3	1.2	1691.9	2307.91			
10	99.3	1.2	1691.9	2307.92			
11	99.3	1.2	1691.6	2307.92			
12	99.5	1.2	20439.71	2307.62	18385.93		
13	100.2	1.2	20460.43	2669.81			
14	100.9	1.2	20478.84	2690.52			
15	101.7	1.2	20499.95	2708.93			
16	102.4	1.2	20521.69	2730.04			
17	103.2	1.2	20542.44	2751.78			
18	103.8	1.2	20560	2772.53			
19	104.2	1.2	20573.55	2790.08			
20	104.6	1.2	20583.78	2803.65			
21	104.8	1.2	20590.71	2813.88			
22	105	1.2	20595.81	2820.8			
23	105.1	1.2	20599.12	2825.9			
24	105.2	1.2	20601	2829.21			
25	105.2	1.2	20602.21	2831.08			
26	105.2	1.2	20603.17	2832.3			
27	105.3	1.2	20603.57	2833.26			
28	105.3	1.2	20604.08	2833.66			
29	105.3	1.2	20604.36	2834.18			
30	105.3	1.2	20604.54	2834.45			
31	105.3	1.2	20604.59	2834.64			
32	105.3	1.2		2834.69		17769.91	26.39
Mole Reflux ratio	100						
Total liquid entering stage	4	at	87.026	C,	1693.942	kmol/h.	
Total liquid entering stage	12	at	88.797	C,	20040.43	kmol/h.	

Table A-12: Modelling results of rectification column

Unit type:	SCDS		Unit name:	Rec. Column	Eqp # 8		
			* Net Flows *				
	Temp	Pres	Liquid	Vapor	Feeds	Product	Duties
Stage	C	atm	kmol/h	kmol/h	kmol/h	kmol/h	MW
1	38.1	0.5	1831.14			520.82	-28.16
2	61.8	0.5	1949.85	2351.97			
3	61.9	0.5	1946.25	2470.68			
4	62	0.5	2050.47	2467.08	101.32		
5	62	0.5	2050.44	2469.98			
6	62	0.5	2050.39	2469.95			
7	62	0.5	2050.33	2469.9			
8	62	0.5	2050.23	2469.83			
9	62	0.5	2050.12	2469.74			
10	62	0.5	2049.95	2469.62			
11	62	0.5	2049.73	2469.46			
12	62.1	0.5	2049.44	2469.24			
13	62.1	0.5	2049.04	2468.95			
14	62.1	0.5	2048.5	2468.55			
15	62.1	0.5	2047.75	2468			
16	62.1	0.5	2046.69	2467.25			
17	62.2	0.5	2045.18	2466.2			
18	62.3	0.5	2042.93	2464.68			
19	62.4	0.5	2039.41	2462.44			
20	62.6	0.5	2033.37	2458.92			
21	63.1	0.5	3120.87	2452.87	1146.66		
22	63.1	0.5	3120.87	2393.72			
23	63.1	0.5	3120.86	2393.72			
24	63.1	0.5	3120.86	2393.71			
25	63.1	0.5	3120.85	2393.71			
26	63.1	0.5	3120.84	2393.7			
27	63.1	0.5	3120.81	2393.69			
28	63.1	0.5	3120.79	2393.66			
29	63.1	0.5	3120.74	2393.64			
30	63.1	0.5	3120.68	2393.59			
31	63.1	0.5	3120.58	2393.53			
32	63.1	0.5	3120.44	2393.43			
33	63.1	0.5	3120.23	2393.29			
34	63.1	0.5	3119.88	2393.08			
35	63.2	0.5	3119.35	2392.74			
36	63.2	0.5	3118.43	2392.2			
37	63.2	0.5	3116.76	2391.28			
38	63.3	0.5	3113.45	2389.62			
39	63.5	0.5	3106.08	2386.31			
40	64.1	0.5	3086.93	2378.93			
41	66.1	0.5	3041.71	2359.79			
42	72.5	0.5	3040.16	2314.56			
43	79	0.5	3076.48	2313.01			
44	81.2	0.5	3090.02	2349.33			
45	81.6	0.5		2362.87		727.15	27.36
Mole Reflux ratio	3.516						
Total liquid entering stage	4	at	61.176	C,	2045.612	kmol/h.	
Total liquid entering stage	21	at	63.116	C,	3120.953	kmol/h.	

HEAT AND POWER GENERATION

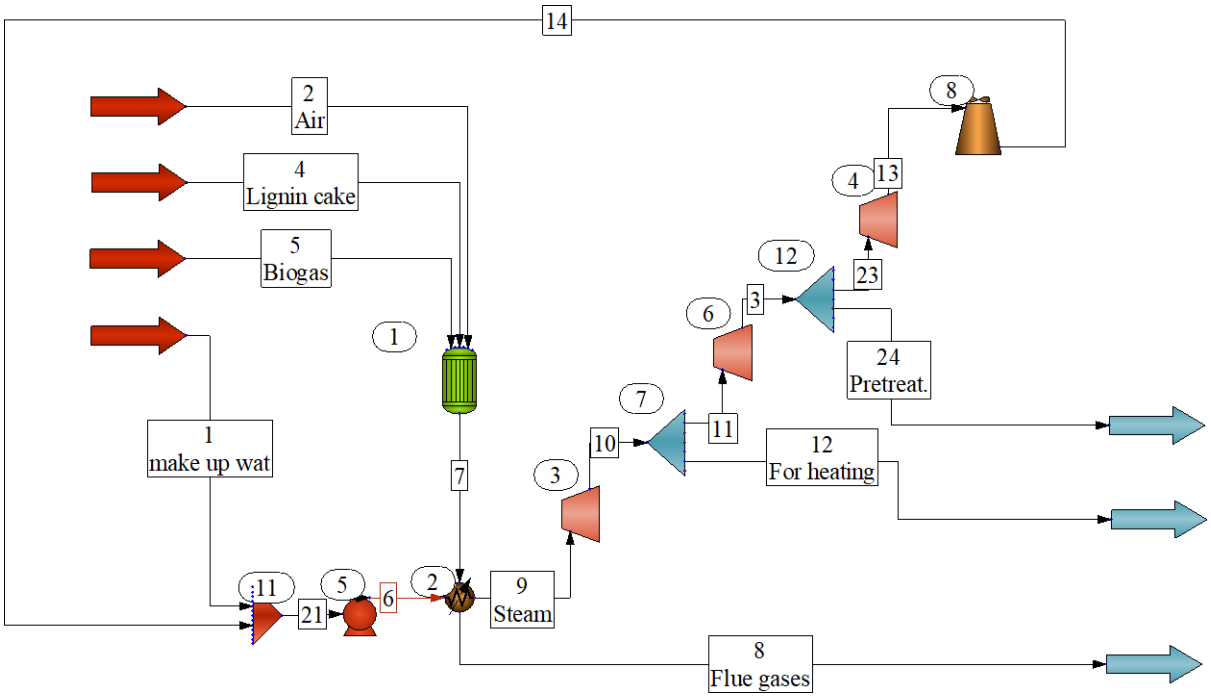

Figure A-4: Chemcad Flowsheet of heat and power generation unit

Table A-13: Combustion reactions in combustor

COMPOUND	REACTANTS	PRODUCTS
Xylan	$C_5H_8O_4 + 5O_2$	$5CO_2 + 4H_2O$
Mannan	Same as Xylan	Same as Xylan
Arabinan	Same as Xylan	Same as Xylan
Galactan	$C_6H_{10}O_5 + 6O_2$	$6CO_2 + 5H_2O$
Sucrose	$C_{12}H_{22}O_{11} + 12O_2$	$12CO_2 + 11H_2O$
Furfural	$C_5H_4O_2 + 5O_2$	$5CO_2 + 2H_2O$
Xylose	$C_5H_{10}O_5 + 5O_2$	$5CO_2 + 5H_2O$
Ethanol	$C_2H_6O + 3O_2$	$2CO_2 + 3H_2O$
Methane	$CH_4 + 2O_2$	$CO_2 + 2H_2O$
Lignin	$C_{7.3}H_{13.9}O_{1.3} + {}_{10.125}O_2$	$7.3CO_2 + 6.95H_2O$
Extractives	$CH_2O + O_2$	$CO_2 + H_2O$
Glucose	$C_6H_{16}O_6 + 6O_2$	$6CO_2 + 6H_2O$
Arabinose	Same as Xylose	
Glucan	Same as Galactan	

Equation A-1 below was used to estimate the heat capacity of biomass components during Chemcad modelling. It was obtained from Dupont, et al., (2014), and it is the average heat capacity of 21 biomass species that was experimentally determined.

$$Cp = 4.340T - 299 \qquad \text{Eq. A-1}$$

Table A-14: Mass balance around heat and power generation

Overall Mass Balance	kmol/h		kg/h	
	Input	Output	Input	Output
Water	20626.24	22624.27	371582	407576
Xylan	10.827	0	1430.43	0
Sucrose	7.493	0	2565	0
Mannan	1.798	0	237.502	0
Arabinan	0.825	0	109.046	0
Galactan	6.591	0	1068.758	0
Furfural	0.024	0	2.343	0
Xylose	6.06	0	909.846	0
Ethanol	0.259	0	11.922	0
Carbon Dioxide	192.877	2081.417	8488.522	91603.14
Methane	185.496	0	2975.91	0
Oxygen	24002.92	21687	768070	693963
Glucan	18.721	0	3035.408	0
Lignin	85.527	0	10476.21	0
Others	668.964	0	20086.56	0
OH-	0.005	0.005	0.093	0.093
Na+	0.008	0.008	0.187	0.187
CH3CO2-	0.003	0.003	0.158	0.158
Sulfuric Acid	0.007	0.007	0.649	0.649
Alpha-D-Glucose	6.122	0	1102.93	0
Arabinose	6.603	0	991.389	0
Ammonium Hydroxi	0.001	0.001	0.02	0.02
Cellulase (Enzym	0.001	0.001	0.016	0.016
Microorganism (C	0.395	0.395	9.73	9.73
Air	241788	241788	7000000	7000000
Total	287615.6	288181	8193154	8193153

Table A-15: Stream composition for heat and power generation

Stream No.	1	2	3	4	5	6	7	8	9	10	11	12	13	14	21	23	24
Temp ^{o}C	25	25	157.3479	47	35	25.2957	6821.799	6722.884	344.7151	178.2353	178.2353	178.2353	99.9743	60	25.1455	157.3479	157.3479
Pressure (atm)	1	5	5.7	5	5	62	5	5	62	9.5	9.5	9.5	1	1	1	5.7	5.7
Total kmol/h	20 450	265 800	13 210	989	385	20 540	267 700	267 700	20 540	20 540	13 210	7 327	85	85	20 540	85	13 130
Total kg/h	368 500	7 768 000	238 000	45 070	11 630	370 000	7 825 000	7 825 000	370 000	370 000	238 000	132 000	1 540	1 540	370 000	1 540	236 500
Flow rates in kg/h																	
Water	368 500	0	238 000	3 045	77	370 000	39 120	39 120	370 000	370 000	238 000	132 000	1 540	1 540	370 000	1 540	236 500
Xylan	0	0	0	1 430	0	0	0	0	0	0	0	0	0	0	0	0	0
Sucrose	0	0	0	2 565	0	0	0	0	0	0	0	0	0	0	0	0	0
Mannan	0	0	0	238	0	0	0	0	0	0	0	0	0	0	0	0	0
Arabinan	0	0	0	109	0	0	0	0	0	0	0	0	0	0	0	0	0
Galactan	0	0	0	1 069	0	0	0	0	0	0	0	0	0	0	0	0	0
Furfural	0	0	0	0	2	0	0	0	0	0	0	0	0	0	0	0	0
Xylose	0	0	0	910	0	0	0	0	0	0	0	0	0	0	0	0	0
Ethanol	0	0	0	0	12	0	0	0	0	0	0	0	0	0	0	0	0
Carbon Dioxide	0	0	0	0	8 489	0	91 600	91 600	0	0	0	0	0	0	0	0	0
Methane	0	0	0	0	2 976	0	0	0	0	0	0	0	0	0	0	0	0
Oxygen	0	768 000	0	0	70	0	694 000	694 000	0	0	0	0	0	0	0	0	0
Glucan	0	0	0	3 035	0	0	0	0	0	0	0	0	0	0	0	0	0
Lignin	0	0	0	10 480	0	0	0	0	0	0	0	0	0	0	0	0	0
Others	0	0	0	20 090	0	0	0	0	0	0	0	0	0	0	0	0	0
Sulfuric Acid	0	0	0	1	0	0	1	1	0	0	0	0	0	0	0	0	0
Alpha-D-Glucose	0	0	0	1 103	0	0	0	0	0	0	0	0	0	0	0	0	0
Arabinose	0	0	0	991	0	0	0	0	0	0	0	0	0	0	0	0	0
Microorganism (C	0	0	0	10	0	0	10	10	0	0	0	0	0	0	0	0	0
Air	0	7 000 000	0	0	0	0	7 000 000	7 000 000	0	0	0	0	0	0	0	0	0

WASTEWATE TREATMENT

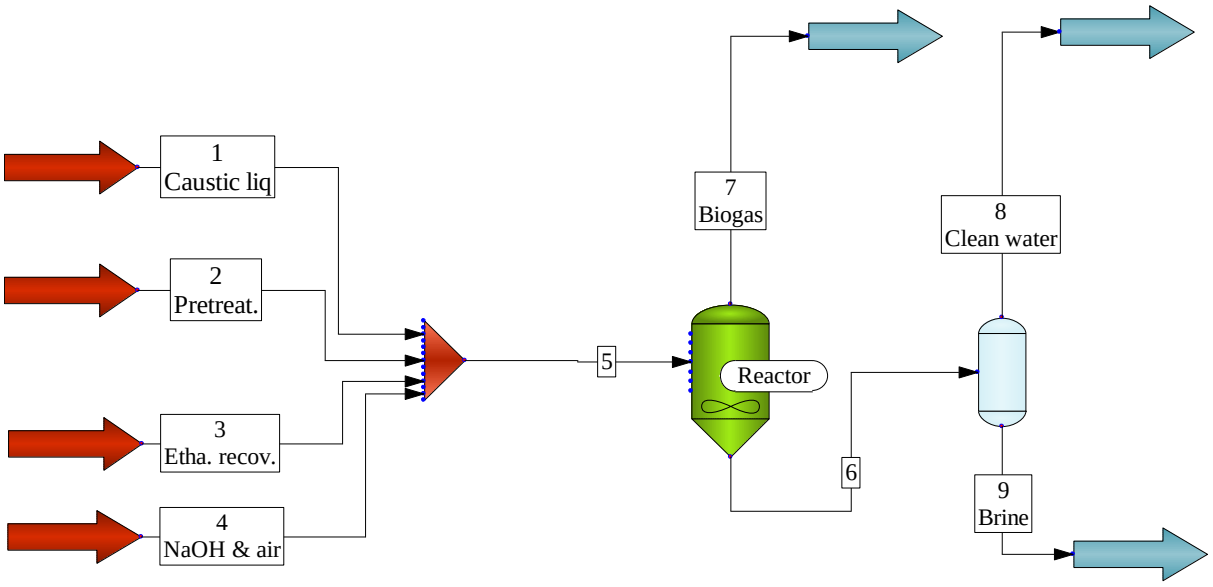

Figure A-4: Chemcad Flowsheet of wastewater treatment

Table A-16: Mass balance around wastewater treatment unit

	kmol/h		kg/h	
	Input	Output	Input	Output
Water	82391.48	82392.78	1484282	1484306
Glucan	8.197	1.148	1329.15	186.081
Xylan	16.651	2.331	2199.926	307.99
Lignin	4.524	4.524	554.15	554.15
Sucrose	8.66	1.212	2964.157	414.982
Others	35.386	4.954	1062.5	148.75
Mannan	1.87	0.262	247.013	34.582
Arabinan	1.698	0.238	224.323	31.405
Galactan	7.617	1.066	1235.065	172.909
OH-	63.859	63.859	1086.071	1086.071
Na+	95.017	95.017	2184.442	2184.442
CH3CO2-	31.158	31.158	1839.747	1839.747
Sodium Hydroxide	5000.375	4999.07	200000	199948
Sulfuric Acid	0.653	0	64.056	0
Furfural	6.217	6.217	597.324	597.324
Xylose	6.701	0.938	1006.071	140.85
Arabinose	7.245	1.014	1087.689	152.277
Ethanol	24.698	3.458	1137.816	159.294
Carbon Dioxide	0	203.994	0	8977.755
Methane	0	186.798	0	2996.798
Microorganism (C	39.014	39.014	960.763	960.763
Oxygen	40.626	2.19	1300	70.086
Sodium Sulfate	0	0.653	0	92.769

Table A-16: Stream composition for waste water treatment unit

Stream No.	1	2	3	4	5	6	7	8	9
Temp ^{o}C	28.0262	45	50.0232	25	34.6654	35	35	25	25
Pressure (atm)	1.5	1	1.5	**5**	5	5	5	5	5
Total kmol/h	53 050	12 180	17 520	5 041	87 790	87 660	383	82 310	5 353
Total kg/h	960 500	219 900	323 600	201 300	1 705 000	1 694 000	11 580	1 483 000	211 000
Flow rates in kg/h									
Water	951 300	219 300	313 600	0	1 484 000	1 484 000	77	1 483 000	1 484
Glucan	1 329	0	0	0	1 329	186	0	0	186
Xylan	788	0	1 412	0	2 200	308	0	0	308
Lignin	554	0	0	0	554	554	0	0	554
Sucrose	150	0	2 814	0	2 964	415	0	0	415
Others	1 062	0	0	0	1 062	149	0	0	149
Mannan	13	0	235	0	247	35	0	0	35
Arabinan	117	0	108	0	224	31	0	0	31
Galactan	63	0	1 173	0	1 235	173	0	0	173
OH-	1 086	0	0	0	1 086	1 086	0	0	1 086
Na+	2 184	0	0	0	2 184	2 184	0	0	2 184
CH3CO2-	1 840	0	0	0	1 840	1 840	0	0	1 840
Sodium Hydroxide	0	0	0	200 000	200 000	199 900	0	0	199 900
Sulfuric Acid	0	0	64	0	64	0	0	0	0
Furfural	0	570	27	0	597	592	5	0	592
Xylose	0	8	998	0	1 006	141	0	0	141
Arabinose	0	0	1 088	0	1 088	152	0	0	152
Ethanol	0	0	1 138	0	1 138	140	19	0	140
Carbon Dioxide	0	0	0	0	0	520	8 458	0	520
Methane	0	0	0	0	0	48	2 949	0	48
Microorganism (C	0	0	961	0	961	961	0	0	961
Oxygen	0	0	0	1 300	1 300	1	69	0	1

GASIFICATION

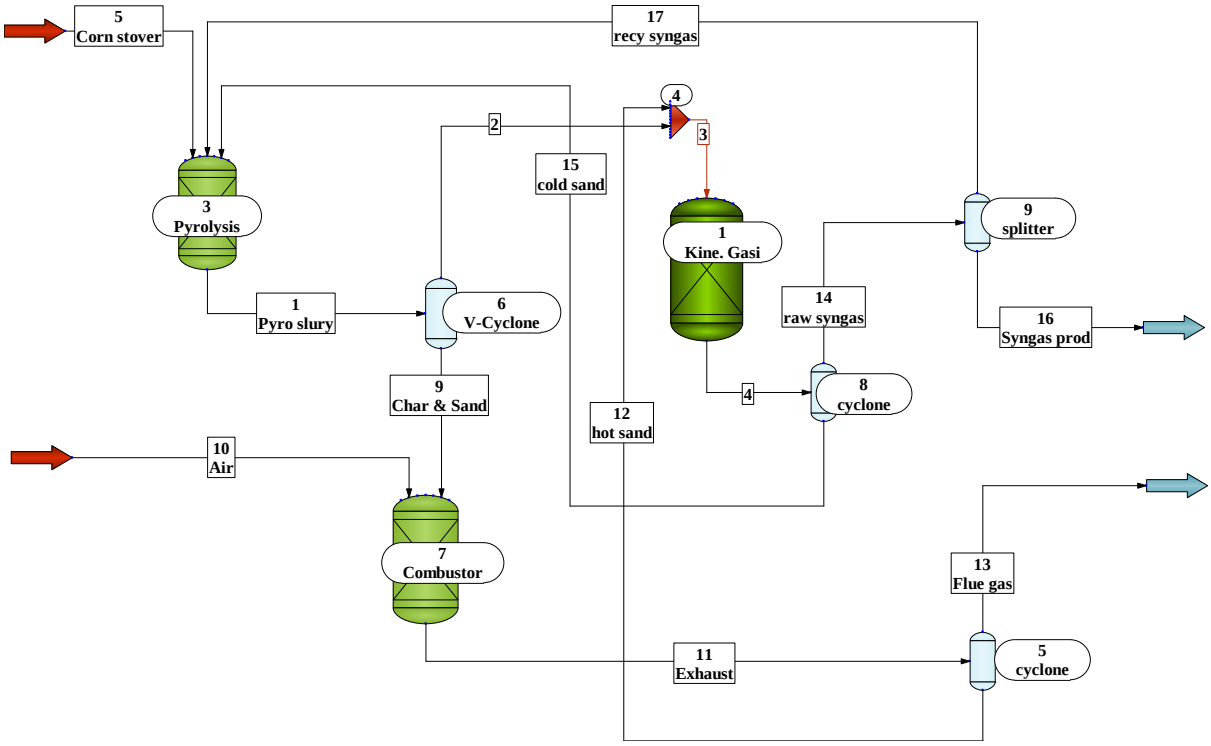

Figure B-1: Chemcad Flowsheet of dual-bed gasification process

Table A-17: Mass balance around gasification process

	kmol/hr		kg/hr	
	Input	Output	Input	Output
Corn stover 2	833.33	0	83333	0
Oxygen	1560.3	124.208	49928	3974.526
Carbon Monoxide	0	735.651	0	20605.59
Carbon Dioxide	0	1999.767	0	88009.73
Methane	0	355.399	0	5701.663
Water	2835.141	2782.685	51075.06	50130.07
Hydrogen	0	478.901	0	965.37
Benzene	0	100.586	0	7857.151
Naphthalene	0	44.894	0	5754.271
Toluene	0	5.475	0	504.481
Total	5228.771	6627.566	184336	183503

Table A-18: Stream composition for gasification process

Stream No.	1	2	3	4	5	9	10	11	12	13	14	15	16	17
Temp (^oC)	760.526	760.5255	958.5684	959.4515	**25**	760	**25**	980	980	980	959.4515	959.4515	959.451	959.4515
Pressure (bar)	1	1	1	1	**1**	1	**1**	1	1	1	1	1	1	1
Total kmol/hr	27 520	5 413	26 080	26 200	3 668	22 040	1 560	22 230	20 670	1 560	5 415	20 790	5 067	347
Total kg/hr	1 385 000	126 300	1 368 000	1 368 000	134 400	1 258 000	49 930	1 308 000	1 242 000	67 180	124 800	1 243 000	116 300	8 478
Flow rates in kg/hr														
Corn stover 2	0	0	0	0	83 330	0	0	0	0	0	0	0	0	0
Oxygen	0	0	0	0	0	0	49 930	5 990	0	3 975	0	0	0	0
Carbon Monoxide	24 190	24 190	24 190	23 960	0	0	0	0	0	0	23 960	0	20 610	3 354
Carbon Dioxide	26 540	26 540	26 540	28 850	0	0	0	60 430	0	63 200	28 850	0	24 810	4 038
Methane	5 928	5 928	5 928	6 630	0	0	0	0	0	0	6 630	0	5 702	928
Water	51 080	51 080	51 080	50 130	51 080	0	0	0	0	0	50 130	0	50 130	0
Hydrogen	991	991	991	1 123	0	0	0	0	0	0	1 123	0	965	157
Carbon	18 160	908	908	1 490	0	16 490	0	0	0	0	0	1 490	0	0
Silicon Dioxide	1 242 000	0	1 242 000	1 242 000	0	1 242 000	0	1 242 000	1 242 000	0	0	1 242 000	0	0
Benzene	4 167	4 167	4 167	7 857	0	0	0	0	0	0	7 857	0	7 857	0
Naphthalene	4 167	4 167	4 167	5 754	0	0	0	0	0	0	5 754	0	5 754	0
Toluene	4 167	4 167	4 167	505	0	0	0	0	0	0	505	0	505	0
Phenol	4 167	4 167	4 167	0	0	0	0	0	0	0	0	0	0	0

SYNGAS CLEANING AND CONDITIONING

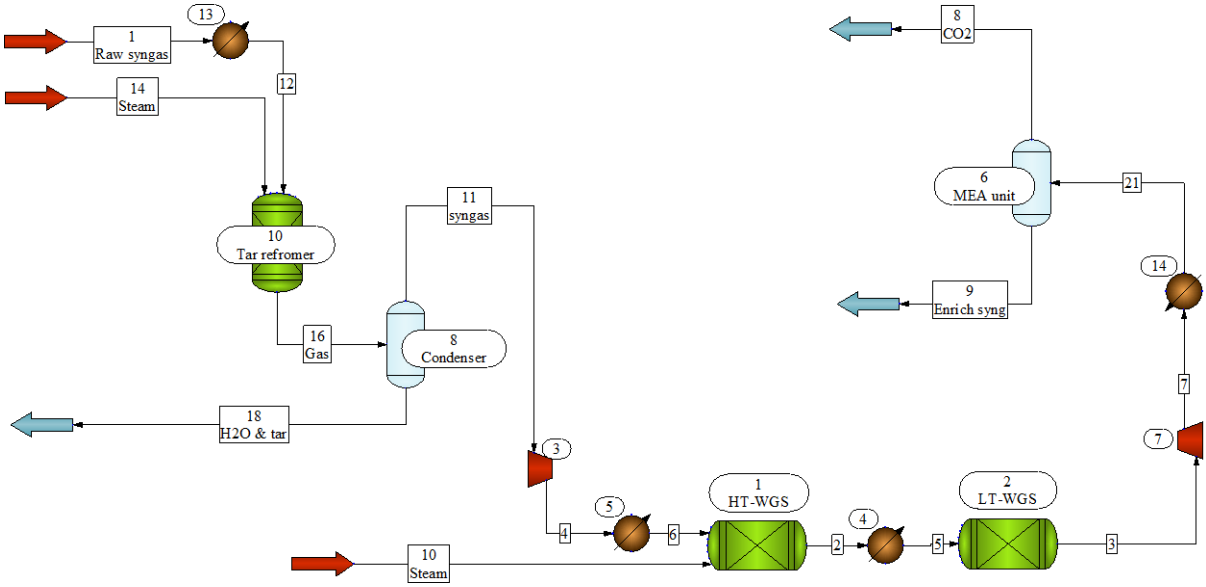

Figure B-2: Chemcad Flowsheet of syngas cleaning and conditioning process. NB. The CO_2 removal sub-process using Monoethanolamine (MEA) solvent was modelled using a Chemcad component separator hereby referred to as “MEA unit”.

Table A-19: Mass balance around gasification process

	kmol/h		kg/h	
	Input	Output	Input	Output
Carbon Monoxide	735.651	486.608	20605.59	13629.89
Carbon Dioxide	563.675	1903.488	24807.32	83772.52
Methane	355.399	355.399	5701.663	5701.663
Water	15049.97	12619.38	271125	227338
Hydrogen	478.902	3412.715	965.37	6879.35
Benzene	100.586	43.109	7857.151	3367.394
Naphthalene	44.894	4.989	5754.271	639.415
Toluene	5.475	0.608	504.481	56.058
Total	17334.55	18826.3	337321	341384.4

Table A-20: Stream composition for syngas cleaning and conditioning

Stream No.	1	2	3	4	5	6	7	8	9	10	11	12	14	16	18	21
Temp C	959.451	408.327	259.1	450.161	230	350	89.416	40	40	**360**	350	40	**350**	350	350	40
Pres (bar)	1	22	22	22	22	22	1.18	1.18	1.18	**22**	5	5	**5**	5	5	1.18
Total kmol/h	5067.00	15420.00	15420.00	4818.00	15420.00	4818.00	15420.00	1410.00	14010.00	10600.00	2685.00	5067.00	1665.00	6091.00	3406.00	15420.00
Total kg/h	116300.00	276800.00	276800.00	85850.00	276800.00	85850.00	276800.00	62050.00	214800.00	191000.00	33770.00	116300.00	30000.00	98310.00	64540.00	276800.00
Flow rates in kg/h																
Carbon Monoxide	20610.00	26850.00	13630.00	51160.00	26850.00	51160.00	13630.00	0.00	13630.00	0.00	30550.00	20610.00	0.00	30550.00	0.00	13630.00
Carbon Dioxide	24810.00	63000.00	83770.00	24810.00	63000.00	24810.00	83770.00	62050.00	21720.00	0.00	0.00	24810.00	0.00	0.00	0.00	83770.00
Methane	5702.00	5702.00	5702.00	5702.00	5702.00	5702.00	5702.00	0.00	5702.00	0.00	0.00	5702.00	0.00	0.00	0.00	5702.00
Water	50130.00	175400.00	166900.00	0.56	175400.00	0.56	166900.00	0.00	166900.00	191000.00	0.06	50130.00	30000.00	60480.00	60480.00	166900.00
Hydrogen	965.40	5928.00	6879.00	4179.00	5928.00	4179.00	6879.00	0.00	6879.00	0.00	3213.00	965.40	0.00	3213.00	0.00	6879.00
Benzene	7857.00	0.08	0.08	0.08	0.08	0.08	0.08	0.00	0.08	0.00	0.00	7857.00	0.00	3367.00	3367.00	0.08
Naphthalene	5754.00	0.06	0.06	0.06	0.06	0.06	0.06	0.00	0.06	0.00	0.00	5754.00	0.00	639.40	639.40	0.06
Toluene	504.50	0.01	0.01	0.01	0.01	0.01	0.01	0.00	0.01	0.00	0.00	504.50	0.00	56.05	56.05	0.01

METHANOL SYNTHESIS FROM SYNGAS

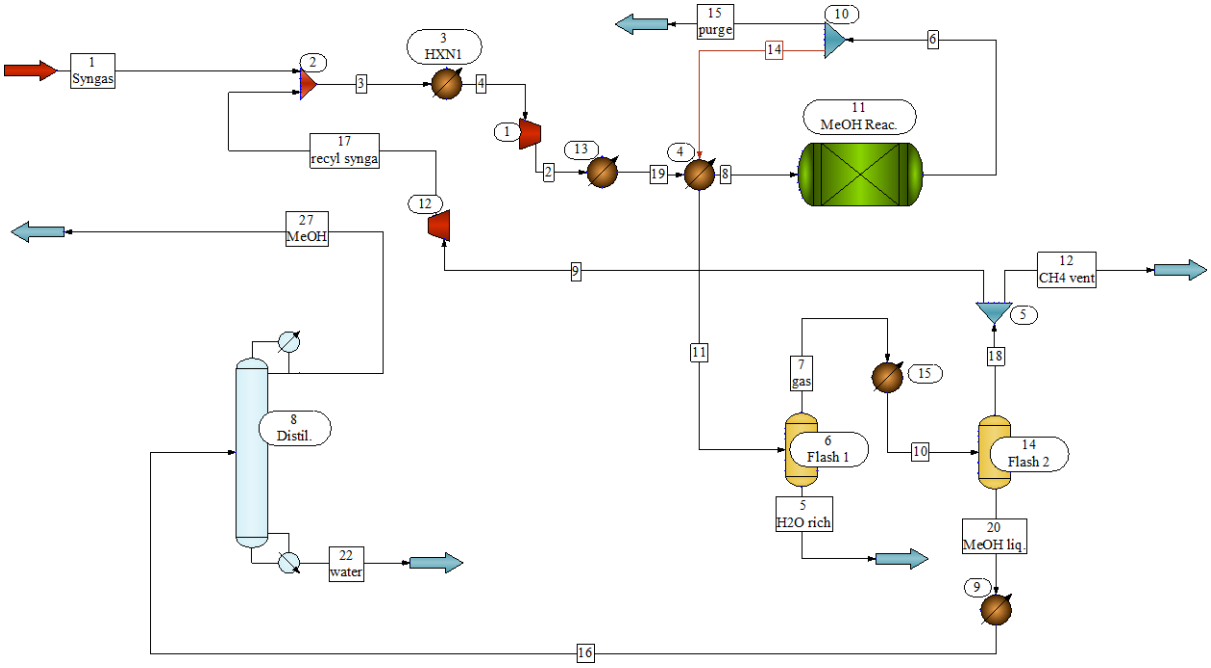

Figure B-3: Chemcad Flowsheet of methanol synthesis from syngas

Table A-21: Mass balance around methanol synthesis from syngas

	kmol/h		kg/h	
	Input	Output	Input	Output
Carbon Monoxide	487	487	13 630	13 631
Carbon Dioxide	683	700	30 080	30 821
Methane	355	359	5 702	5 763
Water	9 262	6 239	166 859	112 391
Hydrogen	3 413	3 413	6 879	6 880
Methanol	0	1 055	0	33 815
Total	14 200	12 253	223 150	203 301

Table A-22: Stream composition for methanol synthesis from syngas

Stream No.	1	2	3	4	5	6	7	8	9	10	11	12	14	15	16	17	18	19	20	22	27
Temp (^oC)	40	214.833	86.4346	150	80	213.094	80	213.094	5	5	210	5	213.094	213.094	25	203.859	5	200	5	211.668	129.79
Pressure (bar)	1.18	110	1.18	1.18	20	110	20	110	20	20	110	20	110	110	20	1.2	20	110	20	20	20
Total kmol/h	1.4E+04	1.7E+05	1.7E+05	1.7E+05	5.2E+03	1.7E+05	1.7E+05	1.7E+05	1.6E+05	1.7E+05	1.7E+05	4.1E+03	1.7E+05	8.7E+02	2.0E+03	1.6E+05	1.6E+05	1.7E+05	4.0E+03	9.1E+02	1.1E+03
Total kg/h	2.2E+05	2.1E+06	2.1E+06	2.1E+06	9.4E+04	2.1E+06	1.9E+06	2.1E+06	1.8E+06	1.9E+06	2.0E+06	4.7E+04	2.0E+06	1.0E+04	5.2E+04	1.8E+06	1.9E+06	2.1E+06	7.2E+04	1.6E+04	3.5E+04
Flow rates in kg/h																					
Carbon Monoxide	1.36E+04	4.6E+05	4.6E+05	4.6E+05	1.4E-11	4.6E+05	4.5E+05	4.6E+05	4.4E+05	4.5E+05	4.5E+05	1.1E+04	4.5E+05	2.3E+03	7.9E-01	4.4E+05	4.5E+05	4.6E+05	1.1E-11	0.0E+00	7.9E-01
Carbon Dioxide	2.17E+04	1.0E+06	1.0E+06	1.0E+06	3.1E-11	1.0E+06	1.0E+06	1.0E+06	9.8E+05	1.0E+06	1.0E+06	2.5E+04	1.0E+06	5.0E+03	7.4E+02	9.8E+05	1.0E+06	1.0E+06	2.4E-11	0.0E+00	7.4E+02
Methane	5.70E+03	1.9E+05	1.9E+05	1.9E+05	5.9E-12	1.9E+05	1.9E+05	1.9E+05	1.9E+05	1.9E+05	1.9E+05	4.7E+03	1.9E+05	9.5E+02	6.2E+01	1.9E+05	1.9E+05	1.9E+05	4.6E-12	0.0E+00	6.2E+01
Water	1.67E+05	1.7E+05	1.7E+05	1.7E+05	9.4E+04	1.7E+05	7.3E+04	1.7E+05	1.5E+03	7.3E+04	1.7E+05	3.7E+01	1.7E+05	8.4E+02	1.7E+04	1.5E+03	1.5E+03	1.7E+05	7.2E+04	1.6E+04	8.6E+02
Hydrogen	6.88E+03	2.3E+05	2.3E+05	2.3E+05	7.1E-12	2.3E+05	2.3E+05	2.3E+05	2.2E+05	2.3E+05	2.3E+05	5.7E+03	2.3E+05	1.2E+03	7.1E-01	2.2E+05	2.3E+05	2.3E+05	5.5E-12	0.0E+00	7.1E-01
Methanol	8.25E-02	0.0E+00	0.0E+00	0.0E+00	0.0E+00	0.0E+00	0.0E+00	0.0E+00	0.0E+00	0.0E+00	0.0E+00	0.0E+00	0.0E+00	0.0E+00	3.4E+04	0.0E+00	0.0E+00	0.0E+00	0.0E+00	3.4E+01	3.4E+04
Benzene	5.83E-02	2.8E+00	2.8E+00	2.8E+00	8.5E-17	2.8E+00	2.7E+00	2.8E+00	2.7E+00	2.7E+00	2.7E+00	6.9E-02	2.7E+00	1.4E-02	8.1E-02	2.7E+00	2.7E+00	2.8E+00	6.6E-17	0.0E+00	8.1E-02
Naphthalene	5.12E-03	2.0E+00	2.0E+00	2.0E+00	6.0E-17	2.0E+00	1.9E+00	2.0E+00	1.9E+00	1.9E+00	1.9E+00	4.9E-02	1.9E+00	9.8E-03	5.8E-02	1.9E+00	1.9E+00	2.0E+00	4.7E-17	5.8E-02	8.1E-13
Toluene	4.35E-19	1.7E-01	1.7E-01	1.7E-01	5.3E-18	1.7E-01	1.7E-01	1.7E-01	1.7E-01	1.7E-01	1.7E-01	4.3E-03	1.7E-01	8.6E-04	5.1E-03	1.7E-01	1.7E-01	1.7E-01	4.1E-18	9.1E-10	5.1E-03
Phenol	0.00E+00	1.5E-17	1.5E-17	1.5E-17	0.0E+00	1.5E-17	1.4E-17	1.5E-17	1.4E-17	1.4E-17	1.4E-17	3.6E-19	1.4E-17	7.3E-20	4.3E-19	1.4E-17	1.4E-17	1.5E-17	0.0E+00	4.3E-19	0.0E+00

APPENDIX B

KEY FINANCIAL DETAILS

Table B-1: Breakdown of major variable operating costs

	Yearly price ($)
Feedstock	$18 487 559
Sulfuric acid	$4 355 972
Ammonium hydroxide	$1 397 922
Sodium Hydroxide	$7 713 481
Make up water	$720 000
Waste disposal cost	$327 797
Other raw materials	$5 603 000
Net electricity credit	-$3 637 840
VARIABLE OPERATING COST	**$34 967 891**

Table B-2: Salary structure of biorefinery' s employees

Plant manager	R850 000	1	850 000
Plant engineer	R750 000	2	1 500 000
Maintenance supervisor	R500 000	1	500 000
Maintenance technician	R400 000	12	4 800 000
Lab manager	R600 000	1	600 000
Lab technician	R500 000	2	1 000 000
Shift supervisor	R450 000	4	1 800 000
Shift operator	R350 000	20	7 000 000
Yard employees	R126 254	4	505 016
Clerks and secretaries	R300 000	3	900 000
TOTAL		60	R19 455 016

Table B-3 : Breakdown of fixed capital Investment for biological conversion.

MAIN CONVERSION AREAS	
Pretreatment	29 485 494
Saccharification & fermentation	25 786 965
Enzyme production	17 054 328
Ethanol recovery	20 752 857
Water treatment	41 711 187
Storage	4 417 687
Power generation (standalone)	69 450 154
Utilities	6 986 110
Total installed equipment cost	215 644 783
Added direct + indirect costs	175 782 860
Shipping cost	10 782 239
Fixed capital investment	**402 209 882**

Maintenance (3% of FCI)
Maintenance HYBRID (3% of FCI)
Insurance (0.7% of Installed capital cost)
Insurance HYBRID (0.7% of Installed capital cost)
Fixed operating cost (standalone)

Table B-4: Capital cost breakdown of major equipment used to model corn stover to methanol biorefinery

		COST DATA OBTAINED FROM LITERATURE							COST ESCALATION DATA		
		Base cost	Base currency	Currency Base Year	Base scale	Base unit scale	Scale factor	Reference	Scale in the present study	Cost after scaling	Cost adjusted to 2019 using CEPCI
GASIFICATION AREA	Indirect gasifier & combustor	6.7	M Euro	2007	20	MWth input	0.72	(Tock, et al., 2010)	387	56.61	72.00
	Tar reformer	93.7	M $	2007	31 000	Syngas flow at exit kmol/hr	0.9	(Liu, et al., 2011)	2 430	9.48	10.96
	Fabric filter	68.8	k $	2002	15.6	m^3 / s	1	(Heyne & Harvey, 2013)	32.78	144.57	222.01
	water scrubber	3	M $	2002	12	m^3 / s	0.7	(Hamelinck, et al., 2004)	32.78	6.03	9.26
	water gas shift	3.36	M $	2007	815	MWLHV (dried biomass)	0.67	(Liu, et al., 2011)	387	2.04	2.36
CO_2 REMOVAL	MEA	5.19	M Euro	2010	17	kg CO_2 esp / s	1	(Heyne & Harvey, 2013)	10.1592	3.14	3.81
METHANOL SYNTHESIS	MeOH reactor	3.5	M Euro	2001	87.5	tonne MeOH / hr	0.72	(Hamelinck & Faaij, 2002))	5.92	0.50	0.85
	recycle compressor	12.9	M Euro	2002	13.2	MWel	0.85	(Hamelinck & Faaij, 2002)	2.2	2.81	4.75
	syngas compressor (before MeOH synthesis	12.9	M Euro	2002	13.2	MWel	0.85	(Hamelinck & Faaij, 2002)	36	30.27	51.13
	MeOH product separation and purification	1.72	M $	2002	4.66	kg / s	0.291	(Larson & Tingjin, 2003)	4.3	1.68	2.58
MEOH PURIFICA-TION	MeOH refining	15.1	M $	2001	87.5	tonne MeOH / hr	0.7	(Larson & Tingjin, 2003)	5.92	2.29	3.53
POWER GENERATION AREA	Boiler/steam generator/ductwork/stack	52	M $	2007	355	Boiler duty MWth	1	(Liu, et al., 2011)	146	21.39	24.73
	Steam cycle (steam turbine/condenser/piping/auxiliaries)	66.7	M $	2007	275	Gross power production MWel	1	(Liu, et al., 2011)	17	4.12	4.77